THE UNIVERSITY OF MICHIGAN
COLLEGE OF ENGINEERING
Department of Chemical and Metallurgical Engineering

Final Report

AN INVESTIGATION OF METAL SPINNING

B. Avitzur
S. Floreen
W. Carleton
E. E. Hucke
D. V. Ragone

UMRI Project 2621

under contract with:

SPINCRAFT, INC.
MILWAUKEE, WISCONSIN

Ref.: Contract No. DA-11-022-ORD-2542
Army Ballistic Missile Agency

administered by:

THE UNIVERSITY OF MICHIGAN RESEARCH INSTITUTE ANN ARBOR

July 1959

PREFACE

This report covers an investigation of the process of spinning of cones. It summarizes the work done during a two year period under contract No. DA-11-022-ORD-2542 of the Army Ballistic Missile Agency and with Spincraft Inc., Milwaukee, Wisconsin. The study covers three distinct aspects and therefore is divided to three parts. Part I covers the theoretical analysis of the mechanism of deformation during power spinning of cones and the dependence of the process variables one on each other. Part II describes and explains the properties of mechanically spun cones, and Part III records the results of cones spun with hand tooling.

While the report can be read as one integral unit, an effort was made to make each section complete as a separate unit. Therefore, repetitions are not avoided. The master plates of progress reports were utilized to edit this final report, and some pages still bear the title of the "Engineering Research Institute" which exists no longer.

The reader can study any part of the report without reference to the others. However, it will be advisable to read first the introductory 19 pages of Part I.

TABLE OF CONTENTS

TABLE OF CONTENTS (Continued)

TABLE OF CONTENTS (Concluded)

LIST OF TABLES

LIST OF FIGURES

LIST OF FIGURES (Continued)

Part II

LIST OF FIGURES (Concluded)

Figure | Page

Part III

ABSTRACT (PART I)

The cone, the roller, and the geometry of the operation are described mathematically. A shear type of deformation is postulated, based on experimental evidence. The displacements, velocities, strain rates, and stress fields are computed for "Mises Material," and hence with Mises stress-strain rate law. The power consumed in the operation is computed from the strain rates and stress fields. The expression for the power is in a form that cannot be solved analytically. A numerical solution is therefore presented in graphical form, where the power and tangential force are plotted for a variety of process variables. The numerical solution is compared with actual measured power and forces.

OBJECTIVE (PART I)

The purpose of this study is to relate the power requirement and the tangential force of mechanical spinning of cones to the process variables.

NOMENCLATURE

X,Y,Z	Rectangular coordinate system with:
O	Origin.
R,θ,Z	Cylindrical polar coordinate system with origin O.
x,y,z	Rectangular coordinate system with:
O'	Origin.
X,Y,Z R,θ,Z x,y,z	Coordinates of a point in space in the corresponding coordinate system.
a_i	(where i = 1,2,3) - The three coordinates of the origin O in the x,y,z coordinates system.
b_j	(where j = 1,2,3) - The three coordinates of the origin O' in the X,Y,Z coordinates system.
a_{ij}	The directional cosines of X,Y,Z axis in the x,y,z coordinate system and vice versa.
r_o	"Round-off" radius of the roller.
ρ_o	The roller's radius.
α_o	Half the included angle of the cone; also the angle between Z and z axis.
R_o	Instantaneous radius at which the roller touches the cone.
$R_{o_{Min.}}$	Cose's radius (R) at the bend.
$R_{o_{Max.}}$	The blank's outer radius.
D_1	Outer diameter of the cone.
S_o	Thickness of the blank.
S_1	Thickness of the final cone.
σ_o	The cone's material yield limit at uniaxial tensile test.
k	Mises yield limit.
N	The speed in rpm.
F	The feed in ipr.

T	Time.
t_o	Initial time.
n	Number of revolutions passed from initial time.
U	Velocity in ipm.
$\bar{U}$	Velocity vector.
U_R	Velocity in R direction in ipm.
U_θ	Velocity in θ direction in ipm.
U_Z	Velocity in Z direction in ipm.
U_{ZP}	Principal part of U_Z component of the velocity.
U_{ZC}	Complementary part of U_Z component of the velocity.
ΔU_{ZP}	Change in U_{ZP}.
ΔU_{ZC}	Change in U_{ZC}.
v	Velocity.
S_t	Circumferential velocity.
S_A	Feed velocity.
S_R	Radial velocity.
$\dot{R},\dot{\theta},\dot{Z}$	Velocities in R, θ, and Z directions.
G, $G(R)$, $G(R,\theta,Z)$, $G(R,\theta,Z,n)$, etc.	The function of the "round-off" surface of the roller.
G_R,G_θ,G_Z,G_T	The partial derivatives of G with respect to R, θ, Z, and T, respectively.
$Z = H(R,\theta,n)$	The function of the "round-off" surface expressing Z explicitly.
A,B,C,D,E,F	Points on the boundaries of the area of contact.
AB,BC,CD,DE,EF,FA	Boundary lines of the area of contact.
R_A,R_B,R_C,R_D,R_E,R_F	Radius at points A,B,C,D,E, and F, respectively.
$\theta_{AB},\theta_{BC},\theta_{CD},$ $\theta_{DE},\theta_{EF},\theta_{FA}$	θ as a function of R along lines AB, BC, CD, DE, EF, and FA, respectively.
Zone 1 Zone 2 Zone 3	Zones of the cone (Fig. 11).

dv	Infinitesimal volume.
ds	Infinitesimal area.
ϵ	Strain.
ϵ_{ij}	Strain components, where: $i = R,\theta,Z$ and $j = R,\theta,Z$.
e	Hydrostatic portion of the strain.
e_{ij}	Strain deviator tensor.
$\dot{\square}$	A dot on top represents time rate, and can be applied to any variable.
$\dot{\epsilon},\dot{\epsilon}_{ij}$, $\dot{e},\dot{e}_{ij}$	These are strain rate, strain-rate components, hydrostatic portion of the strain rate and strain-rate deviator tensor, respectively.
$\square_{ii}$	Repeated index represent summation, like $\epsilon_{ii} = \epsilon_{RR} + \epsilon_{\theta\theta} + \epsilon_{ZZ}$.
δ_{ij}	Unit tensor called "Kronecker delta" and: equal 1 when $i = j$; equal 0 when $i \neq j$.
σ	Stress.
σ_{ij}	Components of stress.
S	Hydrostatic portion of the stress.
S_{ij}	Components of the stress deviator.
τ	Shear stress.
γ	Shear strain.
ν	Poisson's ratio.
E	Young's modulus of elasticity.
γ	Shear angle.
γ'	Instantaneous shear angle.
ξ	Displacement.
b	Strain-hardening coefficient.
δ	Strain-rates ratio factor.
h	Feed marks height.
μ	Proportionality factor in Mises stress-strain-rate law.

I	Strain function.
J_2	The second invariant of stress.
w	Work per unit volume.
$\dot{w}$	Rate of work per unit volume.
$\dot{W}$	Power.
$\dot{W}'$	Weighted power.
$\dot{W}_p'$	Partial weighted power.
$\dot{W}_c'$	Complementary weighted power.
$\dot{W}_{c1}'$; $\dot{W}_{c2}'$	Complementary weighted power consumed over areas 1 and 2, respectively.
$\dot{W}_t$	Power consumed through tangential motion.
$\dot{W}_A$	Power consumed through feed motion.
t	Tangential force.
t'	Weighted tangential force.
F_A	Feed force.
F_R	Radial force.
$\alpha, \alpha_\theta, \alpha_R, \Delta\alpha_R$	Experimental values of shear angles as prescribed in Fig. 23.

PART I

ANALYSIS OF POWER SPINNING OF CONES

I. INTRODUCTION

The aim of this study is to help toward better understanding of the process of spinning, and to develop a method for prediction of the power requirements. The power consumed in the process is of interest for the design of new equipment, for intelligent choice of the best machine for the job, and for the right choice of the process variables for a specified job. Furthermore, this power is the predominant factor dictating the interaction force between the roller and the cone. Therefore it can be later utilized for the determination of the forces.

Spinning is a metal-forming process widely used to fabricate pieces having rotational symmetry. In common spinning practice, a pattern having the final shape of the desired piece is mounted on a lathe. A flat sheet of metal is then clamped to the pattern, and while the pattern and sheet are revolving, the sheet is forced back over the pattern by pressing against the sheet with some type of spinning tool. Reduction in thickness of the sheet may or may not take place. Generally the spinning tool is a roller or a heavy wooden stick.

The process can be done by hand when the spinning is done by a skilled craftsman who knows by experience how to lay the sheet against the pattern; or it can be done mechanically, in which case the forces are applied by some mechanical system.

Many shapes and sizes can be spun; pieces up to 10 feet in diameter are common. Because of the nature of the process, very large

reductions in thickness, up to 75% per pass in some cases, can be achieved. With suitable equipment it is also possible to hot-spin. There seems to be no restrictions as to deformable materials which can be spun. Aluminum, brass, stainless steel, titanium, and super-alloys, for example, have all been successfully spun.

Because of the simplicity of the operation, spinning offers some distinct economical advantages. Lengbridge[8] has shown that spinning is more economical for producing a small number of pieces than deep drawing because of the low setup time and costs. The pattern used for spinning, for example, can often be made of wood, which saves a great deal of tooling expense.

This study deals with the mechanical spinning of cones. It does not pertain to the "formability" problem but it does deal with the effect of the process variables on the power and tangential force for successful operation, where the variables are within their permissible range.

A. THE PROCESS, GENERAL DESCRIPTION

The blank material is a disc of diameter D and uniform thickness S_o. The disc is mounted on a circular conical mandrel, which is clamped to the head of the spinning machine, and rotated. A forming roller is driven on tracks on the bed of the machine parallel to the side of the mandrel. The outer diameter D_1 of the cone (Fig. 1) remains the same

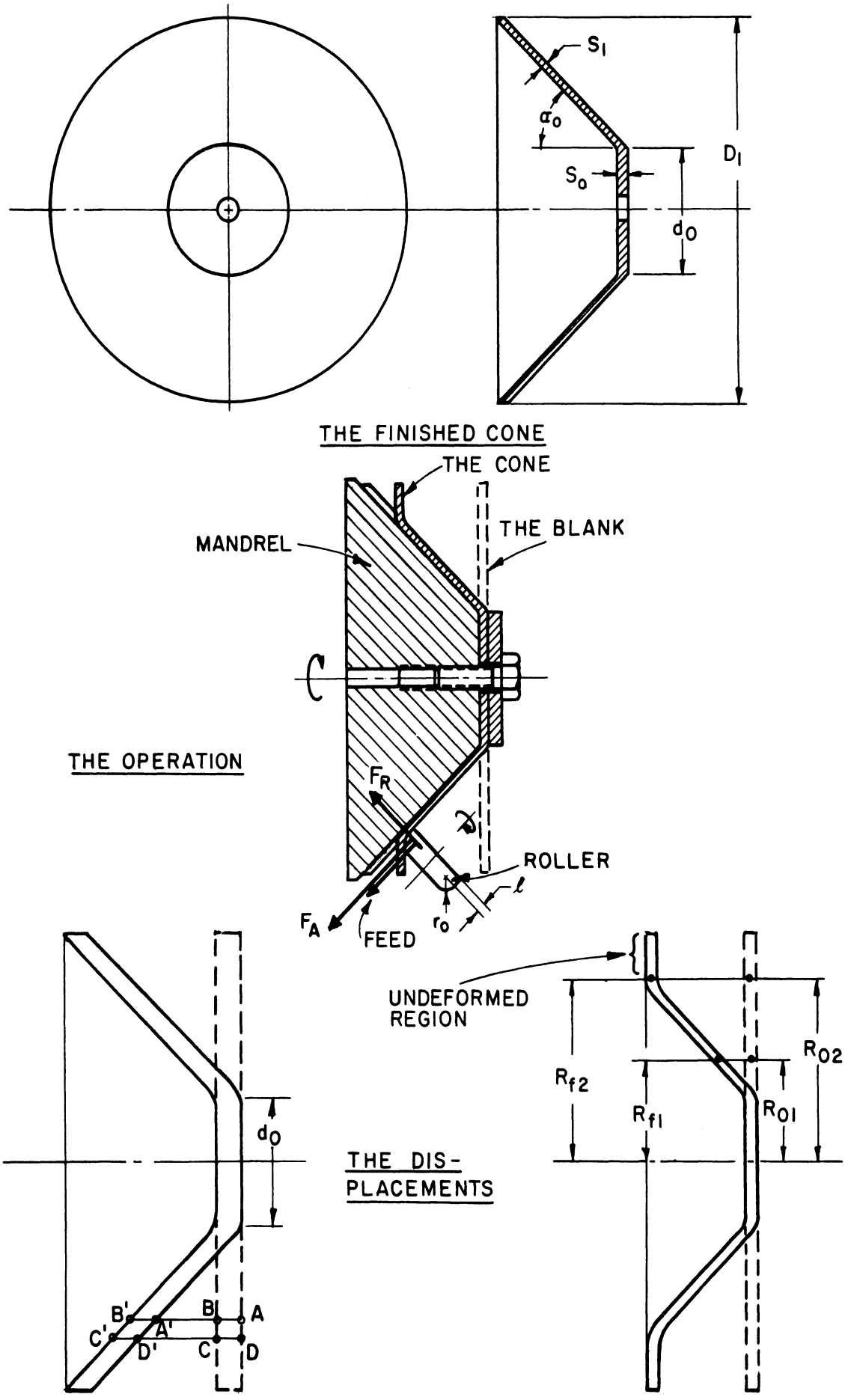

Fig. 1 - The cone, mandrel and operation

as the original diameter of the disc. The thickness of the cone is now:

$$S_1 = S_o \text{ Sin } \alpha_o$$

where: S_1 is the thickness of the final cone,

S_o is the thickness of the blank, and

α_o is half the included angle of the cone.

Spinning operation in which the cone thickness is kept uniform and according to this equation will be defined as spinning according to the "sine law." This type of spinning is called by different names like shear forming, hydro-spinning, flow turning, etc. The displacements and strains will be analyzed in more detail later.

The roller is made of hardened tool steel and mounted on a shaft with ball or roller bearings. There are many shapes of rollers; some are illustrated in Fig. 2. A common feature of all rollers is the "round-off" portion of radius r_o. When thin discs are spun with high feeds, a land is added to the roller to smooth off the feed marks. It is sometimes found convenient to add a front as in shape III of Fig. 2, to push the flange forward.

The relative position of the roller's axis to the side of the mandrel may differ much in different setups. Some examples are shown in Fig. 3.

From this variety of possibilities, a common roller (shape 1) which is oriented with its axis parallel to the side of the mandrel was chosen to be analyzed. The changes in the roller's shape and its positioning might sometimes make the difference between a successful operation or failure. However, the strains and stresses during a successful operation do not differ much from case to case.

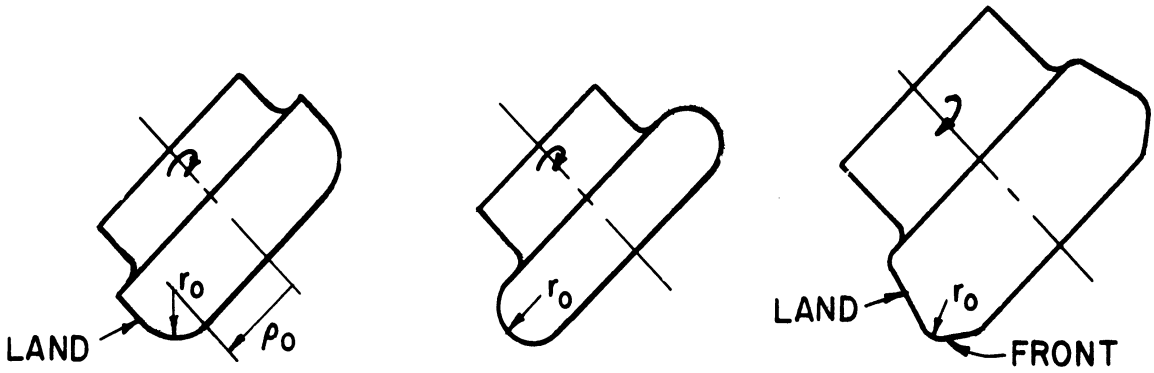

Fig. 2 - The different shapes of the roller

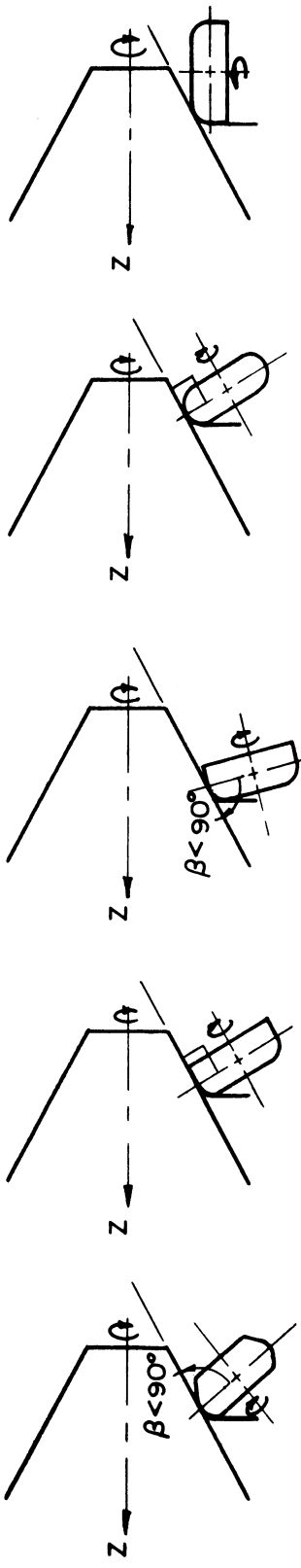

Fig. 3 - The positioning of the roller during forming

II. LITERATURE REVIEW

Until approximately ten years ago, the operation of spinning was done manually. The tool was guided by hand back and forth over the work many times until the material was flatly laid on the mandrel. No instructions were given to the operator concerning the manipulation of the tool. Experience and skill were exercised and the operation was considered an art. The literature of that time is of little value for this study.

In the last ten years, the trend has been toward mass production with power spinning. The advantages of replacing manpower by mechanical power are the same for spinning as for any other industrial process. However, mechanical power requires control-system, and the controls require a prediction of the forces and motions to which the machine has to be set. In spinning operations, as they are performed today, this means the following things: (1) the tool can no longer be manipulated back and forth, but must perform the deformation in one pass; (2) the rotational speed, the feed, and the head in pressure have to be fixed and preset before spinning is started. This presetting is now done by experience and trial-and-error methods.

It became necessary to study the process variables and their effect on the product to eliminate costly errors in the trial-and-error method. The increase in civilian and military items produced by power spinning also explains why more and more attention has lately been directed to the study of this process. Most authors of recent literature

state that a study of deformations, stresses, and forces prevailing during the operation is necessary. Nevertheless, not much has been published on this aspect.

The existing literature can be classified under two categories. One kind of literature describes the process as a shop operation in terms of the product, the machine, and the tooling. No analysis of the deformations and forces is attempted in this kind of literature, and therefore it will not be discussed here. (See Refs. 2, 3, 6, 14, 15 and 16.) The more fundamental publications have an experimental study of the forces versus the process variables, and include various attempts to explain the experimental results. The more pertinent publications in this field with a close relation to this study will be discussed one by one. But first the common factor for all of them should be stated. All studies that try to analyze the stresses and strains deal with Mises Material (For definition see p. 11). All studies express the stress-strain relations by the deformation theory. Most of the analyses were done for the spinning of cones. For cones, all authors accept the "Sine law," but only Reichel[11] realizes the full significance of this law. (For definition of the sine law see p. 4, deformation theory p. 11)

And now it is in order to scan the literature.

Siebel's[13] brief article describes the operation of spinning in general. It gives experimental graphs of the maximum radial and maximum axial forces as functions of wall thickness, roller curvature, and diameter ratio or outer bend radius. The tangential force is computed through the power consumption. This power consumption is computed under

the assumption that the material deforms smoothly from the original shape to the final shape, with no intermediate distortion. In other words, the path of the deformations is neglected; only the end points are considered. Let us refer to this approach as the one of the ideal work. No experimental data are given for the tangential force.

Reichel[11] starts by comparing "deep drawing" to "power spinning." He then describes the deformation pattern in power spinning and stresses the importance of the "Sine Law." He points out that, with the Sine Law, the deformations and stresses take place only under the instantaneous area of contact, and the rest of the material is strain-free. Reichel attempts an explanation of the experimental graphs of the radial and feed forces as functions of some of the variables.

The explanation is based on a calculation of an approximate area of contact. The author admits that this is not the only factor, and points out that some trends cannot be explained this way. He also says that no effect of the lubricant on the measured forces was found. No attempt to compute the power and tangential force was made in the publication.

The work of Feola[5] is mostly an experimental study to determine the radial and feed forces. The effect of the process variables on the buckling and bending of the flange is also discussed by Feola; his conclusions are incorrect because the Sine Law was not followed. A study of the pattern of deformation is included. The forces and power are not computed, and the trends of the experimental forces are not explained.

Colding[4] attempts to analyze the stresses and strains during the process of spinning of cones. However, he analyzes them for a different velocity field from the one he assumes in the beginning. From the stress and strain fields he computes the ideal work and tangential force. He then finds experimentally, with the use of dynamometers, the actual tangential force. He defines an efficiency factor based on ideal and actual tangential forces and plots this efficiency versus an arbitrarily chosen variable combination.

III. THE PROCEDURE

This study can be divided into two parts: the analytical solutions and the experimental verification.

A. The Analytical Solution

The geometry of the operation have been described mathematically. The equations of the cone and the roller have also been formulated. The boundaries of the area of contact between the roller and the cone have then been found.

A shear type of deformation has been postulated, based on experimental evidence.

Two solutions have been derived for the plastic work of deformation: one was based on the incremental theory (Mises stress-strain-rate law), the other, on the deformation theory (stress-strain law). Both solutions were computed for Mises Material (see Fig. 4), which implies:

(1) homogeneous and Isotropic material,

(2) no elastic deformation, and consequently no volumetric change;

(3) no strain-hardening.

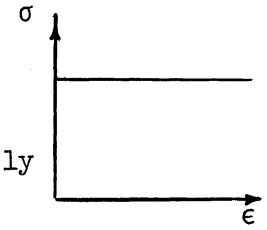

Fig. 4. Stress-Strain curve for Mises Material

However, the deformation theory has an additional solution for the case of linear strain-hardening effect.

The power consumed by friction has been neglected in this study. (see chapter VIII)

a. The Incremental Theory Solution. - The velocity and strain-rate fields were computed using the geometric formulation above. An expression for the plastic work of deformation was then developed. The numerical values are computed using a digital computer.

b. The Deformation Theory Solution. - The solution was simply derived by assuming that the deformation was reached by monotonically increased shear from zero to the final state in a finished cone.

B. The Experimental Verification

Two different types of experiments were conducted.

a. First Set of Experiments. - This set was designed to help choose the right type of deformation that take place during the process. Holes were drilled in the original discs and then plugged. Their direction was traced after the spinning. This series provides support for the choice of shear deformation in the analysis.

b. Second Set of Experiments. - In this set of experiments the forces and power were measured. This set was run separately in two locations. At the Cincinnati Milling Machine Co., a dynamometer was used. Three components of the spinning force were recorded. The axle of the roller is mounted on a three-dimensional dynamometer which is connected to a three-channel recorder. The actual forces for a diversified set of parameters were found. At Spincraft, Inc., the power requirement for the a-c motor driving the mandrel was recorded. The power requirement for a diversified set of parameters was found.

IV. THE ANALYTICAL APPROACH

A. THE PROCESS

For mathematical representation, a model spin was formulated. The geometrical relations between the cone and the roller are shown in Fig. 5. In Fig. 6 the simplified displacements field is described. This displacement field is close to the actual displacements field.

The area of contact between the cone and the roller is that area where the outer surface of the cone and the roller are interfering with each other. This area takes the shape of the roller. The strain field, stress field, work, etc., were computed for the cone under the area of contact only. Although deformations exist outside of this region, they are ignored. This omission is discussed in more detail on page 48 and in Appendix 1.

As Fig. 6 indicates, the radius of any material point remains unchanged during the whole process. Radial planes in the original disc remain radial planes in the deformed cone, so for visual realization one might conceive of the original disc as being constructed from concentric thin cylinders which are slipped axially to form the final cone (see Fig. 7).

The above description does omit one crucial fact. The rings do not slip a full ring at a time. Only the portion of the ring directly affected by the roller is slipped, and as the roller advances it slips a bigger and bigger portion of the ring, until a full revolution is achieved, and the ring as a whole is displaced.

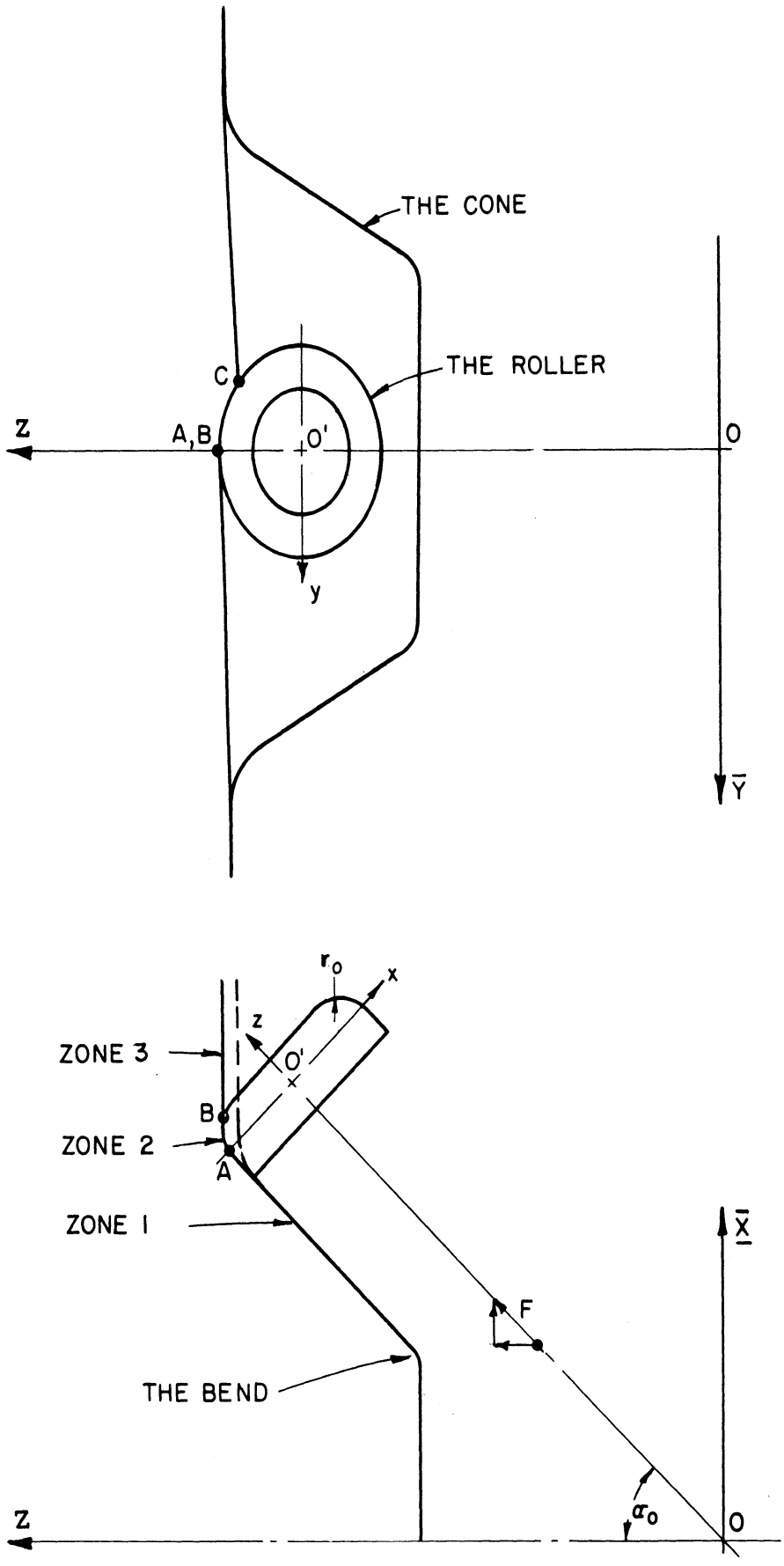

Fig. 5 - The process

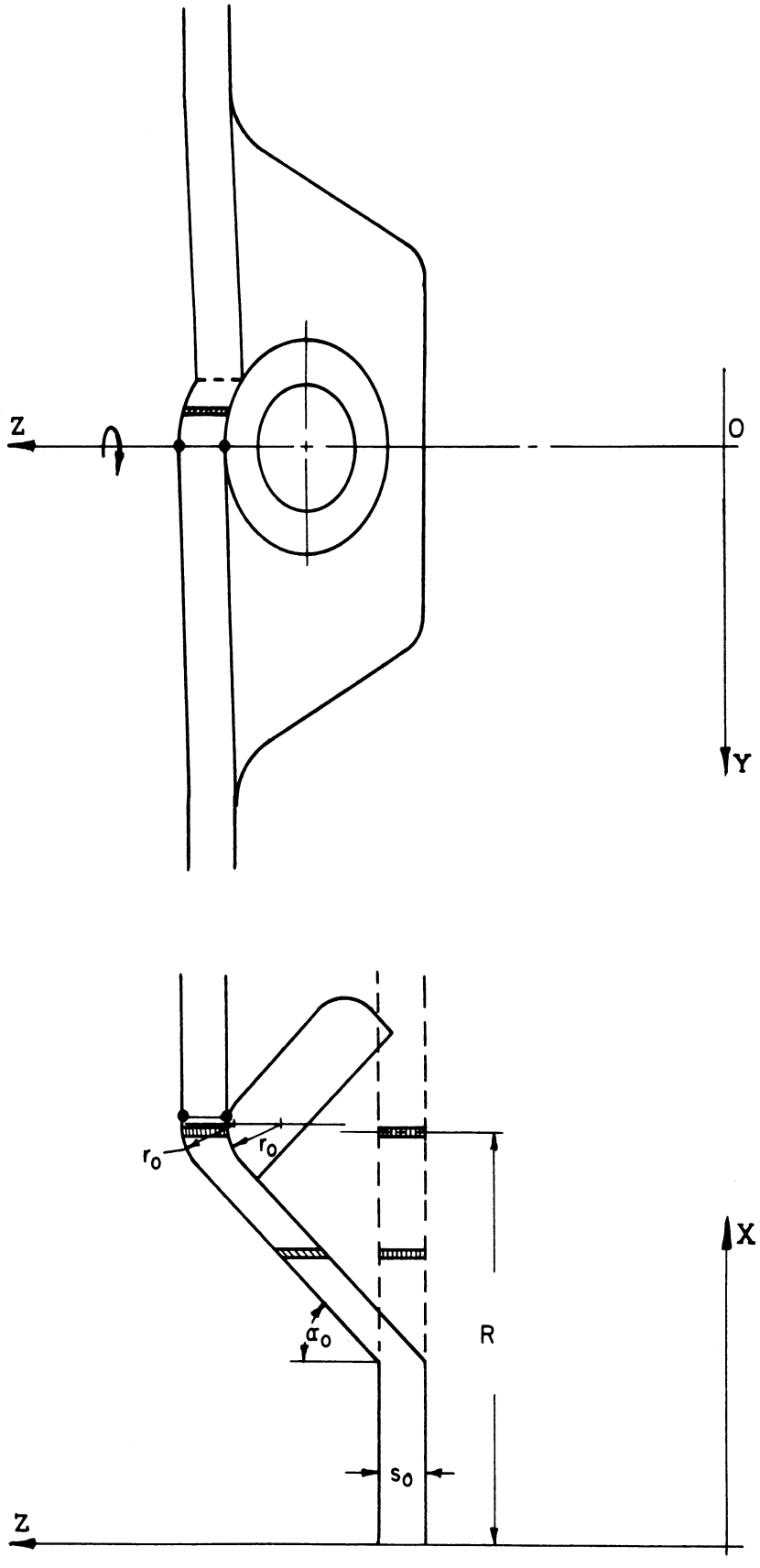

Fig. 6 - The deformation in the process

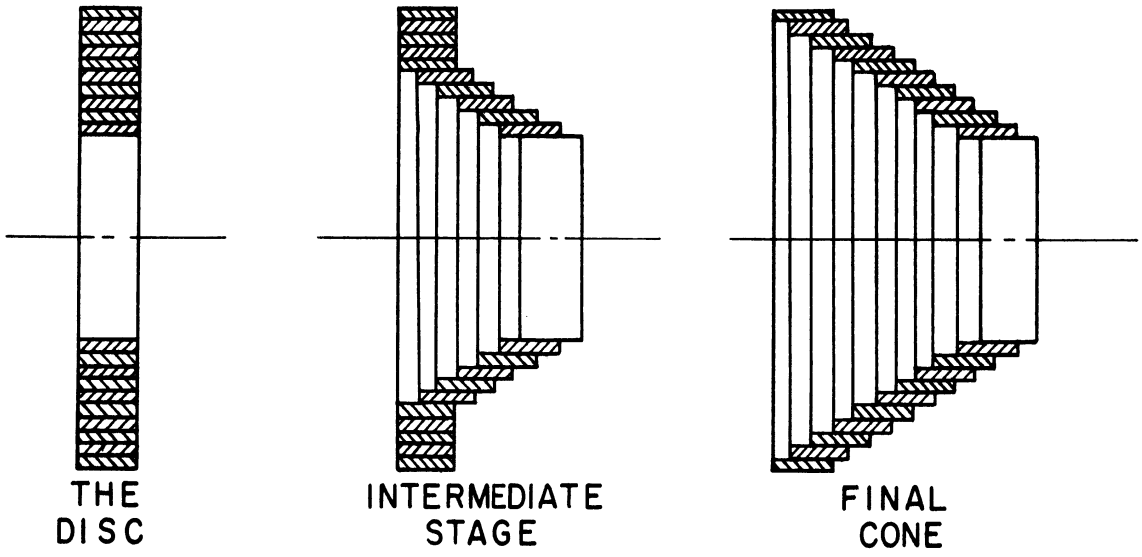

Fig. 7 - Disc analogy

Although at the completion of the deformation the ring is reshaped as a cylinder, during the operation the rings are distorted, and regain their shape only at the end. This distortion is the shear $\epsilon_{\theta Z}$ and is shown in Y-Z plane of Fig. 6.

Figure 8 illustrates the way a disc is displaced if it is opened to form a strip.

This model cone spinning differs in certain points from the actually spun cone. It will be more convenient to discuss these differences while describing the experimental results of the first set of experiments. The justification for choosing this model will be given with the experimental data. Meanwhile, the analysis proceeds for the chosen model.

B. THE PROCESS VARIABLES

To summarize the process in terms of its independent parameters, we classify the parameters in three groups:

(1) the tool parameters,

(2) the cone parameters, and

(3) the process parameters.

The relative position of the tool toward the cone was fixed so that z axis of the tool was parallel to the side of the cone, and the tool feed is in z direction. Thus the positioning is not a variable, and is included in the standard unchanged conditions of the process.

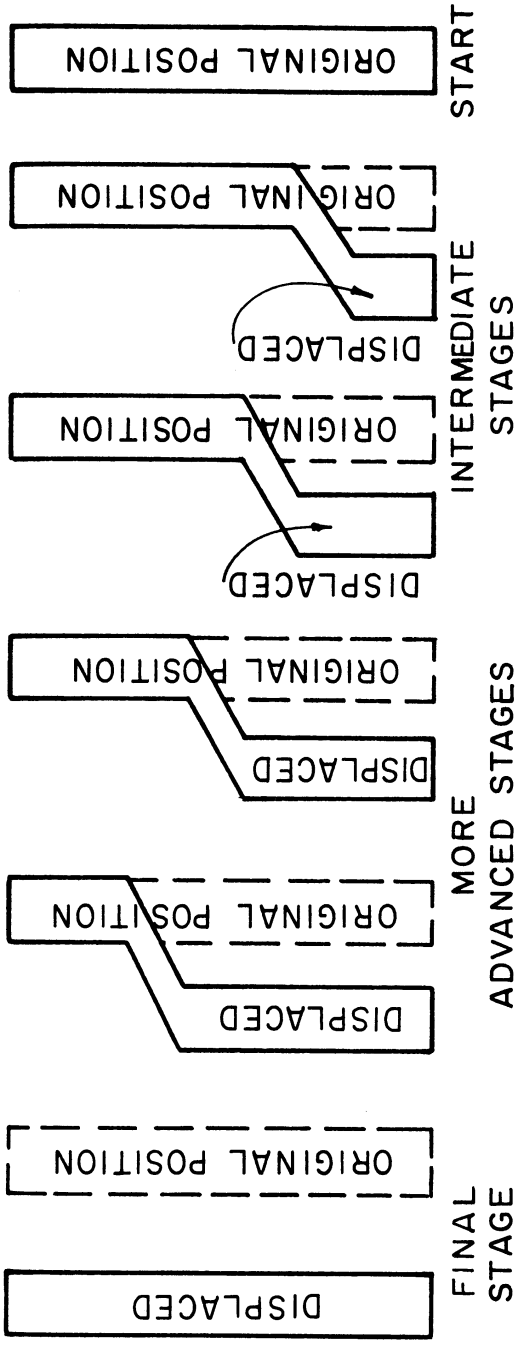

Fig. 8 - Displacing the disc

(a) The tool parameters, using only a tool of shape I in Fig. 2, are:

r_o - the roller's "round-off" radius, and

ρ_o - the roller's radius

(b) The cone parameters are: (see Fig. 1)

α_o - Half the included angle,

R_o - instantaneous radius at which the roller touches the cone,

R_{oMin} - cone's radius (R) at the bend,

R_{oMax} - the blank's outer radius,

S_o - the blank's thickness, and

σ_o - the cone's material yield limit at uniaxial tensile test.

(c) The process parameters are:

N - the speed in rpm, and

F - the feed in ipr.

Of these eight parameters, the cone angle ($2\alpha_o$), the cone bend radius (R_{oMin}) and outer radius (R_{oMax}), as well as the material (σ_o) and the thickness (S_o), are determined by the designer of the cone. The operation can be performed with a wide choice of the other parameters, r_o, ρ_o, N, and F. This study will enable the right choice of these last four parameters as far as the power is concerned. For a good description of the process, see part 1 of Ref. 11.

C. THE VELOCITY FIELD (U)

Let the cone be considered in the R, θ, Z polar coordinate system. Each point of the rotating disc has rotational motion with circumferential velocity:

$$U_\theta = 2\pi RN$$

around the Z axis. No change in the radius R takes place during this process, and therefore the velocity in the radial direction is:

$$U_R = 0.$$

The area of contact between the roller and the cone takes the shape of the roller. Layers at original position $0 \leqslant Z \leqslant S_o$ are identical with each other. The volume under the area of the instaneous contact with the roller has an additional component of the velocity (U_Z) in the Z direction.

Let the velocity U_Z be computed in terms of the other two components of the velocity U_θ and U_R and the geometry of the roller. Let the roller be described as the rigid body $G(R, \theta, Z, T) = 0$. In this analysis, the disc is the flowing medium, and the roller is the rigid body (see Fig. 9).

Stating that the component of the velocity of the flow, Normal to the Rigid Body, (see Ref. 17, p. 18) is the same for the medium as

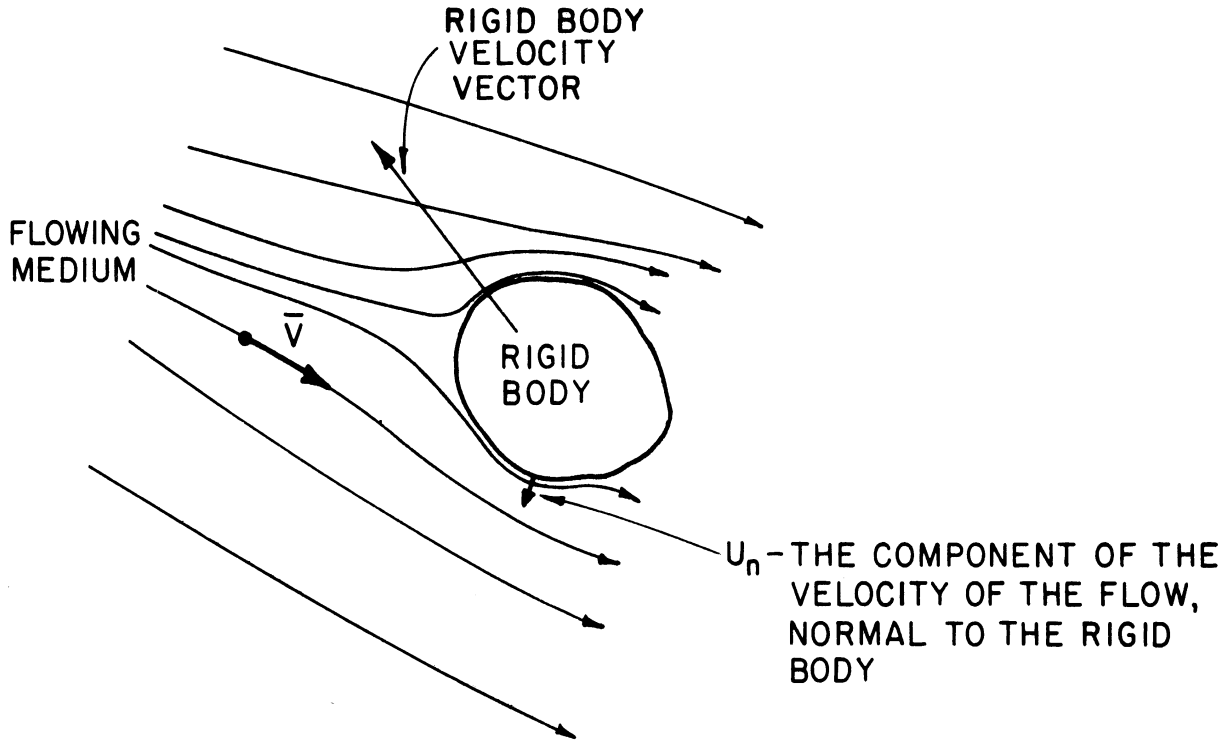

Fig. 9 - Viscous flow around an obstacle

for the rigid body leads to:

$$G_R \cdot \dot{R} + G_\Theta \cdot \dot{\Theta} + G_Z \dot{Z} + G_T = 0$$

where $$G_R = \frac{\partial G}{\partial R}, \; G_\Theta = \frac{\partial G}{\partial \Theta}, \; G_Z = \frac{\partial G}{\partial Z}, \; G_T = \frac{\partial G}{\partial T}$$

$$U_R = \dot{R} = \frac{dR}{dT}, \; U_\Theta = \dot{\Theta} = \frac{d\Theta}{dT}, \; U_Z = \dot{Z} = \frac{dZ}{dT}$$

or $$\bar{U} \cdot \nabla G = U_n = - G_T$$

where: $\bar{U}$ - the velocity vector of the medium

∇G - the gradient of the surface of the rigid body.

$$\frac{dz}{dT} = \frac{-G_R \frac{dR}{dT} - G_\Theta \frac{d\Theta}{dT} - G_T}{G_Z} = - \frac{G_R}{G_Z} \cdot \frac{dR}{dT} - \frac{G_\Theta}{G_Z} \cdot \frac{d\Theta}{dT} - \frac{G_T}{G_Z}$$

Knowing the values $\frac{dR}{dT} = U_R = 0$ and $\frac{d\Theta}{dT} = \frac{U_\Theta}{R} = 2\pi N$,

and also $\frac{G_\Theta}{G_Z} = - \frac{\partial Z}{\partial \Theta}$; $\frac{G_T}{G_Z} = - \frac{\partial Z}{\partial T}$; (Ref. 7, p. 95)

one gets: $$\frac{dZ}{dT} = U_Z = 2\pi N \frac{\partial Z}{\partial \Theta} + \frac{\partial Z}{\partial T}$$

Evaluating the number of revolutions from time $T = t_o$, one gets:

$$n = N \cdot (T - t_o)$$

and deriving with respect to T,

$$\frac{dn}{dT} = N$$

and thus one continues and gets

$$\frac{dZ}{dT} = U_Z = 2\pi N \frac{\partial Z}{\partial \Theta} + \frac{\partial Z}{\partial n} \cdot \frac{dn}{dT} = 2\pi N \frac{\partial Z}{\partial \Theta} + N\frac{dZ}{\partial n} = N \cdot \left[2\pi \frac{\partial Z}{\partial \Theta} + \frac{\partial Z}{\partial n} \right] .$$

Another approach, using Euler's method (the observer is stationary) follows. If the rigid body equation is

$$F(R, \Theta, Z, n) = 0,$$

it gives Z as a function of R, Θ and n.

$$Z = H(R, \Theta, n)$$

$$n = f(T) = N(T-t_o)$$

$$dZ = \frac{\partial Z}{\partial R} dR + \frac{\partial Z}{\partial \Theta} d\Theta + \frac{\partial Z}{\partial n} dn$$

$$U_Z = \frac{dZ}{dT} = \frac{\partial Z}{\partial R} \frac{dR}{dT} + \frac{\partial Z}{\partial \Theta} \frac{d\Theta}{dT} + \frac{\partial Z}{\partial n} \frac{dn}{dT}$$

Inserting the values $\frac{dR}{dT} = U_R = 0$, $\frac{d\Theta}{dT} = \frac{U_\Theta}{R} = 2\pi N$, and $\frac{dn}{dT} = N$, one gets the same expression for U_Z as before.

$$U_Z = N \left[2\pi \frac{\partial Z}{\partial \Theta} + \frac{\partial Z}{\partial n} \right]$$

Summing up the velocity field under direct effect of the roller, one gets:

$$\left.\begin{aligned} U_R &= 0 \\ U_\theta &= 2\pi RN \\ U_Z &= N\left[2\pi \frac{\partial Z}{\partial \theta} + \frac{\partial Z}{\partial n}\right] \end{aligned}\right\} \qquad (1)$$

where the derivatives $\frac{\partial Z}{\partial \theta}$ and $\frac{\partial Z}{\partial n}$ are yet to be defined from the geometry of the roller.

D. THE STRAIN-RATES FIELD

The rates of deformation[12] in cylindrical polar coordinates assume the form:

$$\dot{\epsilon}_{RR} = \frac{\partial U_R}{\partial R}, \quad \dot{\epsilon}_{\theta\theta} = \frac{U_R}{R} + \frac{1}{R} \cdot \frac{\partial U_\theta}{\partial \theta}; \quad \dot{\epsilon}_{ZZ} = \frac{\partial U_Z}{\partial Z}$$

$$\dot{\epsilon}_{R\theta} = \tfrac{1}{2} \cdot \left(\frac{1}{R} \cdot \frac{\partial U_R}{\partial \theta} + \frac{\partial U_\theta}{\partial R} - \frac{U_\theta}{R}\right)$$

$$\dot{\epsilon}_{RZ} = \tfrac{1}{2} \cdot \left(\frac{\partial U_R}{\partial Z} + \frac{\partial U_Z}{\partial R}\right)$$

$$\dot{\epsilon}_{\theta Z} = \tfrac{1}{2} \cdot \left(\frac{\partial U_\theta}{\partial Z} + \frac{\partial U_Z}{R\partial \theta}\right)$$

where $\dot{\epsilon}_{RR}$; $\dot{\epsilon}_{\theta\theta}$; $\dot{\epsilon}_{ZZ}$; $\dot{\epsilon}_{R\theta}$; $\dot{\epsilon}_{RZ}$; $\dot{\epsilon}_{\theta Z}$ are the components of the strain-rate tensor in cylindrical polar coordinates. This description is of the general case where the "Euler Method" is used, which means that the observer is stationary. In the specific case of the velocity field of

Eq. (1), where

$$U_R = 0$$

and

$$U_\theta = 2\pi RN,$$

one can develop the strain-rates field further. Because layers at original position $0 \leqslant Z \leqslant S_o$ are identical with each other, one can infer that no variable is dependent on Z direction. And therefore

$$\dot{\epsilon}_{ZZ} = \frac{\partial U_Z}{\partial Z} = 0$$

and also

$$\frac{\partial U_R}{\partial Z} = \frac{\partial U_\theta}{\partial Z} = 0 .$$

Because $U_R = 0$,

$$\dot{\epsilon}_{RR} = \frac{\partial U_R}{\partial R} = 0$$

$$\dot{\epsilon}_{\theta\theta} = \frac{U_R}{R} + \frac{1}{R}\frac{\partial U_\theta}{\partial \theta} = \frac{0}{R} + \frac{1}{R}\cdot\frac{\partial}{\partial \theta}(2\pi RN) = 0$$

$$\dot{\epsilon}_{R\theta} = \tfrac{1}{2}\left(\frac{1}{R}\cdot\frac{\partial U_R}{\partial \theta} + \frac{\partial U_\theta}{\partial R} - \frac{U_\theta}{R}\right) = \tfrac{1}{2}\left(\frac{\partial}{\partial R}(2\pi RN) - \frac{2\pi RN}{R}\right)$$

$$= \tfrac{1}{2}(2\pi N - 2\pi N) = 0$$

$$\dot{\epsilon}_{RZ} = \tfrac{1}{2}\left(\frac{\partial U_R}{\partial Z} + \frac{\partial U_Z}{\partial R}\right) = \tfrac{1}{2}\cdot\frac{\partial U_Z}{\partial R}$$

$$\dot{\epsilon}_{\theta Z} = \tfrac{1}{2}\left(\frac{\partial U_\theta}{\partial Z} + \frac{\partial U_Z}{R\partial \theta}\right) = \frac{1}{2R}\cdot\frac{\partial U_Z}{\partial \theta}$$

And thus the strain-rates field is given in the form

$$\left.\begin{aligned} \dot{\epsilon}_{RZ} &= \tfrac{1}{2} \cdot \frac{\partial U_Z}{\partial R} \\ \dot{\epsilon}_{\theta Z} &= \frac{1}{2R} \cdot \frac{\partial U_Z}{\partial \theta} \\ \text{All other } \dot{\epsilon}_{ij} &= 0 \end{aligned}\right\} \qquad (2)$$

E. THE STATE OF STRESS

The Levy-Mises[10] stress-plastic-strain-rate law, with the use of stress deviators and strain-rate deviators, is written:

$$\dot{e}_{ij} = \lambda' S_{ij} \qquad (3)$$

where S_{ij} is the stress deviator tensor,

$\dot{e}_{ij}$ is the plastic-strain-rate deviator tensor, and

λ' is the proportionality factor; and is a function of the strain rates.

From the assumption that there is no plastic volumetric change, it follows that the plastic-strain-rate deviator is equal to the plastic strain rate itself.

$$\dot{e} = \frac{1}{3} \dot{e}_{ii}$$

where $\dot{e}$ is the hydrostatic strain

$\dot{e}$ is the hydrostatic strain rate, and

$\dot{e}_{ii} = \dot{e}_{11} + \dot{e}_{22} + \dot{e}_{33} = 0$ (volume constancy);

$$\therefore \dot{e} = \frac{1}{3}\dot{e}_{ii} = 0, \text{ and}$$

$$\dot{\epsilon}_{ij} = \dot{e}_{ij} + \dot{e}\delta_{ij} = \dot{e}_{ij}$$

where δ_{ij} is a unit tensor called "kronecker delta," equaling 1 when i=j and equaling 0 when i≠j

$\dot{\epsilon}_{ij}$ is the plastic-strain-rate tensor.

Because "Mises Material" has no elastic strains, it follows that the plastic strains are the only existing ones. The stress-strain-rate relations become:

$$\dot{\epsilon}_{ij} = \lambda S_{ij} \tag{4}$$

Let a term I be defined such that

$$I = \frac{1}{2}\cdot\dot{\epsilon}_{ij}\dot{\epsilon}_{ij} \tag{5}$$

Substituting (4) in (5), it follows that

$$I = \frac{1}{2}\cdot\dot{\epsilon}_{ij}\,\dot{\epsilon}_{ij} = \lambda^2\cdot\frac{1}{2}S_{ij}\,S_{ij}$$

Substituting "Mises Yield Condition"

$$J_2 = \frac{1}{2}S_{ij}S_{ij} = k^2 \text{ in the preceding equation,}$$

where $J_2 = \frac{1}{2}S_{ij}S_{ij}$ is the second invariant of stress, and

$J_2 = k^2$ postulates that yield occurs when the second invariant of stress reaches a certain limit.

one gets: $I = \mu^2 k^2$

$$\mu = \pm \frac{\sqrt{I}}{k}$$

and Mises "stress-strain-rate" law becomes

$$\dot{\epsilon}_{ij} = \pm \frac{\sqrt{I}}{k} S_{ij} = \pm \frac{\sqrt{\frac{1}{2} \dot{\epsilon}_{kl} \cdot \dot{\epsilon}_{kl}}}{k} \cdot S_{ij} \tag{6}$$

$$\text{or: } S_{ij} = \pm \frac{k \dot{\epsilon}_{ij}}{\sqrt{\frac{1}{2} \cdot \dot{\epsilon}_{kl} \cdot \dot{\epsilon}_{kl}}}$$

The stress deviator field is therefore:

$$\left.\begin{aligned} \sigma_{RZ} = S_{RZ} &= \pm \frac{k \dot{\epsilon}_{RZ}}{\sqrt{\dot{\epsilon}_{RZ}^2 + \dot{\epsilon}_{\theta Z}^2}} \\ \sigma_{\theta Z} = S_{\theta Z} &= \pm \frac{k \dot{\epsilon}_{\theta Z}}{\sqrt{\dot{\epsilon}_{RZ}^2 + \dot{\epsilon}_{\theta Z}^2}} \\ \text{All other } S_{ij} &= 0 \end{aligned}\right\} \tag{7}$$

The sign is to be chosen from physical considerations. Whether it is plus or minus is not relevant in this study.

F. THE POWER

Let the rate of work per unit volume be

$$\dot{w} = \sigma_{ij} \dot{\epsilon}_{ij} \tag{8}$$

where σ_{ij} are the components of the stress tensor.

The stress tensor can be separated into stress deviator and hydrostatic stress.

$$\dot{w} = \sigma_{ij}\dot{\epsilon}_{ij} = (S_{ij} + S\delta_{ij})\dot{\epsilon}_{ij} = S_{ij}\dot{\epsilon}_{ij} + S.\dot{\epsilon}_{ij}\delta_{ij} = S_{ij}\dot{\epsilon}_{ij} + S\dot{\epsilon}_{ii}$$

where: S - the hydrostatic stress $S = \frac{1}{3}\sigma_{ii}$

And because of the incompressibility,

$$\dot{\epsilon}_{ii} = 0;$$

$$\therefore \quad \dot{w} = S_{ij}\dot{\epsilon}_{ij} \tag{9}$$

Substituting for $\dot{\epsilon}_{ij}$ its value from Eq. (6), one gets

$$\dot{w} = \pm \sqrt{S_{ij}S_{ij}} \, \frac{\sqrt{\frac{1}{2}\dot{\epsilon}_{kl}\dot{\epsilon}_{kl}}}{k}$$

Substituting now the yield condition, $J_2 = \frac{1}{2}S_{ij}S_{ij} = k^2$, one gets:

$$\dot{w} = \pm \frac{2k^2}{k}\sqrt{\frac{1}{2}\dot{\epsilon}_{kl}\dot{\epsilon}_{kl}} = \pm 2k\sqrt{\frac{1}{2}\dot{\epsilon}_{ij}\dot{\epsilon}_{ij}}$$

It is now desired to replace k by the yield at uniaxial tensile test.

For uniaxial stress (see Fig. 10):

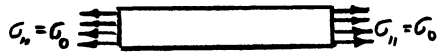

Fig. 10 - Uniaxial tension test.

$$S = \frac{1}{3}\sigma_0 ; \quad S_1 = \frac{2}{3}\sigma_0 ; \quad S_2 = S_3 = -\frac{1}{3}\sigma_0$$

$$\text{All other } S_{ij} = 0$$

Mises Yield condition gives

$$J_2 = \frac{1}{2}S_{ij}S_{ij} = \frac{1}{2}\left(\frac{4}{9} + \frac{1}{9} + \frac{1}{9}\right)\sigma_0^2 = \frac{1}{3}\sigma_0^2 = k^2$$

$$k = \frac{\sigma_0}{\sqrt{3}}$$

It follows that the rate of work per unit volume is:

$$\dot{w} = \pm \frac{2}{\sqrt{3}}\sigma_0 \sqrt{\frac{1}{2}\dot{\epsilon}_{ij}\dot{\epsilon}_{ij}} \qquad (10)$$

Defining work done on a system to be positive, it follows that:

$$\dot{w} = \frac{2}{\sqrt{3}}\sigma_0 \sqrt{\frac{1}{2}\dot{\epsilon}_{ij}\dot{\epsilon}_{ij}}$$

With the particular strain-rate field in this case,

$$\dot{w} = \frac{2}{\sqrt{3}}\sigma_0 \cdot \sqrt{\dot{\epsilon}_{RZ}^2 + \dot{\epsilon}_{\theta Z}^2} = \frac{2}{\sqrt{3}}\sigma_0 \sqrt{\left(\frac{1}{2}\cdot\frac{\partial U_Z}{\partial R}\right)^2 + \left(\frac{1}{2R}\cdot\frac{\partial U_Z}{\partial \theta}\right)^2}$$

$$\dot{w} = \frac{\sigma_0}{\sqrt{3}}\sqrt{\left(\frac{\partial U_Z}{\partial R}\right)^2 + \left(\frac{1}{R}\cdot\frac{\partial U_Z}{\partial \theta}\right)^2}$$

The rate of work for the deformed cone is

$$\dot{W} = \int_{\text{volume}} \frac{\sigma_o}{\sqrt{3}} \cdot \sqrt{\left(\frac{\partial U_Z}{\partial R}\right)^2 + \left(\frac{1}{R} \cdot \frac{\partial U_Z}{\partial \theta}\right)^2} \; dV$$

$$\dot{W} = \frac{\sigma_o}{\sqrt{3}} \int_{\text{Surface}} \left[\int_{Z=0}^{S_o} \sqrt{\left(\frac{\partial U_Z}{\partial R}\right)^2 + \left(\frac{1}{R} \cdot \frac{\partial U_Z}{\partial \theta}\right)^2} \; dZ \right] ds$$

where dV is an infinitesmal volume of $Rd\theta dRdZ$ and
ds is an infinitesmal area of $Rd\theta dR$.

Because the strains are independent on Z direction, one can first integrate with respect to Z and get:

$$\dot{W} = \frac{\sigma_o S_o}{\sqrt{3}} \cdot \int_{\text{surface}} \sqrt{\left(\frac{\partial U_Z}{\partial R}\right)^2 + \left(\frac{1}{R} \cdot \frac{\partial U_Z}{\partial \theta}\right)^2} \; ds$$

$$\dot{W} = \frac{\sigma_o S_o}{\sqrt{3}} \int_{\theta} \int_{R} R \sqrt{\left(\frac{\partial U_Z}{\partial R}\right)^2 + \left(\frac{1}{R} \cdot \frac{\partial U_Z}{\partial \theta}\right)^2} \; dR d\theta \qquad (11)$$

V. MATHEMATICAL DESCRIPTION OF THE PROCESS

A. THE SETS OF AXIS AND THEIR TRANSFORMATION

Consider three coordinate systems, (see Fig.s 5 and 6):

(1) (x,y,z) cartesian coordinate system, with the origin 0'. The axis z is the axis of cylindrical symmetry for the roller, and the origin is the center of the torical portion of the roller.

(2) (X,Y,Z) cartesian coordinate syste, with the origin 0. The axis Z is the axis of cylindrical symmetry for the cone.

(3) (R,Θ,Z) cylindrical polar coordinates with the same origin 0 and Z axis as the second cartesian system.

The directional cosines for transformation from (x,y,z) system to (X,Y,Z) system and vice versa can be represented in the following way.

Table I - Directional Cosines

	x	y	z
X	$\cos \alpha_o$	0	$\sin \alpha_o$
Y	0	1	0
Z	$-\sin \alpha_o$	0	$\cos \alpha_o$

The transformation scheme is according to the following equation.

$$\left.\begin{aligned} x_i &= a_i + a_{ij}X_j \\ X_j &= b_j + a_{ij}x_i \end{aligned}\right\} \qquad (12)$$

where: i = 1,2,3 denote the column number in Table I,
j = 1,2,3 denote the row number in Table I,
a_i = denote the coordinates of the origin 0 in the (x,y,z) coordinates system,
$a_1 = a_2 = 0$
a_3 = -Fn,
b_j = denote the coordinates of the origin 0' in the (X,Y,Z) coordinate system,
b_1 = Fn Sin α_o,
b_2 = 0,
b_3 = Fn cos α_o,
x_1 = x,
x_2 = y,
x_3 = z,
X_1 = X,
X_2 = Y, and
X_3 = Z.

The transformation is now getting this shape:

$$x_1 = x = a_1 + a_{11}X_1 + a_{12}X_2 + a_{13}X_3 = a_{11}X_1 + a_{13}X_3$$
$$= X \cos \alpha_o - Z \sin \alpha_o$$

$$x_2 = y = a_2 + a_{21}X_1 + a_{22}X_2 + a_{23}X_3 = a_{22}X_2 = Y$$

$$x_3 = z = a_3 + a_{31}X_1 + a_{32}X_2 + a_{33}X_3 = a_3 + a_{31}X_1 + a_{33}X_3$$
$$= -Fn + X \sin \alpha_o + Z \cos \alpha_o$$

And applying the second of Eqs. (12), one gets:

$$X_1 = X = x \cos \alpha_o + z \sin \alpha_o + Fn \sin \alpha_o$$

$$X_2 = Y = y$$

$$X_3 = Z = - x \sin \alpha_o + z \cos \alpha_o + Fn \cos \alpha_o$$

The transformation from R, θ, Z system to (X,Y,Z) system is to be performed by:

$$X = R \cos \theta$$

$$Y = R \sin \theta$$

$$Z = Z$$

and from (X,Y,Z) to (R,θ,Z) is performed through

$$R = \sqrt{X^2 + Y^2}$$

$$\theta = \cos^{-1} \frac{X}{\sqrt{X^2+Y^2}} = \sin^{-1} \frac{Y}{\sqrt{X^2+Y^2}} = \tan^{-1} \frac{Y}{X}$$

$$Z = Z$$

The transformation from either system to any other system of the three is now given.

$$\begin{cases} x = X \cos \alpha_o - Z \sin \alpha_o = R \cos \theta \cos \alpha_o - Z \sin \alpha_o \\ y = Y \qquad\qquad\qquad\qquad = R \sin \theta \\ z = X \sin \alpha_o + Z \cos \alpha_o - Fn = R \cdot \cos \theta \cdot \sin \alpha_o + Z \cdot \cos \alpha_o - Fn \end{cases} \tag{13}$$

$$\begin{cases} X = R\cos\theta = x\cos\alpha_o + z\sin\alpha_o + Fn\sin\alpha_o \\ Y = R\sin\theta = y \\ Z = Z = -x\sin\alpha_o + z\cos\alpha_o + Fn\cos\alpha_o \end{cases} \quad (13)$$

continued

$$\begin{cases} R = \sqrt{X^2 + Y^2} = \sqrt{(x\cos\alpha_o + z\cos\alpha_o + Fn\sin\alpha_o)^2 + y^2} \\ \theta = \cos^{-1}\dfrac{X}{\sqrt{X^2+Y^2}} = \cos^{-1}\dfrac{x\cos\alpha_o + z\sin\alpha_o + Fn\sin\alpha_o}{\sqrt{(x\cos\alpha_o + z\sin\alpha_o + Fn\sin\alpha_o)^2+y^2}} = \sin^{-1}\dfrac{Y}{\sqrt{X^2+Y^2}} \\ Z = z = -x\sin\alpha_o + z\cos\alpha_o + Fn\cos\alpha_o \end{cases}$$

B. THE ROLLER

The roller is composed of a half torus and a cylinder. (see Fig. 2 and 5) The half torus exists for $z \geq 0$. Its equations are:

$$\left.\begin{aligned} &\left[\sqrt{x^2 + y^2} - \rho_o\right]^2 + z^2 - r_o^2 = 0 \\ G = &\left[\sqrt{(R\cos\theta\cos\alpha_o - Z\sin\alpha_o)^2 + R^2\sin^2\theta} - \rho_o\right]^2 \\ &+ \left[R\cos\theta\sin\alpha_o + Z\cos\alpha_o - Fn\right]^2 - r_o^2 = 0 \end{aligned}\right\} \quad (14)$$

Let the second of Eqs. (14) be referred to as $G = 0$, or $G(R,\theta,Z) = 0$.

The cylindrical portion of the roller exists only for $z \leq 0$. Its equation is:

$$x^2 + y^2 - (r_o + \rho_o)^2 = 0$$

By transforming this equation to (R,θ,Z) axis, one gets:

$$(R\cos\theta\cos\alpha_o - Z\sin\alpha_o)^2 + R^2\sin^2\theta - (r_o + \rho_o)^2 = 0$$

$$R\cos\theta\cos\alpha_o - Z\sin\alpha_o = \pm\sqrt{(\rho_o + r_o)^2 - R^2\sin^2\theta}$$

$$Z = \frac{1}{\sin\alpha_o}\left[R\cdot\cos\theta\cdot\cos\alpha_o \pm \sqrt{(\rho_o + r_o)^2 - R^2\sin^2\theta}\right]$$

From geometrical considerations, the plus sign is to be chosen for that portion of the roller that is in touch with the cone. The equation of the cylindrical portion of the roller becomes

$$x^2 + y^2 - (r_o + \rho_o)^2 = 0$$

$$Z = \frac{1}{\sin\alpha_o}\left[R\cdot\cos\theta\cdot\cos\alpha_o + \sqrt{(\rho_o + r_o)^2 - R^2\cdot\sin^2\theta}\right] \quad (15)$$

C. THE CONE

Let the cone (see Fig. 11) be separated into three zones. Zone 1 is the already deformed portion of the cone. This zone is bounded by the bend on one end and by the cylinder of the same radius that is described by spiral A. Spiral A is the trace that point A on the roller leaves on the cone. Zone 2 is the zone being deformed. Zone 2 is the region with radius greater than the radius of spiral A and less than the radius of spiral B. Spiral B is the trace that point B on the roller leaves on the cone. Zone 3 is the yet undeformed disc from spiral B and up (see Fig. 11).

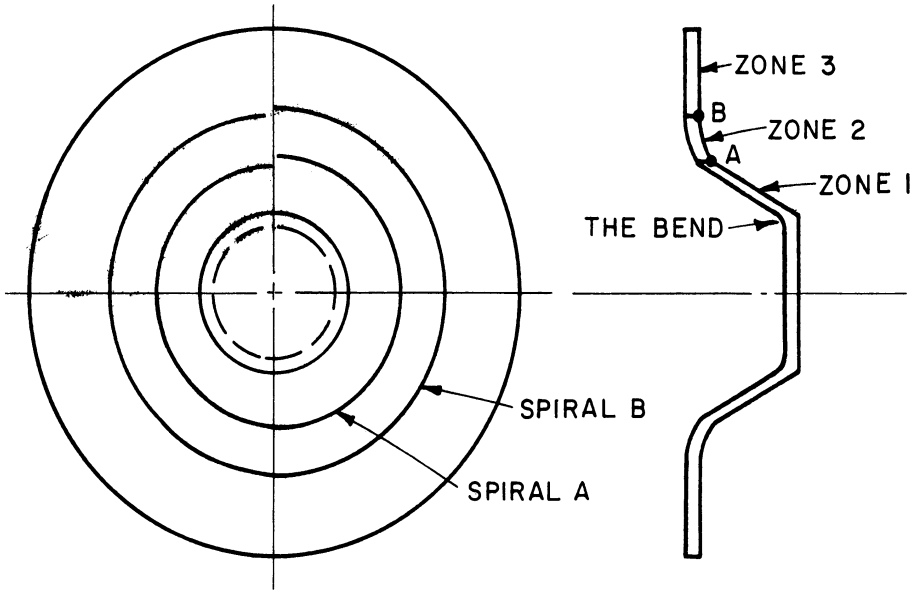

Fig. 11 - Zones of the cone

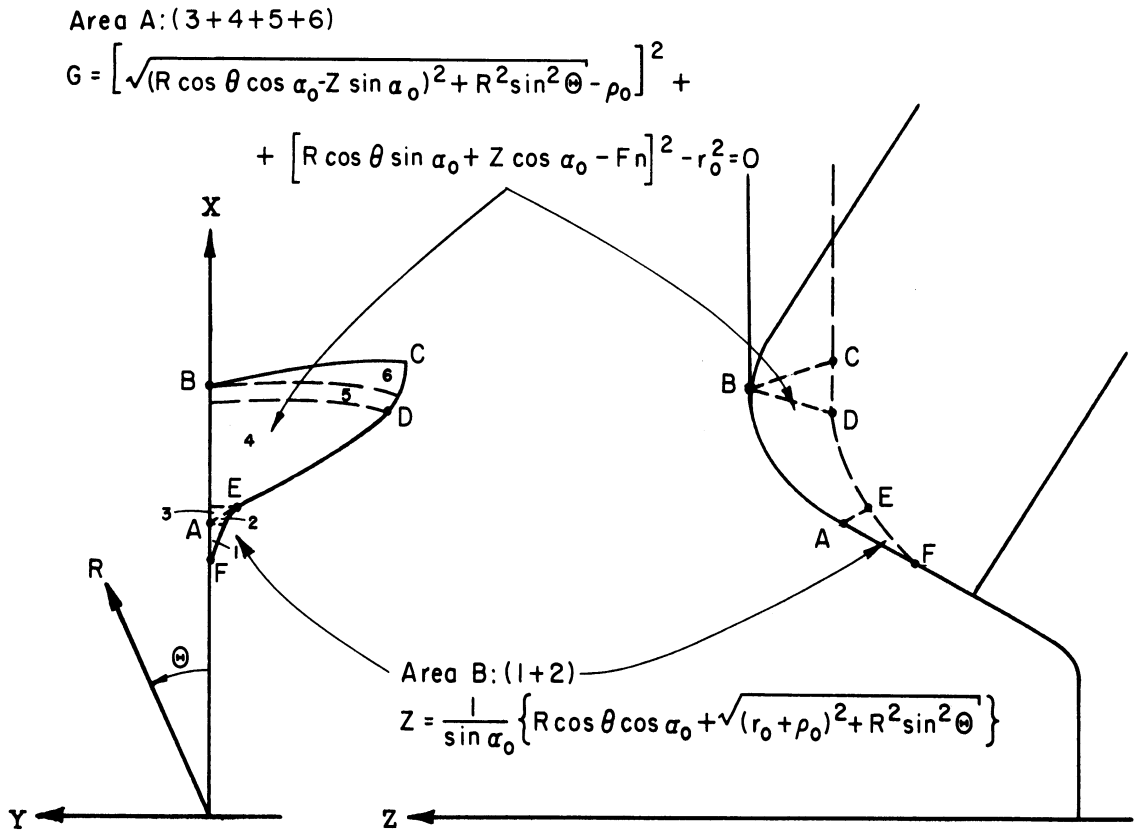

Fig. 12 - Area of contact between the roller and the cone

$$\left.\begin{aligned}
&\underline{\text{Spiral A:}}\quad R_A = F\left(n - \frac{\theta}{2\pi}\right)\sin\alpha_o - (r_o + \rho_o)\cos\alpha_o \\
&\qquad\qquad Z_A = F\left(n - \frac{\theta}{2\pi}\right)\cos\alpha_o + (r_o + \rho_o)\sin\alpha_o \\
&\underline{\text{Spiral B:}}\quad R_B = F\left(n - \frac{\theta}{2\pi}\right)\sin\alpha_o - \rho_o\cos\alpha_o \\
&\qquad\qquad Z_B = F\left(n - \frac{\theta}{2\pi}\right)\cos\alpha_o + \rho_o\sin\alpha_o + r_o
\end{aligned}\right\} \qquad (16)$$

Zone 2 of the Cone

The generating circle AB of the torus (see Fig. 12) is:

$$\text{or:}\quad \begin{cases} (x + \rho_o)^2 + z^2 = r_o^2 \\ y = 0 \\ (R\cos\alpha_o - Z\sin\alpha_o + \rho_o)^2 + (R\sin\alpha_o + Z\cos\alpha_o - Fn)^2 - r_o^2 = 0 \\ \theta = 0 \end{cases} \qquad (17)$$

And thus, zone 2 is:

$$(R\cos\alpha_o - Z\sin\alpha_o + \rho_o)^2 + \left[R\sin\alpha_o + Z\cos\alpha_o - F\left(n - \frac{\theta}{2\pi}\right)\right]^2 - r_o^2 = 0$$

Because the zone of interest is at the contact area between the cone and the roller, for which $\theta \simeq 2\pi$, one can approximate $\frac{\theta}{2\pi}$ by 1. Thus, the approximate equation of the cone at the area of contact is:

$$(R\cos\alpha_o - Z\sin\alpha_o + \rho_o)^2 + \left[R\sin\alpha_o + Z\cos\alpha_o - F(n-1)\right]^2 - r_o^2 = 0$$

$$Z^2 - 2Z\overbrace{\left[\sin\alpha_o\,(R\cos\alpha_o + \rho_o) - \cos\alpha_o\,(R\sin\alpha_o - F(n-1))\right]}^{b}$$

$$+ \underbrace{(R\cos\alpha_o + \rho_o)^2 + \left[R\sin\alpha_o - F(n-1)\right]^2 - r_o^2}_{c} = 0$$

$$Z_{1,2} = b \pm \sqrt{b^2 - c}$$

For the area of contact $Z = Z_2$ (see Fig. 13):

$$Z = b + \sqrt{b^2 - c}$$

where: $b = \rho_o \sin \alpha_o + F(n-1) \cos \alpha_o$ (18)

$$c = (R \cos \alpha_o + \rho_o)^2 + \left[R \sin \alpha_o - F(n-1)\right]^2 - r_o^2$$

Zone 3 of the cone:

For Zone 3 of th cone:

$$Z = F(n - \frac{\theta}{2\pi}) \cos \alpha_o + \rho_o \sin \alpha_o + r_o$$

$$Z \approx F(n-1) \cos \alpha_o + \rho_o \sin \alpha_o + r_o \quad (19)$$

D. THE AREA OF CONTACT

The area of contact between the roller and the cone takes the shape of the roller.

Let the area of contact be composed of two main areas. Area A will be that shaped like the torus, and Area B will be that shaped cylindrically (see Fig. 12). Let the boundary ABCDEFA be defined line by line.

Line AB is the circle described by Eqs. (17).

Line BC The contour of line BC can be found by deriving $\frac{\partial Z}{\partial R} = 0$ on the equation of the torus $G = 0$. However, because the determination of this line gets involved, it may be approximated by a circle passing through point B around the main axis of the torus (see Fig. 14).

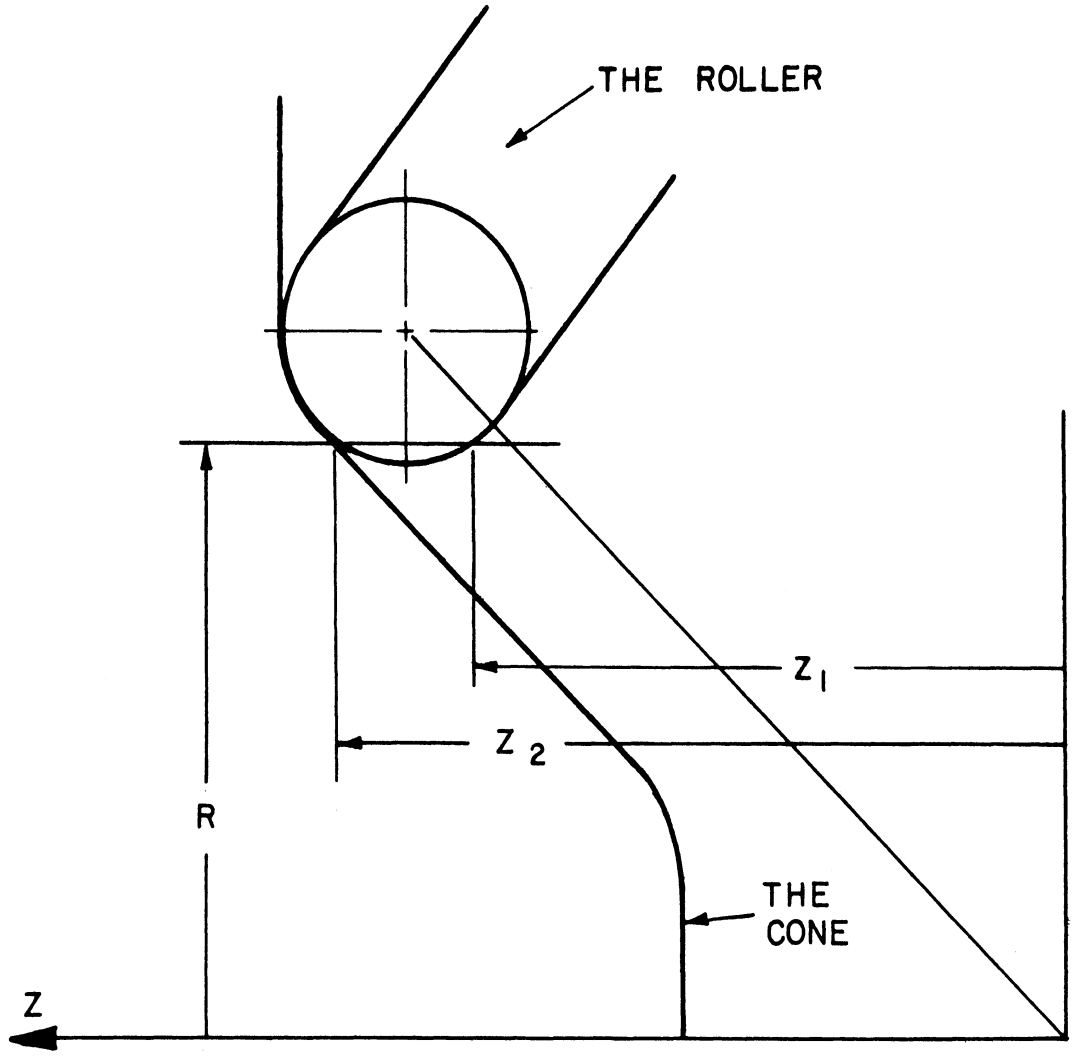

Fig. 13 - Contact region of zone 2 of the cone

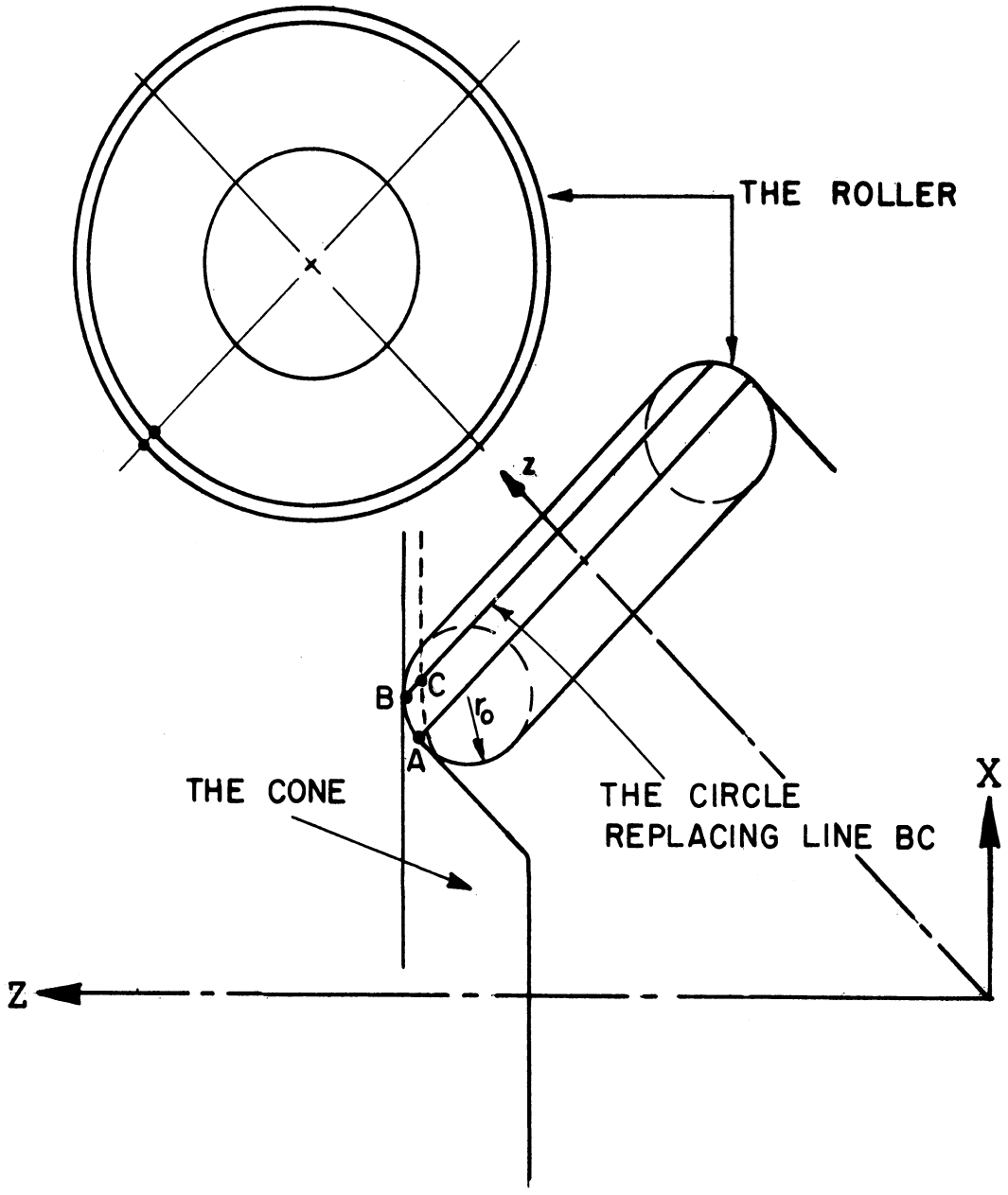

Fig. 14- Line BC

The plane of the circle can be described by:

$$\left.\begin{aligned} z &= r_o \cos \alpha_o \\ \text{And the cylinder} \quad x^2 + y^2 &= (\rho_o + r_o \sin \alpha_o)^2 \end{aligned}\right\} \qquad (20)$$

In the (R,θ,Z) axis, line BC will become:

$$R \cos \theta \sin \alpha_o + Z \cos \alpha_o - Fn - r_o \cos \alpha_o = 0$$

$$(R \cos \theta \cos \alpha_o - Z \sin \alpha_o)^2 + R^2 \sin^2 \theta - (\rho_o + r_o \sin \alpha_o)^2 = 0$$

Inserting $Z = \frac{1}{\cos \alpha_o} (Fn + r_o \cos \alpha_o - R \cos \theta \sin \alpha_o)$ from the first equation into the second equation, one gets

$$[R \cos \theta \cos \alpha_o - (Fn + r_o \cos \alpha_o - R \cos \theta \sin \alpha_o) \tan \alpha_o]^2$$
$$+ R^2 \sin^2 \theta - (\rho_o + r_o \sin \alpha_o)^2 = 0$$

This equation of line BC is written implicitly with respect to R and θ.

Line CD For Line CD the torus G = 0 cuts Zone 3 of the cone, Eq. (19). Repeating the equations once more, one gets:

$$G = \left[\sqrt{(R \cos \theta \cos \alpha_o - Z \sin \alpha_o)^2 + R^2 \sin^2 \theta} - \rho_o\right]^2$$
$$+ [R \cos \theta \sin \alpha_o + Z \cos \alpha_o - Fn]^2 - r_o^2 = 0$$

where:

$$Z = F(n-1) \cos \alpha_o + \rho_o \sin \alpha_o + r_o$$

Line DE At line DE, the torus cuts Zone 2 of the cone:

$$G = \left[\sqrt{(R\cos\theta\cos\alpha_o - Z\sin\alpha_o)^2 + R^2\sin^2\theta} - \rho_o\right]^2$$

$$+ \left[R\cos\theta\sin\alpha_o + Z\cos\alpha_o - Fn\right]^2 - r_o^2 = 0$$

where: $Z = b + \sqrt{b^2 - c}$

$$b = \rho_o\sin\alpha_o + F(n-1)\cos\alpha_o$$

$$c = (R\cos\alpha_o + \rho_o)^2 + \left[R\sin\alpha_o - F(n-1)\right]^2 - r_o^2$$

Line EA is on the plane $z = 0$

From the transformation scheme (Eq. 13)

$$z = R\cos\theta\sin\alpha_o + Z\cos\alpha_o - Fn = 0$$

$$\cos\theta = \frac{Fn - Z\cos\alpha_o}{R\sin\alpha_o}$$

Substituting the right hand of the preceding equation for cos θ in the equation of the cylinder,

$$(R\cos\theta\cos\alpha_o - Z\sin\alpha_o)^2 + R^2\sin^2\theta - (r_o + \rho_o)^2 = 0$$

one gets:

$$\left[(Fn - Z\cos\alpha_o)\cot\alpha_o - Z\sin\alpha_o\right]^2 + R^2\left[1 - \left(\frac{Fn - Z\cos\alpha_o}{R\sin\alpha_o}\right)^2\right]$$

$$= (r_o + \rho_o)^2$$

$$\left[(Fn - Z\cos\alpha_o)\cot\alpha_o - Z\sin\alpha_o\right]^2 - \left(\frac{Fn - Z\cos\alpha_o}{\sin\alpha_o}\right)^2 = (\rho_o + r_o)^2 - R^2$$

$$\left[Fn\cot\alpha_o - Z(\cos\alpha_o\cot\alpha_o + \sin\alpha_o)\right]^2 \cdot \sin^2\alpha_o - (Fn - Z\cos\alpha_o)^2 = \left[(\rho_o + r_o)^2 - R^2\right]\sin^2\alpha_o$$

$$\left[Fn\cos\alpha_o - Z(\cos^2\alpha_o + \sin^2\alpha_o)\right]^2 - (Fn - Z\cos\alpha_o)^2 = \left[(\rho_o + r_o)^2 - R^2\right]\sin^2\alpha_o$$

$$(Fn\cos\alpha_o - Z)^2 - (Fn - Z\cos\alpha_o)^2 = \left[(\rho_o + r_o)^2 - R^2\right]\sin^2\alpha_o$$

$$(Fn)^2(\cos^2\alpha_o - 1) - 2Z(\cos\alpha_o - \cos\alpha_o)Fn + Z^2(1 - \cos^2\alpha_o) = \left[(\rho_o + r_o)^2 - R^2\right]\sin^2\alpha_o$$

$$-(Fn)^2\sin^2\alpha_o + Z^2\sin^2\alpha_o = \left[(\rho_o + r_o)^2 - R^2\right]\sin^2\alpha_o$$

$$Z^2 = (\rho_o + r_o)^2 - R^2 + (Fn)^2$$

$$Z = + \sqrt{(\rho_o + r_o)^2 - R^2 + (Fn)^2}$$

$$\cos\theta = \frac{Fn - Z\cos\alpha_o}{R\sin\alpha_o} = \frac{Fn - \sqrt{(\rho_o + r_o)^2 - R^2 + (Fn)^2}\cos\alpha_o}{R\sin\alpha_o}$$

$$\cos\theta_{AE} = \frac{Fn - \sqrt{(\rho_o + r_o)^2 - R^2 + (Fn)^2}\cos\alpha_o}{R\sin\alpha_o}$$

Line FE Line FE is the intersection of Zone 2 of the cone with the cylindrical portion of the roller. The cone is:

$$Z = b + \sqrt{b^2 - c}$$

where: $$b = \rho_o \sin \alpha_o + F(n-1) \cos \alpha_o$$

$$c = (R \cos \alpha_o + \rho_o)^2 + [R \sin \alpha_o - F(n-1)]^2 - r_o^2$$

And the cylinder is:

$$Z = \frac{1}{\sin \alpha_o} \left[R \cos \theta \cos \alpha_o + \sqrt{(r_o + \rho_o)^2 - R^2 \sin^2 \theta} \right]$$

Solving the equation of the cylinder for cos θ, one proceeds:

$$(r_o + \rho_o)^2 - R^2 \sin^2 \theta = (Z \sin \alpha_o - R \cos \theta \cos \alpha_o)^2$$

$$(r_o + \rho_o)^2 - R^2 + R^2 \cos^2 \theta = R^2 \cos^2 \theta \cos^2 \alpha_o + Z^2 \sin^2 \alpha_o - 2RZ \cos \theta \sin \alpha_o \cos \alpha_o$$

$$R^2(1 - \cos^2 \alpha_o) \cos^2 \theta + 2 RZ \sin \alpha_o \cos \alpha_o \cos \theta - (Z \sin \alpha_o)^2 - R^2 + (r_o + \rho_o)^2 = 0$$

$$\cos \theta = \frac{-RZ \sin \alpha_o \cos \alpha_o}{R^2 \sin^2 \alpha_o} + \frac{\sqrt{(RZ \sin \alpha_o \cos \alpha_o)^2 - R^2 \sin^2 \alpha_o [(r_o + \rho_o)^2 - R^2 - (Z \sin \alpha_o)^2]}}{R^2 \sin^2 \alpha_o}$$

$$\cos\theta = \frac{-Z\cos\alpha_o + \sqrt{(Z\cos\alpha_o)^2 - (\rho_o + r_o)^2 + R^2 + Z^2\sin^2\alpha_o}}{R\sin\alpha_o}$$

$$\cos\theta = \frac{-Z\cos\alpha_o + \sqrt{Z^2 + R^2 - (\rho_o + r_o)^2}}{R\sin\alpha_o}$$

where: $Z = b + \sqrt{b^2 - c}$

$b = \rho_o \sin\alpha_o + F(n-1)\cos\alpha_o$

$c = (R\cos\alpha_o + \rho_o)^2 + [R\sin\alpha_o - F(n-1)]^2 - r_o^2$

Line FA $\theta = 0$

After defining the equations of the line ABCDEFA, the intersection points A, B, C, D, E, F of these lines are to be defined. The radius (R) of these points will be determined. From either of the two equations of the lines passing through any of these points and its radius (R), the angle θ can later be computed.

Point A: $R_A = Fn\sin\alpha_o - (r_o + \rho_o)\cos\alpha_o$

Point B: $R_B = Fn\sin\alpha_o - \rho_o\cos\alpha_o$ (21)

Point C: The value of the radius R_C can be solved from the intersection of the circle BC with Zone 3 of the cone.

Equation (19) of Zone 3, transformed to (x,y,z) axis, will become:

$$Z = F(n-1)\cos\alpha_o + \rho_o\sin\alpha_o + r_o = -x\sin\alpha_o + z\cos\alpha_o + Fn\cos\alpha_o$$

The intersection of Zone 3 with the plane, for which $z = r_o \cos \alpha_o$, will give:

$$F(n-1)\cos \alpha_o + \rho_o \sin \alpha_o + r_o = -x \sin \alpha_o + r_o \cos^2 \alpha_o + Fn \cos \alpha_o$$

$$-F \cos \alpha_o + \rho_o \sin \alpha_o + r_o (1-\cos^2 \alpha_o) = - x \sin \alpha_o$$

$$\therefore \quad x = \frac{1}{\sin \alpha_o} (F \cos \alpha_o - \rho_o \sin \alpha_o - r_o \sin^2 \alpha_o)$$

$$x = F \cot \alpha_o - (\rho_o + r_o \sin \alpha_o)$$

And from Eq. (20) for the circle BC, one gets

$$y^2 = (\rho_o + r_o \sin \alpha_o)^2 - x^2$$

Point C in (x,y,z) axis is defined by

$$\begin{cases} x = F \cot \alpha_o - (\rho_o + r_o \sin \alpha_o) \\ y^2 = (\rho_o + r_o \sin \alpha_o)^2 - x^2 \\ z = r_o \cos \alpha_o \end{cases}$$

From the transformation equation (13), one gets

$$R \cos \theta = x \cos \alpha_o + z \sin \alpha_o + Fn \sin \alpha_o$$

$$R \sin \theta = y$$

$$\therefore \quad R^2 = (x \cos \alpha_o + z \sin \alpha_o + Fn \sin \alpha_o)^2 + y^2$$

$$R_C = \sqrt{(x \cos \alpha_o + z \sin \alpha_o + Fn \sin \alpha_o)^2 + y^2}$$

where: $x = F \cot \alpha_o - (\rho_o + r_o \sin \alpha_o)$

$y = (\rho_o + r_o \sin \alpha_o)^2 - x^2$

$z = r_o \cos \alpha_o$

Point D R_D is defined by the intersection of lines θ_{ED} and θ_{CD}

Point E R_E is defined by the intersection of either two of the three lines: θ_{FE}, θ_{ED} and θ_{AE}.

Point F $R_F = F(n-1) \sin \alpha_o - (\rho_o + r_o) \cos \alpha_o$.

Up to now, n indicated the position of the roller. For practical applications, a term whose physical meaning is easier to visualize should be used. Let the radius R of point A be used, and denoted by R_o:

$$R_o = R_A = Fn \sin \alpha_o - (r_o + \rho_o) \cos \alpha_o$$

$$\therefore \quad Fn = \frac{1}{\sin \alpha_o} \left[R_o + (r_o + \rho_o) \cos \alpha_o \right]$$

This value of Fn is to be inserted wherever it appears.

It is now appropriate to discuss the deflection of the neglected zones.

1. The Zone over Line BC, ($R > R_{BC}$)

The difference between a perfect disc and the actual shape of Zone 3 of the cone diminishes rapidly as R increases over R_B. Therefore, neglecting the plastic deformation work on this zone is justified.

2. Lines CD, DE, EF

The actual strain rate is finite and thus does not confirm with our picture (Fig. 15). The strain-rate field is as described except on that line and very close to it. Therefore the work under the area of contact is computed correctly. The work at the discussed zone (line CDEF) is estimated only (see Appendix 1).

The velocity and strain-rates field

From the equations of the roller, one can compute the values of the following terms:

$$\left.\begin{aligned} U_Z &= N\left[2\pi\,\frac{\partial Z}{\partial \theta} + \frac{\partial Z}{\partial n}\right] \\ \dot{\epsilon}_{RZ} &= \frac{1}{2}\cdot\frac{\partial U_Z}{\partial R} \\ \dot{\epsilon}_{\theta Z} &= \frac{1}{2R}\,\frac{\partial U_Z}{\partial \theta} \end{aligned}\right\} \qquad (22)$$

These terms are long and bulky. Further, under the torus they are expressed as functions of R, θ, Z and n while Z is implicitly deduced from the equation of the torus. Altogether, it is possible by the use of these equations and double integration by numerical methods to solve for the work of deformation. But as this requires much labor, some approximations will be made which will not affect the results appreciably and be less laborious.

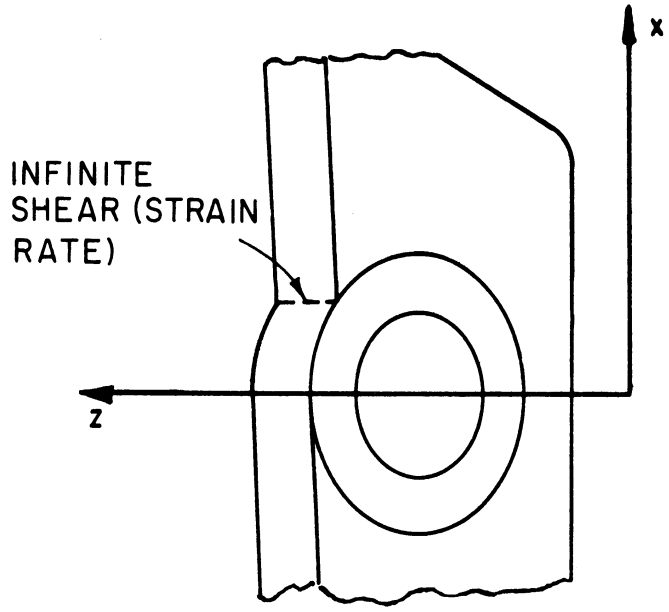

Fig. 15 - The boundary CDEF

VI. SOLVING THE POWER BY THE DEFORMATION THEORY

Let a hypothetical cubic block of unit length be exposed to a pure shear, (see Fig. 16).

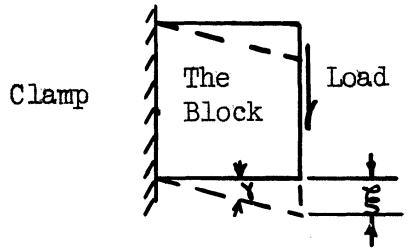

Fig. 16 - Hypothetical block under shearing

Let the load be $k = \frac{\sigma_o}{\sqrt{3}}$, and the shear angle be γ. The distance traveled is $\xi = 1 \cdot \tan \gamma = \tan \gamma$, and the external work of deformation is $W = k \tan \gamma = \frac{\sigma_o}{\sqrt{3}} \tan \gamma$. This is the work of deformation for a unit volume.

The volume worked on the cone is

$$v = 2\pi RN\, S_o\, F \sin \alpha_o \quad \left[\frac{\text{Inch}^3}{\text{Min}}\right]$$

and the relation between α_o and the shear angle γ is $\gamma = 90^o - \alpha_o$. One can now write the power for the spinning of a cone as

$$\dot{W} = 2\pi RN\, S_o\, F \sin \alpha_o \quad \frac{\sigma_o}{\sqrt{3}} \quad \tan \gamma$$

$$\dot{W} = \frac{2}{\sqrt{3}}\, \pi\, \sigma_o\, RN\, S_o\, F \sin \alpha_o \cot \alpha_o$$

$$\dot{W} = \frac{2}{\sqrt{3}}\, \pi\, \sigma_o\, S_o\, N\, F\, R \cos \alpha_o$$

Let now the same approach be introduced to compute the power for spinning of strain-hardened materials.

Let the stress-strain curve and the shear angle and displacement be described as in Figs. 17 and 18.

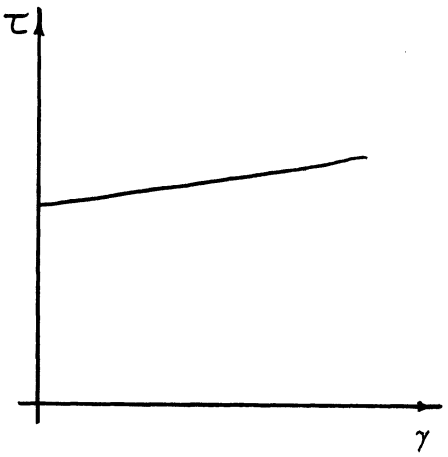

Fig. 17 - Shear stress-shear angle curve

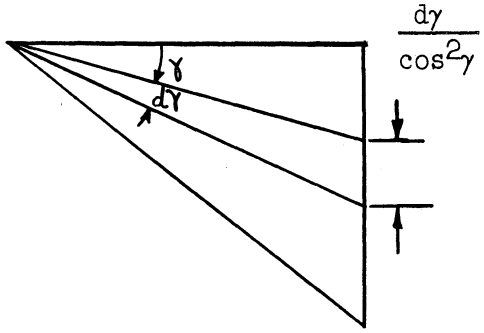

Fig. 18 - Shear angle

The work per unit volume will be

$$w = \int_{\gamma=0}^{\gamma} \tau \frac{d\gamma'}{\cos^2\gamma'} \qquad (23)$$

where γ' is the instantaneous shear angle.

Let the stress-strain curve be approximated by the straight line

$$\tau = \tau_0 + b\gamma$$

where b is the coefficient of strain-hardening, and $\tau_0 = \frac{\sigma_0}{\sqrt{3}}$ is the shear stress at the beginning of yield ;

$$\therefore \tau = \tau_0 + b\gamma = \frac{\sigma_0}{\sqrt{3}} + b\gamma$$

the integral then becomes

$$w = \int_{\gamma=0}^{\gamma} \left(\frac{\sigma_o}{\sqrt{3}} + b\gamma' \right) \frac{d\gamma'}{\cos^2\gamma'} = \frac{\sigma_o}{\sqrt{3}} \int_{\gamma=0}^{\gamma} \frac{d\gamma'}{\cos^2\gamma'} + b \int_{\gamma=0}^{\gamma} \frac{\gamma' d\gamma'}{\cos^2\gamma'}$$

$$w = \frac{\sigma_o}{\sqrt{3}} \tan\gamma + b\,(\gamma' \tan\gamma' + \ln\cos\gamma')_0^{\gamma} = \frac{\sigma_o}{\sqrt{3}} \tan\gamma + b[\gamma \cdot \tan\gamma + \ln(\cos\gamma)]$$

and substituting $\gamma = \frac{\pi}{2} - \alpha_o$, one gets:

$$w = \frac{\sigma_o}{\sqrt{3}} \cot\alpha_o + b\left[\left(\frac{\pi}{2} - \alpha_o\right) \cot\alpha_o + \ln(\sin\alpha_o)\right]$$

This is the work per unit volume. To find the power, one multiplies the work per unit volume by the volume machined per minute.

$$\dot{W} = 2\pi RN\, S_o\, F \sin\alpha_o \left\{ \frac{\sigma_o}{\sqrt{3}} \cot\alpha_o + b\left[\left(\frac{\pi}{2} - \alpha_o\right) \cot\alpha_o + \ln(\sin\alpha_o)\right] \right\}$$

Summarizing the results for perfect plastic material and linearly strain-hardened material, one gets

$$\left.\begin{aligned} &\dot{W} = \frac{2}{\sqrt{3}} \pi\, \sigma_o\, S_o\, N\, F\, R \cos\alpha_o \text{ - for perfectly plastic material} \\ &\dot{W} = \frac{2}{\sqrt{3}} \pi\, \sigma_o\, S_o\, NFR \cos\alpha_o + 2\pi\, \sigma_o S_o\, NFR\, b\left[\left(\frac{\pi}{2} - \alpha_o\right)\cos\alpha_o + \sin\alpha_o \ln(\sin\alpha_o)\right] \end{aligned}\right\} \quad (24)$$

For linearly strain-hardened material where: $\tau = \tau_o + b\gamma = \frac{\sigma_o}{\sqrt{3}} + b\gamma$

VII. SIMPLIFYING THE EQUATIONS FOR NUMERICAL EVALUATION

Repeating here Eq. (11) for the power of plastic deformation (by the incremental theory),

$$\dot{W} = \frac{\sigma_o S_o}{\sqrt{3}} \int_\theta \int_R R \sqrt{\left(\frac{\partial U_Z}{\partial R}\right)^2 + \left(\frac{1}{R} \cdot \frac{\partial U_Z}{\partial \theta}\right)^2}\, dR d\theta \qquad (11)$$

Let a weighted power ($\dot{W}'$) be defined such that

$$\dot{W}' = \frac{\dot{W} \cdot \sqrt{3}}{\sigma_o S_o N} \quad \text{and} \quad \dot{W} = \frac{\sigma_o S_o}{\sqrt{3}} N \dot{W}' ; \qquad (25)$$

then the weighted power is:

$$\dot{W}' = \frac{1}{N} \int_\theta \int_R R \sqrt{\left(\frac{\partial U_Z}{\partial R}\right)^2 + \left(\frac{1}{R} \cdot \frac{\partial U_Z}{\partial \theta}\right)^2}\, dR d\theta \qquad (26)$$

Let $\zeta = \left(\frac{\dot{\epsilon}_{\theta Z}}{\dot{\epsilon}_{RZ}}\right)^2 = \left(\frac{\partial U_Z}{R \partial \theta} \Big/ \frac{\partial U_Z}{\partial R}\right)^2$ so that the equation for the weighted power can be written:

$$\dot{W}' = \frac{2}{N} \int_\theta \int_R R \sqrt{\dot{\epsilon}_{RZ}^2 + \dot{\epsilon}_{\theta Z}^2}\, dR d\theta = \frac{2}{N} \int_\theta \int_R R \sqrt{1 + \zeta}\, \dot{\epsilon}_{RZ}\, dR d\theta \qquad (27)$$

where ζ is the strain-rates ratio factor.

The work of deformation done by the cylindrical portion of the roller will not be computed. The function of this cylindrical portion is to smooth out the feed mark (Fig. 19). These feed marks[4] are minor in size as the following example of a practical case shows.

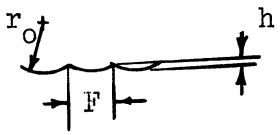

Fig. 19 - Feed marks left by the torus

where h is the feed-marks height.

$$h = r_o - \sqrt{r_o^2 - \left(\frac{F}{2}\right)^2}$$

For example, if r_o = .250 in. and F = .040 in./rev. one gets

$$h = .250 - \sqrt{.250^2 - .020^2} = .0008 \text{ in.},$$

and when reducing F to a half or F = .020 in./rev. one gets

$$h = .250 - \sqrt{.250^2 - .010^2} = .0002 \text{ in.}$$

The amount of the displacement caused by the cylindrical portion of the roller is thus neglected. (The work of deformation caused by the cylindrical portion was computed for a number of cases, and found to be negligible. This part of the work is not included in the report). From here on the equations deal only with the torical portion of the roller.

It is to be expected that γ is a function of R and θ. For $\theta = 0$, one gets $\gamma = 0$, and usually γ is less than .250. For simplicity, and to be able to perform an integration, it will be assumed that γ is independent of R and θ. The constant value of γ will be chosen arbitrarily as that of γ at the point E. The distribution of γ as well as that of $\dot{\epsilon}_{RZ}$ and $\dot{\epsilon}_{\theta Z}$ along line $R = R_B$ and along line ED are available at the General Library of the University of Michigan.

A. INTEGRATING THE POWER

Assuming γ to be a constant, one can take the square root outside of the integral and Eq. (27) becomes:

$$\dot{W}' = \frac{2}{N}\sqrt{1+\gamma}\int_R\int_\theta R\,\dot{\epsilon}_{RZ}\,dR d\theta = \frac{1}{N}\sqrt{1+\gamma}\int_\theta\left[\int_R R\,\frac{\partial U_Z}{\partial R}\,dR\right]d\theta$$

One can perform the integration $\int R\,\frac{\partial U_Z}{\partial R}\,dR$ by substituting $R = U$ and $\frac{\partial U_Z}{\partial R}\,dR = dv$.

But a close check of the equation reveals that, while $\frac{\partial U_Z}{\partial R}$ is changing appreciably for every minor change in R, R itself can be regarded as constant $R = R_o$.

So: $$\int_l^u R\,\frac{\partial U_Z}{\partial R}\,dR \simeq R_o\int_l^u \frac{\partial U_Z}{\partial R}\,dR = R_o\cdot\Delta U_Z$$

The weighted power becomes

$$\dot{W}' = \frac{\sqrt{1+\gamma}}{N}\,R\int\Delta U_Z d\theta \qquad (28)$$

Recalling that

$$U_Z = N\left[2\pi \cdot \frac{\partial Z}{\partial \theta} + \frac{\partial Z}{\partial n}\right]$$

Let:

$$\left.\begin{aligned} U_{ZP} &= 2\pi N \frac{\partial Z}{\partial \theta} \\ U_{ZC} &= N \cdot \frac{\partial Z}{\partial n} \\ \text{and thus:}\quad \Delta U_Z &= \Delta U_{ZP} + \Delta U_{ZC} \\ \Delta U_{ZP} &= 2\pi N \Delta \frac{\partial Z}{\partial \theta} \\ \Delta U_{ZC} &= N \cdot \Delta \frac{\partial Z}{\partial n} \end{aligned}\right\} \qquad (29)$$

Let: The total weighted power $\dot{W}' = \dot{W}'_p + \dot{W}'_c$

where: the partial power is $\dot{W}'_p = \frac{\sqrt{1+\zeta}}{N} R_o \int_\theta \Delta U_{ZP} d\theta$

and the complementary power is $\dot{W}'_c = \frac{\sqrt{1+\zeta}}{N} R_o \int_\theta \Delta U_{ZC} d\theta$

B. COMPUTING THE PARTIAL POWER

$$\dot{W}'_p = \frac{\sqrt{1+\zeta}}{N} R_o \int \Delta U_{ZP} d\theta = \sqrt{1+\zeta} \cdot R_o \cdot 2\pi \int \Delta \cdot \frac{\partial Z}{\partial \theta}\, d\theta$$

$$\dot{W}'_p = 2\pi R_o \cdot \sqrt{1+\zeta} \cdot \Delta Z$$

where: the total $\Delta Z = F \cos \alpha_o$,

and therefore

$$\dot{W}'_p = 2\pi R_o \cdot \sqrt{1+\zeta} \cdot F \cos \alpha_o \qquad (30)$$

The similarity of this partial power to the power computed by the deformation theory is to be noticed. For $\gamma = 0$, $\dot{W}_p$ is the work of deformation computed by the deformation theory, Eq. (24).

C. COMPUTING THE COMPLEMENTARY POWER

The complementary power is

$$\dot{W}_c' = \frac{\sqrt{1+\gamma}}{N} R_o \cdot \int \Delta U_{ZC} d\theta = \sqrt{1+\gamma}\, R_o \int \Delta \frac{\partial Z}{\partial n} d\theta \quad (31)$$

The value of $\frac{\partial Z}{\partial n}$ can be evaluated from Eq. (14), G = 0, of the torus. However, an approximate expression that will be as good for numerical evaluation can be developed.

Let the torus be of infinite radius (ρ_o') (see Fig. 20). The torus which is now a cylinder as described by the circle of radius r_o is

$$(a - Z)^2 + (b - X)^2 = r_o^2$$

$$a - Z = \pm \sqrt{r_o^2 - (b - X)^2}$$

$$Z = a \mp \sqrt{r_o^2 - (b - X)^2}$$

$$Z = a + \sqrt{r_o^2 - (b - X)^2} = a + \sqrt{r_o^2 - (b - R\cos\theta)^2}$$

$$Z = Fn \cos\alpha_o + \rho_o \sin\alpha_o + \sqrt{r_o^2 - [R\cos\theta - (Fn \sin\alpha_o - \rho_o \cos\alpha_o)]^2} \quad (32)$$

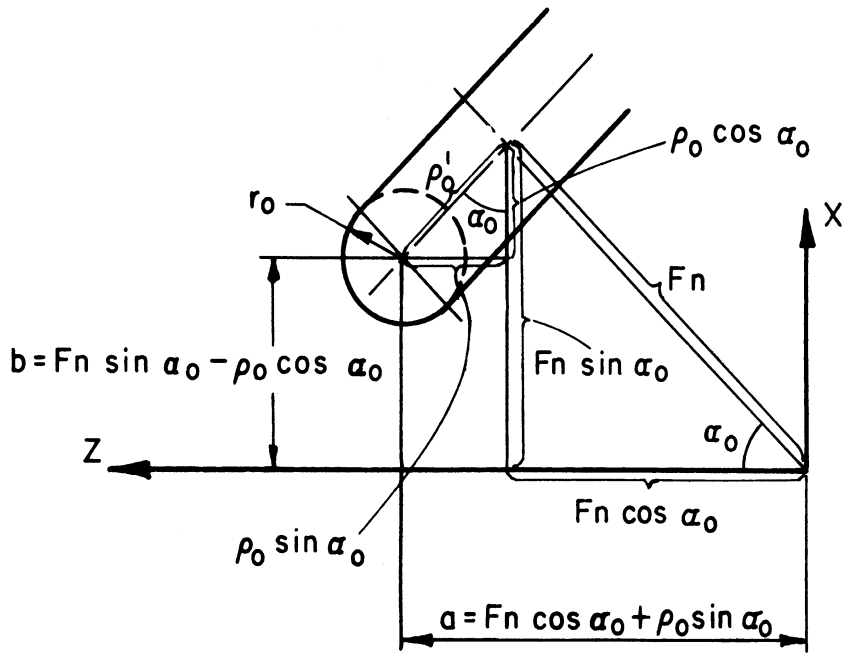

Fig. 20 - Approximating the torus by a cylinder

Differentiating Z with respect to n, one gets

$$\frac{\partial Z}{\partial n} = F \cos \alpha_o + \frac{\left[R \cos\theta - (Fn \sin \alpha_o - \rho_o \cos \alpha_o)\right] \cdot F \sin \alpha_o}{\sqrt{r_o^2 - \left[R \cos \theta - (Fn \sin \alpha_o - \rho_o \cos \alpha_o)\right]^2}}$$

One notices that: $\Delta \frac{\partial Z}{\partial n} = \frac{\partial Z}{\partial n} (R_u) - \frac{\partial Z}{\partial n} (R_l)$

And therefore:

$$\Delta \frac{\partial Z}{\partial n} = F \sin \alpha \left\{ \frac{R_u \cos \theta - (Fn \sin \alpha_o - \rho_o \cos \alpha_o)}{\sqrt{r_o^2 - \left[R_u \cos \theta - (Fn \sin \alpha_o - \rho_o \cos \alpha_o)\right]^2}} \right.$$

$$\left. - \frac{R_l \cos \theta - (Fn \sin \alpha_o - \rho_o \cos \alpha_o)}{\sqrt{r_o^2 - \left[R_l \cos \theta - (Fn \sin \alpha_o - \rho_o \cos \alpha_o)\right]^2}} \right\}$$

where subscripts u denotes upper bound of integration and

l denotes lower bound of integration.

And so, Eq. (31) for the complementary power becomes

$$\dot{W}_c' = \sqrt{1 + \zeta}\, R_o F \sin \alpha_o \cdot \int_{\text{Boundary of the area of contact}} \left\{ \frac{R_u \cos \theta - (Fn \sin \alpha_o - \rho_o \cos \alpha_o)}{\sqrt{r_o^2 - \left[R_u \cos \theta - (Fn \sin \alpha_o - \rho_o \cos \alpha_o)\right]^2}} \right.$$

$$\left. - \frac{R_l \cos \theta - (Fn \sin \alpha_o - \rho_o \cos \alpha_o)}{\sqrt{r_o^2 - \left[R_l \cos \theta - (Fn \sin \alpha_o - \rho_o \cos \alpha_o)\right]^2}} \right\} d\theta \qquad (33)$$

These integrals can be transformed to take the form of elliptic integrals, for which there is a standard procedure for a solution[18]. However, because the boundaries of integration have to be found by a

numerical method (namely, a computer), it was found advantageous to do the integration on the computer also.

D. EVALUATING THE STRAIN-RATES RATIO

Let the approximated torus be used [Eq. (32)]:

$$Z = Fn \cos \alpha_o + \rho_o \sin \alpha_o + \sqrt{r_o^2 - [R \cos \theta - (Fn \sin \alpha_o - \rho_o \cos \alpha_o)]^2}$$

The velocity divided by the number of revolutions per minute is:

$$\frac{U_Z}{N} = \frac{1}{N} \frac{dZ}{dt} = F \cos \alpha_o - \frac{[R \cos \theta - (Fn \sin \alpha_o - \rho_o \cos \alpha_o)] \cdot [-R \sin \theta . 2\pi - F \sin \alpha_o]}{\sqrt{r_o^2 - [R \cos \theta - (Fn \sin \alpha_o - \rho_o \cos \alpha_o)]^2}} \qquad (34)$$

And evaluating $\frac{1}{N} \frac{\partial U_Z}{\partial R}$ and $\frac{1}{N} \frac{\partial U_Z}{\partial \theta}$, one continues:

Let: $(Fn \sin \alpha_o - \rho_o \cos \alpha_o) = \beta$

$$r_o^2 - [R \cos \theta - (Fn \sin \alpha_o - \rho_o) \cos \alpha_o)]^2 = r_o^2 - (R \cos \theta - \beta)^2 = \psi$$

Thus the derivative of $\frac{U_Z}{N}$ from Eq. (34) with respect to R becomes:

$$\frac{1}{N} \frac{\partial U_Z}{\partial R} = \frac{1}{\sqrt{\psi}} \left\{ \cos \theta [2\pi R \sin \theta + F \sin \alpha_o] + (R \cos \theta - \beta) 2\pi \sin \theta \right.$$

$$\left. + \frac{(R \cos \theta - \beta)^2 (2\pi R \sin \theta + F \sin \alpha_o) \cos \theta}{\psi} \right\}$$

$$\frac{1}{N}\frac{\partial U_Z}{\partial R} = \frac{1}{\sqrt{\psi}^3}\left\{\cos\theta\,(2\pi R\sin\theta + F\sin\alpha_o)\left[\psi + (R\cos\theta - \beta)^2\right]\right.$$

$$\left. + (R\cos\theta - \beta)\,2\pi\sin\theta\cdot\psi\right\}$$

$$\frac{1}{N}\frac{\partial U_Z}{\partial R} = \frac{1}{\sqrt{\psi}^3}\left\{r_o^2\cos\theta\,(2\pi R\sin\theta + F\sin\alpha_o) + 2\pi\sin\theta\cdot\psi\cdot(R\cos\theta - \beta)\right\}$$

And the derivative of $\frac{U_Z}{N}$ with respect to θ becomes:

$$\frac{1}{N}\frac{\partial U_Z}{\partial\theta} = \frac{1}{\sqrt{\psi}}\left\{R\sin\theta\left[2\pi R\sin\theta + F\sin\alpha_o\right] + (R\cos\theta - \beta)\,2\pi R\cos\theta\right.$$

$$\left. - \frac{(R\cos\theta - \beta)^2\left[2\pi R\sin\theta + F\sin\alpha_o\right]R\sin\theta}{\psi}\right.$$

$$\frac{1}{N}\frac{\partial U_Z}{\partial\theta} = \frac{1}{\sqrt{\psi}^3}\left\{R\sin\theta\left[2\pi R\sin\theta + F\sin\alpha_o\right]\left[\psi + (R\cos\theta - \beta)^2\right]\right.$$

$$\left. + (R\cos\theta - \beta)\,2\pi R\cos\theta\right\}$$

$$\frac{1}{N}\cdot\frac{1}{R}\cdot\frac{\partial U_Z}{\partial\theta} = \frac{1}{\sqrt{\psi}^3}\left\{r_o^2\sin\theta\left[2\pi R\sin\theta + F\sin\alpha_o\right] + 2\pi\cos\theta\,(R\cos\theta - \beta)\cdot\psi\right\}$$

Recalling that by definition:

$$\zeta = \left(\frac{\dot{\epsilon}_{\theta Z}}{\dot{\epsilon}_{RZ}}\right)^2 = \left(\frac{\frac{1}{R}\cdot\frac{\partial U_Z}{\partial\theta}}{\partial U_Z/\partial R}\right)^2$$

one gets:

$$\gamma = \left\{ \frac{2\pi \cos\theta\,(R\cos\theta - \beta)\ \psi \ - r_o^2 \sin\theta\,[2\pi R \sin\theta + F \sin\alpha_o]}{2\pi \sin\theta\,(R\cos\theta - \beta)\ \psi \ + r_o^2 \cos\theta\,[2\pi R \sin\theta + F \sin\alpha_o]} \right\}^2 \tag{35}$$

where:

$$\beta = Fn \sin\alpha_o - \rho_o \cos\alpha_o$$

$$\psi = r_o^2 - [R\cos\theta - (Fn \sin\alpha_o - \rho_o \cos\alpha_o)]^2$$

VIII. THE TANGENTIAL FORCE

The external power, introduced through the interaction force between the roller and the cone, is consumed by the internal work of deformation and the friction between the roller and the cone. The relative velocity between the roller and the cone is small indeed. The average circumferential velocities of the cone and the roller at the area of contact are equal. The deviation from this velocity is small, because the radius changes very little. The feed velocity of the roller over the cone is significantly small. All in all, it may be assumed that the power consumed by the frictional forces can be neglected. An experimental support for this assumption is given in Ref. 11,§5.5. It is stated there that no measurable difference of the forces between dry and lubricated pieces could be established. The effect of lubrication on rolling coefficient of friction is of about the same order of magnitude as the rolling coefficient of friction. It is therefore to be deducted that if the difference in friction is negligible then the friction itself is negligible. One should remember that if the operation is not done corredtly, the friction can rise.

The friction will therefore be neglected in this study, and only the internal work of deformation will be considered.

The numerical results will be presented in a graphical form. The power is a linear function of the following parameters: Yield limit (σ_o) thickness (S_o) and speed in RPM (N). It will therefore be better to

introduce a weighted tangential force and plot its dependence on the other process variables. The number of graphs will thus be reduced, and the tangential force and power can be found from those graphs and computed for a variety of materials, thicknesses and speeds.

First it will be shown that the greatest portion of the power is absorbed through the tangential component of the force acting between the roller and the cone. Let the force be resolved to its three following components: Tangential Force (t), Radial Force (F_R) directed perpendicular to the side of the cone and Feed Force (F_A) (see Fig. 1). The power consumed can be composed of the total power delivered by these three components of the force separately by each one. In general, the power is the force multiplied by the velocity directed parallel to this force. (The dot product of the force by the velocity). This can be expressed as

$$\dot{W} = t.S_t + F_A.S_A + F_R.S_R$$

where S_t is the circumferential velocity
S_A is the feed velocity, and
S_R is the radial velocity

The roller does not move in the radial direction, or $S_R = 0$.

It follows that $\dot{W} = t.S_t + F_A.S_A = \dot{W}_t + \dot{W}_A$

where: $\dot{W}_t = t.S_t$ - the tangential power

$\dot{W}_A = F_A.S_A$ - the feed power

The "circumferential velocity" is $S_t = 2\pi RN$, and the feed velocity is $S_A = F \cdot N$

The ratio for the "feed power" to the total power is:

$$\frac{\dot{W}_A}{\dot{W}} = \frac{\dot{W}_A}{\dot{W}_A + \dot{W}_t} = \frac{1}{1 + \frac{\dot{W}_t}{\dot{W}_A}} \qquad \frac{1}{1 + \frac{2\pi R}{F}\,\frac{t}{S_A}}$$

A typical case follows (see Table III reading M10).

$$\begin{aligned} F &= .028 \text{ inch/R} \\ R &= 1 \text{ inch} \\ F_A &= 1640 \text{ lb} \\ t &= 100 \text{ lb} \end{aligned}$$

$$\frac{\dot{W}_A}{\dot{W}} \quad \frac{1}{1 + \frac{2\pi}{.028}\,\frac{100}{1640}} \qquad \frac{1}{1 + 13.7} \qquad \frac{1}{14.7} = .068$$

The power consumed by the "feed force" is about 6.8% of the total power. Let the feed power be neglected and the work consumed be regarded as done entirely by the tangential force. One now gets:

$$\dot{W} = t.S_t = 2\,\pi\,R\,N\,t$$

And the tangential force is

$$t = \frac{\dot{W}}{2\pi RN} = \frac{\sigma_o S_o\,\dot{W}}{2\sqrt{3}\,\pi R} \text{ lb.}$$

Let a weighted tangential force (t') be introduced such that:

$$t' = \frac{t}{\sigma_o \, S_o}$$

Equations(36) summarizes the relations between the power, weighted power, tangential force, and weighted tangential force.

$$\left.\begin{aligned}
t &= \frac{\dot{W}}{2\pi RN} = \frac{\sigma_o S_o \, \dot{W}'}{2\sqrt{3}\,\pi R} = \sigma_o \, S_o \, t' \\
t' &= \frac{\dot{W}}{2\pi Rn \, \sigma_o S_o} = \frac{\dot{W}'}{2\sqrt{3}\,\pi R} = \frac{t}{\sigma_o S_o} \\
\dot{W} &= \frac{\sigma_o \, S_o}{\sqrt{3}} \qquad N\dot{W}' = 2\pi RN\sigma_o S_o t' = 2\pi RNt \\
\dot{W}' &= 2\sqrt{3}\,\pi Rt' = \frac{2\sqrt{3}\,\pi R}{\sigma_o \, S_o} \, t = \frac{\sqrt{3}}{\sigma_o \, S_o \, N} \, \dot{W}
\end{aligned}\right\} \quad (36)$$

IX. THE EXPERIMENTAL WORK

Two types of experiments were conducted. One was designed to study the nature of deformation that takes place during the process. The other was designed to measure the forces between the tool and the work during the process.

In usual practice during many spinning operations, the flange (Zone 3) of the cone is distorted. This distortion is very undesirable because a highly distorted flange cannot be worked into a cone and the operation stops or the cone is cracked. This distortion is discussed in Refs. 1, 5 and 11, and some explanations of the factors governing this distortion are given.

It was experiences in this study that the predominent factor governing distortion is the thickness S_1 of the cone. The thickness of all cones studied and analyzed for Part I of this report was kept uniform and according to the "Sine Law". (For the definition of the "Sine Law" see p. 4) In this case the flange is always straight and undistorted.

A. THE EXPERIMENTAL DETERMINATION OF THE NATURE OF THE DEFORMATION

The general pattern of the deformation was first studied by putting grid lines on the original disc and then following the direction they took after deformation. The results of this study are given in Part II. This method showed only the displacement pattern over the surface, ignoring the depth. Later a better technique was used, as follows.

In the original disc .0125-in. holes were drilled and plugged with "sculp" metal (Al. alloy)(see Fig. 21). After the cones were spun, the metal was carefully cut and filed until the holes were revealed. From the

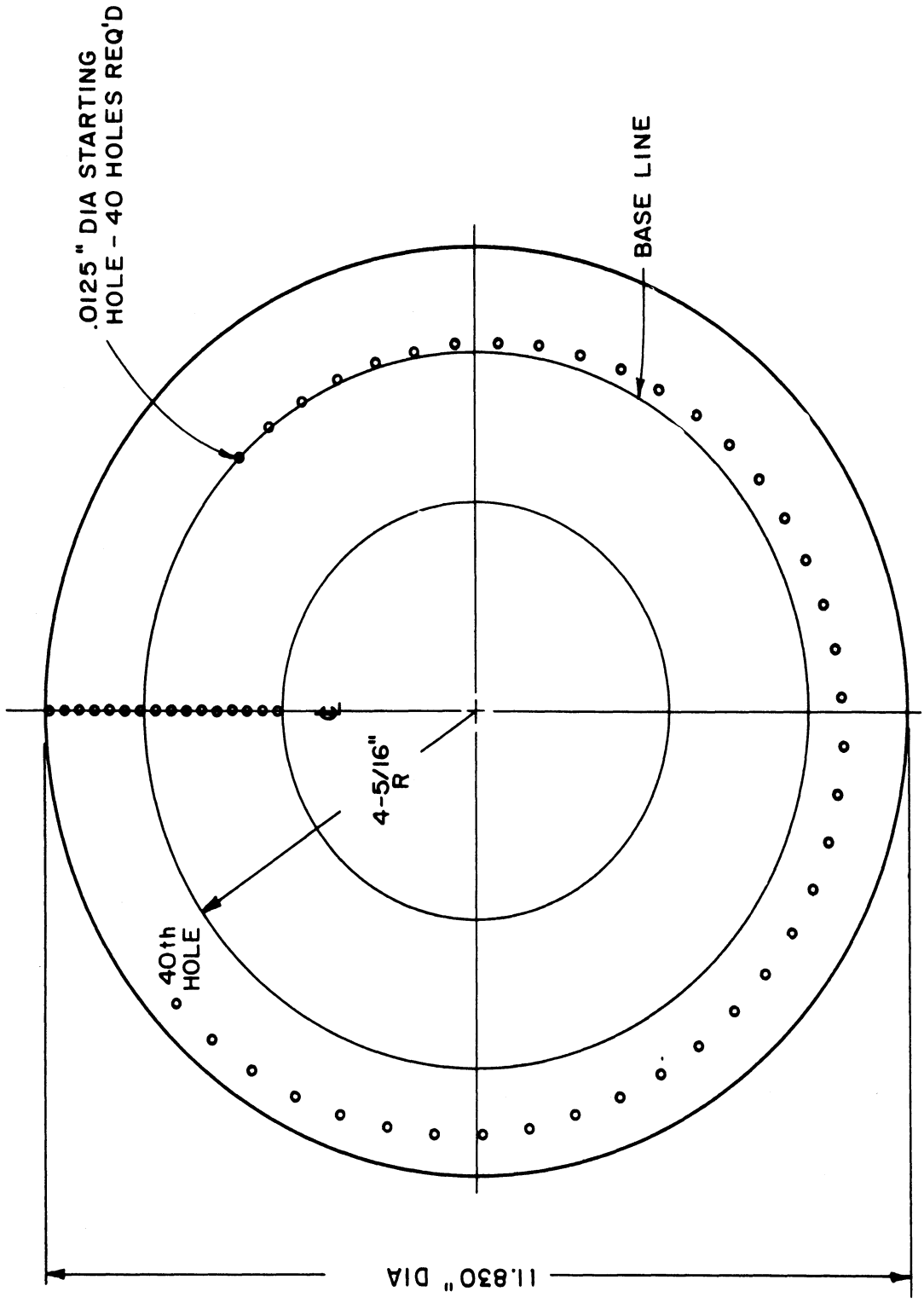

Fig. 21 - Drilled holes in the original disc to study deformation

direction of the plugs, a three-dimensional deformation picture was constructed. A typical picture of the holes is Fig. 22. This cone was spun and checked by Cincinnati Milling Machine Co. as part of a study conducted there.

A top view on the radial line of holes, shows the shear $\epsilon_{R\theta}$ of the cone (see Fig. 23).

The angle α_θ indicate the extent to which the outer surface slipped over the inner surface of the cone. A listing of α, $\Delta\alpha_R$ and α_θ for a variety of cones is given in Table II. $\Delta\alpha_R$ was measured at different radial distances on each cone. α_θ was considered to be zero in the analytical study and compared to $(90-\alpha_o)$, which is the main shear, it is seen to be small enough. No explanation has been found of the odd values of $\Delta\alpha_R$, which prevents inclusion of this distortion in the analytical approach.

The analytical approach assumed a pure shear ϵ_{RZ} which means that $\alpha=0$. This assumption does not hold. For big α_o, it seems that the deformation is closer to pure bend. For smaller α_o, the deformation is closer to pure shear than to bending. It is felt that by assuming pure shear, a computed value for the power will be fairly close to the actual one (see Appendix 2 for the difference between bending and pure shear).

B. MEASURING THE POWER AND TANGENTIAL FORCE

This set of experiments was done in two separate places, one at Cincinnati Milling Machine Company, and the other at Spincraft, Incorporated.

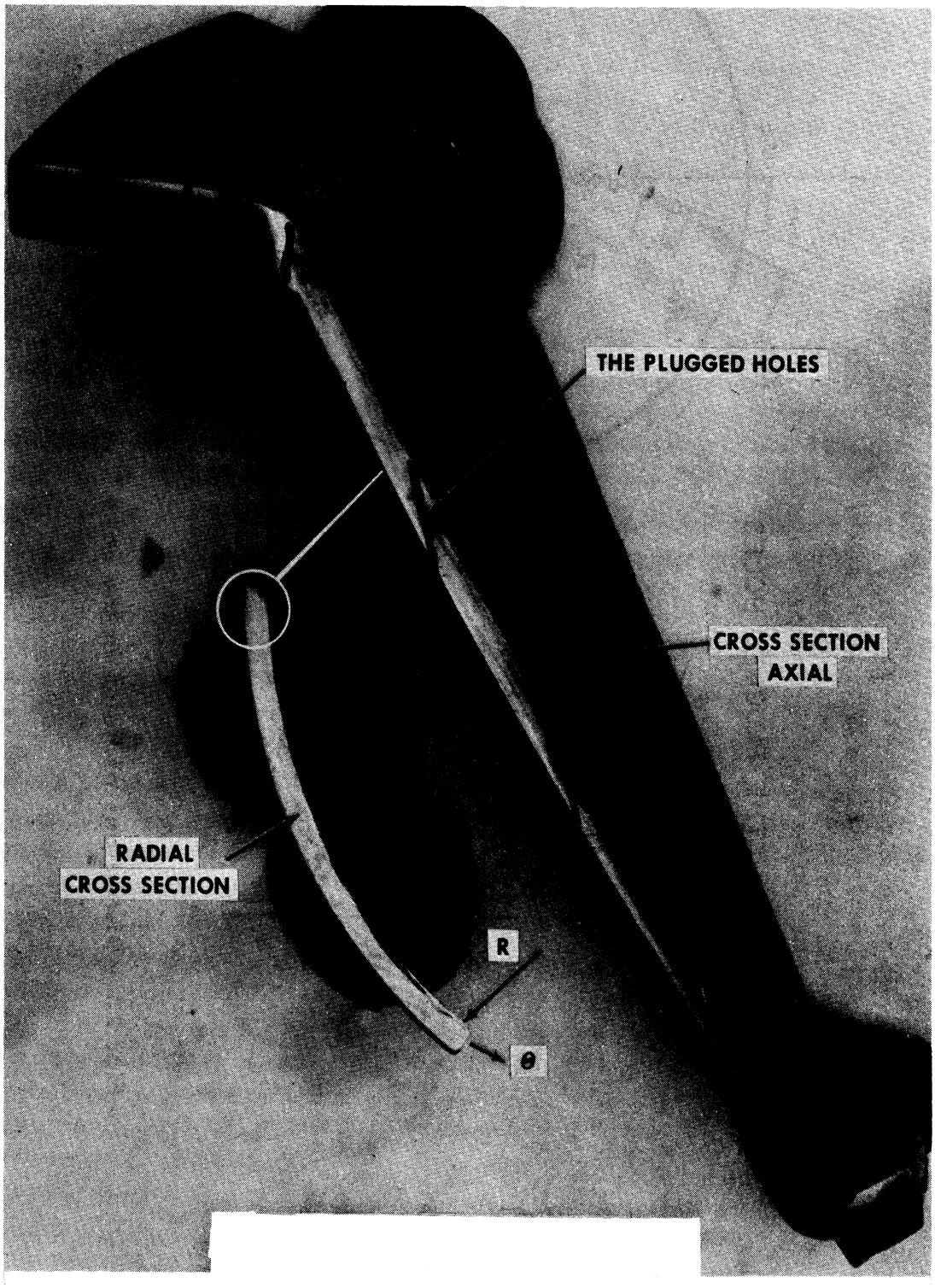

Fig. 22 - A cut of a spun cone

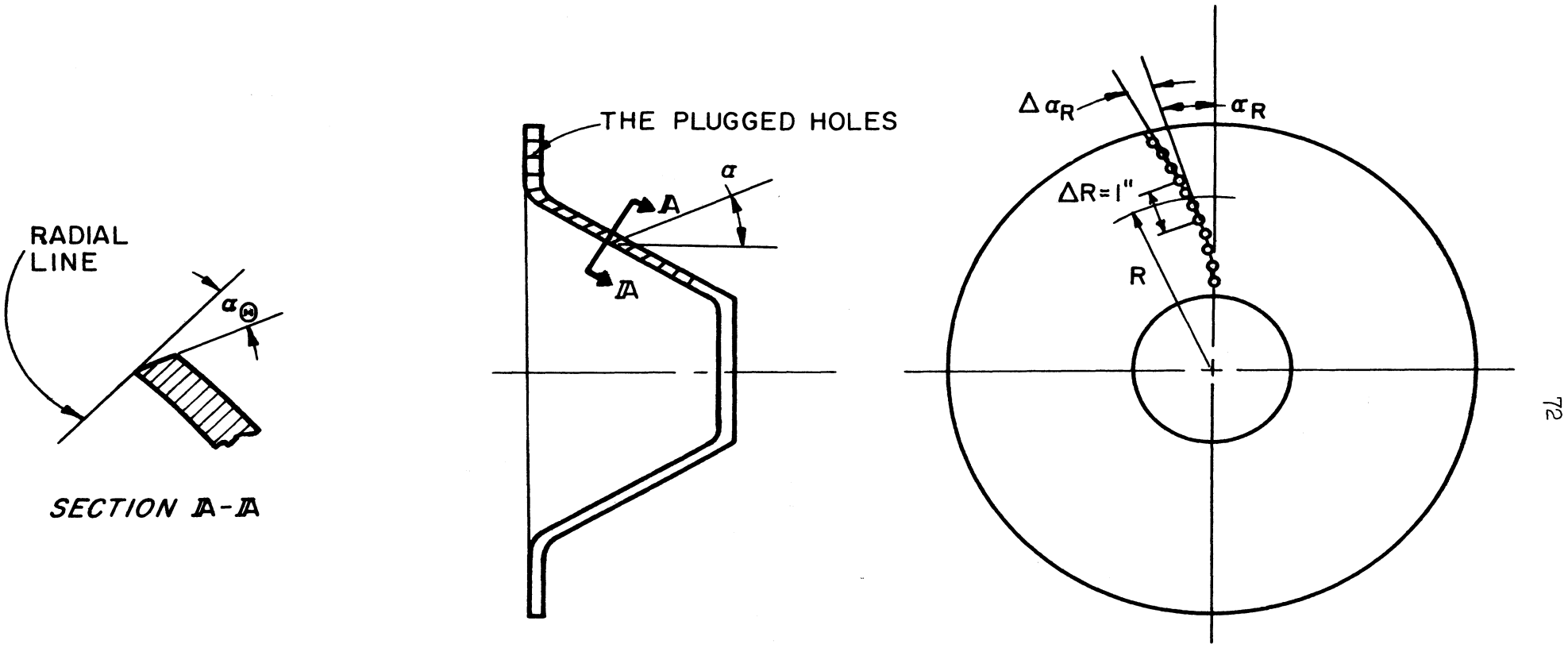

Fig. 23 - Distortions of holes in the cone

Table II - Distortion of Holes Pattern in Spun Cones.

(original thickness S_o = .081 in.)

See Fig. 23

Cone Number	Mat.	Cone Angle, α_o	Radius R	$\Delta \alpha_R$	Average $\alpha_\oplus$	α	$90^o - \alpha$
		Degrees	Inch	$\frac{\text{Degrees}}{\text{inch}}$	Degrees	Degrees	Degrees
1-A-1-R-.5	Al	31.5	4 4.5°	3.5° 0°	6	25	65
1-A-1-R-1	Al	31.5	4 4.5 5	4.5 1.75 2.75	13	22	68
7-A-1-R-.5	Brass	31.5	4 4.5	6 2	12	18	72
9-A-1-R-1	Brass	31.5	3.75 4.25 4.75	3.5 3.5 1.75	17	33	57
1-A-20-R-1	Al	42.5		0	7	35	55
1-A-20-R-5	Al	42.5		0	2	45	45
9-A-3-JJ-R-1	Brass	54	3.25 3.75 4.25 4.75	2 2 3 2	3	23	67

Cincinnati Milling Machine Co. was conducting a study of the spinning operation for quite a long time. Equipment, already constructed, consisted of a three-dimensional dynamometer connected to a 3-channel recorder. The roller is mounted on the dynamometer, and thus the force between the roller and the cone is measured. It was agreed that Cincinnati Milling Machine Co. would run a set of tests designed especially to check the analytical approach developed in this study. For a description of the experimental setup, see Ref. 4. The results are plotted in Fig. 26, 30, 33 and 35. In this study only the tangential force was analyzed.

At Spincraft the power consumption of the a-c motor, which drives the main spindle, was measured. This was done by recording the voltage and current through the motor (see Fig. 24). The data and experimental results are listed in Table IV. The analytical results, compared with the experimental data are plotted in Fig. 27, 28, 29, 31, 32, 34.

One can write the power consumed by the motor to be:

$$\dot{W}_t = \dot{W}_o + \eta \dot{W}$$

where:
$\dot{W}_t$ is the power measured at load,
$\dot{W}_o$ is the power measured at no load,
$\dot{W}$ is the power of deformation consumed by the cone, and
η is the efficiency factor.

The same equation can be transformed to:

$$\dot{W} = \frac{\dot{W}_t - \dot{W}_o}{\eta}$$

The efficiency η for the experiment at Spincraft was arbitrarily chosen at $\eta = 100\%$.

For the analytical solution, a value for the uniaxial yield limit is required. From some cones, a specimen was cut as Fig. 25 shows, and tested on a tensile test machine. Typical stress-strain curves are shown in Fig. A6 and A7. An average flow stress was used instead of the yield limit (see Appendix 3).

The numerical results of the analytical expression are available at the General Library of the University of Michigan.

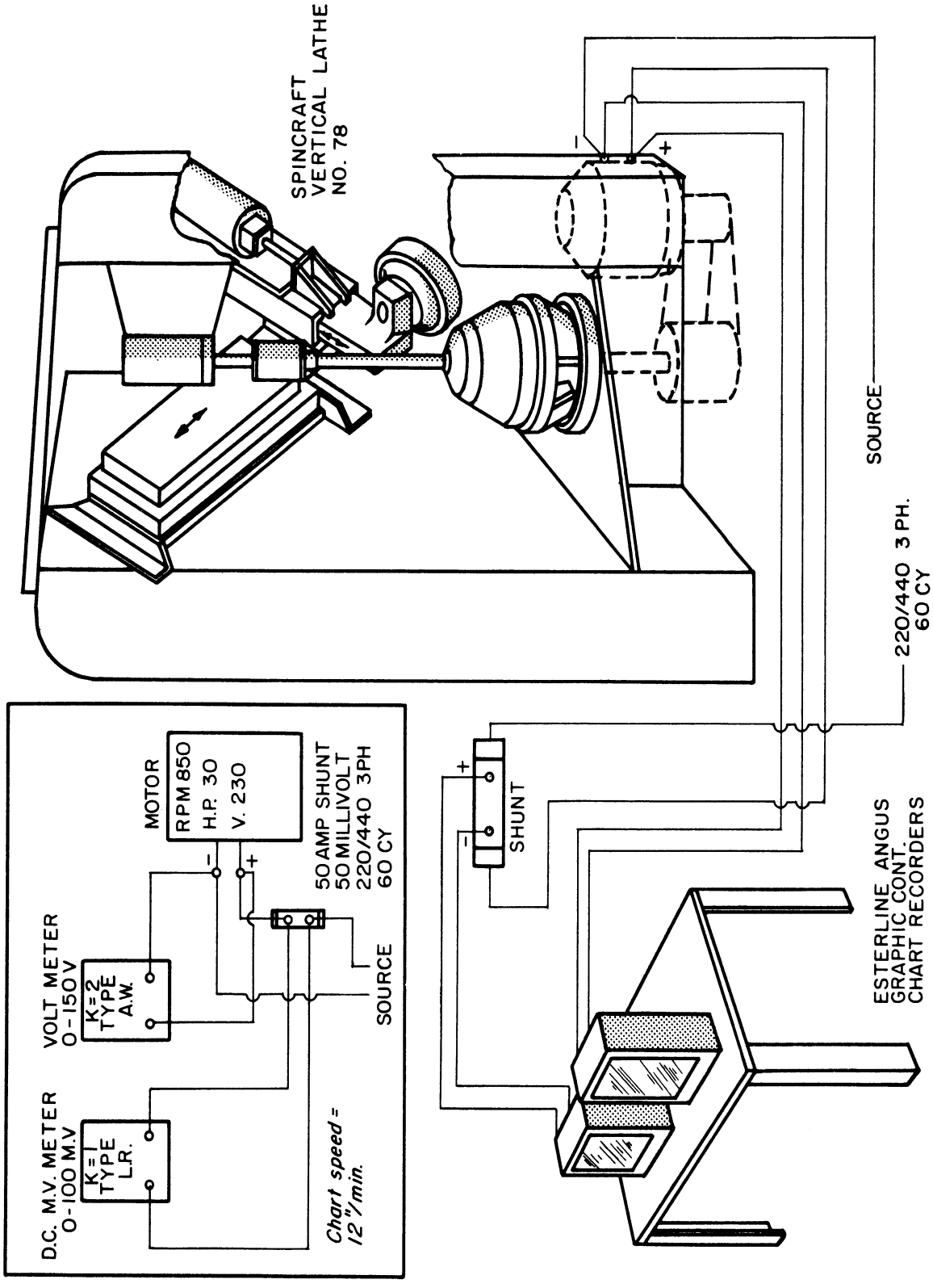

Fig. 24 - Spincraft experimental set up

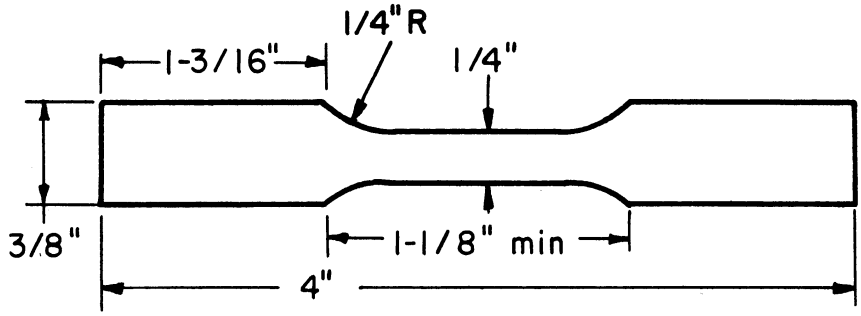

Fig. 25 - Specimen for tensile test

X. RESULTS

The nature of the deformations has been discussed in Ref. 1. Table II gives the deformations as had been found by the holes technique. The effects of each of the parameters, Feed F, cone included angle $2\alpha_o$, cone radius R_o, roller "round-off" radius r_o, and roller radius ρ_o on the power and tangential force, are given in the following graphs.

Knowing these five parameters for an actual case, one finds from the suitable graph the value of the weighted tangential force. By a simple computation, the tangential force and power are obtained:

$$t = \sigma_o S_o t'$$

$$\dot{W} = 2\pi R_o N t = 2\pi R_o N \sigma_o S_o t'$$

where t - the tangential force,

σ_o - yield limit of the actual cone at uniaxial tensile test,

S_o - original disc thickness,

t' - weighted tangential force as found from the graph,

R_o - radius of cone where the force t is applied, and

N - speed of cone in rpm.

TABLE III

Cincinnati Results of Recorded Forces

1	2	3	4	5	6	7	8	9	10	11	12	13	14	15	16	17	18	19	20	21	22	23	24	25	26	27	28	29	30	31	32
	Run Number	Material	Original Thickness	Half Included Angle	Feed per Revolution	Rollers "Round Off"	Rollers Radius	Yield Limit of Worked Cone	Speed				Feed per Minute		Cones Radius		Voltage Drawn		Excess Current Drawn		Power Consumed		Experimental Tangential Force		Weighting Factor		Experimental Weighted Tangential Force				
									Initial	Halfway	Final	Representative			Small	Large	At Small Radius	At Large Radius	At Small Radius	At Large Radius	At Small Radius	At Large Radius	At Small Radius	At Large Radius			At Small Radius	At Large Radius			
			in.	°	ipr	inch		psi	rpm				ipm		inch		volts		amp		lb-in./min		lb		ppi		inch				
			S_o	α_o	F	r_o	ρ_o	σ_o	N_S	N_H	N_F	N	NF		R_1	R_2	V_1	V_2	ΔI_1	ΔI_2	$\dot{W}_1$	$\dot{W}_2$	t_1	t_2			t'_1	t'_2			
															$\dot{W} = 531.V.\Delta I$								$t = \frac{\dot{W}}{2\pi RN}$		$\sigma_o \cdot S_o$		$t' = \frac{t}{\sigma_o \cdot S_o}$				
	M14	1100 Al	.250	35	.021	1/4	7	25000				300	6.3		1.0								75		6250			.012			
	M2	1100 Al	.250	35	.022	1/4	7	25000				300			1.0								50		6250			.008			
	M1	1100 Al	.250	35	.024	1/4	7	25000				300			1.0								95		6250			.015			
	M10	1100 Al	.250	35	.028	1/4	7	25000				300			1.0								100		6250			.016			
	M11	1100 Al	.250	35	.030	1/4	7	25000				300			1.0								120		6250			.019			
	M3	1100 Al	.250	35	.042	1/4	7	25000				300			1.0								130		6250			.021			
	M4	1100 Al	.250	35	.025	1/8	7	25000				300			1.0								155		6250			.025			
	M9	1100 Al	.250	35	.030	1/8	7	25000				300			1.0								120		6250			.019			
	M5	1100 Al	.250	35	.030	1/2	7	25000				300			1.0								105		6250			.017			
	D301	1100 Al	.375	35	.025	1/4	7	25000				300			1.0								200		9370			.021			
	D427	1100 Al	.485	35	.033	1/4	7	25000				300			1.0								300		12000			.025			
	M8	1100 Al	.250	21	.028	1/4	7	25000				300			1.0								130		6250			.021			
	M7	1100 Al	.250	21	.033	1/4	7	25000				300			1.0								105		6250			.017			
	M12	1100 Al	.250	21	.035	1/4	7	25000				300			1.0								115		6250			.0185			

TABLE IV

Spincraft Results of Recorded Power

1	2	3	4	5	6	7	8	9	10	11	12	13	14	15	16	17	18	19	20	21	22	23	24	25	26	27	28	29	30	31	32
	Run Number	Material	Original Thickness	Half Included Angle	Feed per Revolution	Rollers "Round Off"	Rollers Radius	Yield Limit of Worked Cone	Speed				Feed per Minute		Cones Radius		Voltage Drawn		Excess Current Drawn		Power Consumed		Experimental Tangential Force		Weighting Factor		Experimental Weighted Tangential Force				
									Initial	Halfway	Final	Representative			Small	Large	At Small Radius	At Large Radius	At Small Radius	At Large Radius	At Small Radius	At Large Radius	At Small Radius	At Large Radius			At Small Radius	At Large Radius			
			in.	°	ipr	inch		psi	rpm				ipm		inch		volts		amp		lb-in./min		lb		ppi		inch				
			S_o	α_o	F	r_o	ρ_o	σ_o	N_S	N_H	N_F	N	NF		F_1	F_2	V_1	V_2	ΔI_1	ΔI_2	$\dot{W}_1$	$\dot{W}_2$	t_1	t_2			t_1'	t_2'			
																					$\dot{W} = 531 \cdot V \cdot \Delta I$		$t = \frac{\dot{W}}{2\pi RN}$		$\sigma_o \cdot S_o$		$t' = \frac{t}{\sigma_o \cdot S_o}$				
	112	1100-2S-O Aluminum	.081	27.5	.040	3/8	4 7/32	17,000	439	439	439				2 19/32	7.4	232	232	2	4.25	$247 \cdot 10^3$	$555 \cdot 10^3$	34.4	27.2	1380		.0250	.0197			
	113		.081	27.5	.060	3/8	4 7/32	17,000	440	439	435				2 19/32	7.4	232	232	3.3	7	$407 \cdot 10^3$	$860 \cdot 10^3$	56.7	42.5	1380		.0410	.0340			
	114		.081	27.5	.080	3/8	4 7/32	17,000	440	435	430				2 19/32	7.4	230	228	4.5	9.5	$550 \cdot 10^3$	$1150 \cdot 10^3$	76.5	57.5	1380		.0555	.0416			
	115		.081	27.5	.100	3/8	4 7/32	17,000	440	430	410				2 19/32	7.4	240	236	5	12	$638 \cdot 10^3$	$1500 \cdot 10^3$	89.0	78.5	1380		.0645	.0570			
	122		.077	54	.040	3/8	4 7/32	17,000	440	438	432				2 3/8	7 3/4	240	240	1	3	$127.5 \cdot 10^3$	$383 \cdot 10^3$	19.4	18.3	1310		.0148	.0140			
	124		.076	54	.080	3/8	4 7/32	17,000	438	435	432				2 3/8	7 3/4	236	236	2	6	$250 \cdot 10^3$	$750 \cdot 10^3$	38.2	35.8	1290		.0296	.0277			
	125		.076	54	.100	3/8	4 7/32	17,000	438	430	428				2 3/8	7 3/4	236	236	2.5	7.5	$316 \cdot 10^3$	$940 \cdot 10^3$	48.2	45.0	1290		.0374	.0350			
	132		.080	42.5	.040	3/8	4 7/32	17,000	440	438	438				3 5/8	8	236	236	X	4	——	$500 \cdot 10^3$	—	22.7	1360		—	.0167			
	133		.079	42.5	.060	3/8	4 7/32	17,000	440	438	434				3 5/8	8	236	234	3.5	6	$439 \cdot 10^3$	$747 \cdot 10^3$	44.0	34.2	1340		.0328	.0255			
	134		.079	42.5	.080	3/8	4 7/32	17,000	440	435	430				3 5/8	8	234	232	5	8	$620 \cdot 10^3$	$986 \cdot 10^3$	62.0	45.8	1340		.0462	.0342			
	135		.079	42.5	.100	3/8	4 7/32	17,000	440	435	429				3 5/8	8	234	232	5.5	11.5	$685 \cdot 10^3$	$1420 \cdot 10^3$	68.5	65.5	1340		.0510	.0490			
	45		.079	42.5	.080	1/8	4 1/2	17,000	440	435	430				3 5/8	8	236	236	4	8	$503 \cdot 10^3$	$1000 \cdot 10^3$	50.3	46.2	1340		.0375	.0345			
	148		.0805	42.5	.080	3/16	4 1/2	17,000	440	430	430				3 5/8	8	243	243	4.5	9	$580 \cdot 10^3$	$1160 \cdot 10^3$	57.7	53.6	1370		.042	.0390			

THE EFFECT OF THE FEED (F)
ON THE WEIGHTED TANGENTIAL FORCE t'

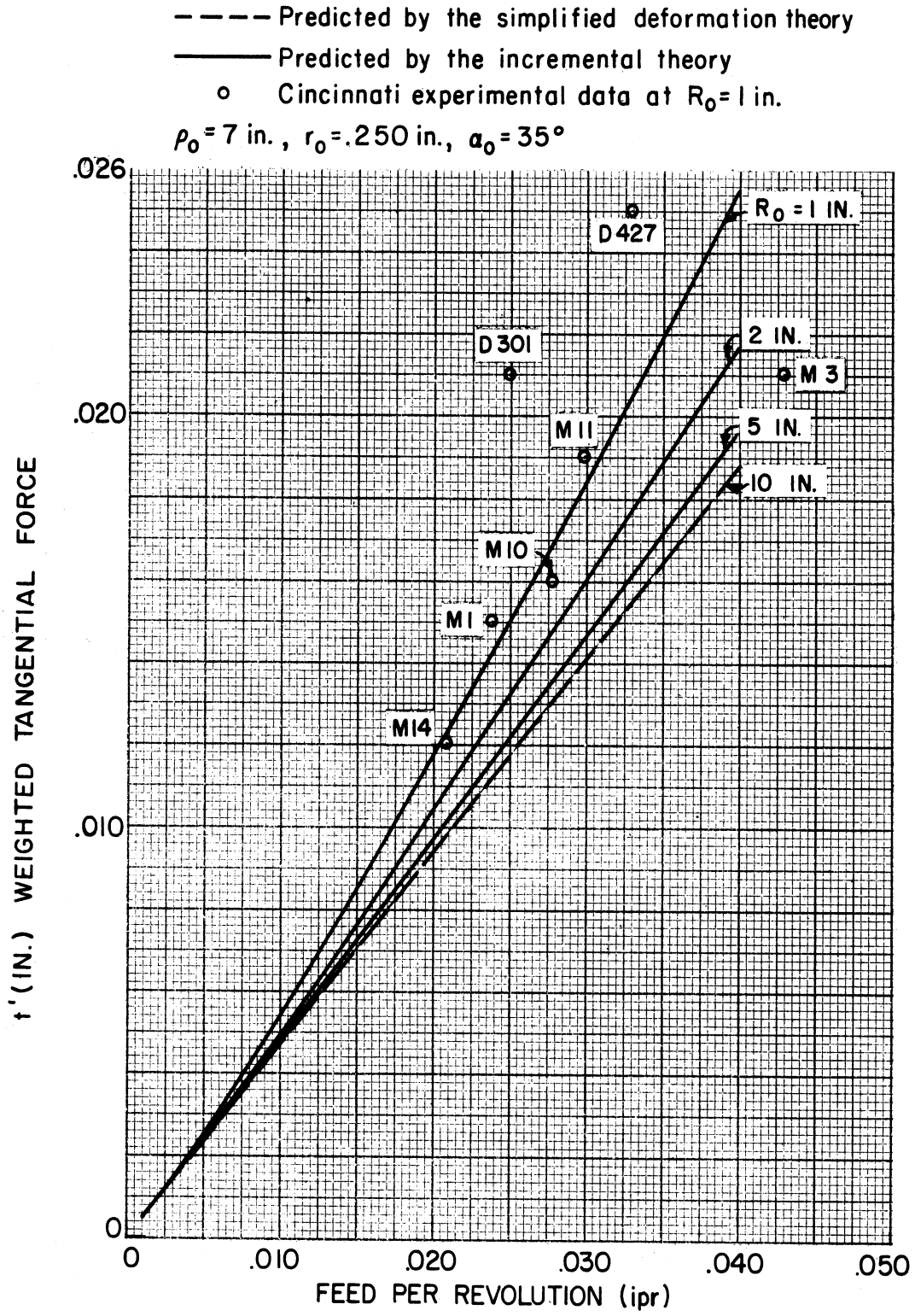

The tangential force $t = \sigma_0 \cdot s_0 \cdot t'$ (lb)

The power $\dot{w} = 2\pi R_0 N t = 2\pi \cdot \sigma_0 \cdot s_0 \cdot R_0 \cdot N \cdot t' \left(\frac{\text{lb in.}}{\text{min}}\right)$

Fig. 26 - Curves of tangential forces versus feeds

THE EFFECT OF THE FEED (F)
ON THE WEIGHTED TANGENTIAL FORCE t'

——— Predicted by the simplified deformation theory
——— Predicted by the incremental theory
o Spincraft experimental data at $R_0 = 2\ 19/32$ in.
× Spincraft experimental data at $R_0 = 7.4$ in.
$\rho_0 = 4.5$ in., $r_0 = 3/8$ in., $\alpha_0 = 27.5$

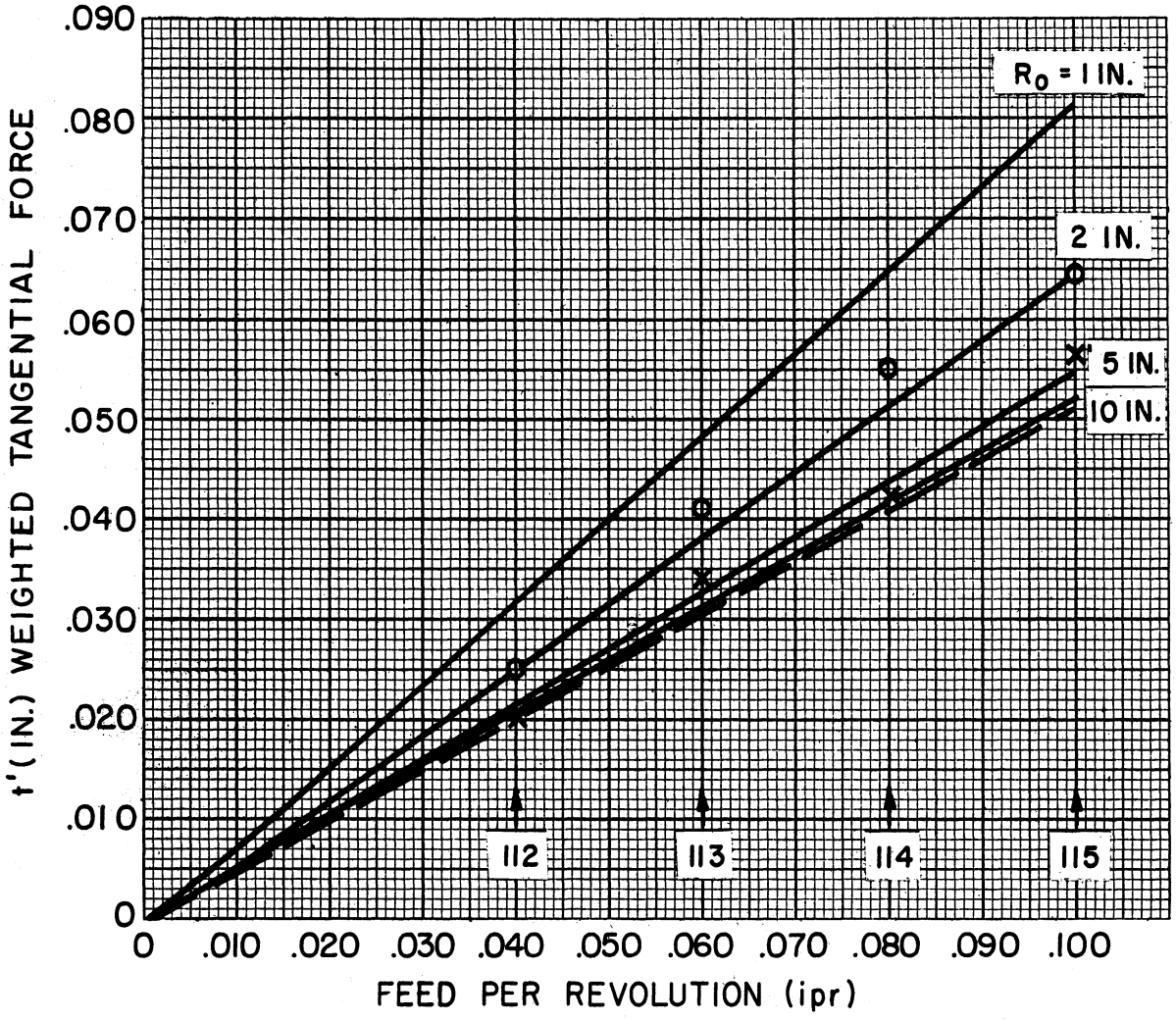

The tangential force $t = \sigma_0 \cdot s_0 \cdot t'$ (lb)

The power $\dot{w} = 2\pi R_0 N t = 2\pi \cdot \sigma_0 \cdot s_0 \cdot R_0 \cdot N t' \left(\frac{\text{lb in.}}{\text{min}}\right)$

Fig. 27 - Curves of tangential forces versus feeds

THE EFFECT OF THE FEED (F)
ON THE WEIGHTED TANGENTIAL FORCE t'

———Predicted by the simplified deformation theory
———Predicted by the incremental theory
o Spincraft experimental data at $R_0 = 3\frac{5}{8}$ in.
× Spincraft experimental data at $R_0 = 8$ in.
$\rho_0 = 4.5$ in., $r_0 = 3/8$ in., $\alpha_0 = 42.5°$

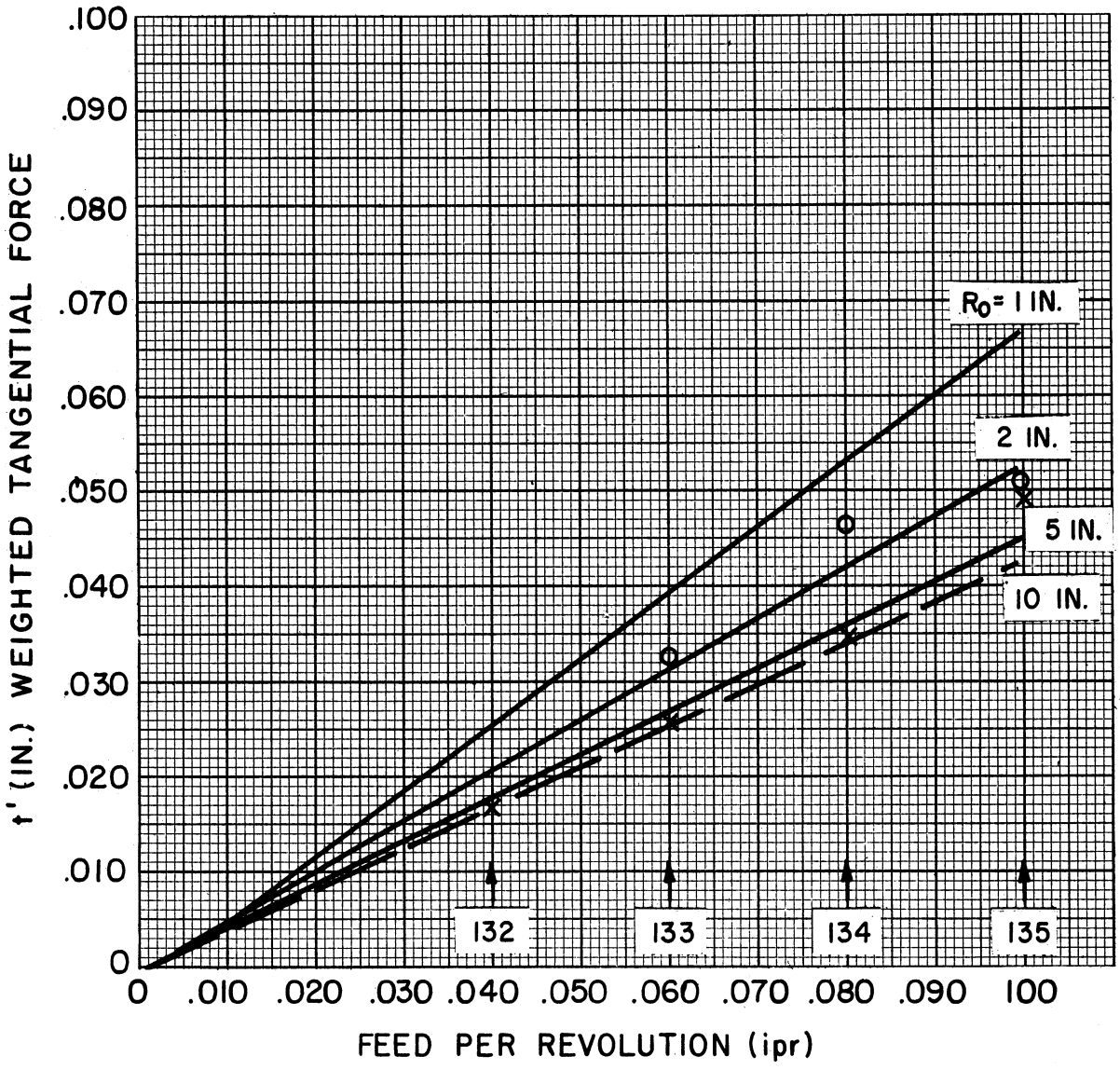

The tangential force $t = \sigma_0 \, s_0 \cdot t'$ (lb)

The power $\dot{w} = 2\pi R_0 N t = 2\pi \cdot \sigma_0 \cdot s_0 \cdot R_0 \cdot N \cdot t' \left(\frac{\text{lb in.}}{\text{min}}\right)$

Fig. 28 - Curves of tangential forces versus feeds

THE EFFECT OF THE FEED (F)
ON THE WEIGHTED TANGENTIAL FORCE t'

———Predicted by the simplified deformation theory

———Predicted by the incremental theory

o Spincraft experimental data at $R_0 = 2\ 3/8$ in.

× Spincraft experimental data at $R_0 = 7\ 3/8$ in.

$\rho_0 = 4.5$ in., $r_0 = 3/8$ in., $\alpha_0 = 54°$

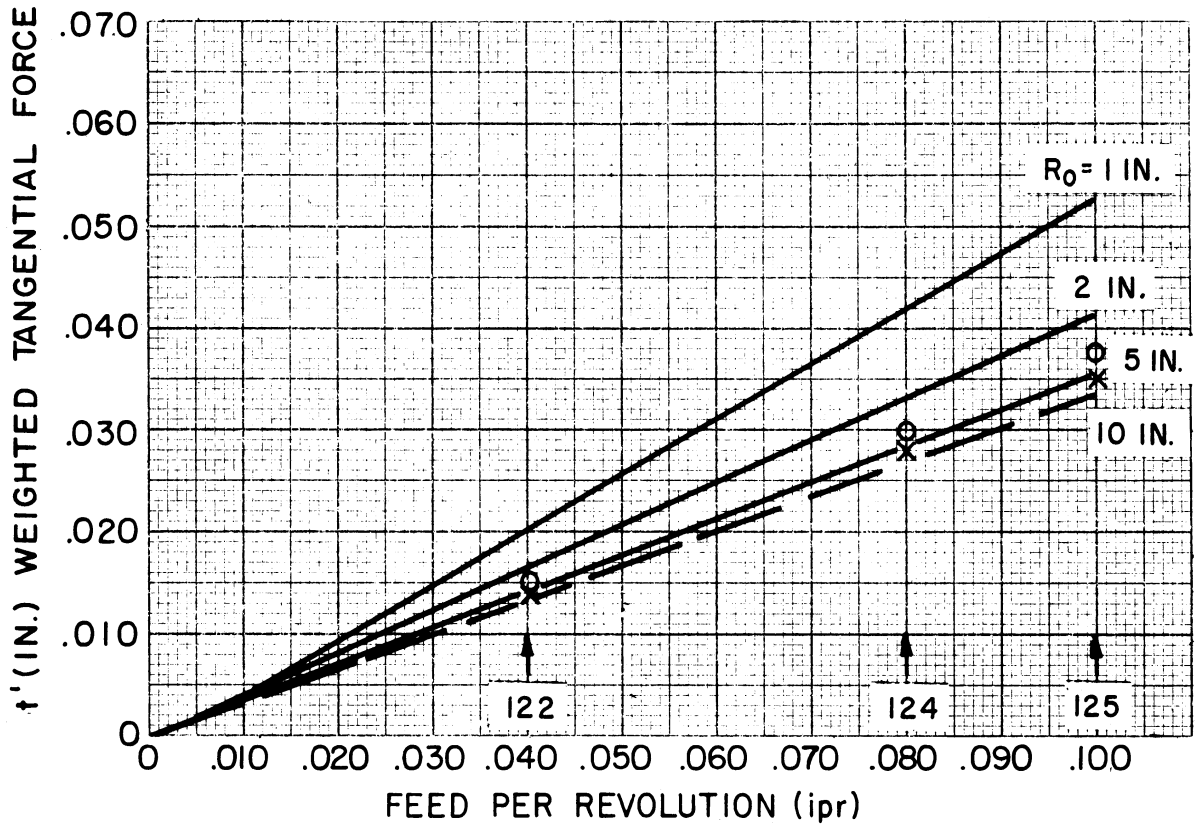

The tangential force $t = \sigma_0 \cdot s_0 \cdot t'$ (lb)

The power $\dot{w} = 2\pi R_0 N t = 2\pi \cdot \sigma_0 \cdot s_0 \cdot R_0 \cdot N \cdot t' \left(\frac{\text{lb in.}}{\text{min}}\right)$

Fig. 29 - Curves of tangential forces versus feeds

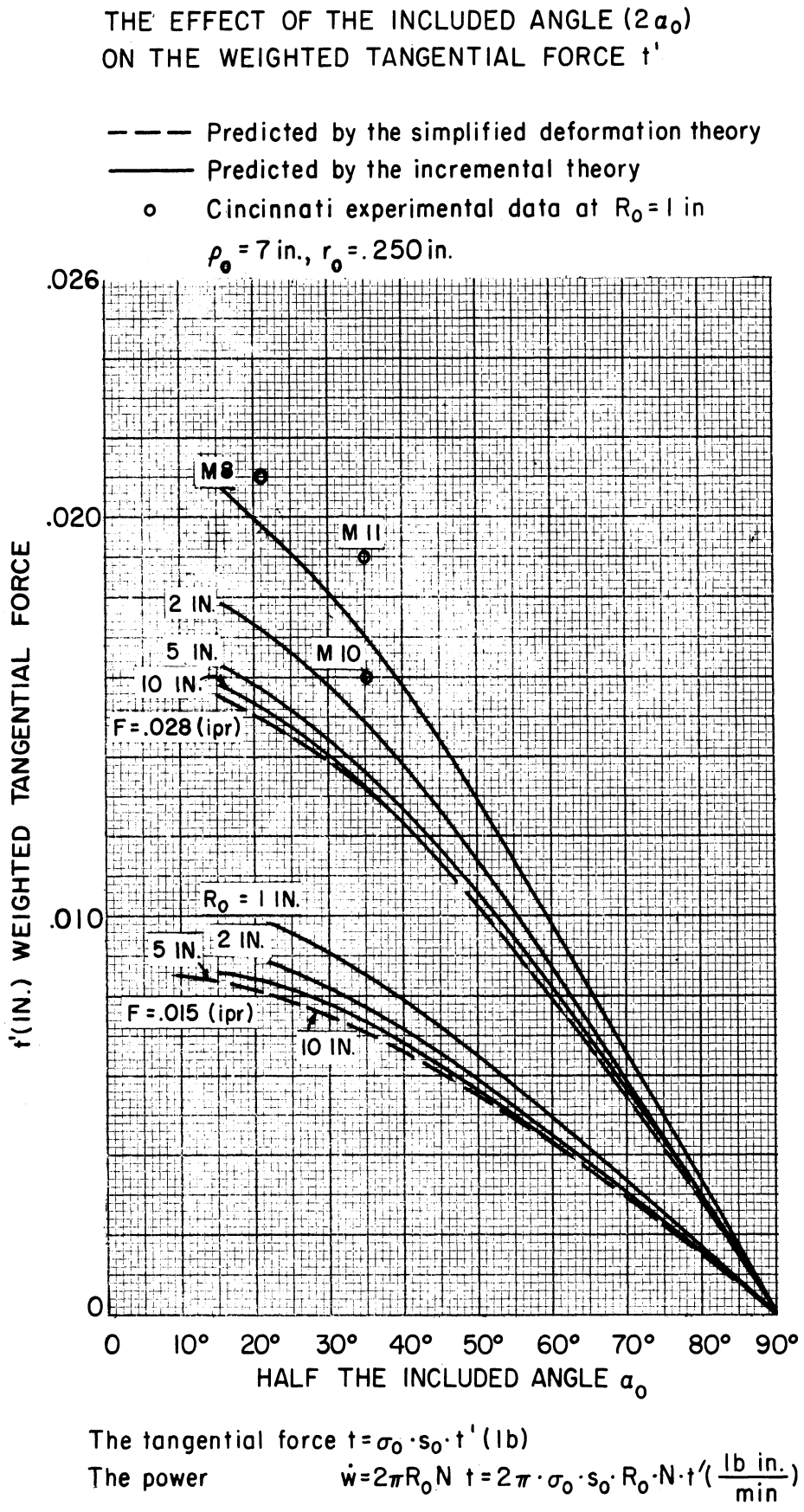

The tangential force $t = \sigma_0 \cdot s_0 \cdot t'$ (lb)

The power $\dot{w} = 2\pi R_0 N \quad t = 2\pi \cdot \sigma_0 \cdot s_0 \cdot R_0 \cdot N \cdot t' \left(\frac{\text{lb in.}}{\text{min}}\right)$

Fig. 30 - Curves of tangential forces versus angles

THE EFFECT OF THE INCLUDED ANGLE ($2\alpha_0$)
ON THE WEIGHTED TANGENTIAL FORCE t'

———Predicted by the simplified deformation theory
———Predicted by the incremental theory
o Spincraft experimental data at $R_0 \approx 3$ in.
× Spincraft experimental data at $R_0 \approx 8$ in.
$\rho_0 = 4.5$ in., $r_0 = 3/8$ in., F = .080 ipr.

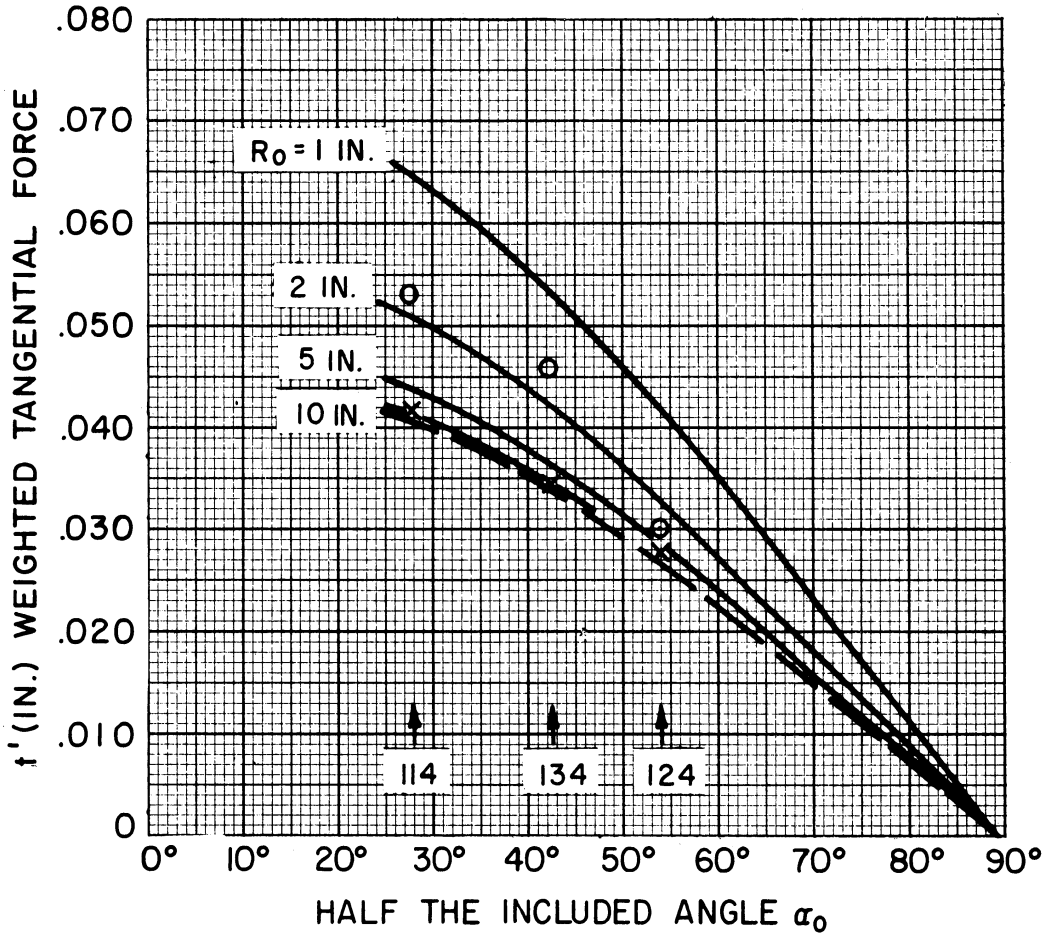

The tangential force $t = \sigma \cdot s \cdot t'$(lb)

The power $\dot{w} = 2\pi R_0 N t = 2\pi \cdot \sigma_0 \cdot s_0 \cdot R_0 \cdot N \cdot t' \left(\frac{\text{lb in.}}{\text{min}}\right)$

Fig. 31 - Curves of tangential forces versus angles

THE EFFECT OF THE INCLUDED ANGLE ($2\alpha_0$)
ON THE WEIGHTED TANGENTIAL FORCE t'

——— Predicted by the simplified deformation theory

——— Predicted by the incremental theory

o Spincraft experimental data at $R_0 \approx 3$ in.

× Spincraft experimental data at $R_0 \approx 8$ in.

$\rho_0 = 4.5$ in., $r_0 = 3/8$ in., F = .100 ipr.

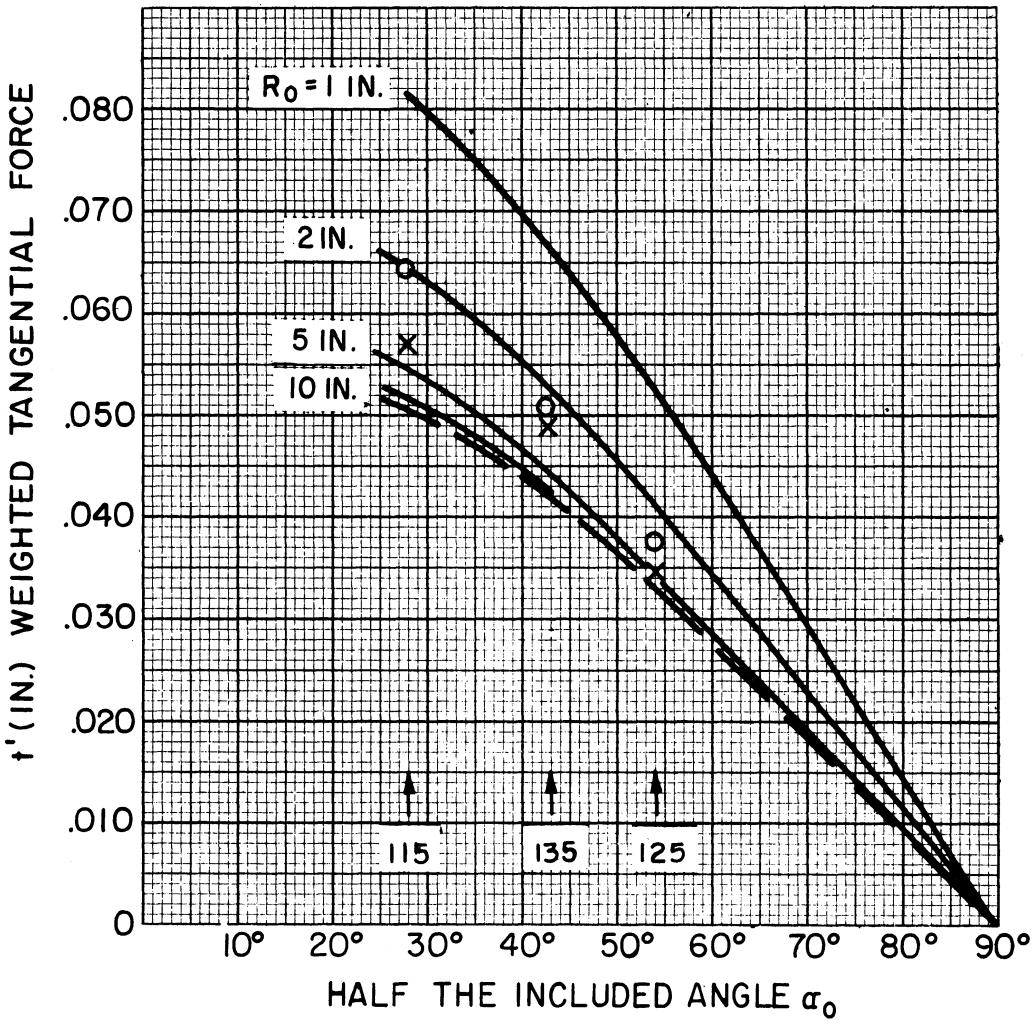

The tangential force $t = \sigma_0 \cdot s_0 \cdot t'$ (lb)

The power $\dot{w} = 2\pi R_0 N t = 2\pi \cdot \sigma_0 \cdot s_0 \cdot R_0 \cdot N \cdot t' \left(\frac{\text{lb in.}}{\text{min}}\right)$

Fig. 32 - Curves of tangential forces versus angles

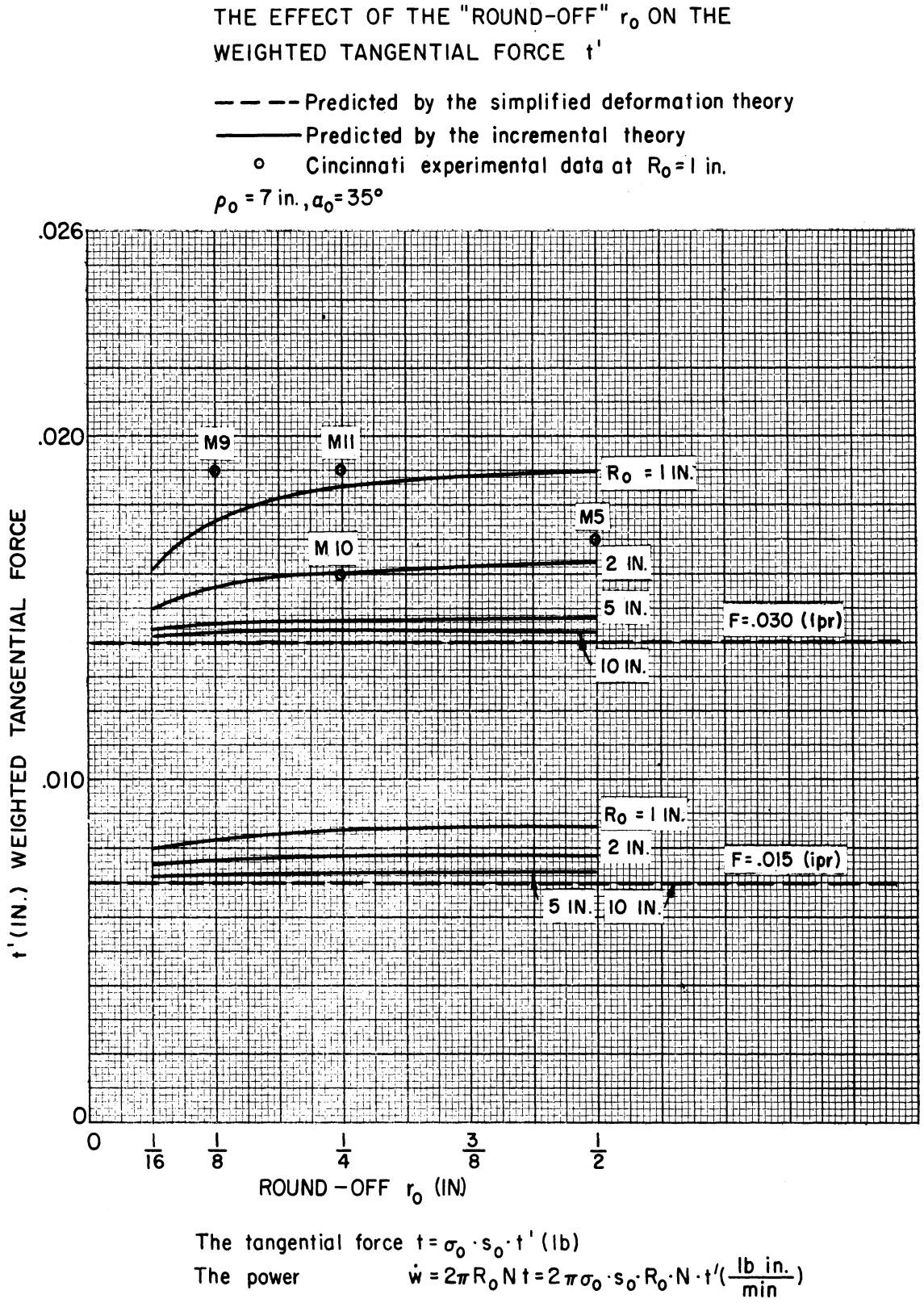

The tangential force $t = \sigma_0 \cdot s_0 \cdot t'$ (lb)

The power $\dot{w} = 2\pi R_0 N t = 2\pi \sigma_0 \cdot s_0 \cdot R_0 \cdot N \cdot t' (\frac{\text{lb in.}}{\text{min}})$

Fig. 33 - Curves of tangential forces versus round-off radii

THE EFFECT OF THE "ROUND-OFF" r_0 ON THE WEIGHTED TANGENTIAL FORCE t'

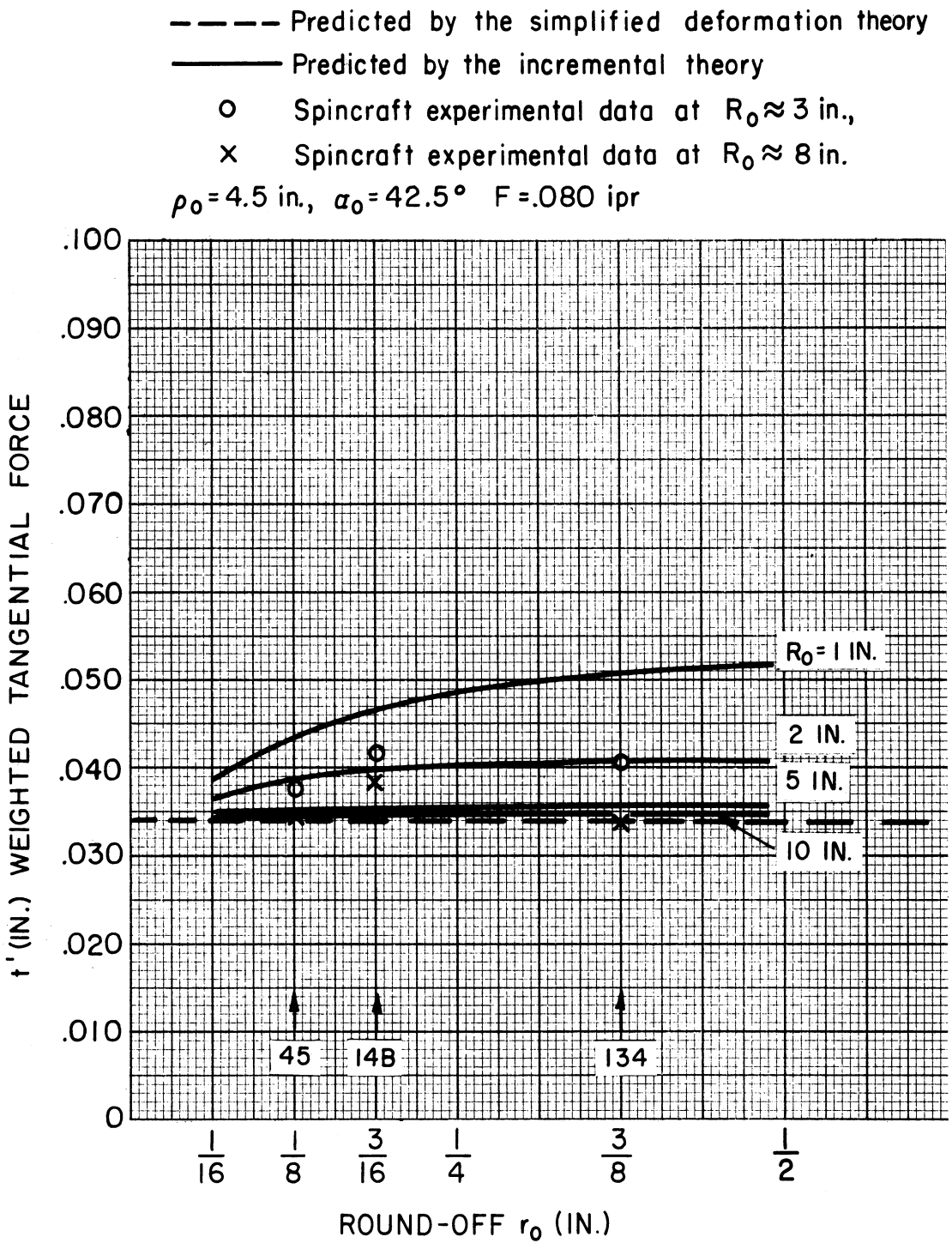

The tangential force $t = \sigma_0 \cdot s_0 \cdot t'$ (lb)

The power $\dot{w} = 2\pi R_0 N t = 2\pi\sigma_0 \cdot s_0 \cdot R_0 \cdot N \cdot t' (\frac{\text{lb in.}}{\text{min}})$

Fig. 34 - Tangential force vs. "Round-off" radius

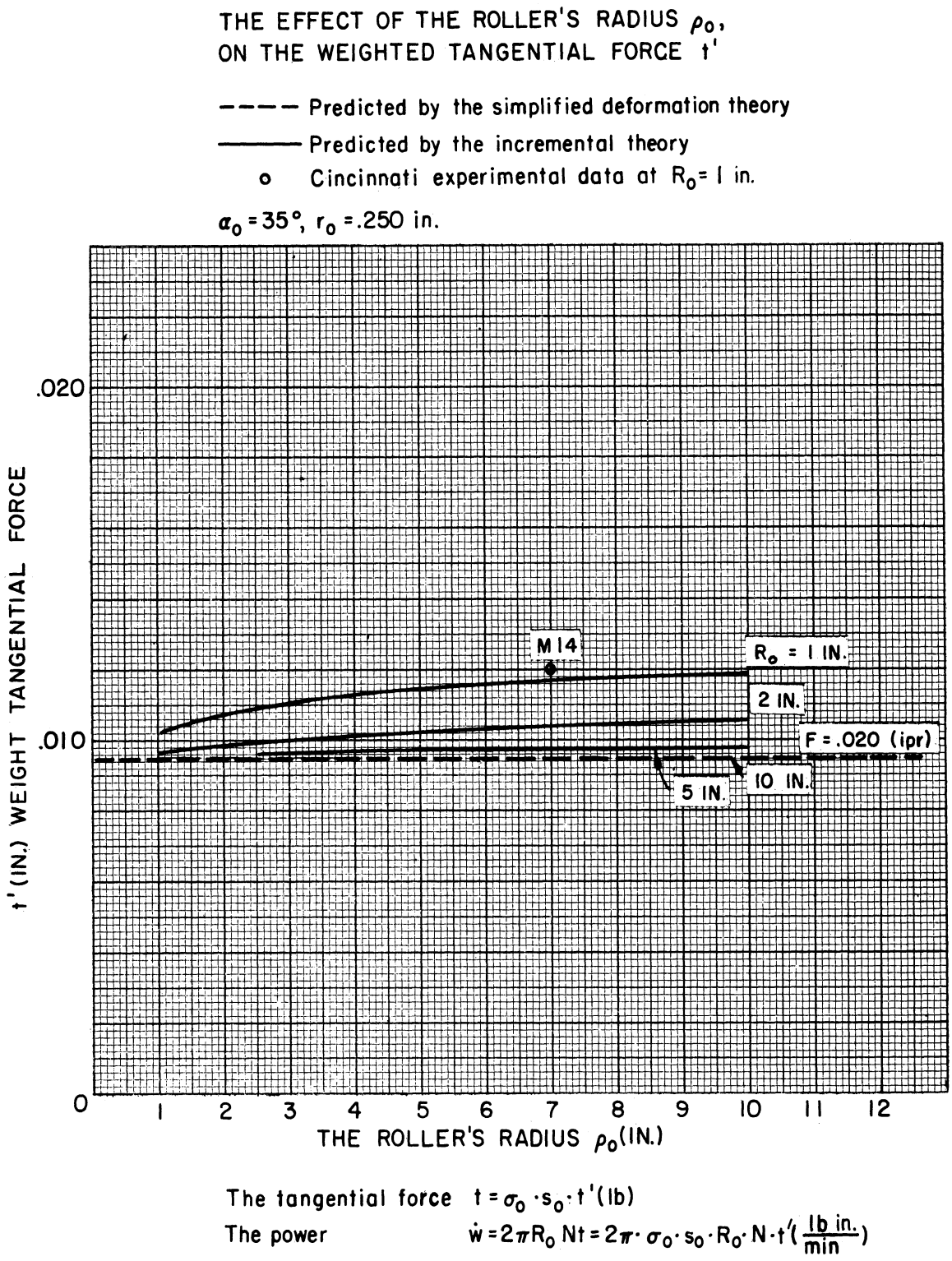

The tangential force $t = \sigma_0 \cdot s_0 \cdot t'$(lb)

The power $\dot{w} = 2\pi R_0 Nt = 2\pi \cdot \sigma_0 \cdot s_0 \cdot R_0 \cdot N \cdot t'$ ($\frac{\text{lb in.}}{\text{min}}$)

Fig. 35 - Curves of tangential forces versus rollers radii

XI. CONCLUSIONS

The effect of the parameters on the tangential force can be summarized as follows.

For any set of parameters, the cone is spun from a minimum R_o at the bend to a maximum R_o at the outer radius. As the radius gets bigger, the tangential force is decreased, but never gets less than the tangential force predicted by the deformation theory. Let this minimum tangential force be called the "most efficient process force." Whenever a change of parameters brings the tangential force closer to the minimum, it will be regarded as making the process more efficient.

(a) The tangential force is linearly dependent on the yield limit σ_o and on the blank's thickness, S_o as long as the thickness is much less than the minimum diameter spun.

(b) Increasing the feed (F) will decrease the efficiency.

(c) The minimum tangential force is proportional to cos α_o. The more deformation is introduced (smaller α_o), the worse is the efficiency.

(d) As the roller round-off radius r_o approaches zero, the efficiency approaches its best value. As r_o gets bigger than about 1/4 in. in practical conditions, a further increase does not change the efficiency very much.

(e) As the roller radius ρ_o approaches zero, the efficiency approaches its best value (see Ref. 11, Part II, p. 255). Here for values of $6" \leqslant \rho_o \leqslant 10"$ the changes in efficiency are very small.

Each one of the effects mentioned above is more noticeable as R_o gets smaller. For very big R_o, the efficiency is approaching its best value for any value of the other parameters.

XII. DISCUSSION

(1) The aim of this study was to find the power consumed in the mechanical spinning of cones.

The information gathered about the process gave the geometrical picture, and some vague idea about the general pattern of the displacements. For the analytical study, a displacement field was postulated, which gave the strain-rates field and the stress-deviator field. The strain-rate field does satisfy automatically the compatability conditions. Because of the very complicated boundaries, which require numerical methods for determination, no attempt was made to check the stresses for satisfaction of the equations of equilibrium. No load-boundary conditions are given, and therefore no steps were taken to satisfy any load distribution. Only the geometrical boundary conditions are satisfied.

Although the above approach is far from giving a rigorous solution for the stress and strain fields, it does give a fairly good approximation of the required work of deformation.

(2) In addition to the solution by the incremental theory, a solution by the deformation theory was given. It is seen that as the radius (R) of the cone increases, the incremental-theory solution approaches the solution given by the deformation theory.

This is explained by the following reasoning. For the incremental theory, in the numerical solution, it was assumed that the ratio γ between the two nonzero strain-rate components was constant. This assumption gave a fairly good value for the power. By assuming γ to be a constant, a

"radial load" was postulated. A "radial load" is one in which each component of strain (and stress) increases with time at the same rate as the others. For this load it has been proven that the incremental theory is in complete agreement with the deformation theory.

In the deformation-theory solution, it was assumed that $\epsilon_{R\theta} = 0$. As the radius of the cone R_o grows bigger, the maximum angle θ of point D on the area of contact gets smaller. The circle R = constant approaches the cord on which $\dot{\epsilon}_{R\theta} = 0$. It is therefore to be expected, as R_o grows and $\epsilon_{R\theta}$ approaches zero, that the solution according to the incremental theory will approach that of the deformation theory.

The deformation-theory solution is therefore a good quick way to find the approximate power requirements.

(3) For the numerical evaluation of the expression for the power, many approximations were made. The original expression could have been evaluated for the exact form of the roller. This would have required a much more complicated program handled by a bigger machine than the IBM 650. This study was mainly conducted to find a way to evaluate the power and to prove the soundness of this way. The shorter and simpler program proved it.

(4) In the set of tests to find the forces, a dynamometer was used in one case and a power measurement in the other. The tangential force measured by the dynamometer showed a wide spread or irreproducibility. The most likely reasons for that spread are: (a) the conditions might not have been under full control, or (b) the dynamometer might be inaccurate.

At any rate, if further tests are to be run, this source of trouble should first be located.

The dynamometer readings were accepted only at the smaller radius R_o = 1 in. As the roller advanced, it started to rub on the flange. In regular operation this rubbing is undesirable and can be eliminated. On any further test, care should be taken to get rid of this rubbing, and have a record of the power for the full length of the operation.

(5) In the set of tests conducted at Spincraft, the power consumption was recorded. If further experiments are to be run, the scaling should be adjusted so that the full range of the current measuring graph paper will be used.

XIII. SUGGESTIONS FOR FUTURE WORK

(1) In the practical setup of a spinning operation, the "radial force" (F_R) and the "feed force" (F_A) are manually adjusted before the operation starts. The adjustment is done by a trial-and-error process. After a cone is spun, its quality and accuracy is measured and the adjustments are made accordingly. This process is lengthy and expensive. A method is desired to predict these forces in advance.

As stated in the introduction, it is believed that the power consumption is the predominant factor dictating the interaction force between the roller and the cone. The tangential component of this force is already computed. The area of contact between the roller and the cone is also defined for magnitude and orientation. It is therefore suggested that by assuming a distribution of the traction over the area of contact one can try to solve for the magnitude and the direction of the interaction force from the tangential component and the contact area. From the interaction force, the radial and feed components can be computed.

(2) The pattern of the deformations was briefly tested in the first set of experiments. Out of this experiment, the shear type of deformation was postulated.

In actual spinning the deformations deviate from the postulated pattern. A more intensive study should be conducted to evaluate the effect of the process variables on the actual deformation pattern.

(3) This study did not deal with the vast field covered by the name of "formability problems." It assumed that the cone can be spun. It is of course obvious, that, taking all the variables constant, success or failure will depend on the right choice of the feed and radial forces. A study of the formability dependence on the cone angle, material, round-off radius, etc., will be beneficial only if those forces are chosen correctly. It is therefore suggested that the external forces required for a successful spinning should be studied first.

(4) The distribution of the stresses and strains under the area of contact should be investigated in detail. Also the "after effect" of spinning is of a great interest. In the study of this "after effect" any effort should be done to determine the residual stresses and the physical and metallurgical properties of the spun cones, and how they are affected by the process variables.

APPENDIX 1

PROGRAM FOR THE IBM 650 DIGITAL COMPUTER

It now remains to solve numerically the following sets of equations. From the deformation theory

$$\dot{W} = \frac{2}{\sqrt{3}} \pi \sigma_o S_o \, NFR_o \cos \alpha_o$$

$$\dot{W}' = 2\pi \, F \, R_o \cos \alpha_o$$

$$t = \frac{\sigma_o S_o}{\sqrt{3}} \, F \cos \alpha_o$$

$$t' = \frac{F}{\sqrt{3}} \cos \alpha_o$$

And from the incremental theory:

$$\dot{W}' = 2\pi \, F \, R_o \sqrt{1 + \gamma} \cos \alpha_o$$

$$+ \sqrt{1 + \gamma} \, R_o F \sin \alpha_o \int \left\{ \frac{R_u \cos \theta - \beta}{\sqrt{r_o^2 - (R_u \cos \theta - \beta)^2}} - \frac{R_l \cos \theta - \beta}{\sqrt{r_o^2 - (R_l \cos \theta - \beta)^2}} \right\} d\theta$$

Boundary of the area of contact

where: $$\gamma = \left\{ \frac{2\pi \cos \theta \, (R \cos \theta - \beta) \, \psi - r_o^2 \sin \theta \cdot (2\pi R \sin \theta + F \sin \alpha_o)}{2\pi \sin \theta \, (R \cos \theta - \beta) \, \psi - r_o^2 \cos \theta \cdot (2\pi R \sin \theta + F \sin \alpha_o)} \right\}^2$$

$$\beta = Fn \sin \alpha_o - \rho_o \cos \alpha_o$$

$$\psi = r_o^2 - [R \cos \theta - (Fn \sin \alpha_o - \rho_o \cos \alpha_o)]^2$$

$$\dot{W} = \frac{\sigma_o S_o}{\sqrt{3}} N \dot{W}'$$

$$t' = \frac{\dot{W}'}{2\sqrt{3}\pi R}$$

$$t = \sigma_o S_o t'$$

For the integration, the boundaries of the area of contact are to be computed. Because the cylindrical portion of the roller is disregarded, area B is omited. Let the remaining area of contact be approximated by the configuration of Fig. A1.

The integration will be done for Area 1 and for Area 2.

For area 1: $R_u = R_B = Fn \sin \alpha_o - \rho_o \cos \alpha_o$

$R_1 = R_A = R_o$

$\theta_u = \theta_E$

$\theta_1 = 0$

For area 2: $R_u = R_B = Fn \sin \alpha_o - \rho_o \cos \alpha_o$

$R_1 = R_{ED}(\theta)$ = R of line ED as a function of θ

$\theta_u = \theta_D$

$\theta_1 = \theta_E$

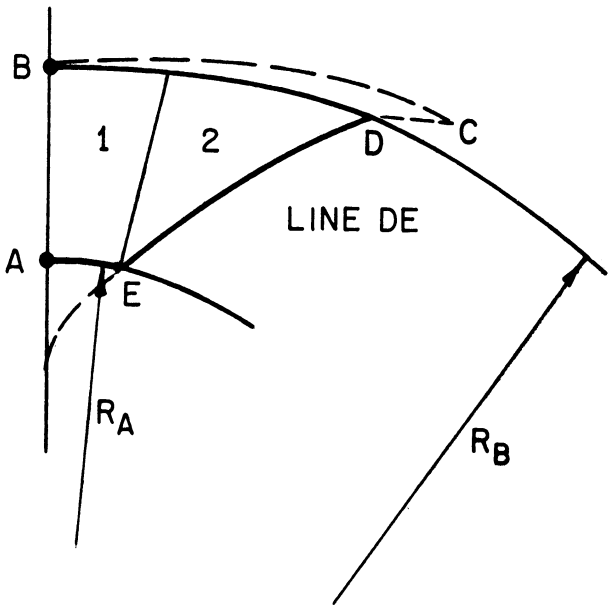

Fig. A1 - Approximated area of contact

For simplicity (and to save drum locations on the computer), let R_1 of area 2 be linearly dependent on θ

$$R_1 = R_o + (R_B - R_o) \frac{\theta - \theta_1}{\theta_u - \theta_1}$$

To solve for θ_E and θ_D, one solves the equation of the torus:

$$G = 0$$

$$Z = b + \sqrt{b^2 - c}$$

$$b = \rho_o \sin \alpha_o + F(n-1) \cos \alpha_o$$

$$c = (R \cos \alpha_o + \rho_o)^2 + [R \sin \alpha_o - F(n-1)]^2 - r_o^2$$

for θ when $R = R_o$ and when $R = R_B$, respectively. Newton's method of successive approximations will be used.

The equation $G(R,\theta) = 0$ is to be solved for R_o, for example. Thus $G(R_o,\theta) = 0$ is given; it is necessary to solve for θ. According to Newton's method:

$$\theta_1 = \theta_o - \frac{G(R_o\ \theta_o)}{G_\theta(R_o\theta_o)}$$

where θ_o is an approximation of the exact solution.

θ_1 is now closer to the exact solution of θ than θ_o is. If θ_o is replaced by θ_1 and the computation is repeated, the solution approaches the exact value more and more closely. Repetition of the operation yields any desired accuracy.

Let:

$$G(\cos\theta) = \left[(R\cos\theta\cos\alpha_o - Z\sin\alpha_o)^2 + R^2(1-\cos^2\theta) - \rho_o\right]^2 + \left[R\cos\theta\sin\alpha_o + Z\cos\alpha_o - Fn\right]^2 - r_o^2 = 0$$

where: $Z = b + \sqrt{b^2 - c}$

$$b = \rho_o \sin\alpha_o + F(n-1)\cos\alpha_o$$

$$c = (R\cos\alpha_o + \rho_o)^2 + \left[R\sin\alpha_o - F(n-1)\right]^2 - r_o^2$$

$$\frac{\partial G(\cos\theta)}{\partial(\cos\theta)} = 2\left[(R\cos\theta\,\alpha_o - Z\sin\alpha_o)^2 + R^2(1-\cos^2\theta) - \rho_o\right] \cdot$$

$$\frac{(R\cos\theta\cos\alpha_o - Z\sin\alpha_o)\,R\cos\alpha_o - R^2\cos\theta}{\sqrt{(R\cos\theta\cos\alpha_o - Z\sin\alpha_o)^2 + R^2(1-\cos^2\theta)}}$$

$$+\ 2\left[R\cos\theta\sin\alpha_o + Z\cos\alpha_o - Fn\right]R\sin\alpha_o$$

The value of cos θ will be solved by Newton's method for any desired R.

$$\cos\theta_1 = \cos\theta_o - \frac{G(\cos\theta_o)}{\frac{\partial G(\cos\theta_o)}{\partial(\cos\theta_o)}}$$

Then the value of θ itself will be computed.

After solving for θ_E and θ_D, the program will solve for the value of Γ at these two points. The valve of Γ at θ_D will be used as a representative value for an average of Γ.

The integration of the terms under the integral is done by Simprson's rule for numeric integration.

As Fig. 18 shows, some work is done along the boundary CDEF, which is not included in the work of deformation under the area of contact. A direct computation of this work seems difficult. To account for this work, it was assumed that the additional work is proportional to the value of $\dot{\epsilon}_{\theta Z}$ and it has been added to the correcting factor under the root $(\sqrt{1 + \zeta})$.

Let the equation for the main power be written as:

$$\dot{W}_p' = 2\pi F R_o \cdot \sqrt{1 + a\cdot\zeta} \cdot \cos \alpha_o$$

where a is a multiplying factor to account for the work at the boundary CDEF.

The "IT"[9] language for an IBM 650 was used in this solution with the library sub-routines of the University of Michigan Statistical Research Laboratory.

Before presenting the program, the assignment list is given:

Table V - Assignment List for the Results

C5 - R_o radius at point A

C6 - ρ_o roller radius

C7 - r_o Roller "round-off" radius

C8 - α_o Half included angle

C9 - F Feed per revolution

C10 - Half the number of intervals used in Simpson integration

Y1 - $\dot{W}1$ Complementary weighted power at area 1

Y2 - $\dot{W}2$ Complementary weighted power at area 2

Y9 - $\dot{W}9$ Principal weighted power

Y11 - $\dot{W}11$ Total weighted power by the deformation theory

Y13 - t' Weighted tangential force by deformation theory

Y14 - t' Weighted tangential force by incremental theory

Y19 - $\dot{W}19$ Total weighted power by the incremental theory

I0 - Identification number for the set of parameters (see Table VII)

I1 - Percent of Y1 of total power

I5 - Percent of Y2 of total power

I4 - Percent of Y4 total power

I9 - Percent of Y9 of total power

I17 - Percent of power by incremental theory to power by deformation theory

C110 - Cos θ_E

C111 - Cos θ_D

C113 - Strain-rates ratio $\sqrt{}$ at point E

C114 - Strain-rates ratio $\sqrt{}$ at point D

Table VI - Genera Assignment List

C1 - R
C2 - θ } coordinates position in space
C3 - Z

C4 - N - Speed in rpm

C5 - R_o - Radius at point A

C6 - ρ_o - Roller radius

C7 - r_o - Roller "round-off" radius

C8 - α_o - Half the included angle of the cone

C9 - F - Feed in ipr

C10 - Half the number of intervals used in Simpson integration

C11 - Sin θ

C12 - cos θ

C13 - sin α_o

C14 - cos α_o

C23 - $\rho_o \sin \alpha_o$

C26 - F sin α_o

C27 - n - The number of revolution passed from time T = 0

C28 - F·n

C32 - $R \cos \theta \cos \alpha_o - Z \sin \alpha_o$

C33 - $\sqrt{(R \cos \theta \cos \alpha_o - Z \sin \alpha_o)^2 + R^2 \sin^2 \theta}$

C37 - $R \cos \theta \sin \alpha_o + Z \cos \alpha_o - Fn$

C42 - $(r_o + \rho_o) \cos \alpha_o$

C46 - $r_o + \rho_o$

C50 - θ_E, θ at the point E

C55 - $F(n-1) \cos \alpha_o$

C56 - $\rho_o \sin \alpha_o + F(n-1) \cos \alpha_o = b$

C57 - F(n-1)

C61, C62, C63, C64 — Temporary variables used to compute the complementary power

C69 - $\rho_o \cos \alpha_o$

C72 - $R_B = Fn \sin \alpha_o - \rho_o \cos \alpha_o$

C73 - $R \cos \theta - (Fn \sin \alpha_o - \rho_o \cos \alpha_o)$

C74 - r_o^2

C75 - $r_o^2 - [R \cos \theta - (Fn \sin \alpha_o - \rho_o \cos \alpha_o)]^2$

C76 - $F \sin \alpha_o + 2\pi R \sin \theta$

C77 - $2\pi [R \cos \theta - (Fn \sin \alpha_o - \rho_o \cos \alpha_o)] \cdot C75$

C78 - (C77 * C11) + C74 * C12 * C76

C79 - (C77 * C12) - C74 * C11 * C76

C80 - C79/C78

C83 - $C = (R \cos \alpha_o + \rho_o)^2 + [R \sin \alpha_o - F(n-1)]^2 - r_o^2$

C94 - (C56 * C56) - C83

C95, C96, C97 — Multiplying factors

C100 - $\sqrt{\frac{1 - C111*C111}{C111*C111}}$

C101 - $G_{ED}(R,\theta,Z)$ The function G = 0 along line ED

C102 - $\frac{\partial G_{ED}(R,\theta,Z)}{\partial(\cos \theta)}$

C103 - C101/C102

C110 - $\cos \Theta_E$

C111 - $\cos \Theta_D$

C113 - $\sqrt{}$ at point E, strain rates ratio at point E

C114 - $\sqrt{}$ at point D, strain rates ratio at point D

C121 - $\rho_o \sin \alpha_o + F(n-1) \cos \alpha_o + r_o$

Y1 - $\dot{W}1$ - Complementary weighted power at area 1

Y2 - $\dot{W}2$ - Complementary weighted power at area 2

Y9 - $\dot{W}9$ - Principal weighted power

Y11 - $\dot{W}11$ - Total weighted power by the deformation theory

Y13 - t' - Weighted tangential force by the deformation theory

Y14 - t' - Weighted tangential force by the incremental theory

Y19 - $\dot{W}19$ - Total weighted power by the incremental theory

I0 - Identification number for the set of parameters (Table VII)

I1 - Percent of Y1 of total power

I2 - Alphabetic variable - "NOT"

I3 - Alphabetic variable - "GOOD"

I4 - Data for machine decission

I5 - Percent of Y2 of total power

I6 - Data for machine decission

I8 - Data for machine decission

I9 - Percent of Y9 of total power

I17 - Percent of power by incremental theory to power by deformation theory

TABLE VII

IDENTIFICATION NUMBER (IO) KEY

$\rho_o \equiv$ C6		$\alpha_o \equiv$ C8			F ≡ C9		$r_o \equiv$ C7		$R_o \equiv$ C5	
Radius, in.	Code	Degrees	Code	Radians	Feed	Code	Radius, in.	Code	Radius, in.	Code
1	01	15	15	0.26179900	.015	15	1/16 = .0625	01	1	01
2	02	21	21	0.36651900	.020	20	2/16 = 1/8 = .125	02	2	02
3	03	30	30	0.52359900	.021	21	3/16 = .1875	03	3	03
4	04	31.5	31	0.54977900	.030	30	4/16 = 1/4 = .250	04	4	04
5	05	35	35	0.61086500	.035	35	5/16 = .3125	05	5	05
6	06	42.5	42	0.74176600	.039	39	6/16 = 3/8 = .375	06	6	06
7	07	45	45	0.78539800	.040	40	7/16 = .4375	07	7	07
8	08	54	54	0.94247800			8/16 = 1/2 = .5	08	8	08
9	09	60	60	1.04719800					9	09
10	10	75	75	1.30899600					10	10

Example:

The variables: ρ_o = 7 in., α_o = 35°, F = .025 ipr, r_o = 1/4 in., R_o = 5 in.

The code: IO = 07 35 25 04 05

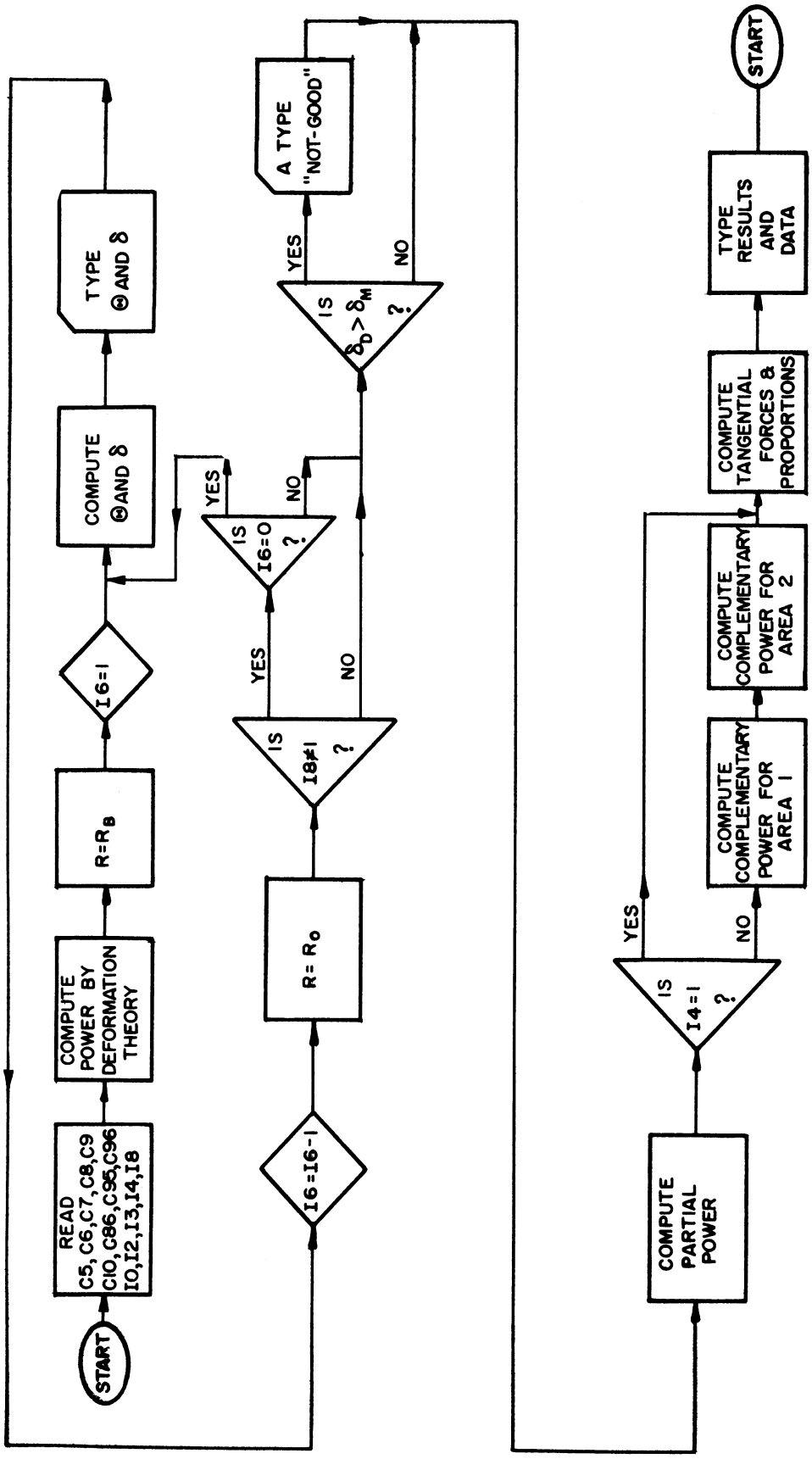

δ - STRAIN - RATE RATIO AT THE POINT DEFINED BY R AND θ

δ_M - CRITICAL VALUE OF δ

δ_D - δ AT POINT D

Fig. A2 - Flow diagram for computer program

Program for Power and Tangential Force

```
0007        I0,C5...C10,C86 READ                F
            C13=Q22EKC8Q                        F
            C14=Q21EKC8Q                        F
            C23=C6*C13                          F
            C69=C6*C14                          F
            C46=C6+C7                           F
            C26=C9*C13                          F
            C42=C46*C14                         F
            C27=(C5+C42)/C26                    F
            C28=C9*C27                          F
            C57=C9*(C27-1.)                     F
            C55=C57*C14                         F
            C56=C55+C23                         F
            C121=C56+C7                         F
            C72=(C28*C13)-C69                   F
            Y11=6.2831853*C5*C9*C14             F
            C1=C72                              F
            I6=1                                F
0006        C12=.99                             F
            C83=((C6+C1*C14)*C6+C1*C14)+((
            C57-C1*C13)*C57-C1*C13)-C7*C7F
            C94=(C56*C56)-C83                   F
            G22IFC94V0.                         F
            C94=0.                              F
0022        C3=C56+Q20EKC94Q                    F
0015        C32=(C1*C12*C14)-C3*C13             F
            C33=Q20EK((C32*C32)+C1*C1*(1.-
            C12*C12))Q                          F
            C37=(C1*C12*C13)+(C3*C14)-C28F
            C101=((C33-C6)*(C33-C6))+(C37*
            C37)-C7*C7                          F
            C102=2.*(((C33-C6)*(C32*C1*C14
            )-C1*C1*C12)/C33)+C1*C13*C37        F
            C103=C101/C102                      F
            C12=C12-C103                        F
            G15IFAC103WC86                      F
            C(110+I6)=C12                       F
            C73=(C1*C12)-C72                    F
            C11=Q20EK(1.-C12*C12)Q              F
            C74=C7*C7                           F
            C75=C74-C73*C73                     F
```

```
                C76=C26+6.283*C1*C11                    F
                C77=6.283*C73*C75                       F
                C78=(C77*C11)+C74*C12*C76               F
                C79=(C77*C12)-C74*C11*C76               F
                C80=C79/C78                             F
                C(113+I6)=C80*C80                       F
0011            TI0TC(113+I6)TC(110+I6)                 F
                I6=I6-1                                 F
                C1=C5                                   F
                G14IFI8U1                               F
                G6IFI6U0                                F
0014            G3IFAC114WC95                           F
0020            Y9=Y11*(Q20EK(1.+C96*C114)Q)            F
                G19                                     F
0003            ATI2TI3                                 F
                G20                                     F
0019            G18IFI4U1                               F
                C12=Q20EK((1.-C12*C12)/C12*C12
                )Q                                      F
                C50=Q23EKC12Q                           F
                C3=Q27EK0.KC50KC10K1K2K9Q               F
0002            C12=Q21EKC3Q                            F
                C61=(C5*C12)-C72                        F
                C62=(C7*C7)-C61*C61                     F
                C62=AC62                                F
0004            C63=C61/(Q20EKC62Q)                     F
                C61=C72*C12-1.                          F
                C62=(C7*C7)-C61*C61                     F
                C62=AC62                                F
0005            C64=C61/(Q20EKC62Q)                     F
                Y1=C5*C9*C13*C64-C63                    F
                G2                                      F
0009            Y1=Y1*(Q20EK(1.+C96*C114)Q)             F
                C100=Q20EK((1.-C111*C111)/C111
                *C111)Q                                 F
                C101=Q23KC100Q                          F
                C3=Q27EKC50KC101KC10K2K10K16QF
0010            C12=Q21EKC3Q                            F
                C61=C5-C72+(C72-C5)*C12*(C3-C5
                0)/(C101-C50)                           F
                C62=(C7*C7)-C61*C61                     F
```

```
                C62=AC62                                F
                C63=C61/(Q20EKC62Q)                     F
                C61=C72*C12-1.                          F
                C62=(C7*C7)-C61*C61                     F
                C62=AC62                                F
                C64=C61/(Q20EKC62Q)                     F
                Y2=C5*C9*C13*C64-C63                    F
                G10                                     F
0016            Y2=Y2*(Q20EK(1.+C96*C114)Q)             F
0018            Y19=AY1+AY2+AY9                         F
                I17=100.*Y19/Y11                        F
                Y13=.5*Y11/1.73205*3.14159*C5F
                Y14=.5*Y19/1.73205*3.14159*C5F
                G23IFI4U1                               F
                I1=100.*Y1/Y19                          F
                I5=100.*Y2/Y19                          F
                I9=100.*Y9/Y19                          F
0012            TI0TY1TY2TY9TY19                        F
0008            TI0TI1TI5TI9                            F
0023            TI0TC5TC6TC7TC8                         F
0001            TI0TC9TC10TC86TC96                      F
0021            TI0TC95TI4TI8TI17                       F
0013            TI0TY11TY9TY13TY14                      F
0017            TI0TC50TC101                            F
                G7                                      F
                H                                      FF
```

COMPARING THE STRAIN RATES

```
0007    I0,C5...C10,C86 READ                    F
        C13=Q22EKC8Q                            F
        C14=Q21EKC8Q                            F
        C23=C6*C13                              F
        C69=C6*C14                              F
        C46=C6+C7                               F
        C26=C9*C13                              F
        C42=C46*C14                             F
        C27=(C5+C42)/C26                        F
        C28=C9*C27                              F
        C57=C9*(C27-1.)                         F
        C55=C57*C14                             F
        C56=C55+C23                             F
        C72=(C28*C13)-C69                       F
        I6=5                                    F
        C43=(C72-C5)/5.                         F
0001    C1=C72-I6*C43                           F
0006    C12=.99                                 F
        C83=((C6+C1*C14)*C6+C1*C14)+((
        C57-C1*C13)*C57-C1*C13)-C7*C7F
        C94=(C56*C56)-C83                       F
        G22IFC94V0.                             F
        C94=0.                                  F
0022    C3=C56+Q20EKC94Q                        F
0015    C32=(C1*C12*C14)-C3*C13                 F
        C33=Q20EK((C32*C32)+C1*C1*(1.-
        C12*C12))Q                              F
        C37=(C1*C12*C13)+(C3*C14)-C28F
        C101=((C33-C6)*(C33-C6))+(C37*
        C37)-C7*C7                              F
        C102=2.*(((C33-C6)*(C32*C1*C14
        )-C1*C1*C12)/C33)+C1*C13*C37 F
        C103=C101/C102                          F
        C12=C12-C103                            F
        G15IFAC103WC86                          F
        C(105+I6)=C12                           F
        C73=(C1*C12)-C72                        F
        C11=Q20EK(1.-C12*C12)Q                  F
        C74=C7*C7                               F
        C75=C74-C73*C73                         F
        C76=C26+6.283*C1*C11                    F
        C77=6.283*C73*C75                       F
        C78=(C77*C11)+C74*C12*C76               F
        C79=(C77*C12)-C74*C11*C76               F
        C80=C79/C78                             F
        C(113+I6)=C80*C80                       F
```

```
0002        TIOTC(113+I6)TC79TC78TC(105+I6
0002        )                                F
            I6=I6-1                          F
            I7=I6+1                          F
            G3IFI7U0                         F
            G1                               F
0003        I6=1                             F
            C43=(1.-C105)/5.                 F
            C1=C72                           F
            C12=1.                           F
0004        C73=(C1*C12)-C72                 F
            C11=Q20EK(1.-C12*C12)Q           F
            C74=C7*C7                        F
            C75=C74-C73*C73                  F
            C76=C26+6.283*C1*C11             F
            C77=6.283*C73*C75                F
            C78=(C77*C11)+C74*C12*C76        F
            C79=(C77*C12)-C74*C11*C76        F
            C80=C79/C78                      F
            C(118+I6)=C80*C80                F
0005        TIOTC(118+I6)TC79TC78TC12        F
            C12=C12-C43                      F
            I6=I6+1                          F
            G4IFC12WC105                     F
            G7                               F
            H                               FF
```

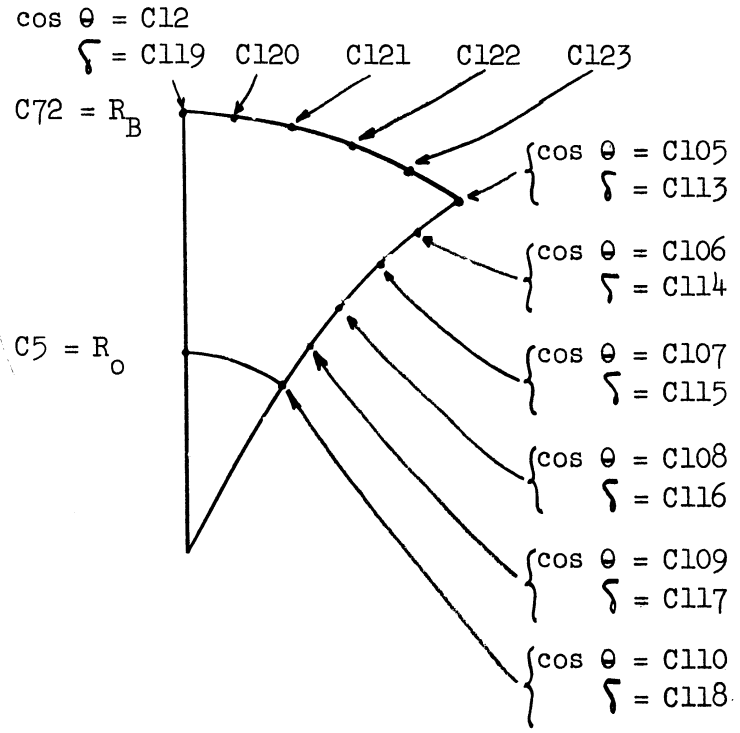

Fig. A3 - Locations of computed strain rates

APPENDIX 2

COMPARING THE TANGENTIAL FORCES FOR SHEAR AND BENDING

The type of deformation that takes place can be assumed as bending or shear, as will be explained immediately. The actual deformation can be anything between these two types (see Fig. A4).

A. BEND

Each point on the central surface remains at its previous radial distance (R) from the axis Z. The straight lines AB and CD remain straight and perpendicular to the surface. AB becomes A'B' and CD becomes C'D'. The length A'B' = AB sin α_o.

B. SHEAR

Shear was described earlier (Fig.6). Each point remains at its previous distance (R) from the center (Z axis). The straight lines AB and CD remain straight with no change in length. However, in this case they are no longer perpendicular to the surface, but parallel to the Z axis.

Let the tangential force be computed with the deformation theory. For shear deformation the tangential force was found to be:

$$t_s = \frac{S_o \sigma_o}{\sqrt{3}} F \cos \alpha_o$$

For pure bending the steps are as follows:

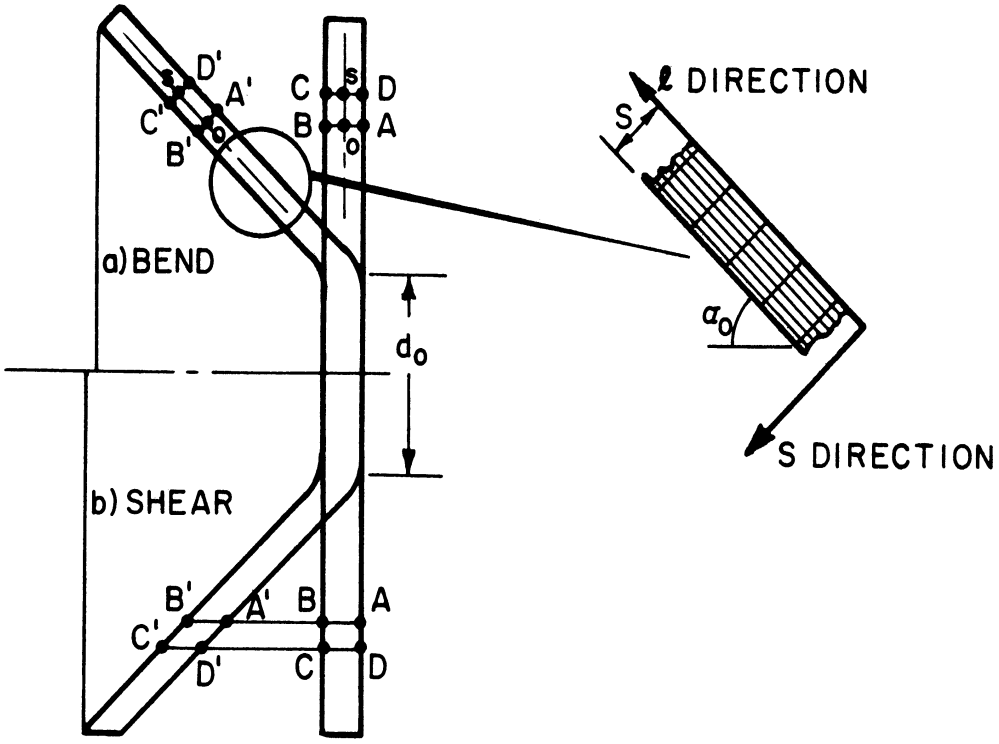

Fig. A4 - The shear and bending strains

Let the power be:

$$\dot{W} = V \int \sigma_o d\phi = V\sigma_o \phi$$

where: V is the volume deformed per minute
σ_o the yield limit under uniaxial tension
ϕ the effective logaritmic strain

Let ϕ_θ be the circumferential logarithmic strain at the middle surface

ϕ_S be the width average logarithmic strain

ϕ_1 be the length logarithmic strain (see Fig. A4)

The middle surface has no circumferential change in length, and therefore

$$\phi_\theta = 0$$

The thickness is reduced from S_o to $S_1 = S_o \sin \alpha_o$

and therefore: $$\phi_S = \ln \frac{S_1}{S_o} = \ln (\sin \alpha_o)$$

From the volume constancy, one gets

$$\phi_1 = -\phi_S - \phi_\theta = -\phi_S$$

The definition of the effective strain in the absence of shear strains

$$\phi = \frac{2}{3} \sqrt{\frac{1}{2} \left[(\phi_\theta - \phi_1)^2 + (\phi_1 - \phi_S)^2 + (\phi_S - \phi_\theta)^2 \right]}$$

in this case reduces to

$$\phi = \frac{2}{3}\sqrt{\frac{1}{2}\left(\phi_S^2 + 4\phi_S^2 + \phi_S^2\right)} = \frac{2}{\sqrt{3}}\phi_S = \frac{2}{\sqrt{3}}\ln(\sin\alpha_o)$$

The volume deformed per minute is:

$$V = 2\pi RN\, S_o\, \Delta R = 2\pi RN\, S_o\, F \sin\alpha_o$$

And thus:

$$\dot{W} = 2\pi RN\, S_o\, F \sin\alpha_o\, \sigma_o \frac{2}{\sqrt{3}} \ln(\sin\alpha_o)$$

And the tangential force

$$t_c = \frac{\dot{W}}{2\pi RN} = 2\, S_o \frac{\sigma_o}{\sqrt{3}} F \sin\alpha_o \ln(\sin\alpha_o)$$

For comparison purposes let a weighted tangential force be defined such that

$$t' = \frac{t\sqrt{3}}{S_o\ \sigma_o}$$

The bending assumption gives

$$t_c' = 2F \sin\alpha_o \ln(\sin\alpha_o)$$

The shear assumption gives

$$t_S' = F\cos\alpha_o$$

Figure A5 describes the weighted tangential force for a feed of .100 ipr for half included angle from $\alpha_o = 0$ to $\alpha_o = 90^o$.

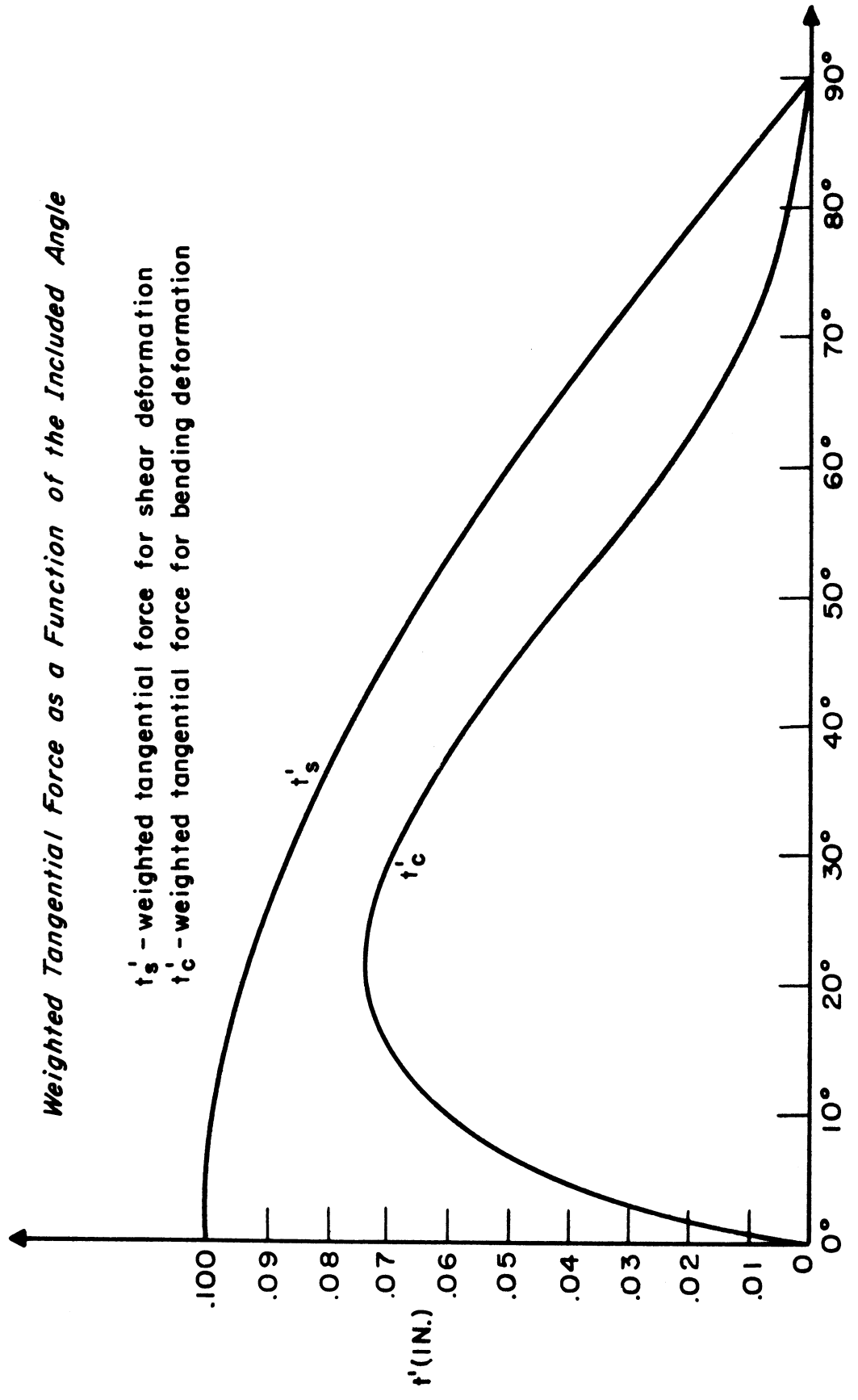

Fig. A5 - Comparing shear deformation to bending

APPENDIX 3

EVALUATING THE YIELD LIMIT

In the analytical approach, Mises material was considered. The characteristics of the material were thus presented by a single value of the yield limit (σ_o). Actual materials, however, have an elastic range as well as a strain-hardening effect. The most convenient way to present the characteristics of an actual material is by its tensile test recording of a uniaxial stress plotted against the strain. For the check of the numerical answer against the experimental power consumed, a representative value for σ_o is to be chosen from the tensile test data.

First, the question of the elastic portion of the deformation was considered. Steel with modulus of elasticity of 30,000,000 lb/inch^2 and with extremely high yield limit of σ_o = 80,000 lb/inch^2 will serve as an example. For this particular material, the strain at yield with uniaxial stress will be

$$\epsilon_{yield} = \frac{80,000}{30,000,000} < .003$$

Let the shear at 45° to the principal axis be found for this case. The shear stress $\tau = \frac{\sigma_o}{2}$

The shear strain is $\gamma = \frac{(1 + \nu)}{E}\tau \approx \frac{1.5}{2} \cdot \frac{\sigma_o}{E} \approx .0022$

Transferring the radians to degrees, one gets maximum shear in the elastic range of .13° for original angle of 90°.

The shear strain at yield is much smaller than the minimum shear (5^{o}) considered in this study. The elastic deformation was considered as part of the plastic deformation. This assumption has only a negligible effect on the numerical results, as is clearly illustrated in Figs. A6 and A7, where a stress-strain curve and a True stress-True strain curve are plotted. Both figures are for the same material. Note the difference in scale on the strain axis.

From the actual recording an average value was picked up and denoted to be the representative yield limit σ_{o}. The value of σ_{o} is neither far from the minimum nor from the maximum value of the stress on the chart.

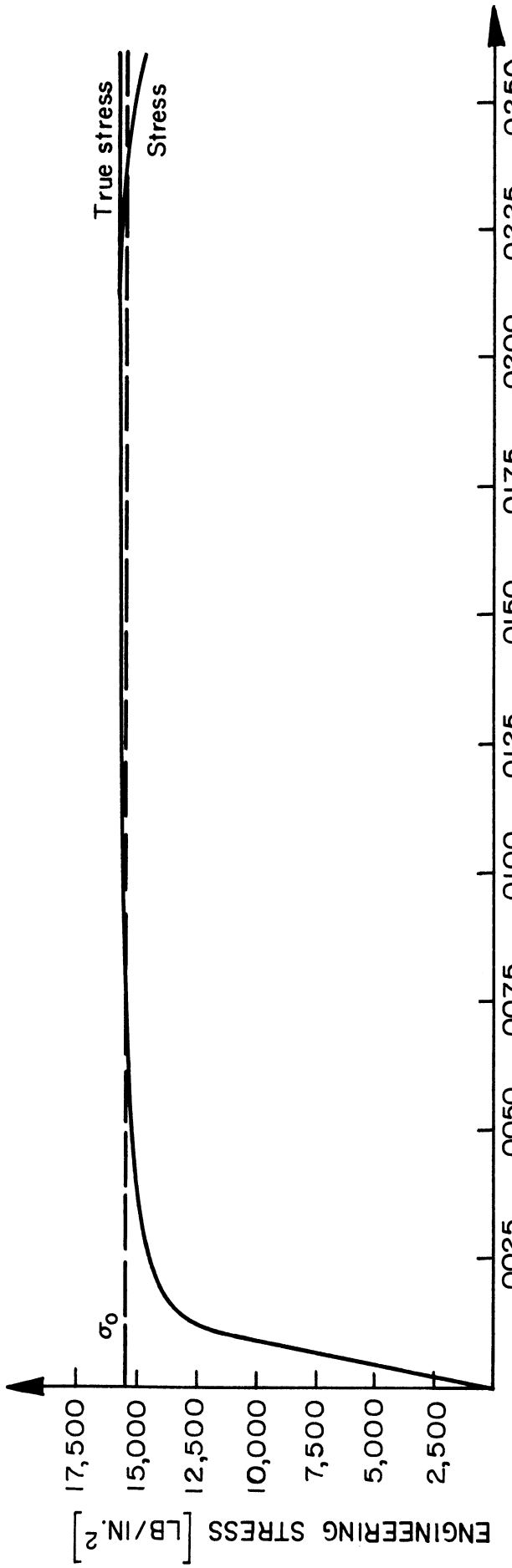

Fig. A6 – Stress-strain curve for Al. 1100-(2S)-H

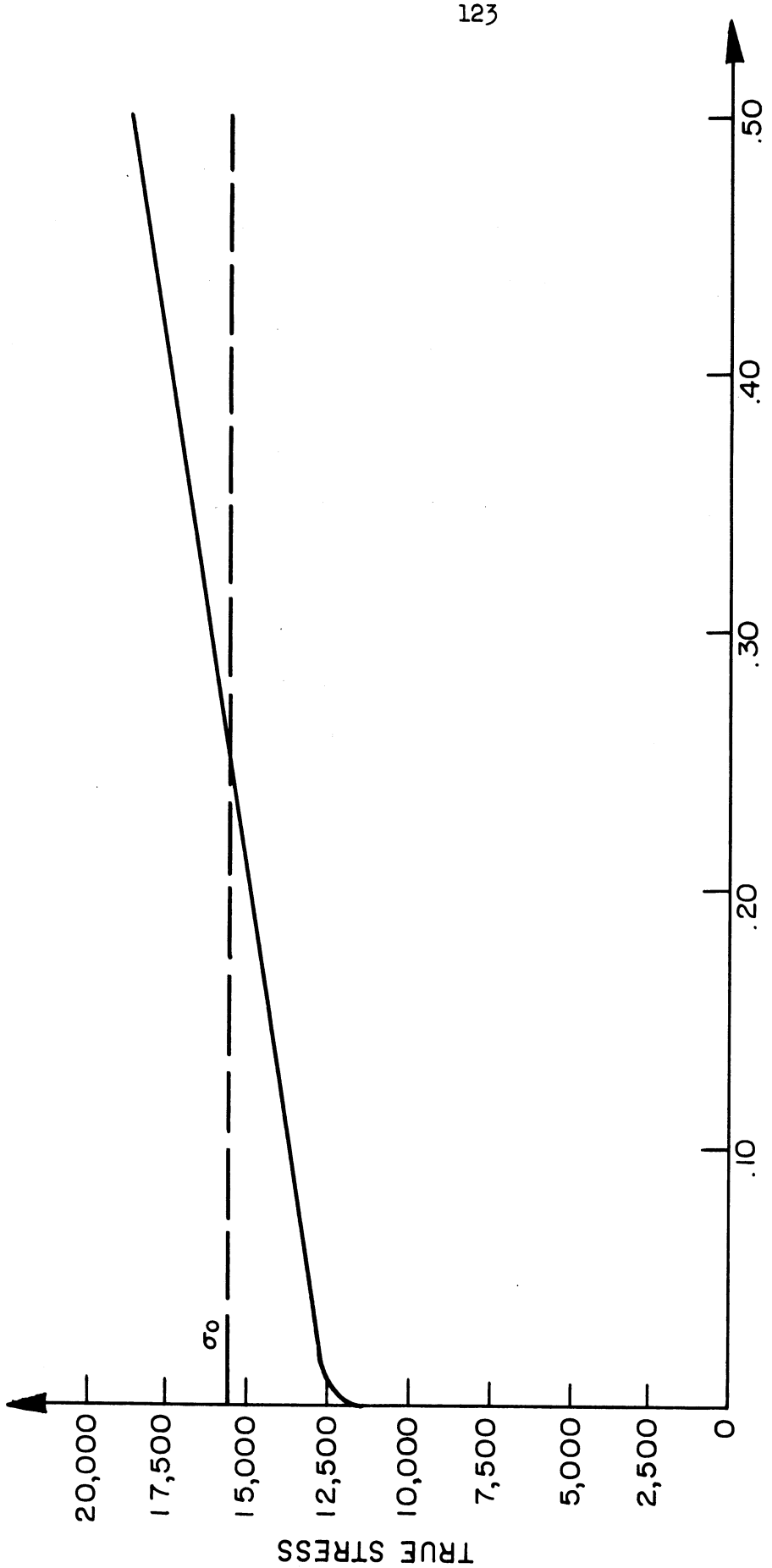

Fig. A7 – True stress-true strain for Al. 1100-(2 S)–H

APPENDIX 4

THE FEED MECHANISM

It has been stated on several occasions that the feed pressure and hence the feed force are kept constant (at about 700 psi) for all sets of variables. It is our understanding that the feed force is a dependent variable. This force is dictated by the resistance of the spun cone which varies with the independent variables like, feed, thickness, cone angle, material, etc. A good flow control valve installed in the proper feed system will give practically constant speed for a wide range of feed forces.

The pressure at the pressure control valve is the outlet pressure of the pump and may also be the inlet pressure to the flow control valve. This pressure is not the feed pressure. For examples of typical Hydraulic feed systems, see Fig. A-8.

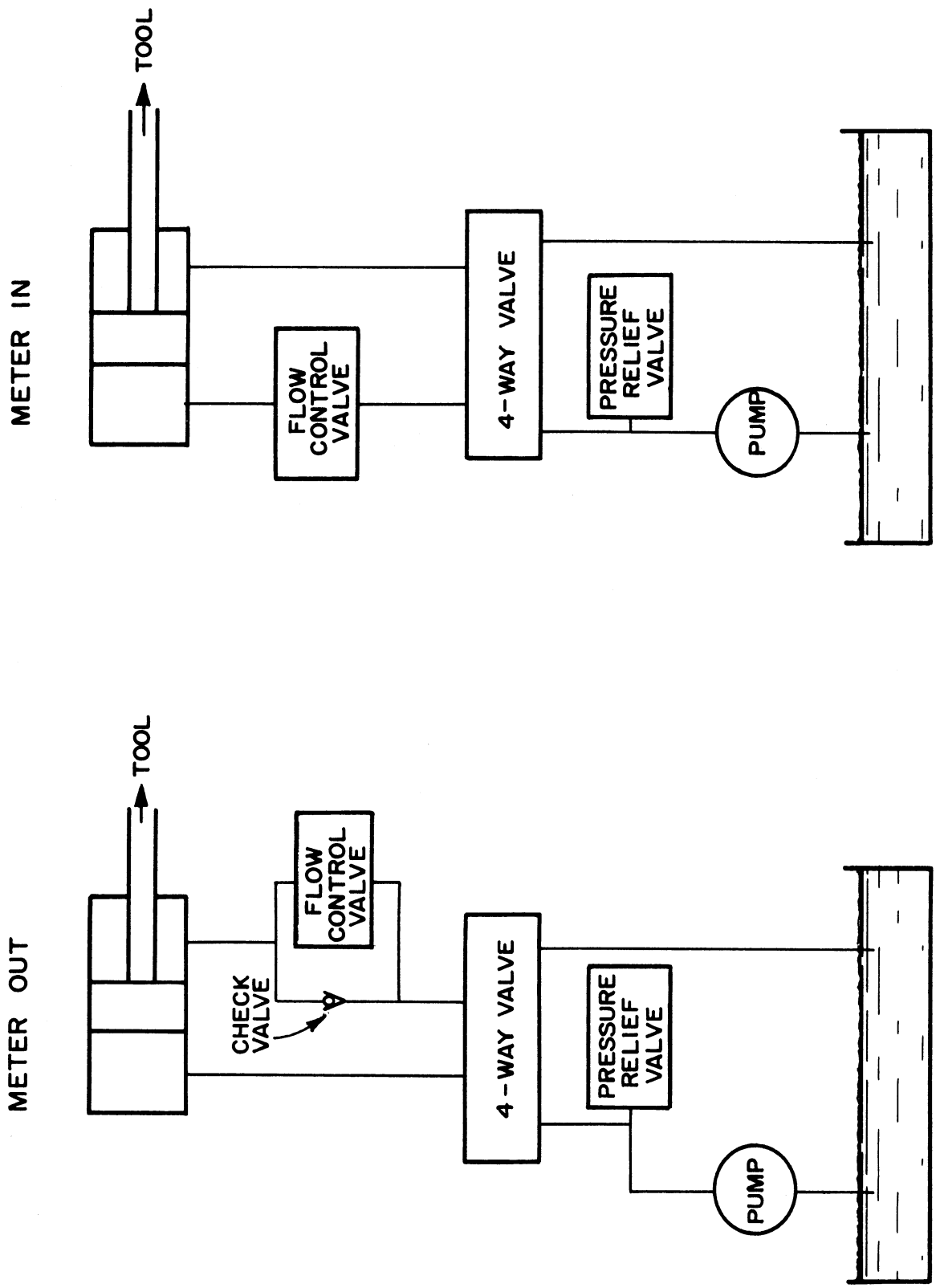

Fig. A8 - Typical feed systems

REFERENCES

1. Avitzur, B., Carleton, W. D., Floreen, S., Hucke, E. E., and Ragone, D. V., Mechanically Spun Cones, Univ. of Michigan Eng. Res. Inst. Report 2621-4-P, Ann Arbor, June 1958.

2. Avitzur, B., Carleton, W. D., Floreen, S., Hucke, E. E., and Ragone, D. V., Hand Spun Cones, Univ. of Michigan, Eng. Res. Inst. Report 2621-5-P, Ann Arbor, November 1958.

3. Banta, F., "Design Possibilities for Automatic Spinning," Product Engineering, 25, 189 (November, 1954).

4. Colding, B. N., Shear Spinning, ASME paper No. 59-PROD-2, 1959.

5. Feola, J. N., Experimental Analysis of Shear Deformation, unpublished M.S. thesis, Syracuse University, January 1955.

6. Heater, J. N., "Power Roll Forming: Machining Without Chips," Tool Engineering, 99-102 (October 1956).

7. Kaplan, W., Advanced Calculus, Addison-Wesley Publishing Company, Inc., Cambridge, Mass., 1953.

8. Lengbridge, J., "Economics of Spinning and Drawing," Tool Eng., 30, 89-94 (1953).

9. Perlic, A. S., Smith, J. W., and Van Zoeren, H. R., Internal Translator (IT), A compiler for the IBM 650, Univ. of Mich. Statistical Res. Lab., January 1957.

10. Prager, W., and Hodge, P. G., Jr., Theory of Perfectly Plastic Solids, John Wiley and Sons, Inc., New York, pp. 30-31, 1951.

11. Reichel, H., "Roll Spinning of Cone Shaped Aluminum Parts," Fertigungstechnik, 8, Part 1, No. 5, 181-184 (April 1958); Part 2, No. 6, 252-260 (June 1958).

12. Rouse, H., (Editor), Advanced Mechanics of Fluids, John Wiley and Sons, Inc., New York, 1959. p. 204.

13. Siebel, E., and Droge, K. A., "Forces and Material Flow in Spinning," Werkstattstechnik und Maschinenbau, 45, No. 1, 6-9 (January 1955).

14. Spencer, L. F., "Why Not Spin It," Iron Age, 167, 105 (March 1951).

15. Sporck, C. L., and Busch, W. H., Floturn - A Production Process as Well as a Development, ASME Paper No. 57-SA-98, 1957.

16. Stalker, K. W., Roll Forming - Chipless Production A. S. M. E. Paper No. 57-A-271, 1957.

17. Streeter, V. L., Fluid Dynamics, McGraw-Hill Book Company, Inc., New York, 1948.

18. Von karman, T., and Biot, M. A., Mathematical Methods in Engineering McGraw-Hill Book Co., New York, pp. 119-130, 1940.

PART II

INVESTIGATION OF MECHANICALLY SPUN CONES

I. INTRODUCTION

In spite of the relatively wide useage of spinning as a forming process there is very little information concerning the mechanical properties of spun pieces. Several investigations (2,3,4,5,6) have noted a considerable increase in hardness after spinning; and a general increase in the tensile strength and fatigue resistance (4,5,6). The effects produced by spinning appear to be quite similar to those produced by cold rolling, with the microstructures of spun pieces show grains elongated in the direction of spinning (5). To date, however, there has been no systematic attempt to determine how the mechanical properties in spun pieces vary with the shape of the piece, amount of reduction, and so forth.

In the present investigation an attempt was made to determine the mechanical properties of spun materials, and also to study the plastic deformations produced by the spinning operation. A series of pieces were mechanically spun on a machine equipped with suitable guages and controls so that the various forces, feed rates, and other variables employed could be measured. After spinning, sections were cut from the pieces and the mechanical properties measured. Also, the dimensions of the pieces were measured before and after spinning in order to determine the nature of the deformations.

II. APPARATUS AND PROCEDURE

Materials

Various materials were used in this investigation. Cartridge brass (70% Cu-30 Zn), 1100(2S) Aluminum, Mild Steel (1020), and 17-7 and AM350 Stainless Steels. The materials were purchased in the form of annealed sheet. The brass sheet was .081" thick. Two thicknesses of aluminum sheets were used, .081" and .125", so that the effect of sheet thickness could be determined. The mild and stainless steels were of about .080" thickness.

Tests on As-Received Sheet

A series of hardness and tensile tests were performed on some of the as-received sheets to determine the variations in properties between sheets of the same material, and also to determine the extent of anisotropy in the sheets.

A further series of tensile tests were performed to determine the effect of the size of the tensile specimen on the tensile properties. The standard ASTM tensile specimens for sheet materials is one inch wide and eight inches long. It was felt that a specimen of this size would be too large for testing many of the spun pieces. Therefore tensile tests were conducted to determine the variation in tensile properties when smaller specimens were used.

Spinning Procedure

The spinning of the test pieces was done by Spincraft Inc. of Milwaukee, Wisconsin. The pieces were spun in the form of truncated cones. A photograph of a typical cone is given in Figure 1.

The different reductions were obtained by varying the apex angles of the cones. The angles selected as shown schematically in Figure 2, were 63°, 85°, and 108°. In all cases the final diameters of the cones were approximately constant, and equal to the original diameter of the unspun blank. This deformation process has also been called stretch-forming, roll-forming, hydroforming, and flow turning by various authors. For the brass cones this diameter was approximately 12 inches. For the aluminum cones of both thicknesses as well as for the steels the diameters were about 16 inches.

To aid in the study of the deformation process a number of cones were spun to 50% or 95% of completeness. These cones are shown schematically in Figure 3.

To further the study of the deformation process, grids were layed out on the blanks of most of the cones that were fully spun. The grids, as shown schematically in Figure 4, consisted of two sets of points laid out at 90° to each other. Originally these grids were placed on the spun surface of the cones, that is to say the surface on which the spinning tool was applied. It was found however, that the tool tended to erase the grids during the spinning operation. The grids then were placed on the under surface of the cones, the surface that laid against the pattern, and these grids were preserved. By measuring the grids in a cone after spinning, the amount

of the deformation of the piece could be ascertained. A series of small holes forming a grid pattern gave unsatisfactory results due to tearing during the spinning.

All of the cones at each set of runs were spun on the same machine and by the same operator. The machine was equipped with pressure guages, and a recording of the pressures, feed rates, spinning tool, was kept for each of the cones. A complete listing of all the cones that were spun and the spinning variables that were used is presented in Table I. The spinning variables listed in this table may be described as follows:

No load RPM - The speed of rotation of the lathe before the spinning tool was applied in revolutions per minute.

Full Load RPM-The speed of rotation of the lathe during the spinning operation (revolutions per minute).

Head-in Psi- The radial pressure (pressure in the cylinder forcing the tool in a direction perpendicular to the pattern) applied by the spinning tool against the piece. (pounds per square inch.)

Table forward iPM - The rate at which the tool traveled forward axially (inches per minute)

Roller radius - (See figure 5)

Roller land - (See figure 5)

Comments - Observations made by the operator during the spinning operation.

The following are kept constant for all the cones.

Table forward pressure = 700 psi = axial pressure, the pressure. parallel to the pattern (see Appendix 4 of Part I).
Clamp pressure = 600 psi - Pressure holding the sheet to the pattern.
Roller material and pattern material were of steel.
The lubricant used was the same Spincraft blend.

Testing of Spun Cones

1. Measurements of Mechanical Properties.

Tensile specimens were cut from all of the fully spun cones. In all cases a 4" specimen was used, as is shown schematically in Figure 6. The specimen had dimensions that are one-half of those of the standard ASTM 8" specimen. Four specimens were taken from each cone for the aluminum and brass only, two in an axial direction and two in a tangential direction (Figure 7). The specimens were taken with their axis either parallel or perpendicular to the original rolling direction of the sheets so that the effect of any anisotropy in the sheets could be determined.

Some curvature was noted in many of the specimens because of the curvature of the material from which they were cut. These specimens were straightened by hand, which might have caused some deviations in the recorded tensile properties. These deviations appear to be unavoidable, but are probably very small since the sheets were already in a heavily cold-worked condition.

Hardness readings were taken on the surface of a number of the cones. In some cases however, the variations in thickness of the specimens made accurate measurements difficult. Micro-hardness measurements were made on the cross sections of several cones in order to measure the variation in hardness from the spun surface to the surface lying against the pattern. Several additional spot tests were also made on some of the cones. These tests will be described later in the report.

2. Measurements of Deformations.

Two types of deformation measurements were made, measurements of the thickness, and measurements on the grids distorting the fully-spun cones.

Thickness measurements were made on all the cones and consisted merely of cutting pieces from the cones and measuring the thickness with a micrometer.

The grid measurements were made before the cones were sectioned and consisted of locating the points in the grid with a divider and measuring the distance between the divider points on a scale. The grid measurements were rather complex because the different types of deformation that were found. A full description of how these various deformations were measured will be given under "Results".

III. RESULTS

1 - Tests on Standard Sheets.

On the basis of the tensile and hardness tests of the as-received sheets it was concluded that the anisotropy in the sheets was negligible. These tests also showed that there was no significant difference in properties between sheets of the same material, except for a slight difference between the .125" and .081" aluminum. In this case it was found that the .125" aluminum had slightly lower tensile and hardness values that the .081" sheet. The average, as-received properties of the three types of sheet are summarized in Table II.

Tests using 4" and 8" sized tensile specimens are also listed in Table II. The results show that the 4" specimen had comparable tensile properties to the standard 8" specimen. In view of this similarity it seems likely that the 4" specimens that were used in the testing of cones, gave properties that would approximate very closely those that would be obtained using the standard 8" specimens.

2 - Mechanical Properties in Spun Cones.

The results of the tensile tests on the spun cones are summarized in Tables II and VI. The results show that the tensile and yield strengths increase as the cone angle decreases, or, in other words, the tensile properties increase with the increasing reductions in thickness, as would be expected. The elongations values decrease with increasing reductions which again is what would be expected.

In general it was found that the orientation of the specimens in the cone had no effect on the tensile properties. In some cones the specimen in

the axial direction had slightly higher tensile strengths than those taken in a longitudinal direction, or vice versa, but these variations were not systematic. These local variations probably represent characteristics of an individual cone only and not the overall process.

In the same manner it was found that the original rolling direction of the sheet had no effect on the tensile properties. This result is not surprising since the anisotropy in the as-received sheets are negligible.

Some difficulty was encountered in performing the tensile tests because of the variations in thickness in the specimen. The magnitude of these thickness variations will be brought out in the next section. It should be pointed out however, that the specimens failed at the region of smallest cross-section. Therefore the reported tensile values are not representative of an average reduction of the cone but of some localized spot in the cone where the thickness was a minimum.

Finally the tensile data show that there is no significant difference in the properties of the .081" and .125" aluminum cones. Hence it would appear that the original thickness of the sheet, at least in the range studied, has no significant effect on the resultant mechanical properties.

The surface hardness of the spun cones are tabulated in Table IV. A great deal of scatter was observed in the hardness readings, and for this reason the average hardnesses only are tabulated in Table IV. The hardness values in general increase with increasing reduction in the expected manner.

Knoop microhardness readings were taken on the cross sections of a number of cones, but once again the scatter in the data tended to mask the

hardness variations. The data for one of these cones is given in Table V, and plotted in Figure 8. Because of the scatter in the data the hardness values are probably best plotted as a band, as shown in Figure 8.

To determine just how much scatter might be found in microhardness readings of this order of magnitude, several pieces of the as-received sheet were cold-rolled to similar reductions in area. Microhardness measurements were then made on these pieces and the average variation was determined by statistical analysis. It was found that the variations in the cold-rolled pieces were of the same order of magnitude as those found in the cones. Hence the variations found in the cones appear to be due primarilly to the inherent scatter in the method of measuring the hardness, and not to variations in the cones themselves.

In general the hardness tabulated in Table V are typical of the cones examined, and the decrease in hardness with distance from the spun surface (Figure 8) is representative of most of the cones. Metallographic examination of the cones also show the variation in hardening under the spun surface. Some photomicrographs of cross-sections of the brass cones are given in Figure 9. The photomicrographs show that the spun surface of the cone is highly deformed, and that the deformation decreases as the distance below the spun surface increases.

As mentioned above, most of the cones showed a progressive decrease in hardness with increasing depth below the spun surface. Several cones however, showed a slight increase in hardness just below the spun surface. (Figure 10) In order to confirm this observation several additional tests were made on one of these cones.

The first test consisted of cutting a small section from the spun portion of one of these cones and measuring the Rockwell B hardness of the spun surface in the conventional manner. A layer of material was then removed from the spun surface by immersing the piece in concentrated nitric acid. The hardness of the newly exposed surface, which lay several thousanths under the original spun surface, was then measured. Another layer was then removed and the hardness measured again. Repeating this procedure several times gave the results shown in Figure 11. The figure shows that there appears to be a distinct increase in hardness in the region under the spun surface.

A second test consisted of immersing the piece in acid before and then measuring the X-ray line breadth after each surface removal. The results are shown in Figure 12. The increase in line breadth shows that the region under the spun surface shows greater distortion than the surface.

In another test, several pieces of the cone were annealed at various lengths of time at 626°F and then examined metallographically. Courser grains were found under the surface which shows that recrystallization began in this region. This would be true only if the region had a larger amount of energy stored up through a larger distortion. Table VI gives yield limit, strength and elongation for cones spun from various materials and than heat treated.

In view of these results it appears that the region under the surface of this cone is really harder than the spun surface. The reason for this behavior is probably due to the partial recovery of the spun surface of the cone. Considerable heat is generated during spinning, and this heat could cause partial recovery of the highly deformed region at the spun surface.

The region under the surface however, would not be subjected to temperatures as high as the surface temperature and therefore would not recover. Thus, after the spinning was completed the region under the surface would be the more distorted because no recovery had taken place.

There does not seem to be any reason in terms of the pressures, feed rate, and other spinning variables, why some cones should show partial recovery while others did not. A possible explanation may be that insufficient lubricant was used during spinning of these pieces. This would increase the friction between the spinning tool and the sheet, and therefore produce a higher temperature in the sheet. Unfortunately there is no data to indicate whether or not this was the case.

In general the mechanical properties of spun pieces are similar to those produced by rolling. A comparison of the properties produced by these two methods are shown in Figure 13 and 14. The agreement seems quite good, particularly for the aluminum. Hardness values are not included in the aluminum data because of the uncertain values found.

Thus for these materials the tensile properties of a spun piece can be estimated by knowing the properties produced by cold rolling to the same reduction.

It must be recognized that the properties are not completely analogous, in view of the variations in work hardening from one surface to the opposite surface in a spun piece. This variation may be very important when one used a spun piece in some service application. Spinning produces a much more non-homogeneous deformation than rolling, and it is only the average value taken through the whole cross-section of the piece which gives comparable properties

with a cold rolled piece. Furthermore, as will be brought out in the next section, there may be large variations in thickness in a spun piece. The tensile properties of a spun piece are dependent upon its minimum thickness and not on the average thickness. Thus care must be taken to locate the region of minimum thickness and use the tensile value for the reduction in this region and not those for the overall reduction when making any estimates. With these limitations in mind however, it would seem fairly reliable estimates of the mechanical properties can be made from rolling data.

3 - Deformations in Spun Cones. (Aluminum and Brass Cones Only)

The thicknesses found in spun cones are summarized in Figure 15. In these plots the thickness of each of the aluminum and brass cones is plotted against the distance from the bend, that is, the radial distance from the spot where spinning began. As would be expected, the thickness of the cones depends upon the cone angle, with the smaller angle cones having smaller thicknesses. In general the results show this, but they also show that there may be considerable variations in thickness in a single cone, and also between cones of the same included angle. In general it appears that the variations in thickness are greater in the brass cones than in the aluminum ones.

Comparison of the results of the 50%, 95%, and fully spun cones for the same cone angle show that the thickness does not appear to be influenced by how much of the cone has been spun. In other words, it does not appear that further spinning on the piece alters the thickness of the portion that has already been spun. Thus the thickness at any region in the cone is

dependent only upon the forces that act on that particular region, and is not affected by deformations taking place in other regions of the cone; that is, the plastic deformation takes place under the roller. Comparison of the thickness measurements of the 0.081" and 0.125" aluminum cones shows that the variations in thickness along the cone are of the same magnitude. Hence, the original thickness to have little effect on this aspect of the deformation. This result is in agreement with the mechanical tests, which showed that the tensile properties were the same.

The grid distortions found in the fully spun cones are shown schematically in Figure 16. As shown in the figure, two types of distortion were found. The first is a radial elongation of the grids because of the increase in length of the sheet in the spun region. The second is a tangential movement of the grids because of the shearing action of the spinning tool. The magnitude of this shear was determined by extending an original line of the grid from the unspun region of the cone and measuring the distance of this new extended line to the grid points. No change in the width of the grids was noticed.

The radial elongations vs the distance from the bend for the various cones are shown in Figure 17. In these figures the distance from the bend was taken at half the distance between the two grid points that give the corresponding elongation value. The overall elongation, that is the elongation between the first and last point, are also plotted. The results show that there are considerable variations in the elongations in the cones. It should be pointed out again however, that the grids were on the underside of the cones

and thus only approximate the deformation of the whole piece. Once again the results on the aluminum sheets also suggest that the elongation is not affected by the original thickness.

Conservation of volume requires that there should be a direct relationship between the elongation and the thickness in a deformed piece. Comparison of the radial elongations and thicknesses in the fully spun cones are presented in Figure 18. The figures show that there is a simple linear relationship between the two.

The tangential movements of the grids are plotted in Figure 19 as a function of the distance from the bend. This distortion should be due to the shearing force, and if the shear force were constant these curves would be straight lines. In the present case it appears that the shearing force was usually lower at the start, and then increased slightly.

The overall results show groups of cones which seem inconsistent insofar as their deformation is concerned. The first set includes 4A1B and 4A1C. In these cones the thicknesses are greater than would be expected on the basis of the thickness values for the other 125" aluminum cones. The operators comments (Table I) note that not much spinning was done on cone 4A1C. The same could probably be said for 4A1B. It is interesting to compare the thicknesses of these two cones with that of the third cone, 4A1A, that was spun to this shape. The thicknesses of the first two cones are on the order of .096" while the thickness of 4A1A is about .066". Thus a difference in thickness of approxiamtely 30% can be found in pieces of the same geometry. The spinning forces were not the same for these three cones, however.

The other data which appears out of line involves the tangential displacements in cones 3A3P and 3A3F, and 4A2M and 4A3E. It seems reasonable to assume that the amount of tangential displacement would increase with increasing reductions in thickness. In these two sets of cones however, the order of displacement is reversed. That is, a cone with greater reductions show less displacement and vice versa. The reason for this effect will be discussed in the following section.

IV. DISCUSSION

In order to correlate the deformations in the cones with the spinning variables used (Table I) it is necessary to establish certain basic assumptions. The first assumption is that spinning may be treated as a plastic flow problem, and that the general laws of plasticity are obeyed. The second assumption is that it would be desirable to spin a piece in which the thickness is constant. This assumption is certainly not the only one that could be made, and the problem could be treated equally well using other apporaches. On the basis of strength, response to heat treatment, and other metallurgical variables, however, this second assumption is a very practical one. For example the age-hardening characteristics and the corrosion resistance could be markedly different in various regions of a spun piece if the deformation was not uniform. The final assumption is that the diameter of the piece after spinning is equal to the diameter of the unspun blank.

On the basis of these assumptions the thickness of the cone should be a function of the cone angle, and can be expressed by the relation:

$$S_1 = S_o \sin \alpha_o$$

where S_1 = thickness of the spun section
S_o = thickness of the blank
α_o = half the cone angle

(For further discussion see Part I of this report)

From the above equation the required thicknesses of the spun sections of the cones can be calculated. These calculated thicknesses are listed in Table III.

A comparison of the calculated thicknesses with those actually found in the cones shows that in most cases there is a distinct departure from the ideal case of constant thickness. Since the thickness of a cone is controlled by the spinning variables that were used, the problem is to show how changes in the spinning variables cause departures from constant thickness. Unfortunately the data are not sufficiently complete to make a fully rigorous solution possible. It is possible however, to show in general how the thickness is influenced by the spinning variables.

On the basis of the thicknesses found in cones of the same geometry but spun to 50%, 95% and fully complete, it would appear that the thickness at any spot in the cone is determined solely by the action of the spinning tool as it went by that spot. In other words, the thickness at any spot is due only to the instantaneous spinning forces acting at the spot. Once the spot has been deformed its thickness is unaffected by the deformations in other regions of the cone. Thus variations in thickness must be due to variations in the applied forces, or to the variation in the resultant force. The resultant force is composed of the three components, Head-in force, Feed force and Tangential force. (See Figure 20) The Feed and Tangential force are dependent variables. The Head-in force is controlled by the operator and is an independent variable in standard practice.

The force which primarilly controls the thickness is the head-in force. Siebel and Droge show that the change in thickness is almost directly proportional to the head-in pressure. Thus one should find that when this force is large the thickness is small, and vice versa. Comparison of the thickness data with the head-in pressures in Table I support this conclusion

quite well. The magnitude of this force is of course dependent upon the material being spun. Thus one finds pressures on the order of 20-25 psi for the aluminum cones and 300-500 psi for the brass cones.

The magnitude of the head-in pressure will also depend upon the cone angle. Smaller cone angles will require a greater reduction in thickness and consequently a greater head-in pressure. The relative change in pressure with thickness will of course be dependent upon the plastic properties of the material.

In the present investigation the applied radial pressures is kept constant during the spinning of each single cone. Thus some question might be raised as to why the thickness of the cone varies as a function of the distance from the bend, if the pressure were constant.

The answer to this question hinges upon the resistance of the sheet to deformation. The resultant thickness depends upon the net force applied to the material, which is the sum of the applied forces (pressures) minus the sum of the resisting forces in the material. These resisting forces are a function of the distance from the bend. Thus the net force and consequently the thickness will be a function of the distance from the bend.

Let us consider the case where the spinning tool is still near the bend. (Figure 21) Ahead of the tool there is a ring of metal which is as-yet unspun. Now this ring of metal will be stressed because of the deformation that has already taken place in front of this ring. These stresses will then act to either aid or hinder the deformation stresses of the spinning tool.

Suppose that the head-in pressure is too small, and that the thickness of the spun region near the bend is therefore larger than the ideal thickness. The outer ring is then being pulled inward and consequently there is a tensile stress built up in the metal at the point where the spinning tool is being applied. This tensile stress favors the reduction in thickness and therefore the thickness should be less at this region. Continued spinning therefore should decrease the thickness of the piece. Further out from the bend however, some point must be reached where the stresses in the ring become too small because the size of the ring has been progressively decreasing. The helping stress will then become progressively smaller until it becomes zero at the final outer edge of the cone. The thickness will therefore become greater toward the outer edge of the cone.

By the same style of reasoning it can be shown that when the head-in pressure is too large that the thickness should be less than the ideal thickness at the region near the bend. In this case however, the unspun ring will exert a compressive stress which will tend to act against the head-in pressure. Thus the thickness will increase with increasing distance from the bend. When the unspun ring becomes small the compressive stresses will be lessened, and thus the thickness will decrease at the outer edge of the cone.

On the basis of this type of reasoning the cone thicknesses should vary as shown schematically in Figure 22. Comparison of the predicted thickness variations with the actual variations found in the cones shows fairly good agreement. For example, cones 4A1A, 4A1C, 5A1F, and 5A1G have thicknesses that are greater than the predicted value, and in these cones the thickness is greater at the bend, decreases slightly, and then increases, in accordance

with the general theory. For cones where thickness is less than the calculated value, the theory does not seem to hold as well. These cones have low thickness values at the bend and increase in thickness with increasing distances from the bend, in the expected manner. A decrease in thickness does not generally occur at some further distance from the bend, as would be predicted. Examples of this type are cones 5A2J, 5A2R, and 6A2S. It may be that some other variable is coming into play in these cases, such as the feed rate, which is tending to further affect the deformation.

The results also show that some of the cones are approaching the ideal condition where the thickness is the calculated thickness. These cones are 3A3DD, 3A2N, 3A1D, 3A3EE, 3A1E, 3A3FF, 3A1H, and 5A15. Thus it seems possible to produce cones of constant thickness by a proper selection of spinning variables. As mentioned previously, the results are not suitable for making a rigorous analysis, but they do show in which direction the variables should be altered in order to produce the calculated thickness.

In addition to the cone angle and the head-in pressure, other variables which will affect the deformation are the feed rate and the roller radius.

While all of the discussion thus far has been based on the thickness of the piece, the other deformations noted in the cones may also be related to the spinning variables in the same manner. The radial elongation was shown to be proportional to the thickness, for example, and thus the elongations in the cones can be explained in the same manner as the thicknesses.

The tangential displacements are also influenced by the spinning variables, but in this case the relationship is more uncertain. The tangential displacements are due to the tangential force produced in the cones. No

direct measurement of this tangential force was made. The tangential force is actually a resultant force obtained from the head-in and axial forces, and thus is dependent upon the magnitudes of these forces. It is also dependent upon the cone angle. Furthermore the tangential force should also be dependent upon the friction between the roller and the cone, and although the same lubricant was used throughout, there is no guarantee that the friction force was constant.

In general one would expect to find that the tangential displacement increases with increasing applied pressures, and this seems to be true in most cases. The exceptions to this were noted in the results section, in which the displacements of several of the aluminum cones do not vary in this expected manner. A number of the spinning variables were altered between these cones and therefore it is not easy to assign the cause the the exceptions to a single variable. From an overall comparison of the variables in Table I, though, it would appear that the difference in the roller diameter is the most likely cause. The cones which show too much deflection were formed with the 3/8" radius roller, while those showing too little deflection were formed with the 1/8" radius roller. In view of the comments already made concerning the effect of the roller radius it would seem likely that a larger radius roller would tend to produce a greater tangential force, and vice versa. A difference in the friction could also account for the differences in deflection however, and therefore a definite conclusion cannot be made. In any case this concern over the tangential displacement may be of little importance since it would not be of major concern in determining the properties of the piece.

The foregoing discussion has been intended to describe how the deformations produced by spinning are controlled by the various spinning variables. It should not be implied however, that the variables that were discussed are the only ones which will affect the deformation. Examples of the variables that have not been systematically varied are; rotational speed of the spinning lathe, spinning tool shape, lubrication, and the initial blank temperature. It is expected that the effects of these variables will be considered in future work.

V. CONCLUSIONS

On the basis of this investigation the following conclusions can be made concerning the properties of spun pieces.

1 - Mechanical Properties.

a) The tensile and yield strength and hardness of spun pieces increases with increasing reductions.

b) The tensile elongations decrease with increasing reductions.

c) The tensile properties and hardness produced by spinning are in general quite similar to those produced by cold rolling to the same reduction. Thus, to a first approximation, the mechanical properties of spun pieces may be estimated from the cold-rolled properties. (Some care must be taken to locate the region of minimum thickness in the spun piece because this is where tensile failure will occur).

d) There is a difference in the degree of cold working from the spun surface to the opposite surface. In some cases the maximum residual distortion may occur beneath the spun surface, presumably because of the recovery of the spun surface.

e) For the thickness studied, the resultant mechanical properties do not depend on the original thickness of the sheet.

2 - Deformations.

a) There may be large variations in thickness of spun pieces, and also large variations in thicknesses between pieces spun to the same reduction.

b) In the same manner there may be large variations in the elongations and the tangential displacements in the pieces.

c) Spinning to 50%, 95% or 100% completion does not appear to alter the deformations in the pieces.

d) It seems that a qualitative picture of the deformation process can be used to describe the deformation process, and how the thickness should vary in terms of the spinning variables. In general the spinning variables should act as follows:

1. The reduction in thickness is controlled primarily by head-in pressure, and large head-in pressure should cause large reductions.

2. Smaller feed rates should cause greater reductions.

3. Small roller radius should increase the reduction, and probably tend to decrease the tangential displacements.

4. The rotational speed of the lathe do not appear to be an important variable, and small changes in speed should not affect the reduction.

REFERENCES

1. J. Lengbridge. Tool Eng. 30 (1953) 89.

2. J. R. Young - Machinery - London 86 (1955) 187.

3. F. L. Banta - Product Eng. 25 (1954) 189.

4. K. Stalker and K. Moore - Am - Machinist 99 (1955) 126.

5. Anon. - Product Eng. 27 (1956) 135.

6. K. W. Stalker - ASME preprint no. 57-A-271 - 1958.

7. E. Siebel and K. Droge - Werkstatt and Mach. 45 - 1955.

8. Ludwigson, D. C., and Hall, A. M., The Physical Metallurgy of Precipitation Hardened Stainless Steels. DMIC Report 111, April 20, 1959, Defense Metals Information Center, Battelle Memorial Institute, Columbus 1, Ohio.

9. Roberts, D. A., Roach, D. B., and Hall, A. M., Physical and Mechanical Properties of Nine Commercial Precipitation Hardenable Stainless Steels. DMIC Report 112, May 1, 1959, Defense Metals Information Center, Battelle Memorial Institute, Columbus 1, Ohio.

10. Roach, D. B., and Hall, A. M., The Engineering Properties of Precipitation Hardenable Stainless Steels. TML Report No. 48, July 20, 1956. Titanium Metallurgical Laboratory, Battelle Memorial Institute, Columbus 1, Ohio

Table I - Listing of Spun Cones

Sample No.	%Spun	No Load RPM	Full Load RPM	Head-in psi	Table Forward l p.m.	Roller Rad.	Roller Land	Comments
5A1G	50	400	400	400	20	1/8"	1/4"	Metal not completely on block. Not enough head-in pressure.
5A1F	95	400	40	300	20	1/8"	1/4"	Metal did not lay down on block completely. Not enough head-in pressure.
5A1J	100	400	400	500	20	1/8"	1/4"	Large amount of head-in pressure required to metal on block.
3A1D	50	350	350	25	28	1/8"	1/4"	Unspun portion of blank distorted due to excess table forward.
3A1E	95	350	350	25	25	1/8"	1/4"	Cut down table forward speed to eliminate wrinkle on end.
3A1H	100	350	350	25	25	1/8"	1/4"	O.K.
4A1C	50	350	350	50	28	1/8"	1/4"	Speed of spindle unchanging during spinning. Not much spinning was done.
4A1B	95	350	320	50	28	1/8"	1/4"	Increase table speed to eliminate spirals.

Sample No.	%Spun	No Load RPM	Full Load RPM	Head-in psi	Table Forward l p.m.	Roller Rad.	Roller Land	Comments
4A1A	100	350	300	50	20	1/8"	1/4"	Table forward speed too slow spirals occur in spinning. Spindle speed drop occurs at maximum stroke.
6A2S	50	440	440	500	20	1/8"	1/4"	O.K.
5A2R	95	440	440	550	20	1/8"	1/4"	O.K.
5A2T	100	400	400	425	20	1/8"	1/4"	O.K.
3A2N	50	400	400	25	48	1/8"	1/4"	O.K.
3A20	95	400	400	25	48	1/8"	1/4"	O.K.
3A2P	100	400	400	20	48	1/8"	1/4"	O.K.
4A2K	50	350	350	50	25	1/8"	1/4"	Table forward was too slow. Spirals occured on large end.
4A2L	95	350	350	50	28	1/8"	1/4"	Table forward too slow spindle speed too slow. Spirals occured.
4A2M	100	400	400	50	48	1/8"	1/4"	Increased speed of spindle and table forward to eliminate spirals. Piece good.

Sample	%Spun	No Load RPM	Full Load RPM	Head-in psi	Table Forward l p.m.	Roller Rad.	Roller Land	Comments
6A3GG	50	500	480	375	20	1/8"	1/4"	Head-in pressure too great. Metal flared back against roller.
6A3HH	95	500	480	300	20	1/8"	1/4"	Head-in pressure still too great. Metal falring back.
5A3JJ	100	500	480	275	20	1/8"	1/4"	O.K.
3A3DD	50	460	460	10	42	3/8"	3/16"	O.K.
3A3EE	95	460	460	10	42	3/8"	3/16"	O.K.
3A3FF	100	460	460	10	42	3/8"	3/16"	O.K.
4A3AA	50	400	400	25	28	1/8"	1/4"	Roller too sharp and head-in pressure too great. Material tends to back over radius of roller.
4A3BB	95	460	460	15	28	3/8"	3/16"	O.K.
4A3CC	100	460	460	15	28	3/8"	3/16"	O.K.

Cone angle $2\alpha_o$ = 85° blanks thickness = .080"

Sample	Material	%Spun P	RPM Start	RPM Final	Head-in psi	Table Forward ipr	Roller Round-off radius
4-1	Al.5086	95	350	335	105	.040	1/8
4-2	17-7 PH S.S.	95	350	325	850	.040	1/8
4-3	AM350 S.S.	95	350	325	950	.040	1/8
4-4	Mild Steel	95	340	332	450	.040	1/8
4-5	Al-1100	95	440	430	25	.080	1/8
3-1	Al-1100	95	440	435	60	.080	1/2

For all Specimens

Table forward psi = 700 (See Appendix 4 of Part 1)

Clamp psi = 600

Lubricant = Socony Spincraft Blend #1.

Legend

In the sample numbers, the first number refers to the material.

No. 5 and 6 = brass

No. 3 = .081" aluminum

No. 4 = .125" aluminum

TABLE II

Tensile Tests Data on As-Received Sheets

Material	Total Length	Width Test Section	Avg. Tensile Strength psi	Avg. Yield Strength psi	% Elong.
Brass					
.081" thick	9"	.562"	47,650	16,400	57
	8"	.500"	47,500	16,800	65
	7"	.423"	48,500	17,000	65
	6"	.500"	47,700	17,500	67
	6"	.378"	48,200	19,500	63
	5"	.338"	48,100	17,800	70
	4"	.500"	47,800	17,800	70
	4"	.250"	47,100	17,200	65
	4"	.125"	52,100	20,300	60+
Aluminum					
.081" thick	8"	.500"	13,600	5,400	41
	6"	.375"	13,600	5,700	40
	4"	.250"	13,600	6,200	37
Aluminum					
.125" thick	8"	.500"	11,100	4,100	40
	4"	.250"	11,600	4,600	38

TABLE III - Tensile Properties of Spun Cones

Each value is average of two specimens, one parallel and one perpendicular to the original rolling direction.

radial direction = direction from center of cone to outer edge.
tangential direction = direction parallel to outer edge of cone or perpendicular to radial direction.

Cone	Cone Angle	Thickness Experimental	Thickness Theoretical	Tensile Strength (psi)	Yield Strength psi.2% offset	Elongation % 1"
Brass 5-A-1J--radial dir.	63°	.042	.0423	79,900	75,100	7
tang. dir.	63°	.042		86,000	68,000	9
Brass 5-A-2J--radial dir.	85°	.051	.0548	77,800	62,500	10
tang. dir.	85°	.051		80,000	63,200	*
Brass 5-A-3J--radial dir.	108°	.063	.0655	69,500	66,200	9
tang. dir.	108°	.063		71,100	57,800	12
.081" Al 3A1H-radial dir.	63°	.044	.0423	18,500	17,190	9
tang. dir.	63°	.044		18,600	17,250	9
.081" Al 3A2P-radial dir.	85°	.051	.0548	17,700	16,150	10
tang. dir.	85°	.051		17,900	16,900	9.5
.081" Al 3A3FF-radial dir.	108°	.062	.0655	15,950	15,050	12
tang. dir.	108°	.062		15,800	15,070	11
.125" Al 4A1A-radial dir.	63°	.072	.0653	19,200	18,400	8.5
tang. dir.	63°			19,200	17,950	10
.125" Al 4A2M-radial dir.	85°	.080	.0845	18,250	17,300	9.5
tang. dir.	85°			18,950	17,600	10.5
.125" Al 4A3CCradial dir.	108°	.098	.1010	16,150	15,050	13.5
tang. dir.	108°			16,100	14,900	15

* Both specimens broke at gage marks.

MECHANICALLY SPUN

Table IV

Hardness of Spun Surface of Mechanically Spun Cones

Cone	Average Hardness Rockwell B Scale
63° Brass	87
85° Brass	85
108° Brass	80
	Average Brinnel Hardness No. 500 Kg load 10 mm ball
63° 081" Al	30
85° 081" Al	28
108° 081" Al	27
63° 125" Al	29
85° 125" Al	27
108° 125" Al	27

Table V - Microhardness Readings on Cross-sections of cone 6A3GG.
Knoop indenter, 1000 gram load.
Positions 1 and 2 are in the unspun section of the cone. The remaining positions are all at a various region in the spun section.

Position on Specimen	Total thickness (relative units)	Distance from Spun surface (relative units)	Knoop Hardness Number
1	202	25	79.9
		65	83.4
		105	76.2
		145	77.7
		185	78.8
2	200	20	75.2
		60	83.0
		100	80.7
		140	81.1
		180	79.5
3.	180	20	164.6
		50	157.1
		80	166.9
		110	159.2
		135	143.4
		160	133.1
4	174	20	176.4
		48	165.7
		76	170.4
		104	168.0
		132	139.0
		154	133.9
5	170	17	182.8
		55	180.2
		83	171.5
		101	163.5
		129	149.0
		153	123.8
6	160	15	171.5
		42	178.9
		69	165.7
		96	168.0
		123	153.0
		145	152.0

Position on Specimen	Total thickness (relative units)	Distance from Spun Surface (relative units)	Knoop Hardness Number
7	158	15	182.8
		42	188.2
		69	182.8
		96	178.9
		123	157.1
		145	149.0
8	152	18	185.4
		48	180.2
		78	186.8
		108	165.7
		134	149.0
9	147	18	193.7
		48	186.8
		78	175.2
		108	169.2
		129	155.0
10	146	18	198.1
		48	180.2
		78	178.9
		108	160.2
		130	154.0
11	149	18	188.2
		48	184.1
		78	177.7
		108	158.1
		130	145.2

TABLE VI

Tensile Test Data

(For Various Materials and Various Heat Treatment)

Cone Included Angle $\alpha = 2\alpha_o = 85^\circ$

Run No.	Material	Heat Treatment			Yield Limit	Ultimate Strength	Percent Elongation
		Name	Description	Criteria	Psi	Psi	%
135	1100 Al	Annealed			6000	13,600	40
		Work Hardened	Spun cone, about 30% reduction of area	.2% Offset	16,000	17,200	10.8
		Stress relieved	420°F for 1 hour and air cooled		13,500	16,400	15.6
4-4	M.S.	Normalized	1650°F for 1 hour and air cooled	upper yield limit	49,800	67,300	14.0
		Stress relieved	1050°F for 1 hour and air cooled		59,000	63,000	18.0
			950°F for 1 hour and air cooled		65,500	68,000	15.0
			850°F for 1 hour and air cooled		67,000	71,000	13.0
		Work Hardened	Spun cone, about 30% reduction of area	.2% offset	68,000	75,000	7.7
4-2	17-7 S.S.	Stress relieved	1050°F for 1.5 hrs and air cooled	.2% offset	125,000	182,500	20
		R.H.* 950°F	1750°F for 10 min. and air cool, 2 hrs. interval, -100°F for 8 hrs., 30 min interval 950°F for 1 hr and air cooled		220,000	228,000	12.6

Run No.	Material	Heat Treatment		Yield Limit	Ultimate Strength	Percent Elongation
		Name	Description Criteria	Psi	Psi	%
		T H* 1050°F	1450°F for 1.5 hrs. and air cool, 1050°F for 1.5 hrs and air cool	176,000	185,000	12.6
		Work Hardened	Spun cone, about 30% reduction of area	120,000	180,000	19
4-3	M350 S.S.	SCT*	1710°F for 30 min and water cool,-100°F for 3 hrs.,850°F for 3 hrs and air cool	214,000	229,000	20.6
		Double Age *	1375°F for 3 hrs and air cool. 850°F for 3 hrs and air cool	162,000	193,000	20
		CRT*	850°F for 3 hrs and air cool	186,000	224,000	18.8
		Work Hardened	Spun cone, about 30% reduction of area	138,000	225,000	22

* See Refs. 8, 9, and 10.

Fig. 1. Photograph of spun cone.

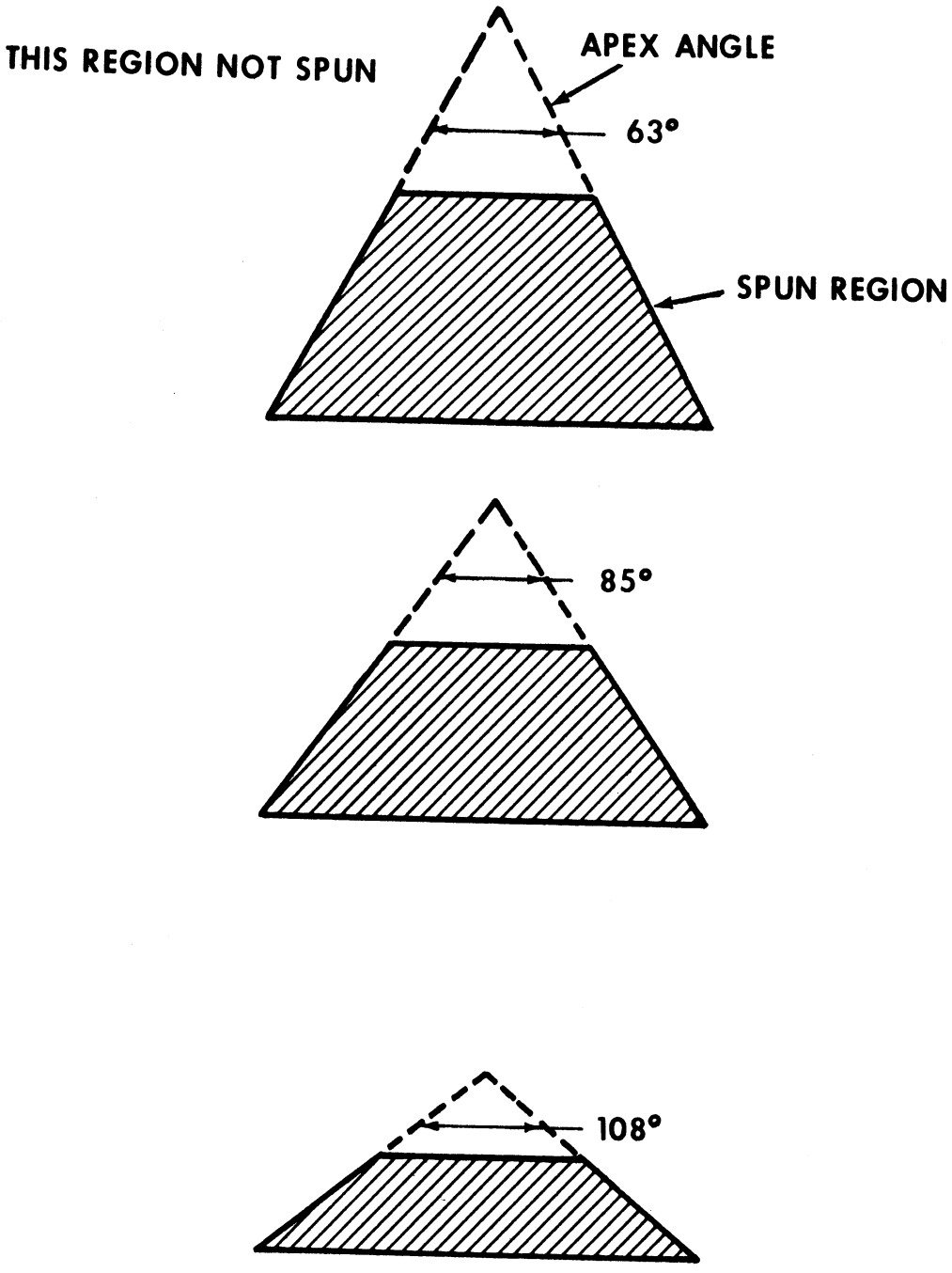

SCHEMATIC VIEW SHOWING CONE ANGLES

FIG. 2

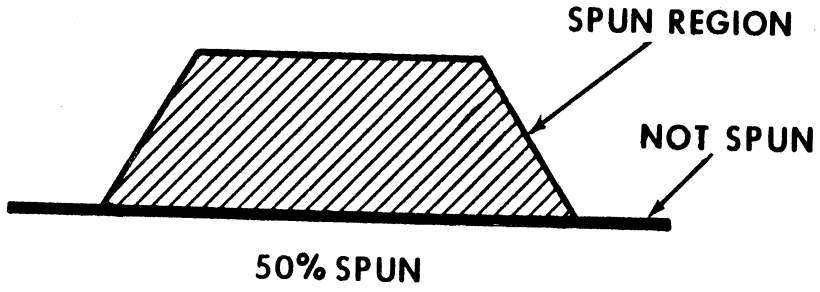

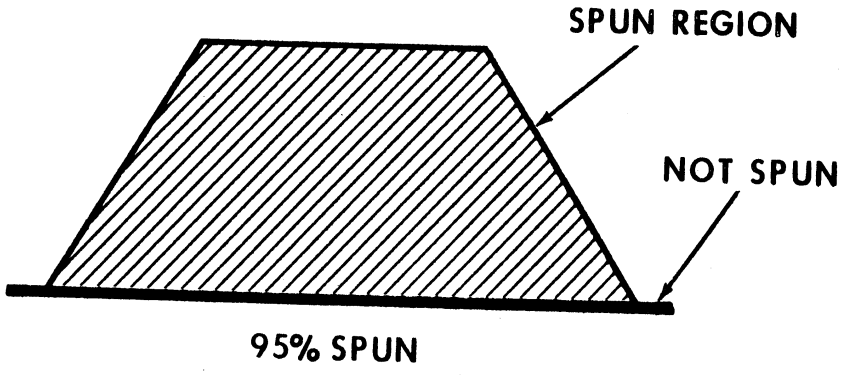

SCHEMATIC VIEW SHOWING 50% AND 95% SPUN CONES

FIG. 3

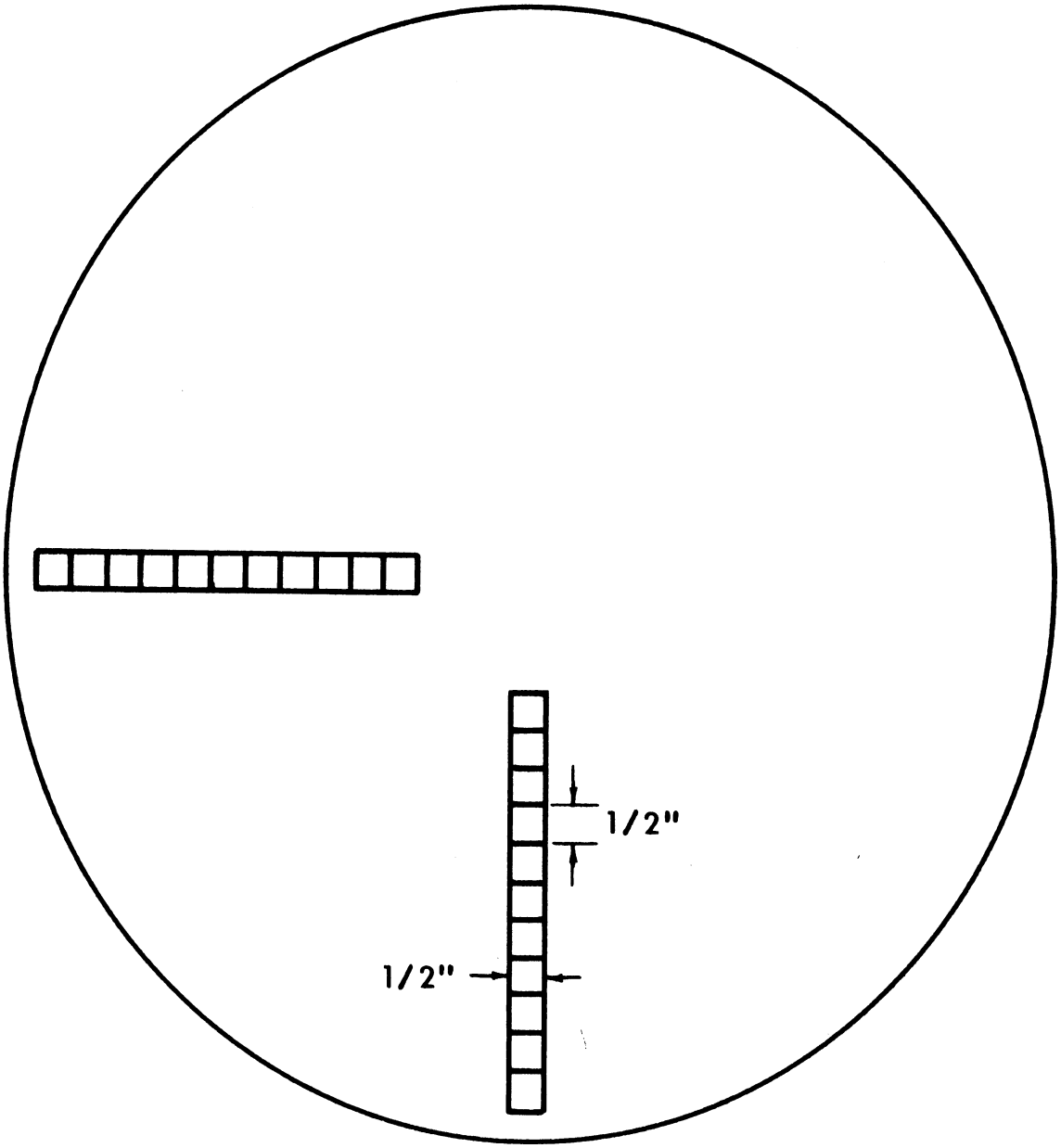

LAYOUT OF GRIDS ON BLANKS BEFORE SPINNING

FIG. 4

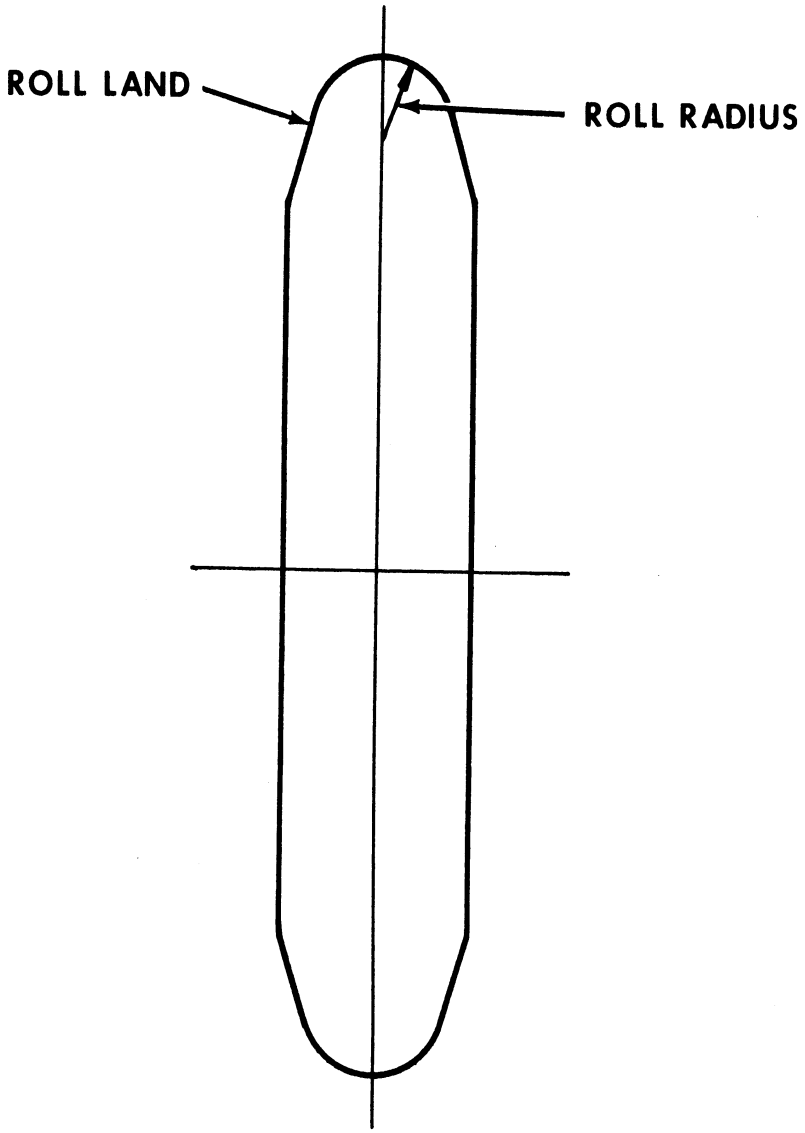

SCHEMATIC VIEW OF ROLLER
SHOWING RADIUS AND LAND

FIG. 5

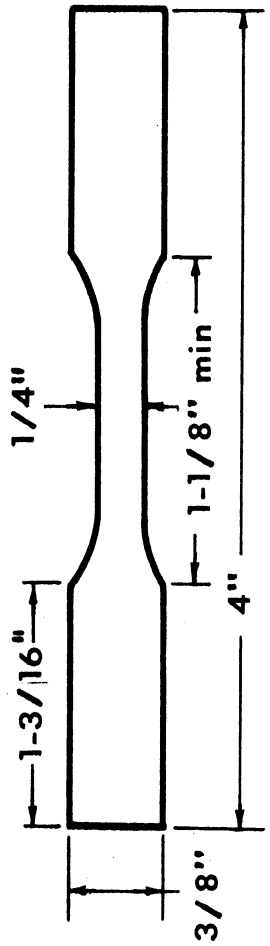

FOUR INCH TENSILE SPECIMEN

FIG. 6

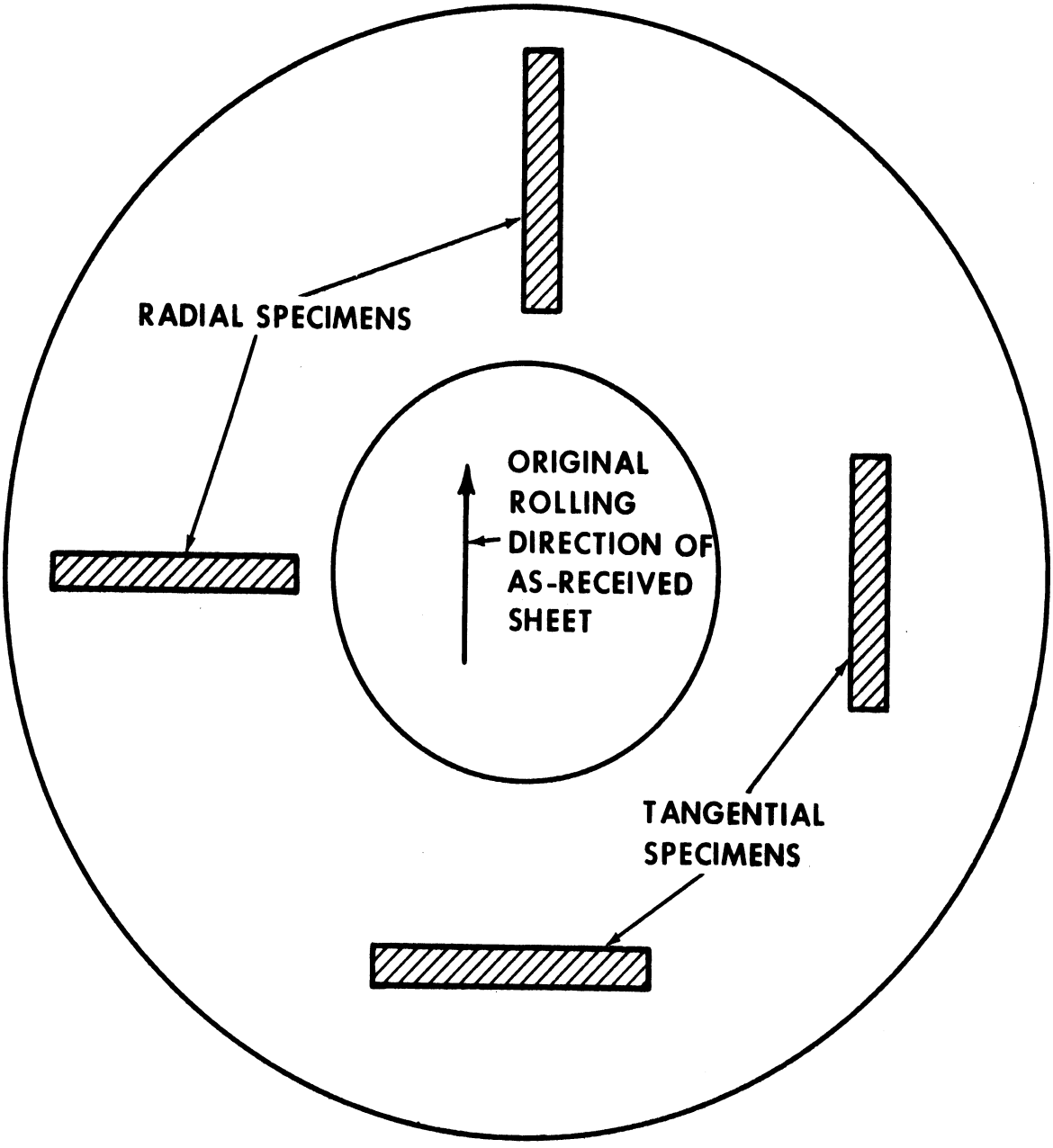

LOCATIONS WHERE TENSILE SPECIMENS WERE CUT FROM CONES

FIG. 7

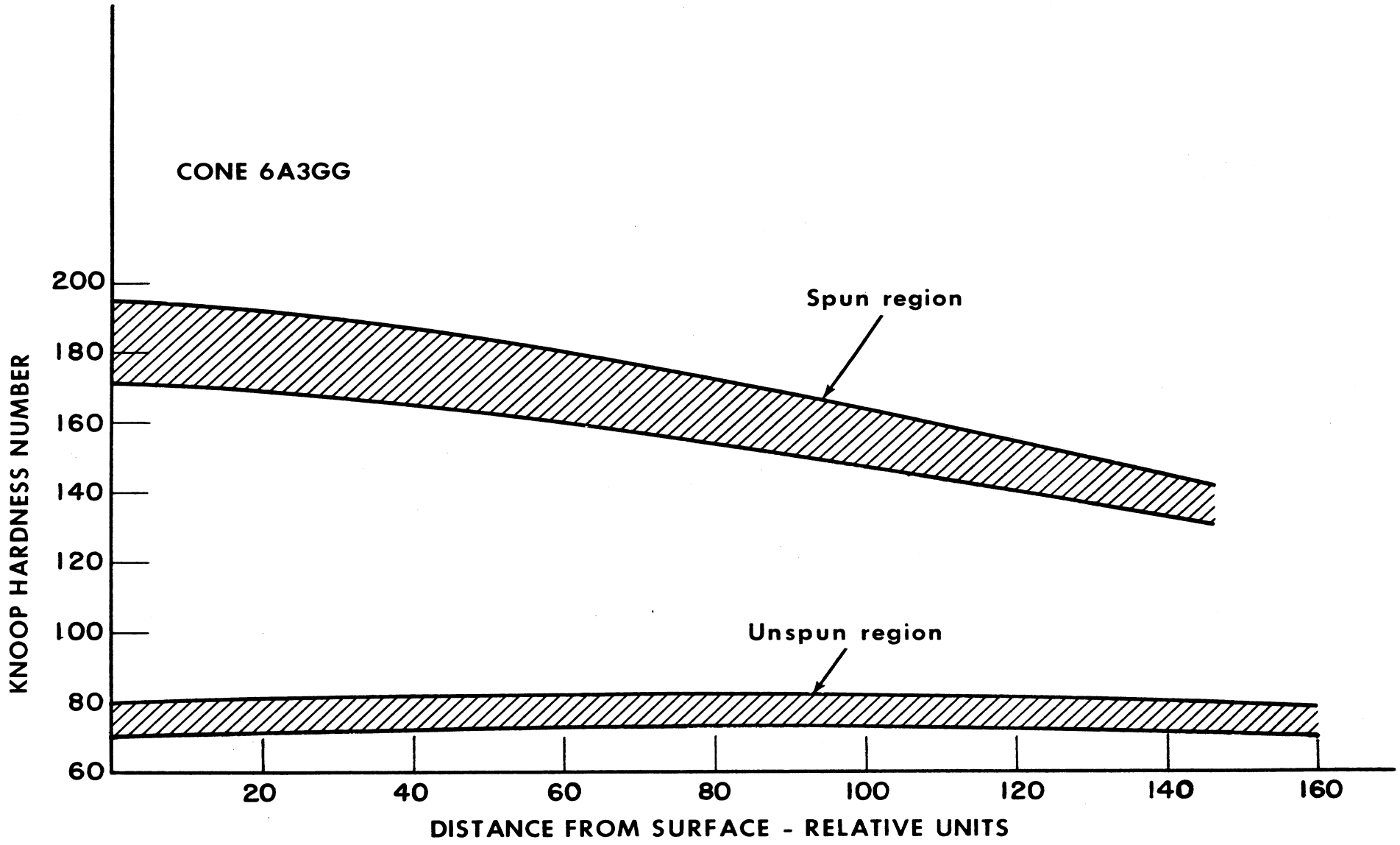

VARIATION IN MICROHARDNESS WITH DEPTH BELOW SPUN SURFACE

FIG. 8

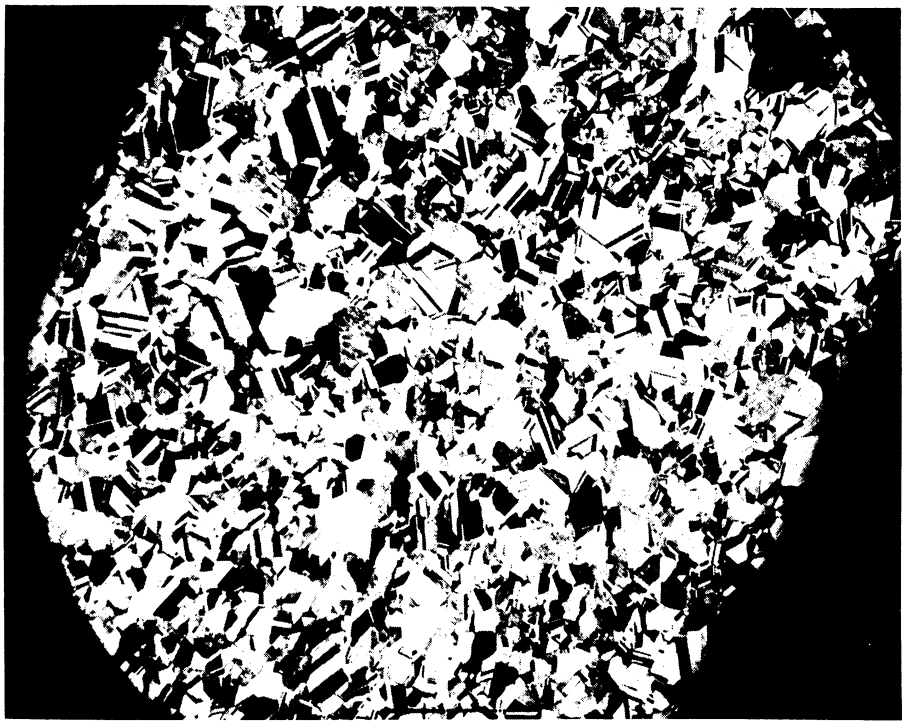

(a) Unspun center portion of cone.

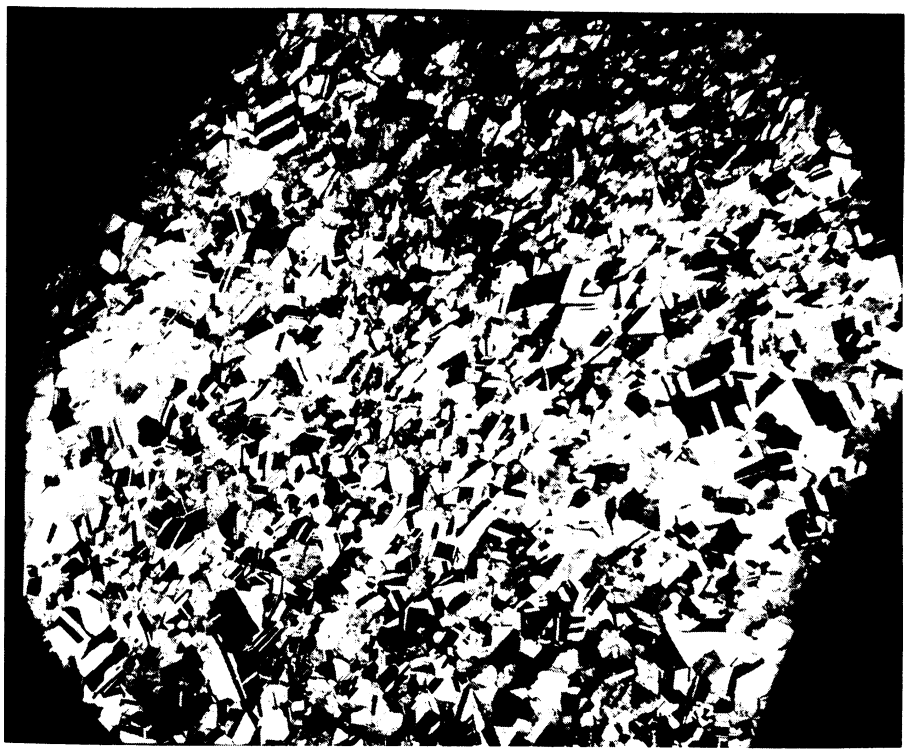

(b) Region at bend of cone. Note beginning of cold worked microstructure.

Fig. 9. Photomicrographs of cone 6A3GG. All photos 100X. Pictures tilted to show complete cross section.

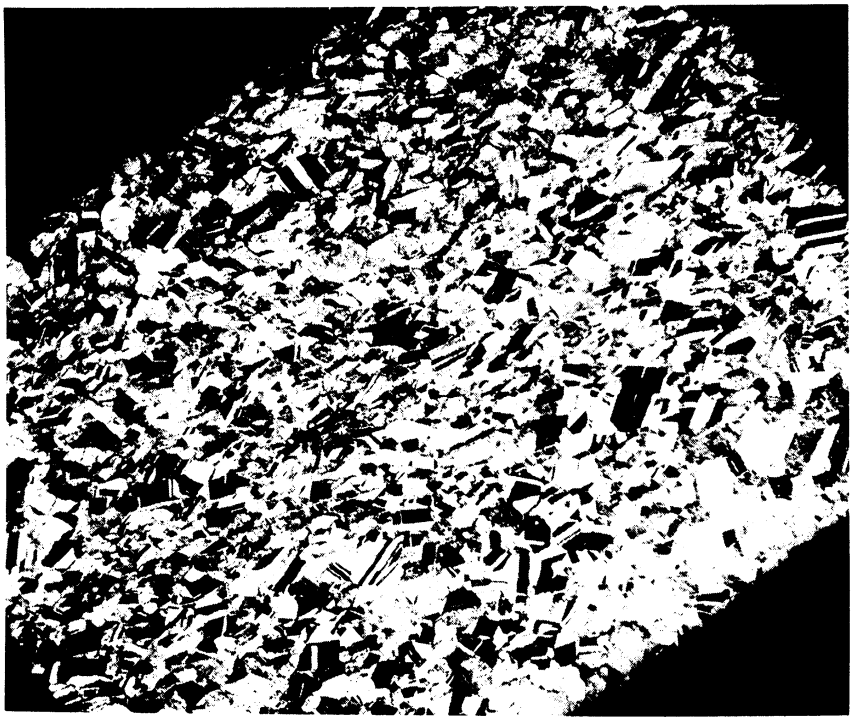

(c) Spun region of cone. Note difference in microstructure at top (spun surface) and bottom.

Fig. 9. Continued

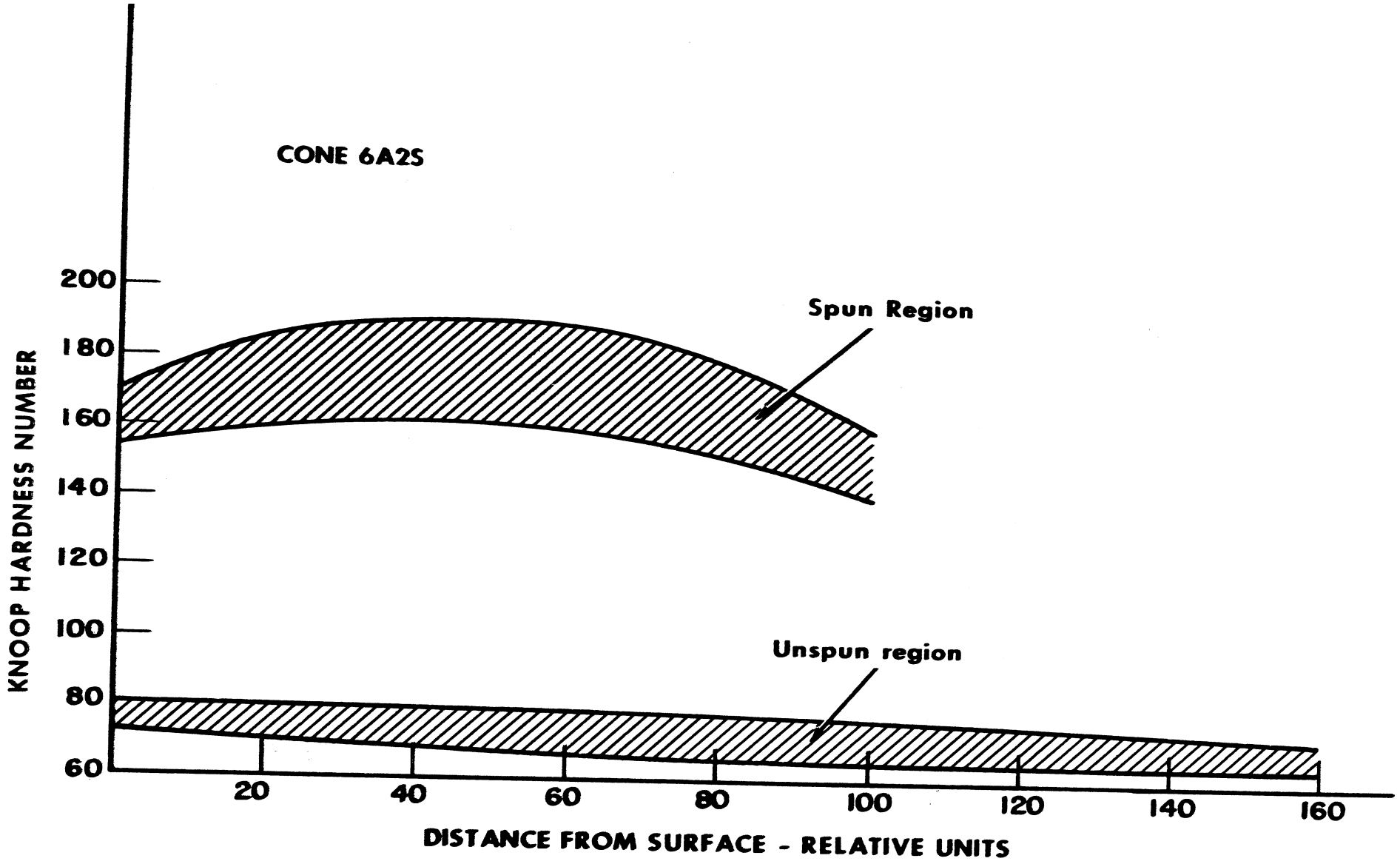

VARIATION IN MICROHARDNESS WITH DEPTH BELOW SPUN SURFACE

FIG. 10

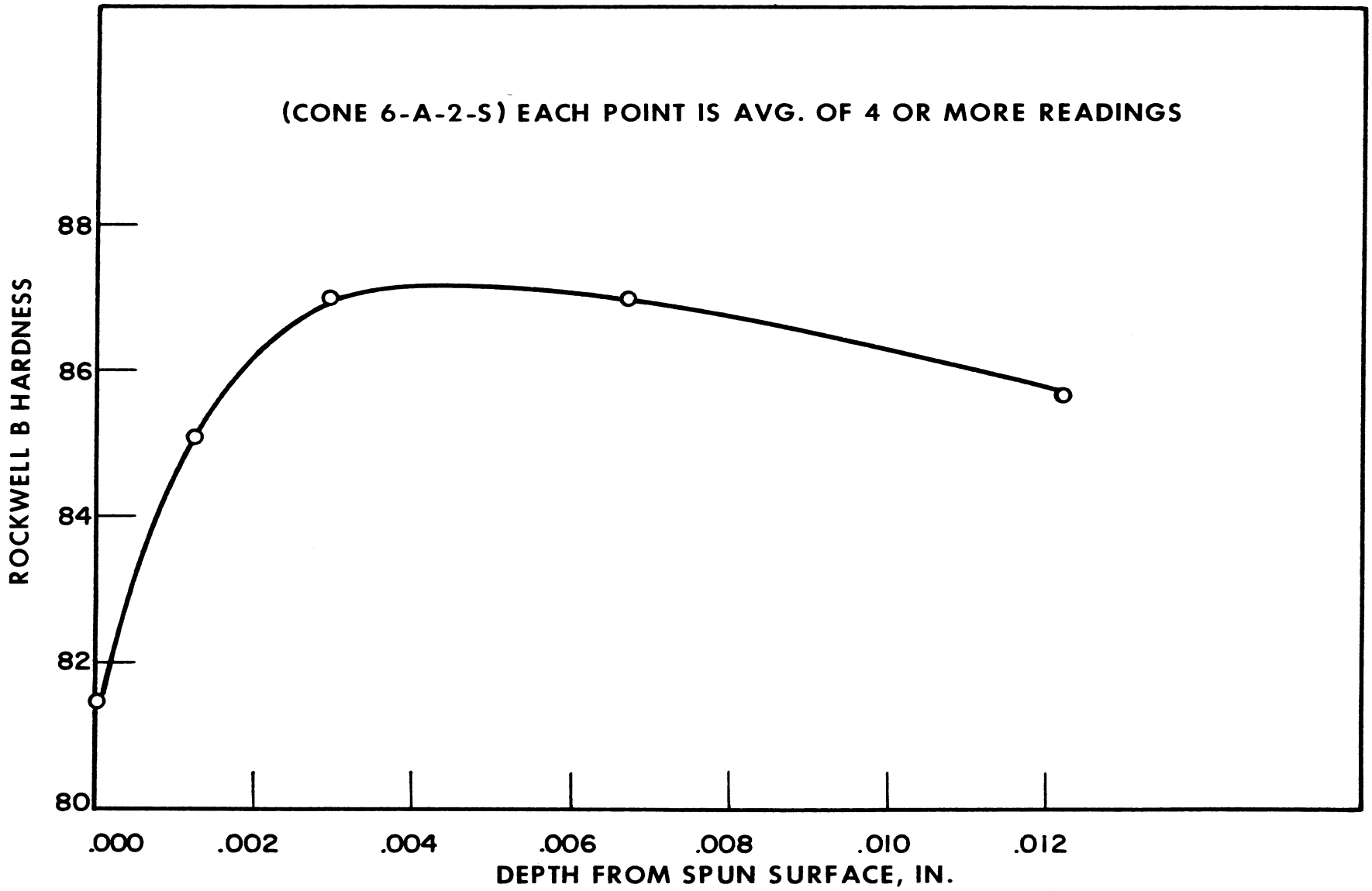

VARIATION OF HARDNESS WITH DEPTH FROM SPUN SURFACE

FIG. 11

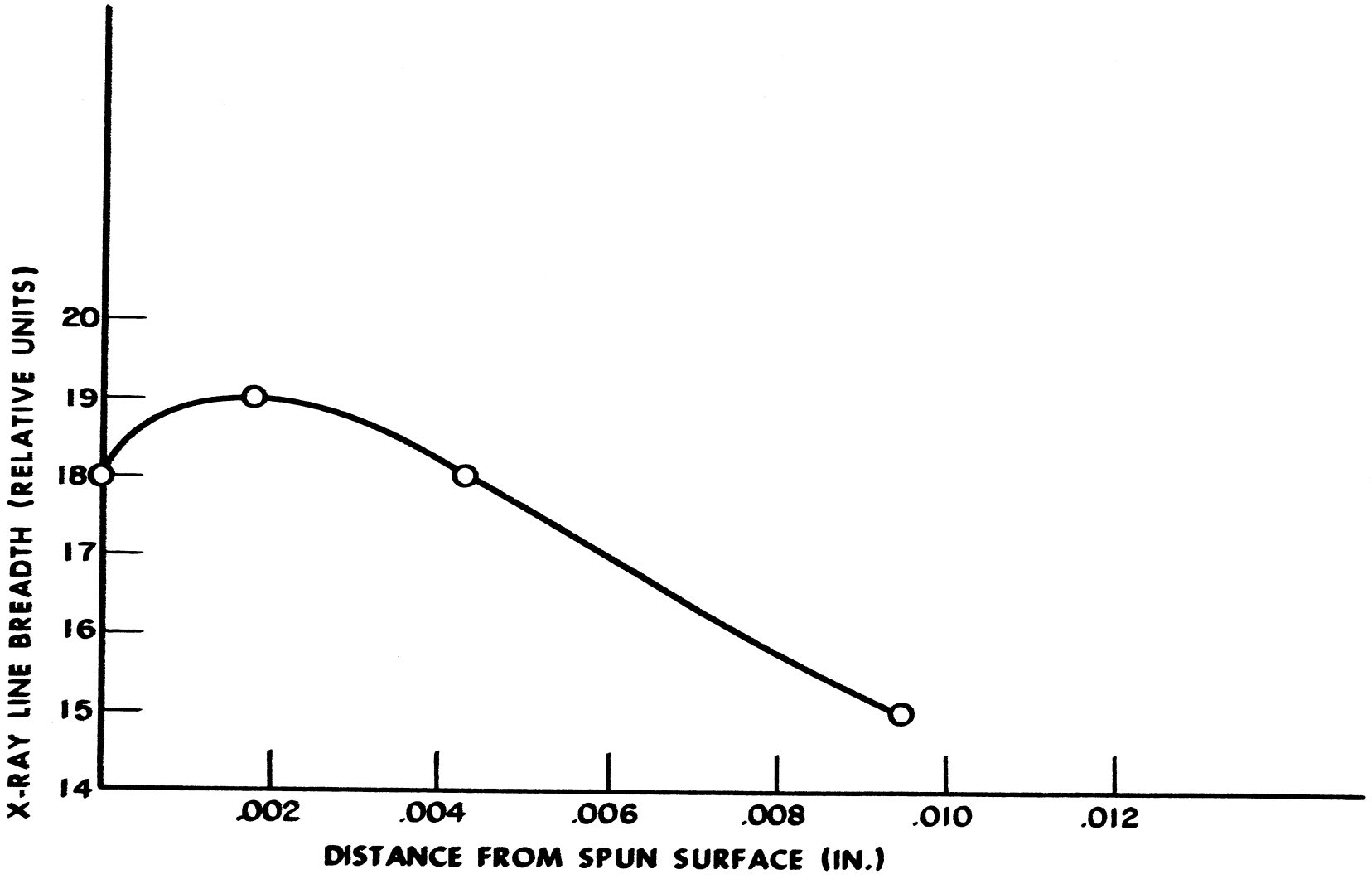

X-RAY LINE BREADTH vs DISTANCE FROM SPUN SURFACE CONE 6A2S

FIG. 12

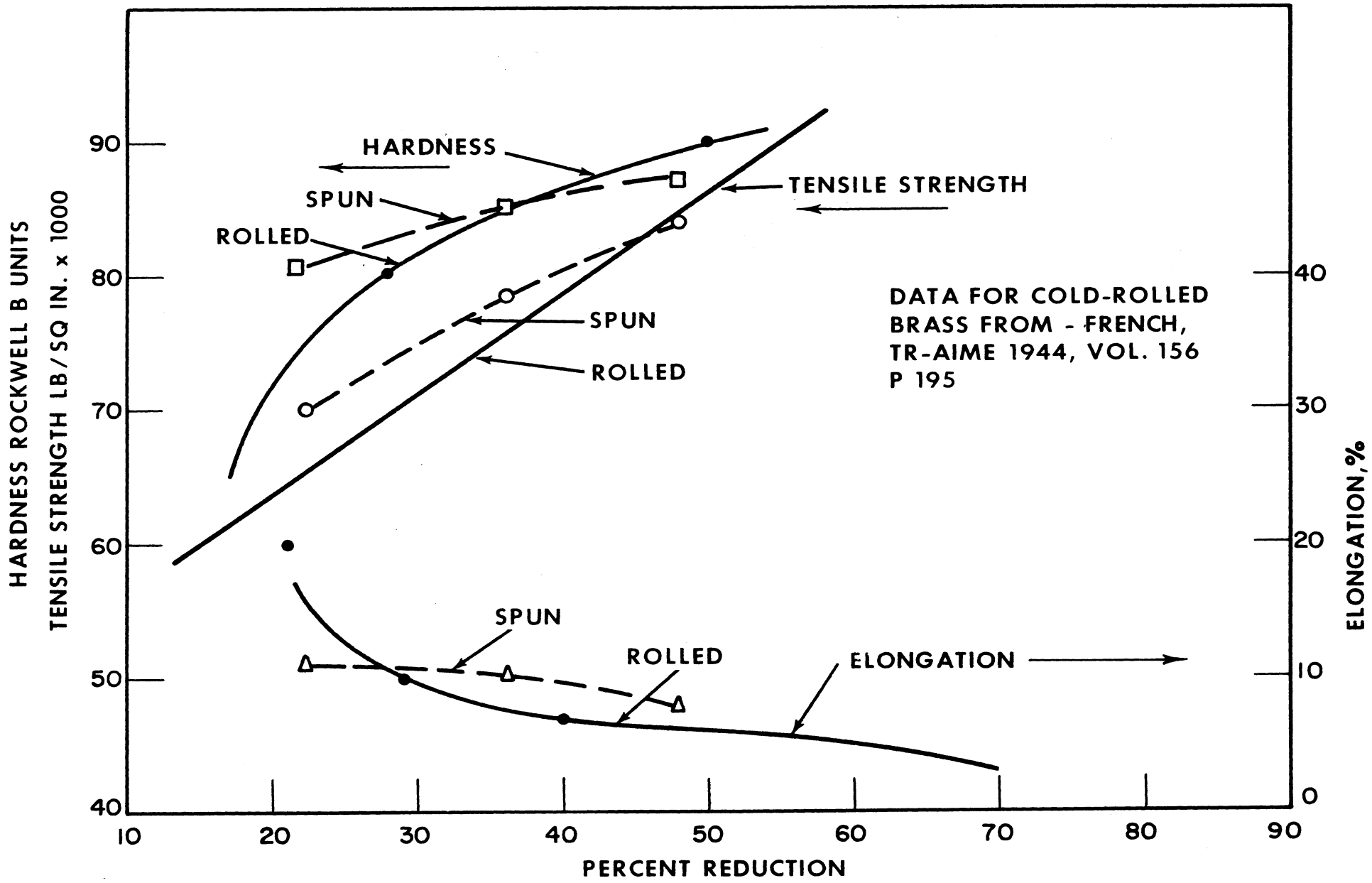

COMPARISON OF MECHANICAL PROPERTIES OF BRASS PRODUCED BY SPINNING AND ROLLING

FIG. 13

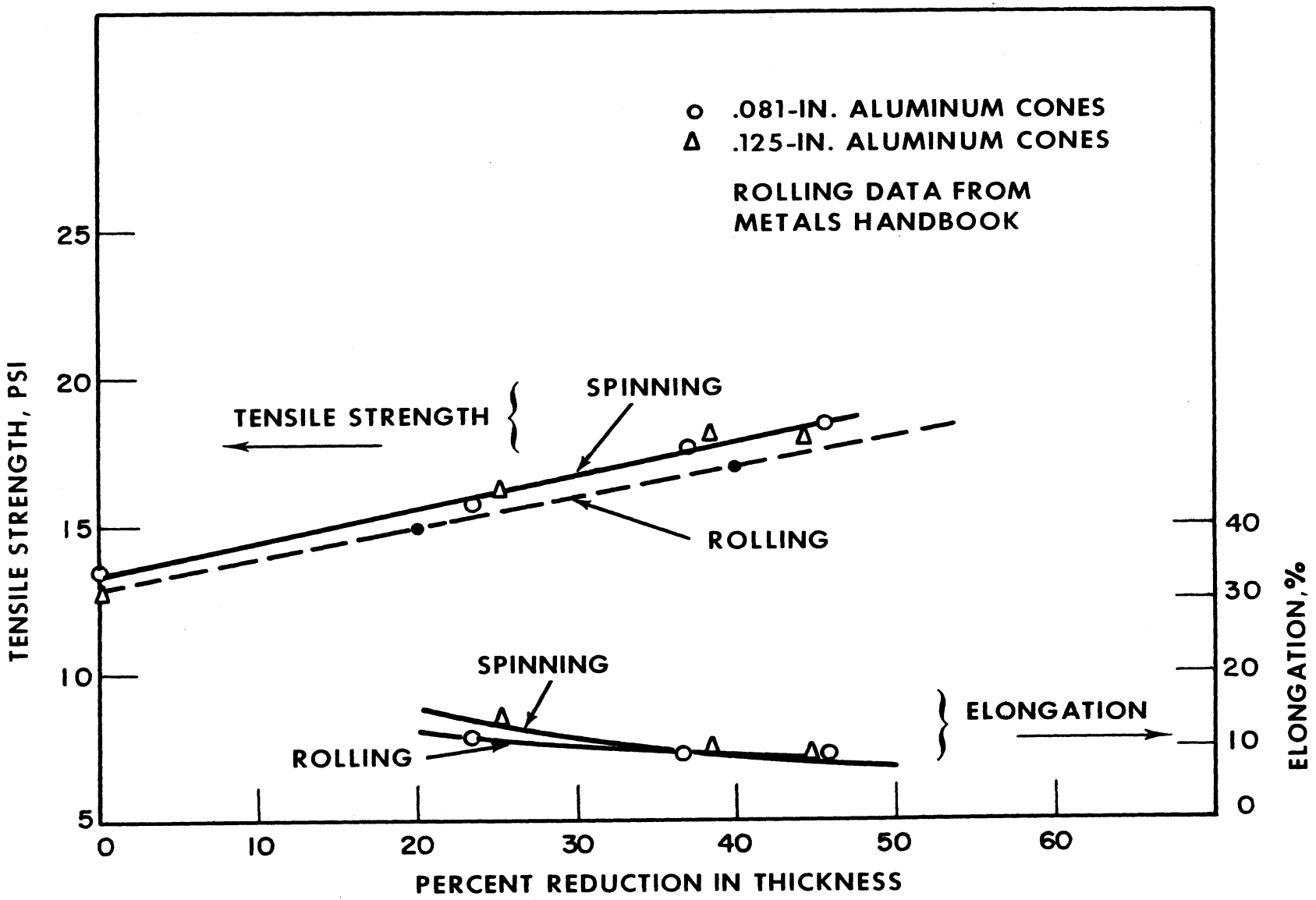

COMPARISON OF MECHANICAL PROPERTIES OF ALUMINUM PRODUCED BY SPINNING AND ROLLING

FIG. 14

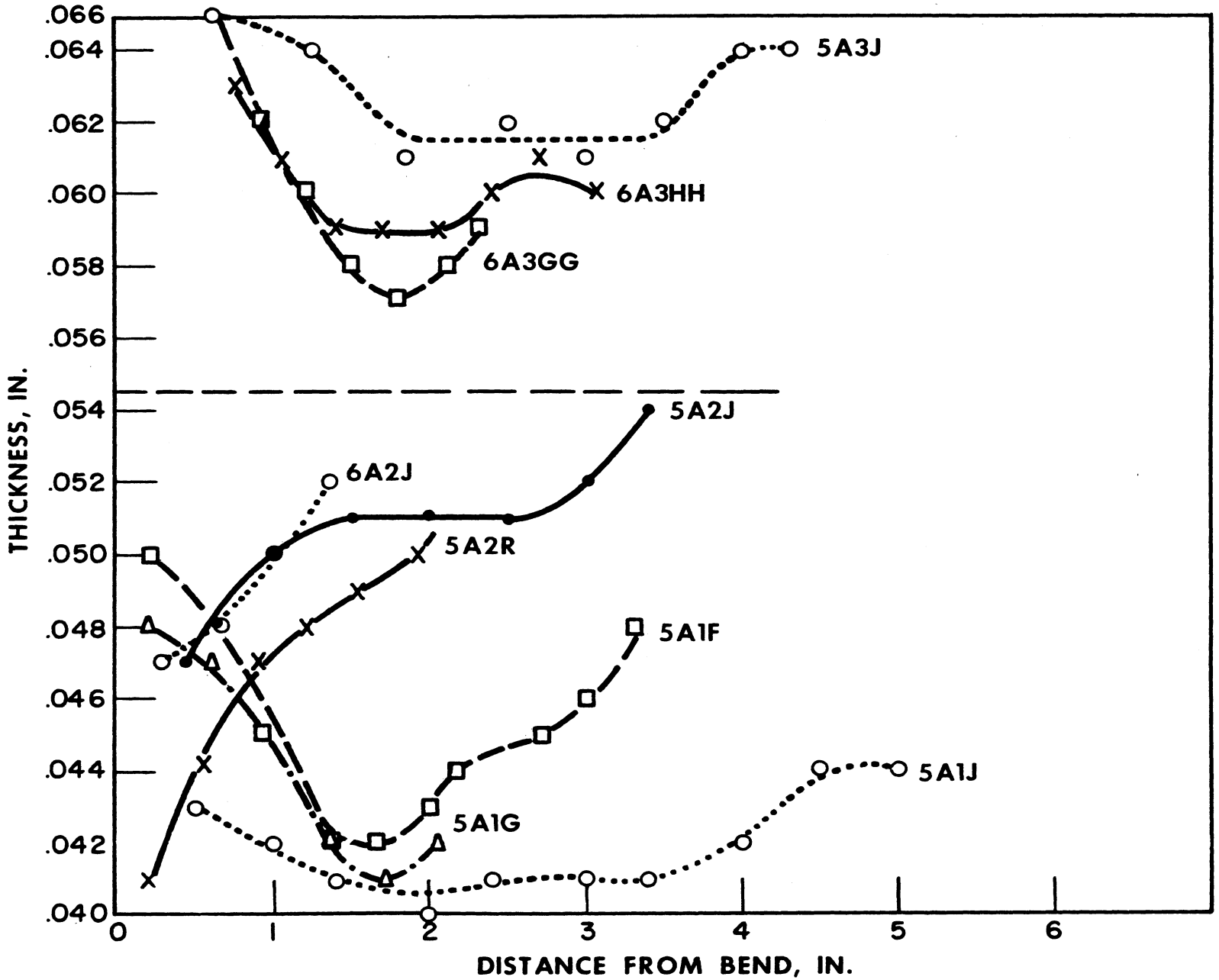

THICKNESS vs. DISTANCE FROM BEND - BRASS CONES

FIG. 15a

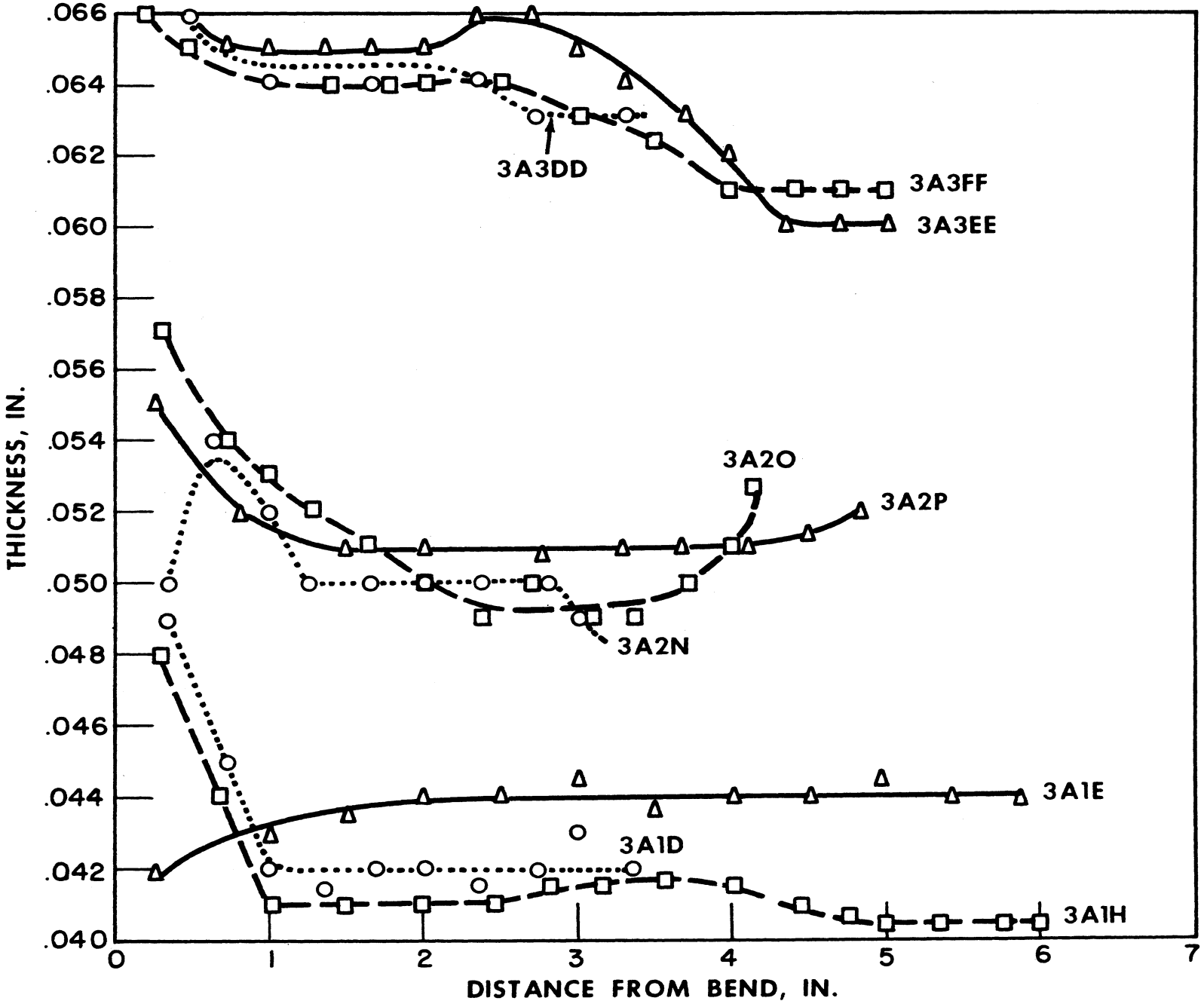

THICKNESS vs. DISTANCE FROM BEND - .081-IN. ALUMINUM CONES

FIG. 15b

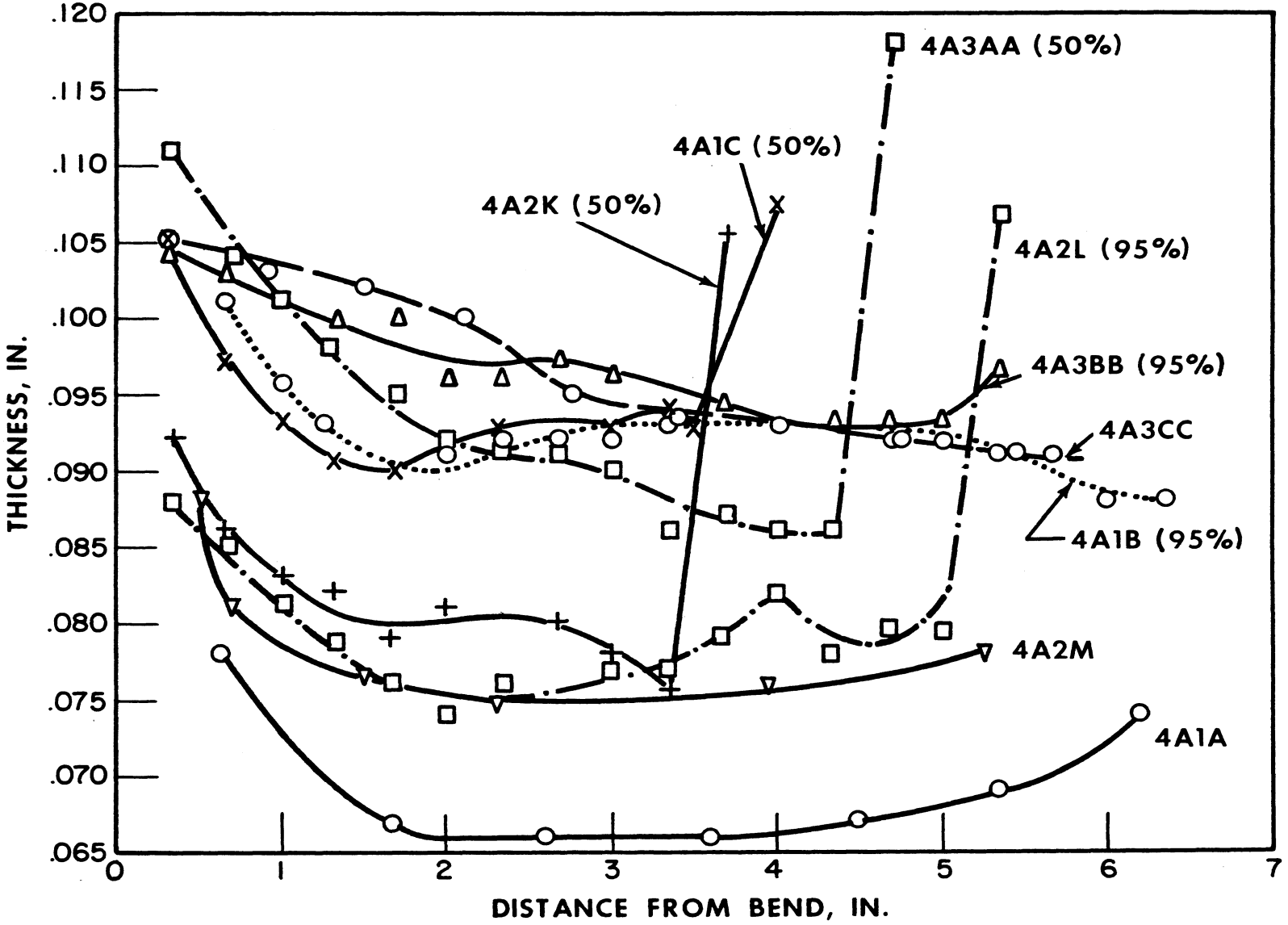

THICKNESS vs. DISTANCE FROM BEND - 0.125-IN. ALUMINUM

FIG. 15c

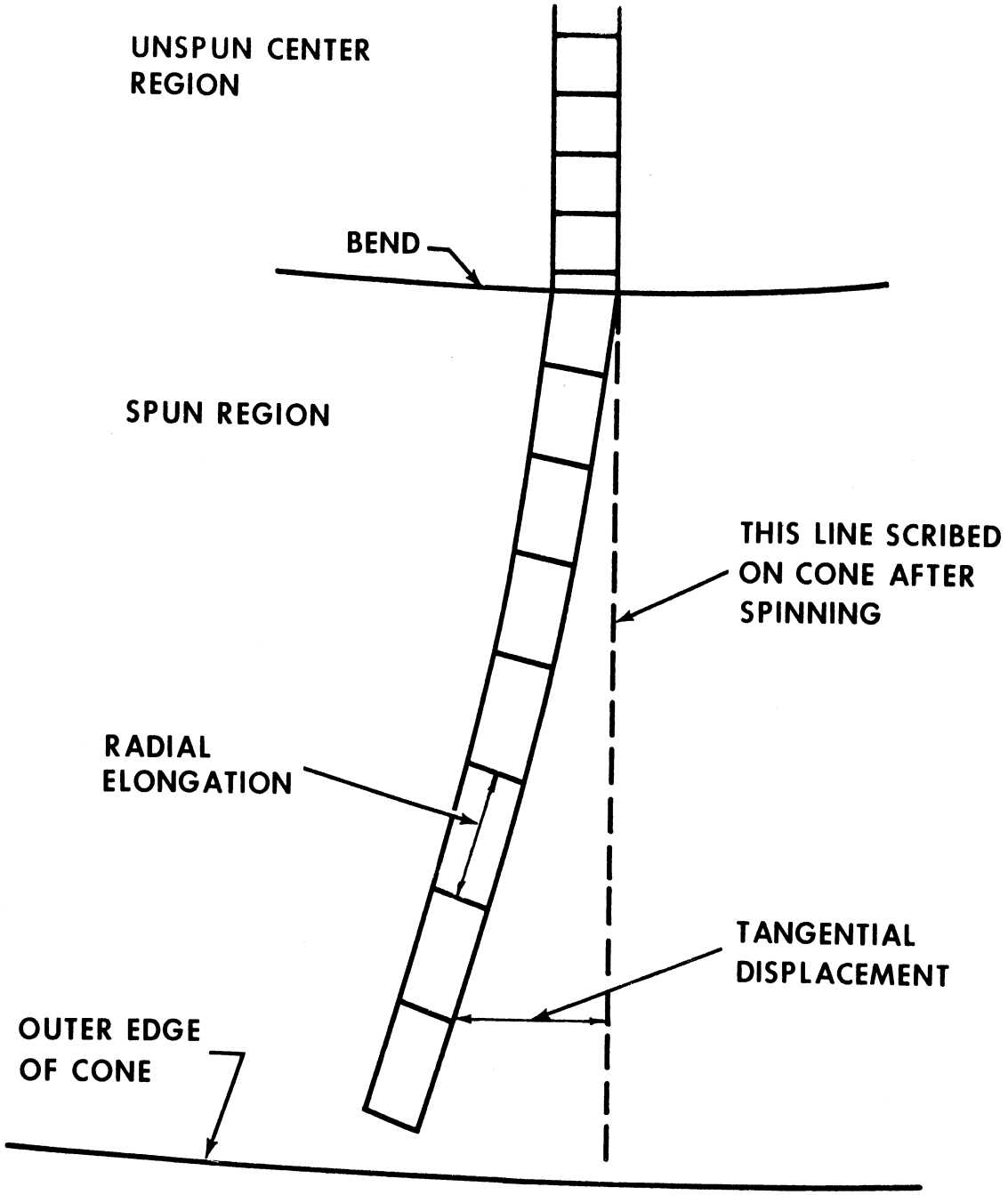

GRID DISTORTIONS IN FULLY SPUN CONES

FIG. 16

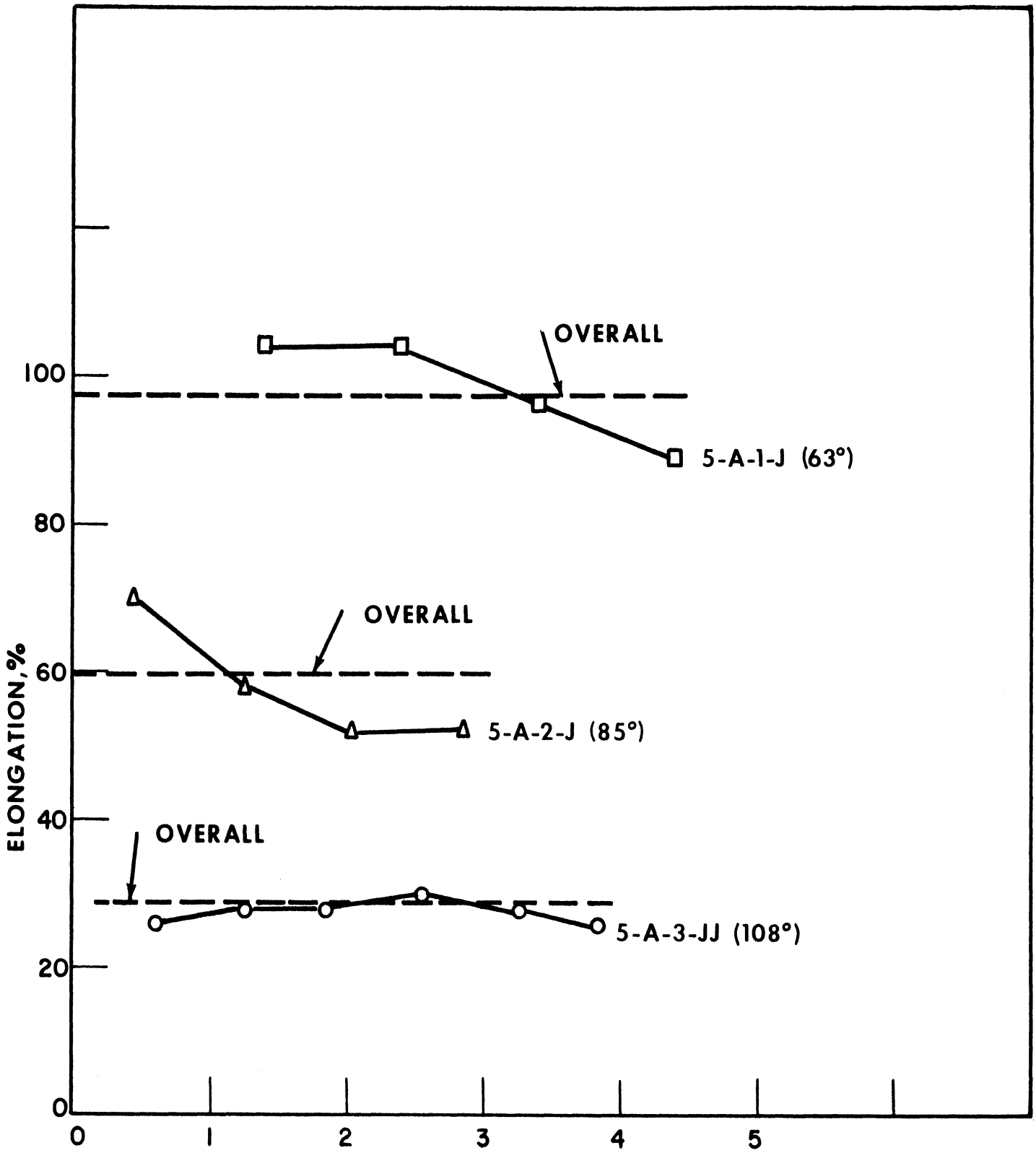

RADIAL GRID ELONGATION—BRASS CONES

FIG. 17a

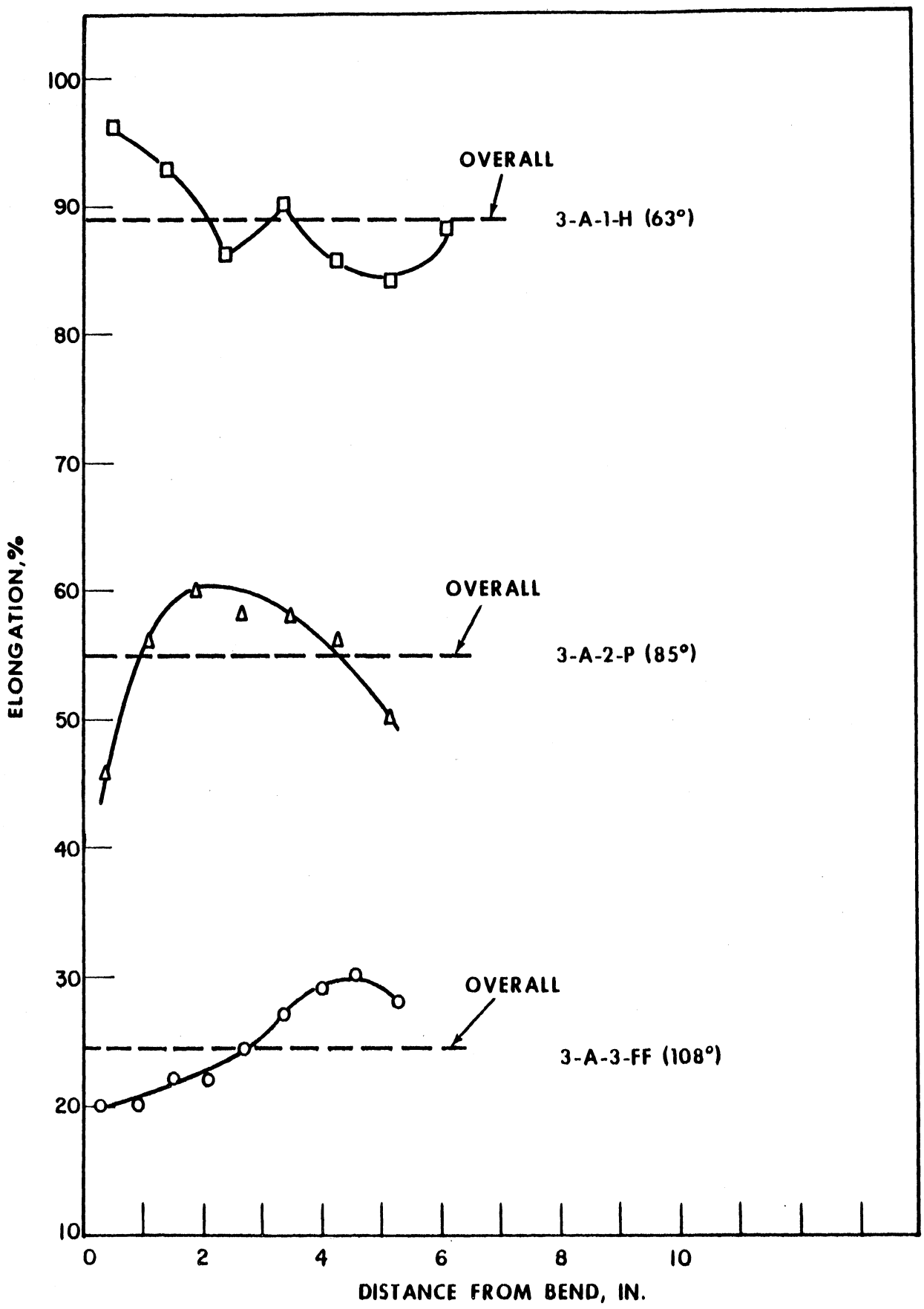

RADIAL GRID ELONGATION – .081-IN. ALUMINUM CONES

FIG. 17b

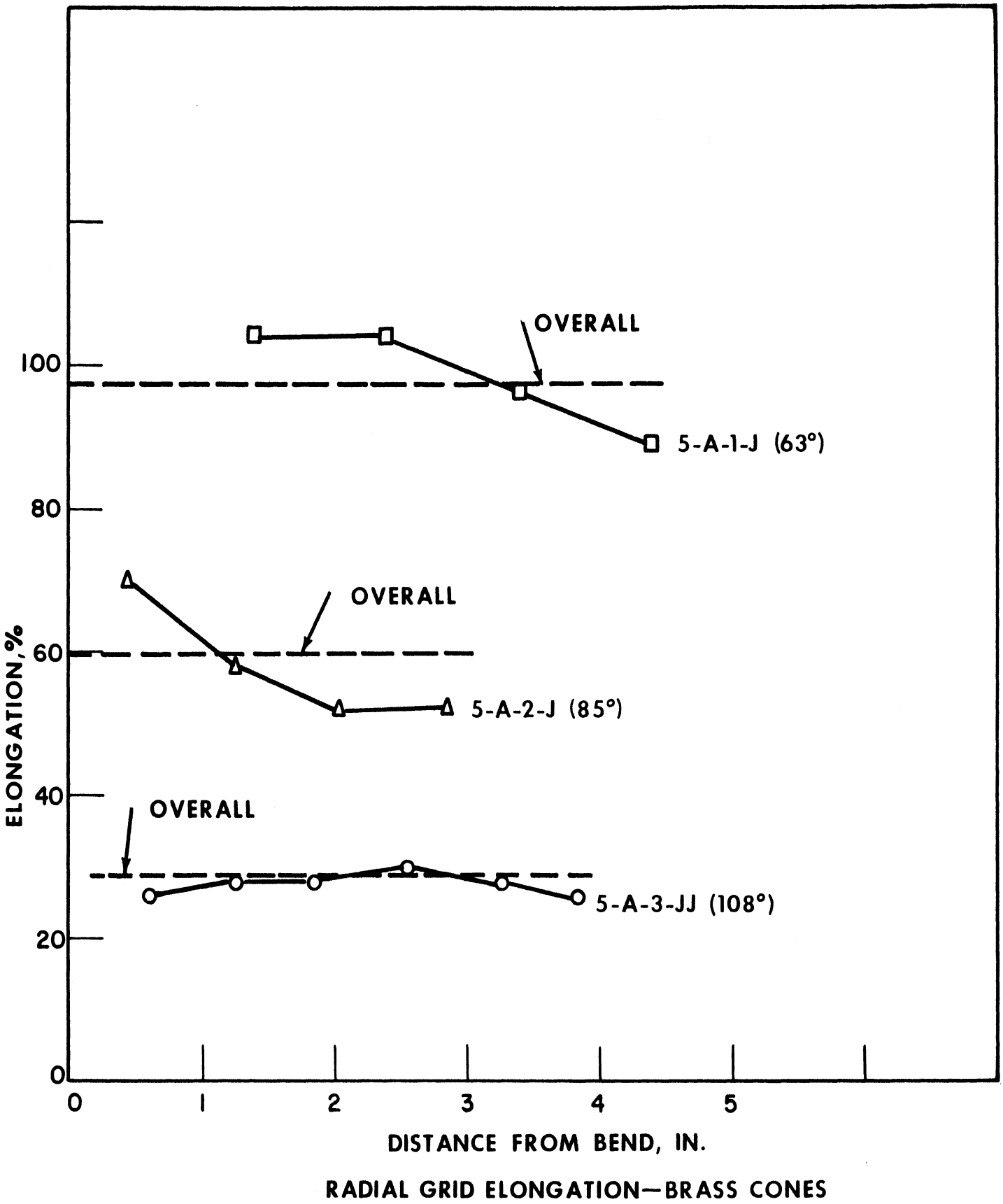

RADIAL GRID ELONGATION—BRASS CONES

FIG. 17a

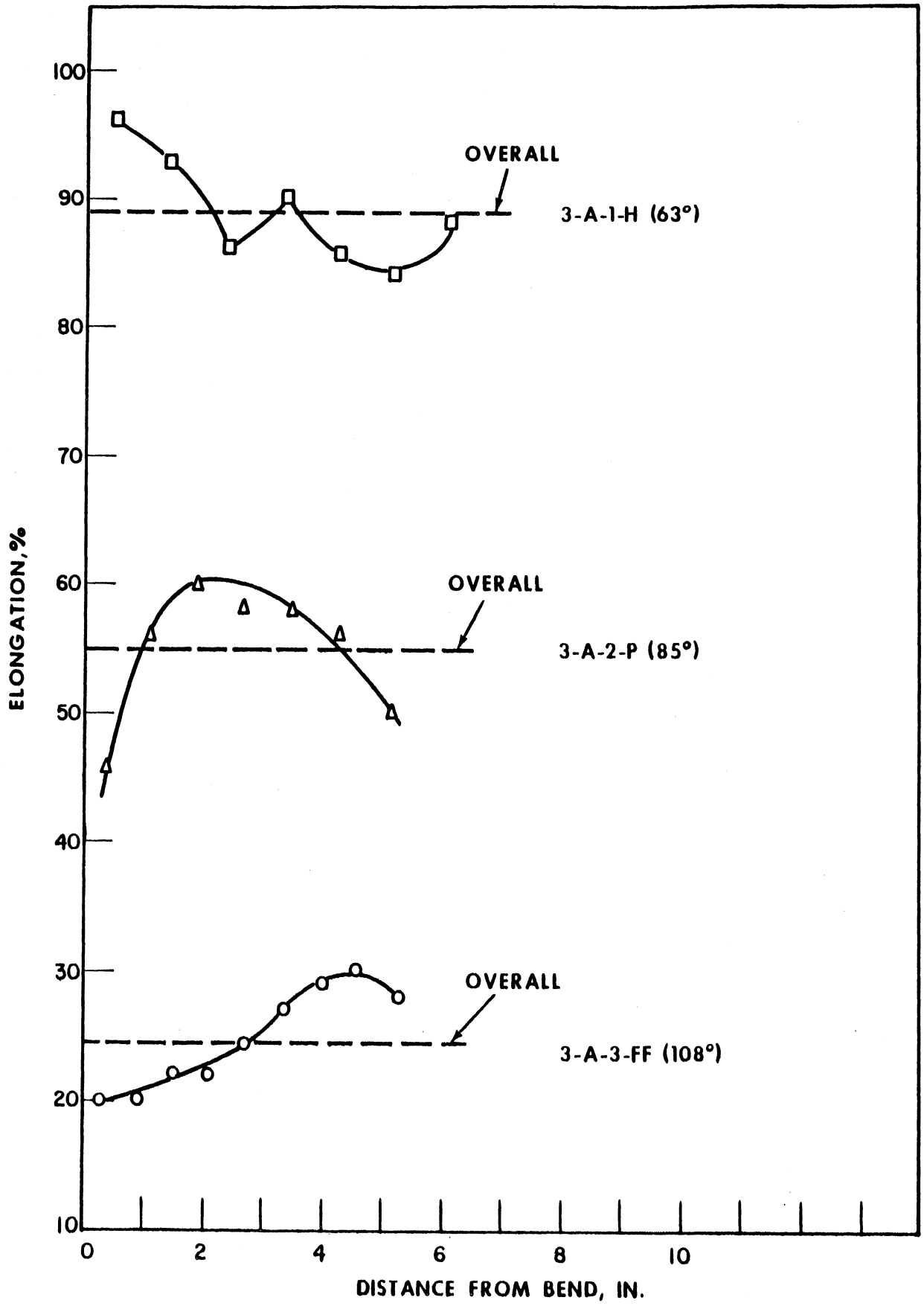

RADIAL GRID ELONGATION — .081-IN. ALUMINUM CONES

FIG. 17b

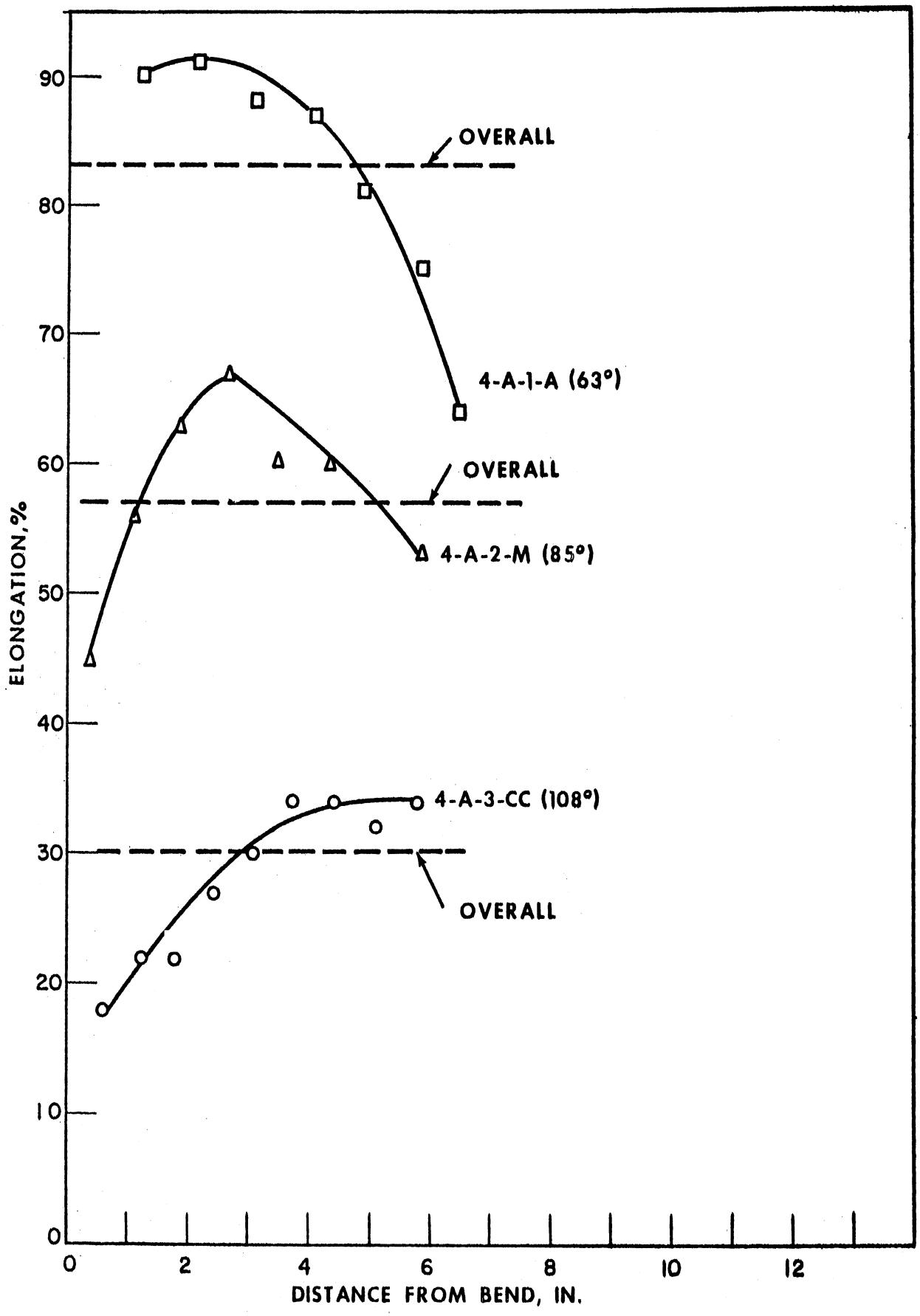

RADIAL GRID ELONGATION-.125-IN. ALUMINUM CONES

FIG. 17c

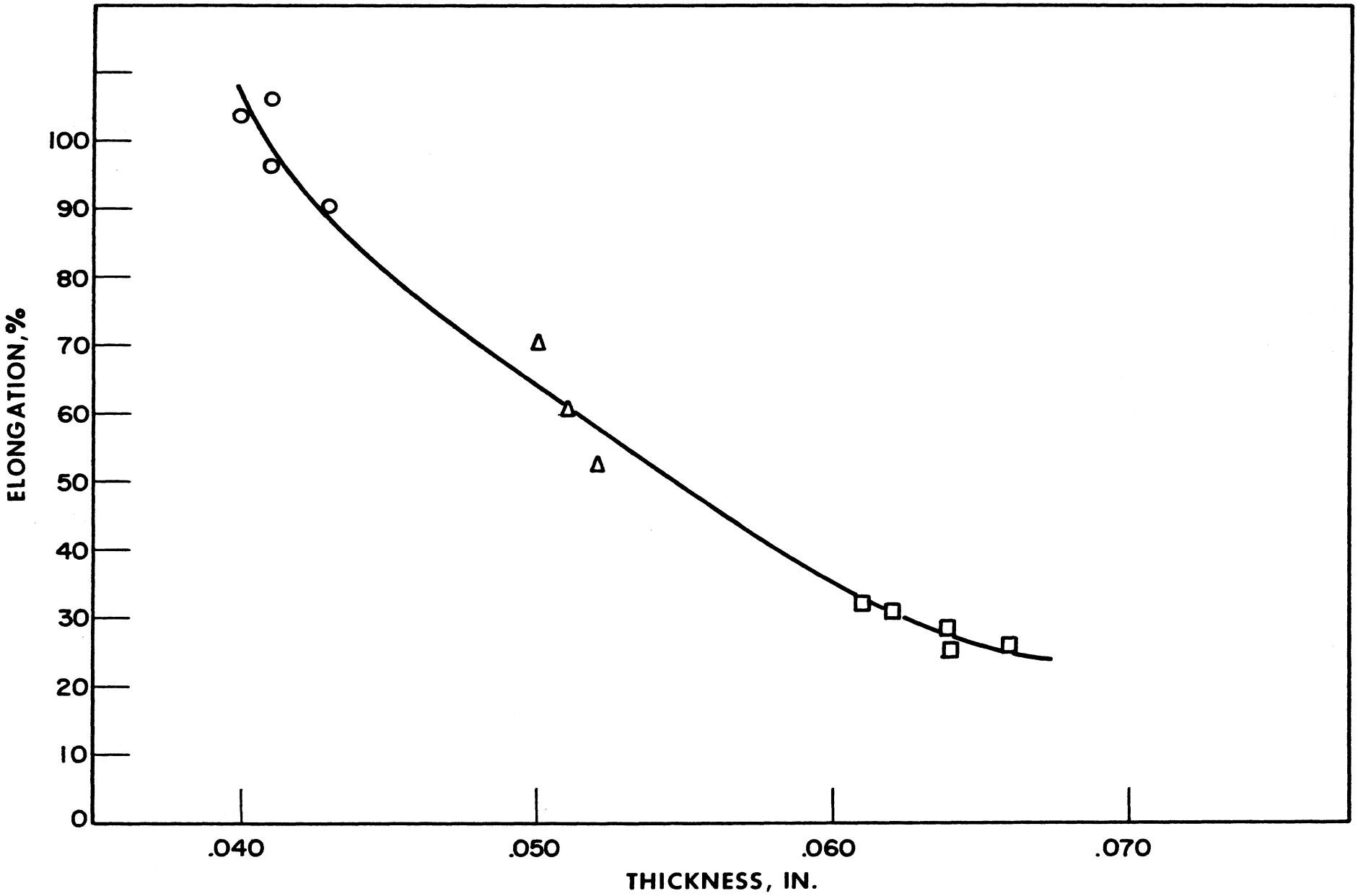

ELONGATION vs. THICKNESS—BRASS CONES

FIG. 18a

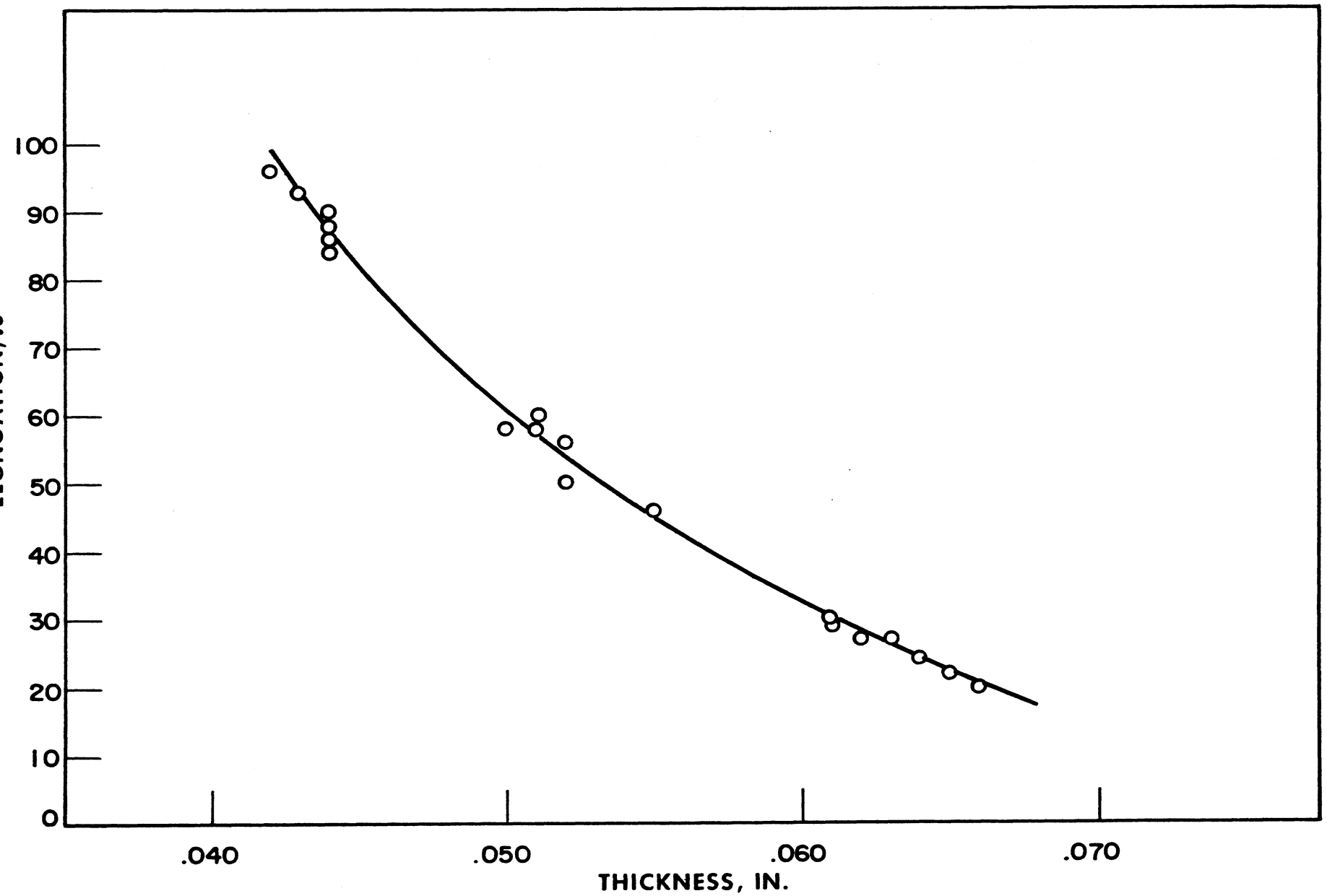

ELONGATION vs. THICKNESS– .081-IN. ALUMINUM CONES

FIG. 18b

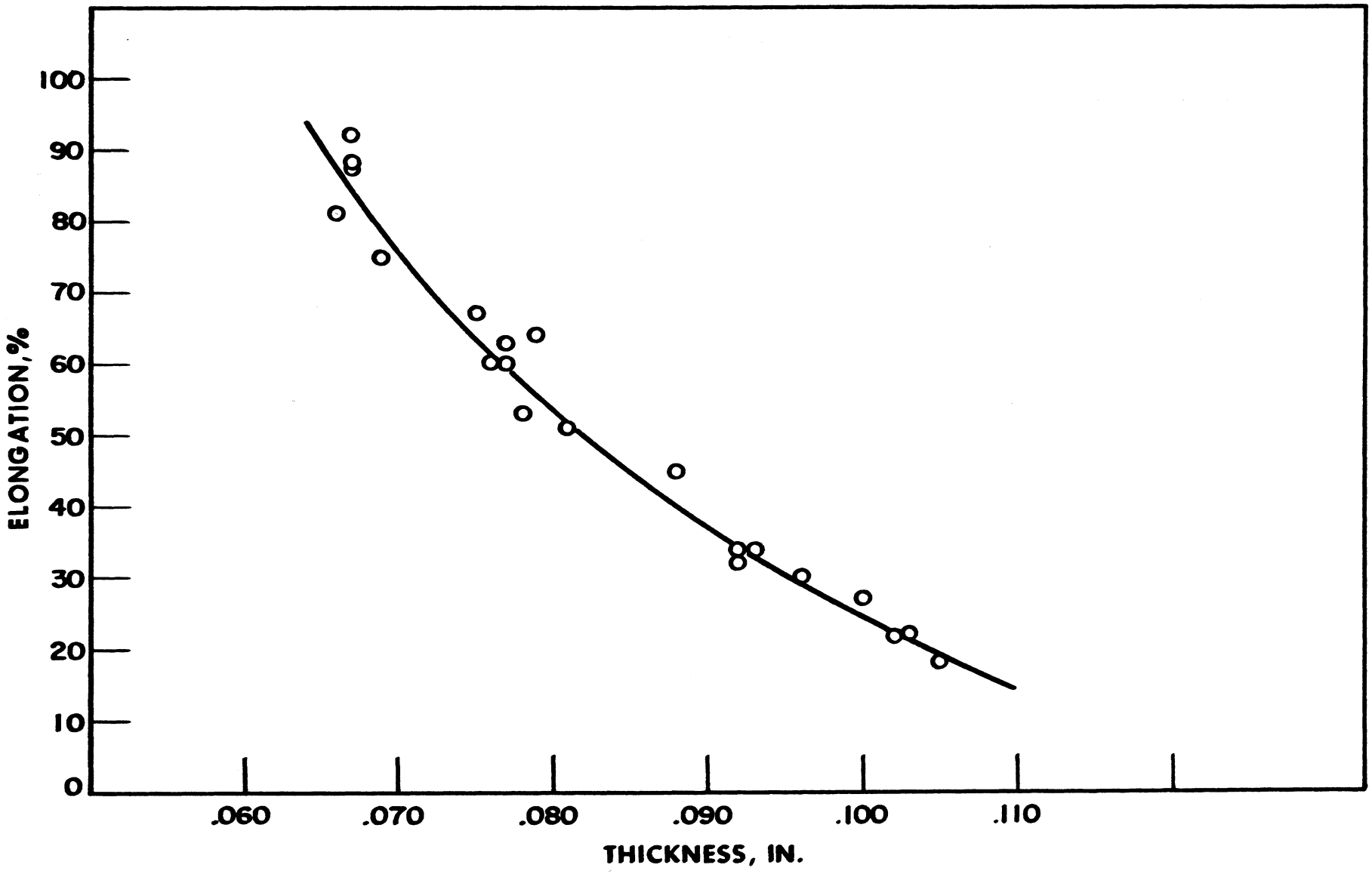

ELONGATION *vs.* THICKNESS—.125-IN. ALUMINUM CONES

FIG. 18c

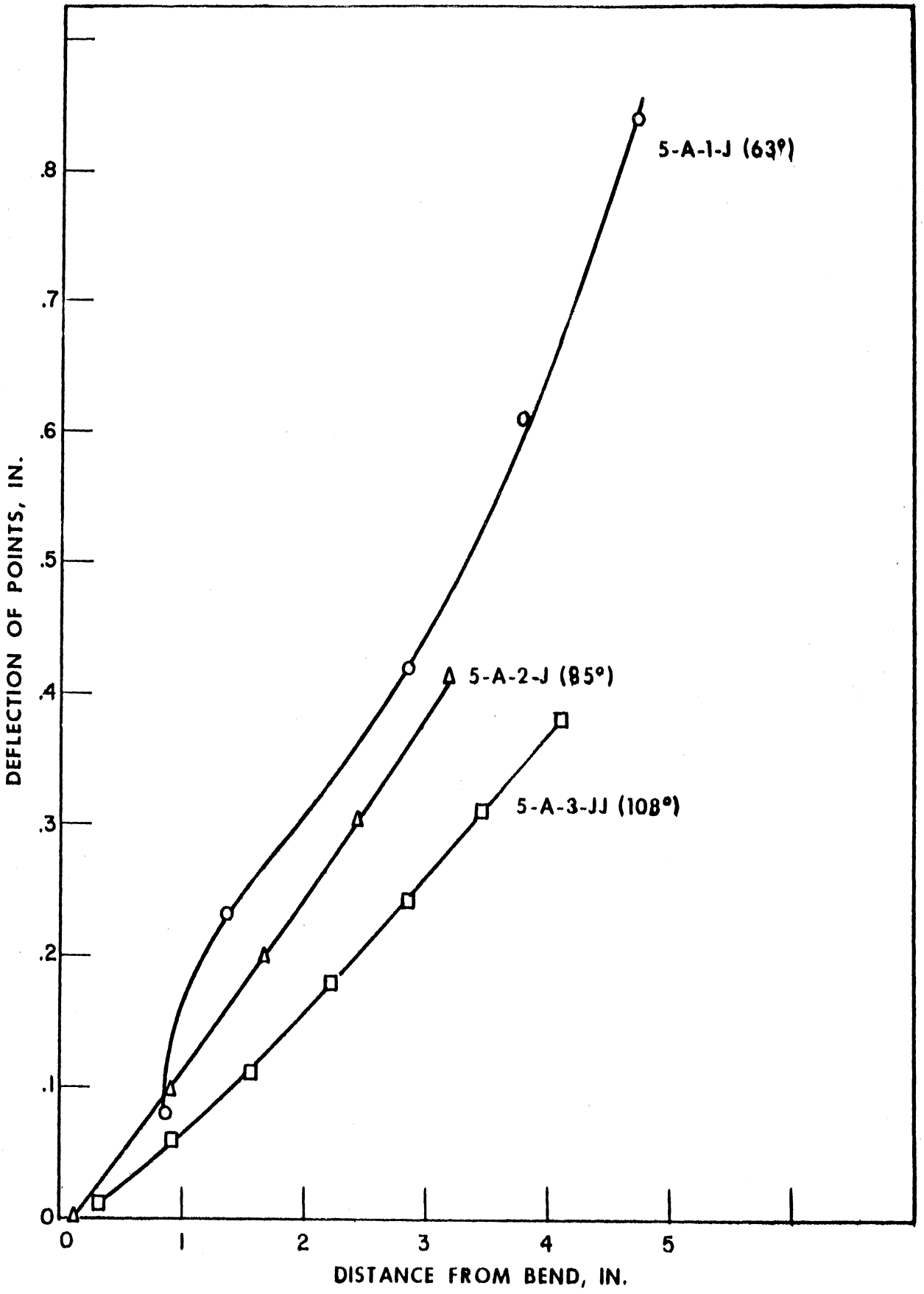

TANGENTIAL GRID MOVEMENT – BRASS CONES.

FIG. 19a

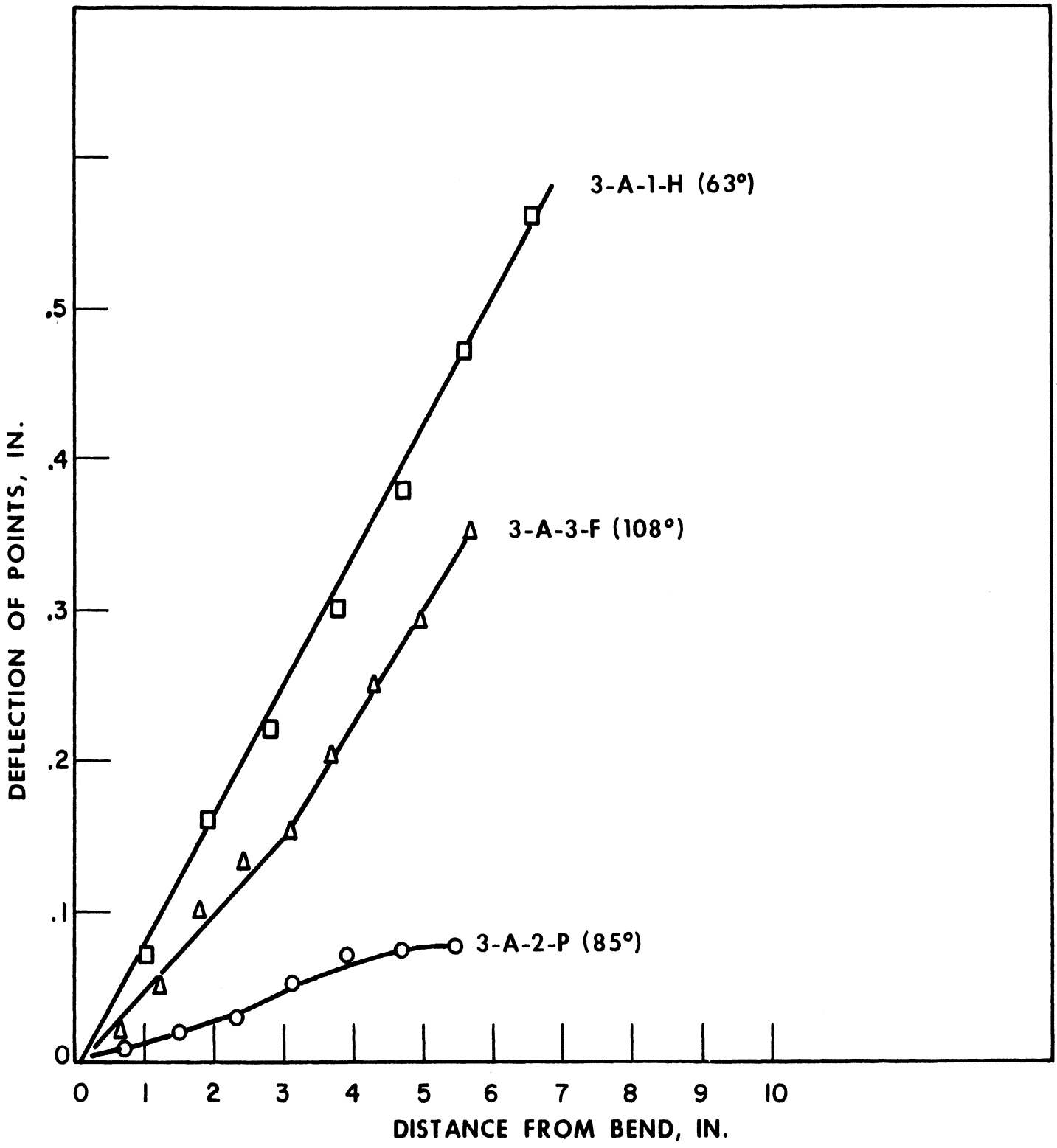

TANGENTIAL GRID MOVEMENT-.081-IN. ALUMINUM CONES

FIG. 19b

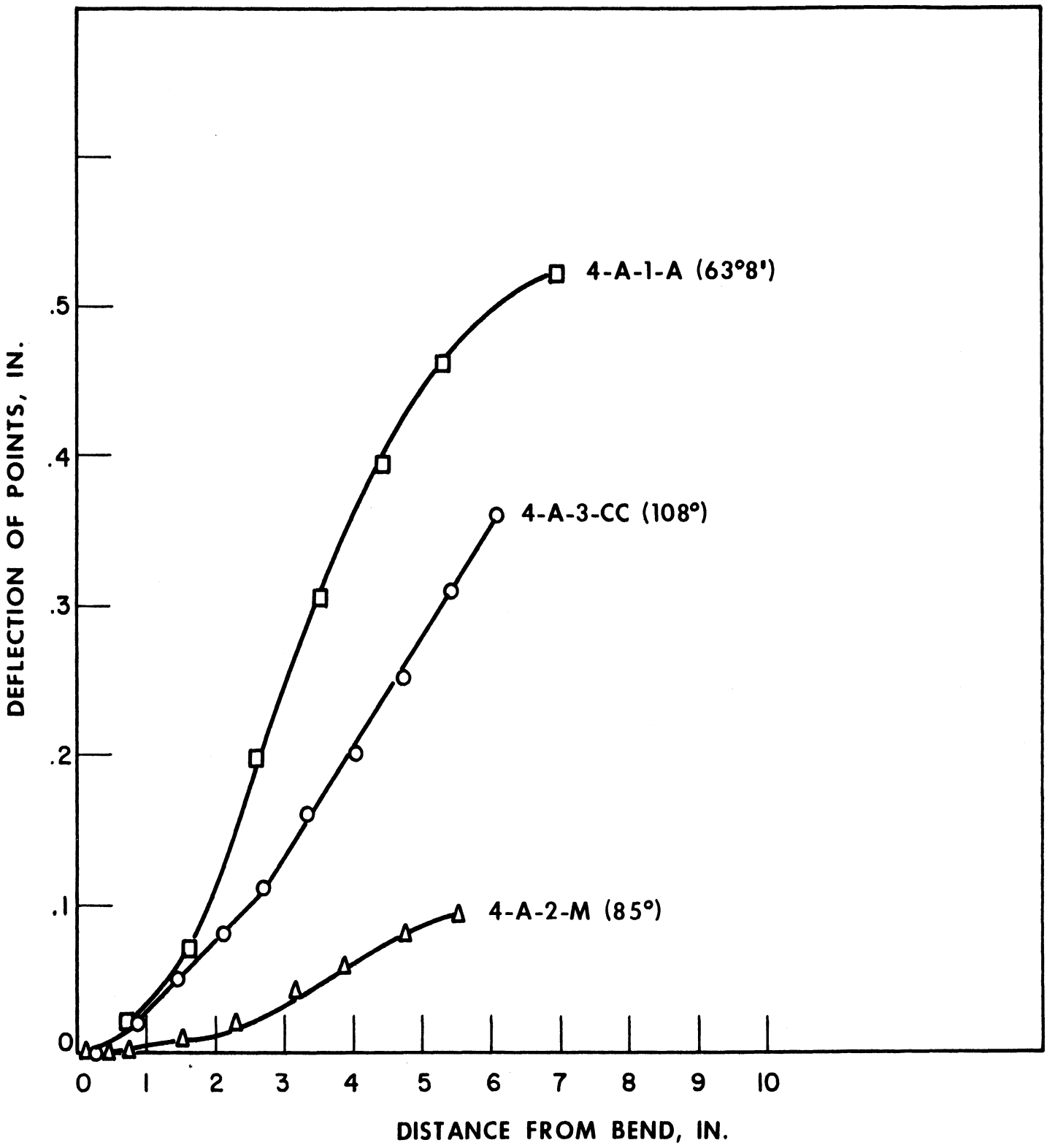

TANGENTIAL GRID MOVEMENT–125-IN. ALUMINUM CONES
FIG. 19c

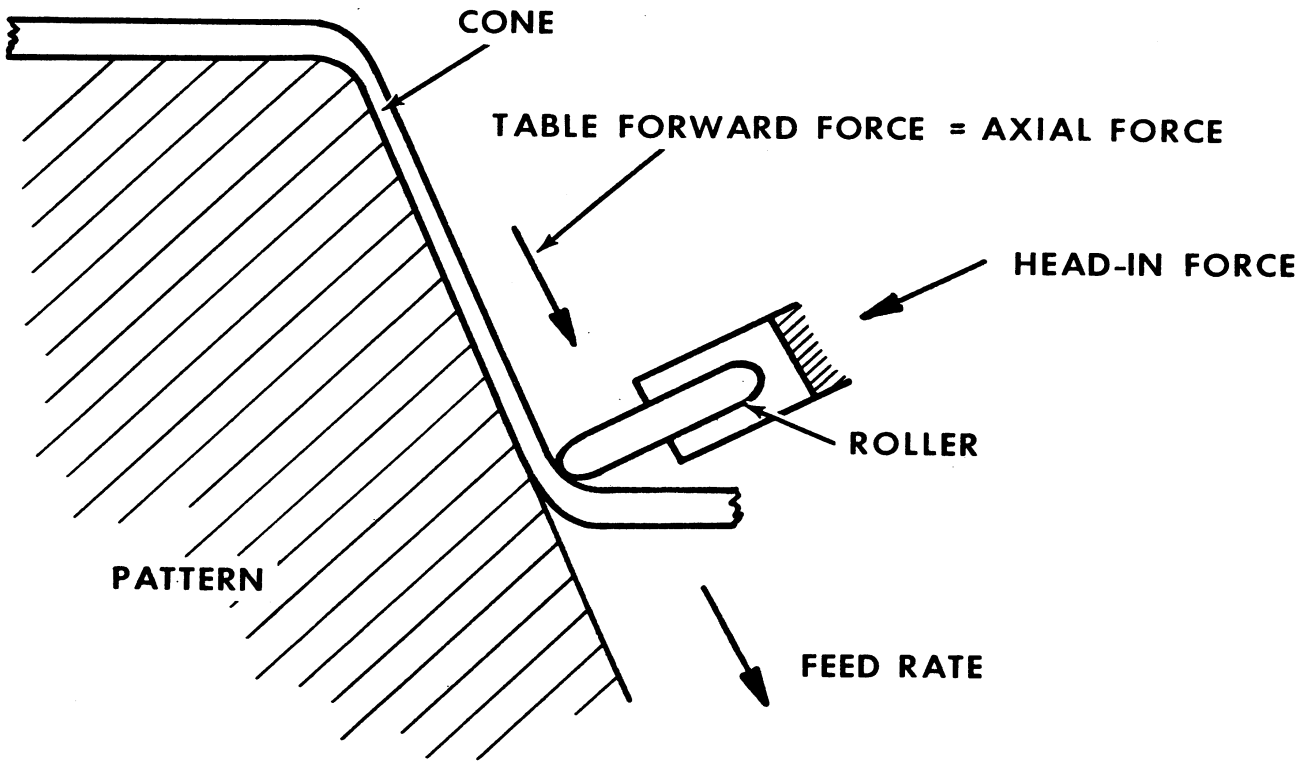

SCHEMATIC VIEW OF SPINNING FORCES

FIG. 20

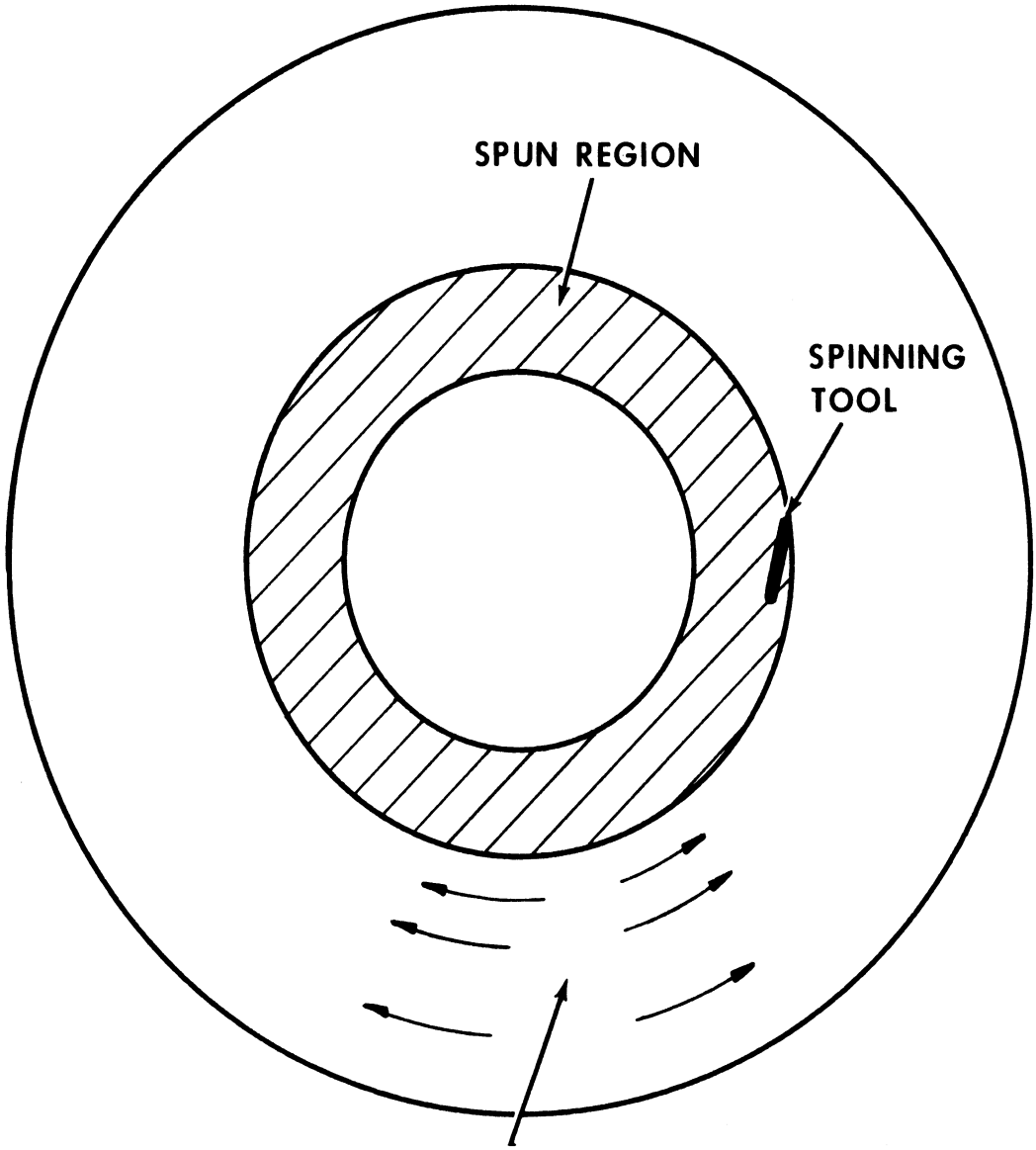

ELASTIC STRESSES DURING SPINNING

FIG. 21

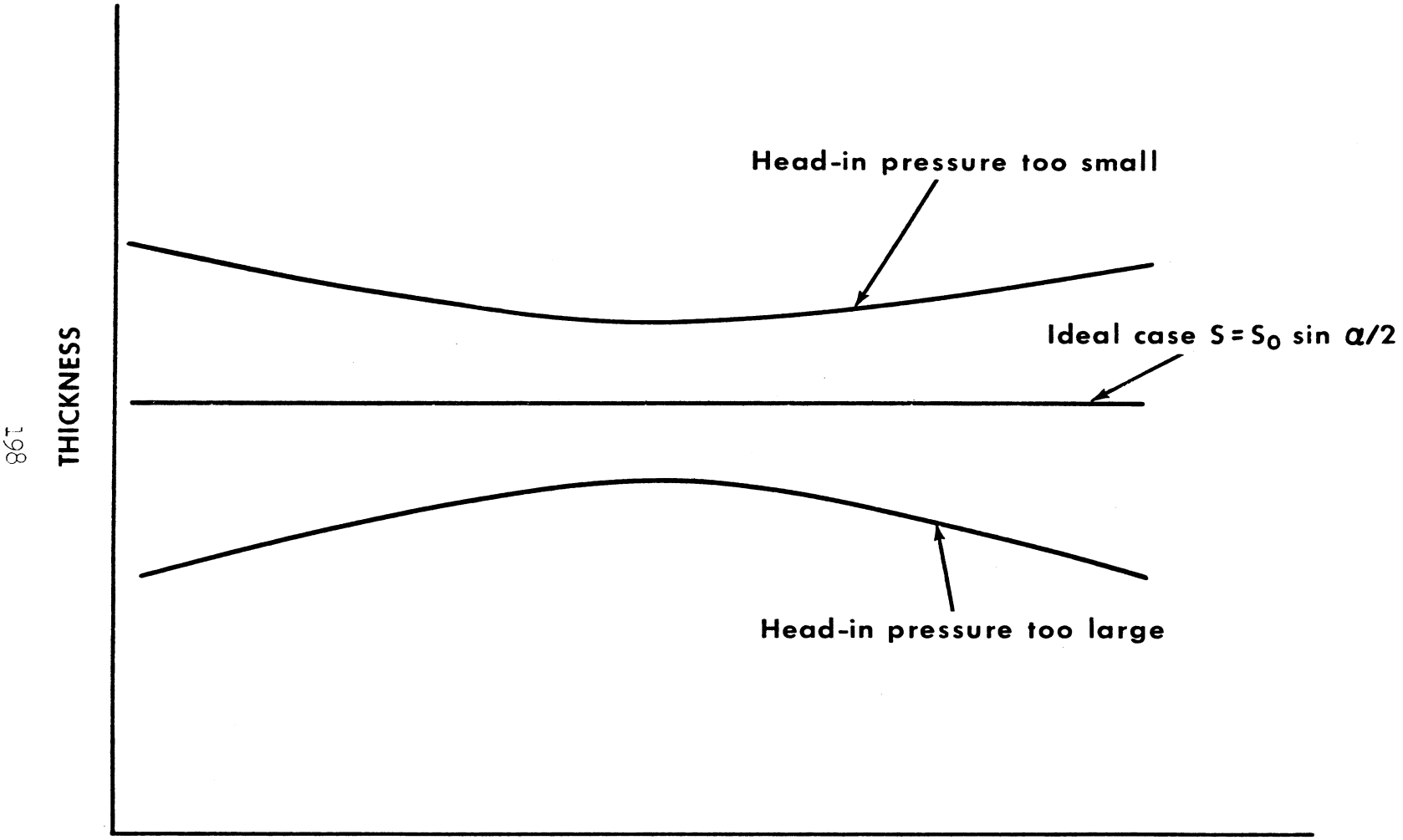

PREDICTED VARIATION IN THICKNESS vs DISTANCE FROM BEND

FIG. 22

PART III

INVESTIGATION OF HAND SPUN CONES

I. INTRODUCTION

This investigation is concerned with the mechanical properties and deformations in materials which have been hand spun. Essentially this work is a continuation of a previous investigation made of mechanically spun pieces (Part II). The previous investigation showed that the properties of pieces which are mechanically spun are generally very similar to those produced by cold-rolling to an equivalent reduction. The investigation also showed that the deformations found in spun pieces could be explained in an overall way on the basis of the various forces, feed rates, etc., that were used to fabricate the pieces.

In this investigation a series of pieces were spun by hand to the same dimensions as the mechanically-spun pieces. Hand spinning is what the name implies. The shaping of the metal is done by a skilled craftsman who used a specially-designed instrument called a spinning tool to form a sheet over the pattern.

Hand spinning is different from mechanical spinning in two important respects. In the first place the applied force and rate of feed used by the man doing the spinning are not kept constant, as is usually the case in mechanically spinning. Secondly, the hand spinner may make a number of passes on the same piece until he believes the deformation is correct, while in mechanical spinning only one pass is commonly used to fabricate the piece.

The hand spinner can use whatever force, feed rate, and number of passes that he feels is necessary to form the piece. Because of this freedom any mathematical analysis of the plastic deformation, such as is possible in mechanical spinning, is out of the question. An investigation of this type

therefore, must of necessity be confined to a general evaluation of hand spun pieces in terms of the mechanical properties and types of deformations.

II. EXPERIMENTAL PROCEDURE

In the present investigation a number of the experimental procedures were identical with those used for the mechanically spun cones. For a more complete description of these procedures the reader should refer to that section of the report. For the sake of convenience however, the entire procedure will be briefly described.

1 - Materials.

The materials used were 1100 aluminum and cartridge brass (70%Cu). The materials were purchased in the form of annealed sheets. The thickness of the brass sheets were .081". Two thicknesses of aluminum sheet were used, .081" and .125". Previous tests (Part II) showed that there were no significant differences in mechanical properties between sheets of the same alloy, and also that the anisotropy in the sheets are negligible.

2 - Spinning Procedure.

The pieces were spun by the Spincraft Corp. of Milwaukee, Wisconsin. All of the pieces were spun by the same man and on the same machine.

The pieces were spun into the form of truncated cones having the same dimensions as the mechanically spun cones. The three cone angles that were used were the same as for the mechanically spun cones. A sketch showing the general shape of the spun cones is presented in Figure 1, and a photograph of a typical cone is given in Figure 2. All of the cones were spun to completion.

As was previously done, grids were placed on a number of the sheets before they were spun. The sheets were then spun so that the grids were located on the inner side of the cones; that is on the side that was opposite to the side on which the spinning tool was applied. A sketch showing the grids that were used is given in Figure 3.

A listing of the cones that were spun to date together with the spinning procedures that were used is presented in Table I. Several different sizes and shapes of spinning tool were used. These tools are shown schematically in Figure 4. The number of passes that were used varied from 1 to 24. The comments in the table are those made by the man who performed the spinning.

3 - Testing of Spun Cones.

The tensile properties were determined by machining tensile specimens from some of the cones. Four specimens were taken from each cone, as shown in Figure 5. The tensile specimen that was used is shown in Figure 6. This specimen has dimensions that are one-half those of the standard 8" ASTM tensile specimen for sheet materials. Previous tests (Part II) showed that the 4" and 8" specimen gave approximately the same tensile properties. Thus the measured tensile properties should approximate those obtained using the standard 8" specimens.

Hardness tests were made on the spun surfaces of all the cones. Several of the cones were cross-sectioned and microhardness measurements were made across the thickness of the sheet. Thickness measurements were made on the spun regions of all the cones.

The grid deformations in the cones were measured before the cones were sectioned. The measurements consisted in locating the grid points with a divider and then measuring the divider points on a scale. The deformations found in the grids were rather complicated. The various measurements that were made will be discussed more fully in the next section.

III. RESULTS

1. Mechanical Properties.

The tensile properties of the spun cones are listed in Table II. Because of the negligible anisotropy in the as-received sheet, the original rolling direction should not have any significant effect on the tensile properties. For this reason the tensile properties of the two specimens taken parallel and perpendicular to the original rolling direction are averaged in the table. The results show, as would be expected, that the tensile and yield strength increase with increasing reduction, and that the elongation decreases. The scatter in the tensile data is large however, much more so than was found for the mechanically spun cones.

The hardness measurements on the spun surfaces of the cones also showed considerable scatter. In many cases the curvature and surface roughness of the pieces made accurate measurements difficult. Because of these variations only the average hardness values have been reported. These values are listed in Table III. The results show that the hardness increases with reduction, as would be expected.

The average variation in microhardness in the cross sections of some of the cones is shown schematically in Figure 7. It was found in general that the microhardness was fairly constant over the cross-section, as shown in the Figure. This result is rather surprising. Since the spinning tool is applied to only one surface of the sheet one might expect to find a decrease in hardness from the spun surface to the opposite surface. This latter type of hardness gradient was encountered in the mechanically-spun pieces. However no such gradient was encountered in the present case.

In general the mechanical properties of the hand-spun cones showed less work hardening than the mechanically spun cones. No doubt this reflects the differences in modes of deformation in the two cases.

2. Deformations.

The thicknesses of the spun regions of the cones as a function of the distance from the bend are plotted in Figure 8. The results show that there may be distinct variations in thickness in hand-spun pieces. Similar thickness variations were also found in the mechanically spun pieces. In some of the present cones however, for example the 108° angle aluminum cones, the thickness variations were much less than those found in the mechanically spun cones. The result is not too surprising when one considers that any number of passes can be made on a hand spun piece until the operator feels that the thickness is uniform. Also the 108° mechanically spun cones were particularly of bad quality. When the operator was not primarilly concerned with producing a uniform thickness, as shown by the comments in Table I, there are much greater variations in thickness.

The grid distortions in the cones are shown schematically in Figure 9. In general three types of distortions were found, an elongation of the grid, a tangential displacement, and a decrease in the width of the grid. (Figure 9) The magnitude of these various distortions in the cones are summarized in Figures 10 to 12.

It would be expected that there should be a direct relationship between the thickness and the elongation values. These relationships are shown in Figure 13. The results show that there is a general relationship but with a good deal of scatter.

The tangential displacements in the hand spun cones are in some cases entirely different from those found in the mechanically spun cones. In a number of the hand spun cones having a 63^{o} cone angle a negative displacement was found in the region near the bend. No negative displacement was found in any of the mechanically-spun cones.

Finally a decrease in the width of the grids was found in some of the 63^{o} cones, which was not found in the mechanically-spun cones. Only those cones showing a significant decrease in grid width (greater than .01 inches) are plotted in the figures. Once again, only the 63^{o} cone angle pieces show this behavior.

While the 63^{o} cones showed these new types of deformation, the other cones displayed deformations that were more similar to the deformations in the mechanically-spun cones. No decrease in the width of the grids or negative tangential displacements were observed. The only striking characteristics of these cones are, as mentioned, the uniform thicknesses in some of them and the consistent way in which the radial elongations vary.

IV. DISCUSSION

It would be very desirable to make some generalizations concerning the properties of hand spun pieces. To some extent this is possible. The results show that the mechanical properties, such as tensile strength and hardness, are increased by increasing amounts of reduction. In the mechanically spun pieces these properties after spinning were very close to the properties produced by cold rolling to the same reduction (1). The hand spun pieces do not show this agreement, in most cases being lower than the cold-rolled properties. Also the hand spun pieces show a good deal more scatter in the measured values. Thus one might conclude that hand spinning does in general work harden a piece, but that an accurate estimate of the resultant properties cannot be made.

Some of this same scatter in data is also found in the deformation measurements. For example in the 63° cones the width of the grids was decreased and the tangential displacements were negative in some regions. As was pointed out, these results are unique. No such deformations were found in any of the mechanically-spun cones, or in the cones hand spun to other cone angles.

Because of the lack of information concerning the applied forces, feed rates, and so on, it is difficult to make any analysis of the deformations. Both the grid width and the tangential displacements should be dependent upon the tangential force applied to the cone during spinning; that is, upon the force acting along the circumference of the cone. If this force were quite large it could decrease the width of the grids. The

negative tangential displacements are harder to explain. This displacement should be due to the shearing of the metal, and since the piece is always revolving in the same direction one would expect the shear to always be in the same direction. It might be possible however, if the tangential force were very large at the outer edge of the cone, for the region near the bend to be bent back in the reverse direction. This is because the piece is clamped to the pattern at the center of the cone. The net effect of the force revolving the cone at the center and the retarding force at the outer edge would be to produce a flow in the negative direction between these two forces. Thus one would expect to find a negative displacement near the bend, and a decrease in the grid width near the outer edge, which is generally the case in these cones. Whether this is actually what happened is difficult to say. It is interesting to note however, that these distortions were only found in the 63° angle cones, where the total applied force and therefore the tangential force would be greater.

Although the deformations in some cones were rather unusual, in others they were what might be expected and also quite uniform. The radial elongations for example, all showed the same general behavior. This uniformity probably reflects the consistent way in which the spinner formed the pieces. The thicknesses of some of the pieces were also very uniform, as was pointed out in the case of the 108° aluminum cones. This uniformity in thickness could be a very desirable property in many spun pieces, and it is significant that while hand spinning may produce more scatter in mechanical properties, it also may produce more uniformity in dimensions.

It is difficult to assess the influence of the various spinning tools that were used to produce the cones. With mechanical spinning the shape of the spinning tool appears important. In the present case however, variations in the force, feed rate, and so on would probably hide the influence of the tool shape. One important factor which has not been studied however, is the surface condition of the piece. To some extent the surface condition will depend on the shape of the tool and thus to some extent dictate the proper tool for the job.

From an overall point of view it would seem that the one distinct feature of hand spinning, as opposed to mechanical spinning is the greater range of properties it produces. This greater range can be either helpful or harmful, depending on what is desired in the finished piece. Thus if uniform mechanical properties are desired, hand spinning is probably inferior to mechanical spinning. Economic considerations must also enter into any comparison of the two processes. It would probably be more economical to produce a small number of pieces, or pieces having more intricate shapes, by hand spinning. A full evaluation of this is beyond the scope of this report, however.

Finally it should be pointed out that there are several important factors.which have not been evaluated in this investigation, but which must be considered in evaluating hand-spun pieces. The most important one of course is the man doing the spinning. In the present investigation all of the spinning had been done by one man. Naturally if another man did the spinning the results would be different to some degree, depending upon the skill of the man. In the present case the man who did the spinning was a

skilled spinner who has spent a number of years in the trade. Talent is very hard to evaluate however, and it is impossible to tell whether the results represent the work of an average spinner or not. The important thing is to note that at least slightly different results would be expected from each man who performs the work.

Other factors are the material being spun, and the shape and dimensions of the piece. Both the materials used in this investigation might be considered as being fairly easy materials to spin. In the same way the cones represented shapes that were quite easy to fabricate. The skill of the spinner also enters in here, but with more difficult materials and shapes even the most skillful spinners might have trouble producing uniform results.

V. CONCLUSIONS

To date this investigation of hand spun pieces has shown the following:

1 - The mechanical properties such as tensile and yield strength and hardness are somewhat lower than those found in mechanically spun pieces.

2 - The scatter in properties is greater than for the mechanically spun pieces.

3 - The deformations in hand spun pieces are similar to those in mechanically spun pieces in most cases. Two new deformations were found in some of the hand spun pieces which have not been detected before. A tentative reason has been advanced for this behavior.

TABLE I - Listing of Cones - Roller and Friction Spinning - 63° Block

Sample No.	Roller Shape	Roller Material	Lubricant	No. of Spinning Passes	Comments
3-R-1-a	4" Dia. 1-1/4" Rad.	Ampco Bronse	Heavy Grease	2 Minimum	Intended to lay metal on block in one pass. Metal springs off. Two passes required. Metal thickness unobserved.
3-R-1-b Grid Full	Multi Rad. 3/4 - 2-1/2	Ampco Bronze	Heavy Grease	24 Multiple	Intended to hold maximum metal thickness to affect the grid lines.
4-R-1-c Grid Full	Multiple Rad. 3/4-2-1/2 x 5" Dia.	Ampco Bronze	Heavy Grease	11 Multi	Eight passes, then changed spindle speed to 252 RPM to eliminate chatter.
6-R-1-e	1-1/4" Rad. 4" Dia.	Ampco Bronze	Heavy Grease	9 Minimum	Metal would not lay down on the block. Spin helper was used.
6-R-1-f Grid Full	1-1/4" Rad. 4" Dia.	Ampco	Heavy Grease	11 Multi	OK - no attempt to hold metal thickness.
2-F-1-A	3-1/2" Dia. Ball friction	Unicut	Naptha Soap and H. Grease	13 Multiple	Spun part in conventional manner to obtain proper metal flow and hold metal thickness.
2-F-1-B	3-1/2" Dia. Ball	Unicut	Soap and Grease	6 Minimum	Spun with minimum amount of strokes to lay metal on block.

Sample No.	Roller Shape	Roller Material	Lubricant	No. of Spinning Passes	Comments
6-F-1-C	3-1/2" Dia. Ball	Unicut	Soap and Grease	10	Large radius of friction ball apposed. Operator's efforts to lay metal on block.
8-F-1-D	3-1/2" Dia. Ball	Unicut	Soap and Grease	6	OK

85^{o} Block

Sample No.	Roller Shape	Roller Material	Lubricant	No. of Spinning Passes	Comments
2-R-2-A	1" Rad.	Ampco Bronze	Heavy Grease	1 min.	Good. Metal thickness regard unheeded.
2-R-2-B Grid Full	1" Rad.	Ampco	Heavy Grease	9 multi	Good. Spun to maintain metal thickness.
9-R-2-C	1" Rad.	Ampco	Heavy Grease	4 min.	Good.
9-R-2-D	1" Rad.	Ampco	Heavy Grease	7 multi	Good.
2-F-2-A	4"Ball	Unicut	H. Grease and Soap	7 min.	Good. Attempted to spin without breakdown of edge. More passes were required.

Sample No.	Roller Shape	Roller Material	Lubricant	No. of Spinning Passes	Comments
2-F-2-B Grid Full	4" Ball	Unicut	Grease and soap	2	Good Edge breakdown spun with less passes.
9-F-2-C	4" Ball	Unicut	Grease and soap	5 min.	Good. Disregard metal thickness.
9-F-2-D	4" Ball	Unicut	Grease and soap	9 Multi	Good. Spun to maintain metal thickness.
			108° Block		
2-R-3-A	Multi Rad. 3/4" -2-1/2" x 5" Dia.	Ampco	H. Grease	12 Multi	OK - Spun conventionally.
2-R-3-B	Multi Rad. 3/4" -2-1/2" x 5" Dia.	Ampco	H. Grease	1 Minimum	OK - No attempt to retain metal thickness.
8-R-3-A	Multi Rad. 3/4: -2-1/2" x 5" Dia.	Ampco	G. Grease	10 Multi	OK
8-R-3-B Grid	3/4: -2-1/2" x 5" Dia.	Ampco	H. Grease	2 Minimum	OK - No regard for metal thickness.
2-F-3-A	3" Sphere	Unicut	H. Grease	10 Multi	OK - Crimped edge to stiffen blank. Multiple passes to impose stress.

Sample No.	Roller Shape	Roller Material	Lubricant	No. of Spinning Passes	Comments
2-F-3-B	3" Sphere	Unicut	Naptha Soap and H. Grease	1 Minimum	OK - Crimped edge. No regard for metal thickness.
8-F-3-A	3" Sphere	Unicut	Grease and Soap	2 Minimum	OK - More effort required by operator to lay metal on block. Approximately 3" l compared to roller spinning.
8-F-3-B	3" Sphere	Unicut	Grease and Soap	Multi	OK - Same as 8-F-3-A.

Sample Numbers

1st number in code refers to material
2,3 = .081" aluminum
4 = .125" aluminum
6-9 = brass

TABLE II

Tensile Properties of Hand Spun Cones

Each value is average of two specimens, one parallel and one perpendicular to the original rolling direction of the sheet.

rad = radial direction - direction from center of cone to outer edge.
tan = tangential direction - direction parallel to outer edge of cone, or perpendicular to radial direction.

63^{o} Angle Cones

Cone		Tensile Strength (psi)	Yield Strength .2% offset (psi)	%Elongation
Brass 8FiD	rad	73,700	57,000	7.2
	tan	66,700	49,000	7.9
Brass 6FiC	rad	64,000	48,800	12.5
	tan	55,000	41,000	29.0
Brass 6K1F	rad	64,800	45,200	15.7
	tan	63,400	42,400	16.5
Brass 6K1E	rad	76,000	53,800	6.8
	tan	61,500	40,200	14.0
Brass 6R1G	rad	73,800	50,600	4.8
	tan	63,400	48,900	11.8
081 Al 2F1A	rad	15,300	13,200	16.8
	tan	14,800	12,800	16.4
081 Al 3R1A	rad	17,100	15,600	10.8
	tan	17,400	15,800	8.8
081 Al 3R1B	rad	15,300	13,200	16.5
	tan	15,000	12,800	17.4
081 Al 2F1B	rad	15,600	13,600	15.6
	tan	15,100	13,000	13.6
125 Al 4R1C	rad	14,600	12,200	21.6
	tan	14,400	12,400	20.8

85^{o} Angle Cones

Cone	Tensile Strength Psi	Yield Strength .2% offset (Psi)	% Elongation
Brass 9F2C rad	70,800	68,200	13.3
tan	65,300	64,700	16.4
Brass 9F2D rad	70,100	63,000	17.2
tan	60,200	57,600	23.4
Brass 9R2C rad	70,300	68,500	14.8
tan	65,600	65,400	14.8
Brass 9R2D rad	67,200	65,700	12.5
tan	61,200	58,400	25.0
Al 2F2A rad	16,900	16,600	18.7
tan	16,500	16,200	17.2
Al 2F2B rad	18,500	18,200	12.5
tan	17,200	17,100	12.5
Al 2R2A rad	18,100	17,500	12.3
tan	17,500	16,700	14.9
Al 2R2B rad	16,200	15,500	19.6
tan	15,700	15,000	21.9

108° Cone Angles

Cone		Tensile Strength (psi)	Yield Strength .2% offset (psi)	%Elongation
Brass 8R3A	rad	64,800	85,000	13.1
	tan	59,000	49,000	24.0
Brass 8F3A	rad	64,800	58,000	14.0
	tan	58,400	49,600	21.1
Brass 8F3B	rad	59,100	39,000	15.2
	tan	60,500	51,700	16.1
Brass 8R3B	rad	61,800	55,000	18.7
	tan	58,800	47,800	12.2
081 Al 2R3B	rad	14,200	13,200	14.7
	tan	13,700	12,500	16.3
081 Al 2R3A	rad	15,400	14,000	12.3
	tan	15,500	13,500	16.6
081 Al 2F3A	rad	14,900	12,600	15.1
	tan	14,600	12,500	15.3
081 Al 2F3B	rad	15,700	14,200	15.5
	tan	15,100	13,900	14.8

TABLE III

Hardness of Spun Surface of Hand Spun Cones

Brass Cones	Average Hardness - Rockwell B Scale
63° angle	76
85° angle	72
108° angle	69

Aluminum Cones	Average Brinell Hardness No. 500-Kg load 10 mm Ball
63° angle .081" thick	29
63° angle .125" thick	27
85° angle .081" thick	28
108° angle .081" thick	27

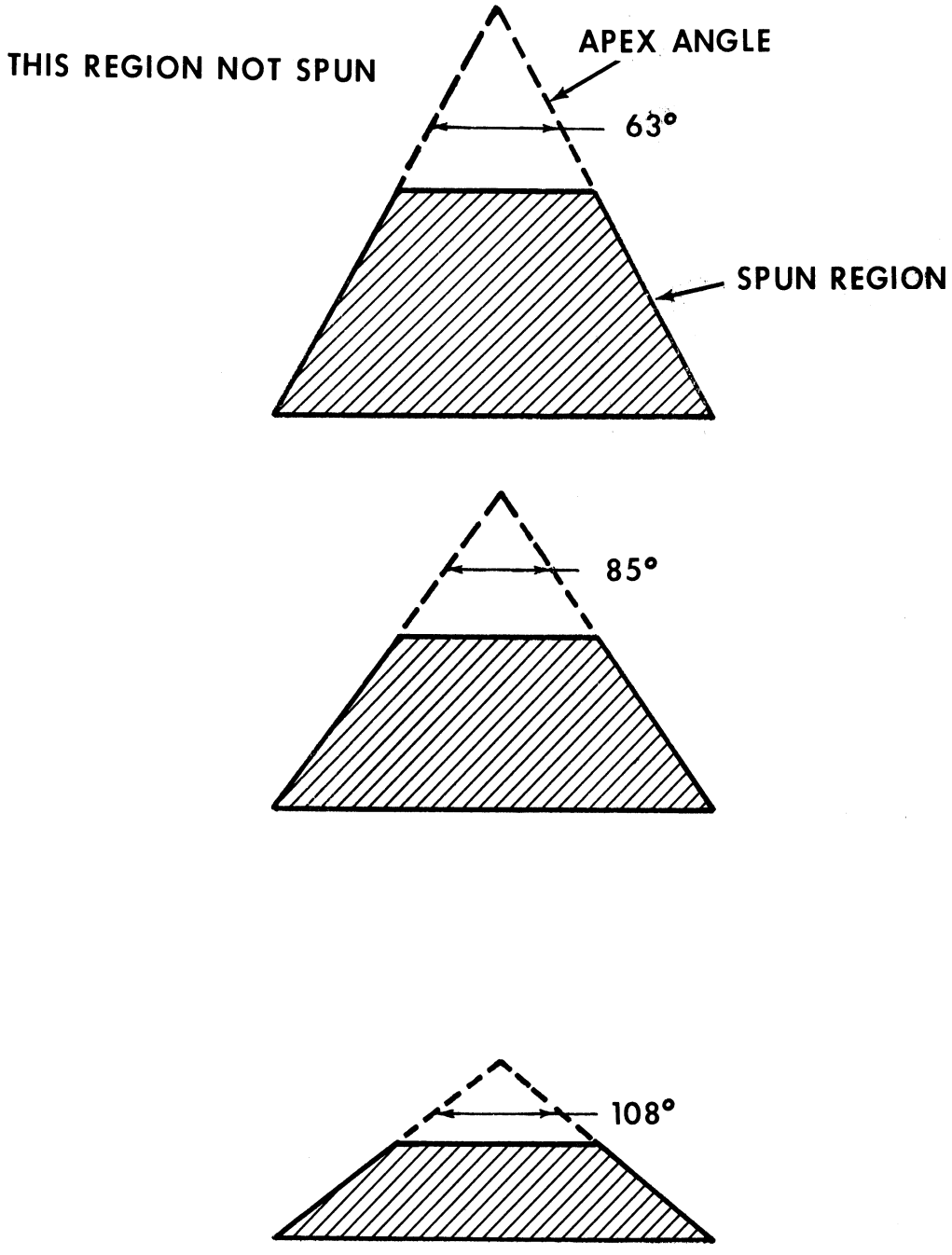

SCHEMATIC VIEW SHOWING CONE ANGLES

FIG. 1

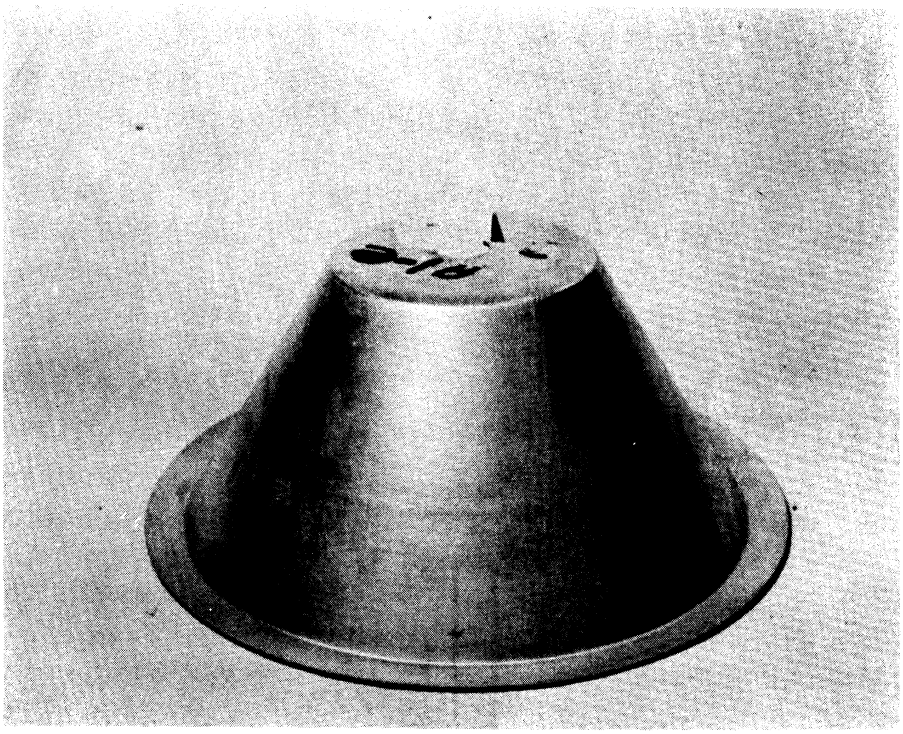

Fig. 2. Photograph of spun cone.

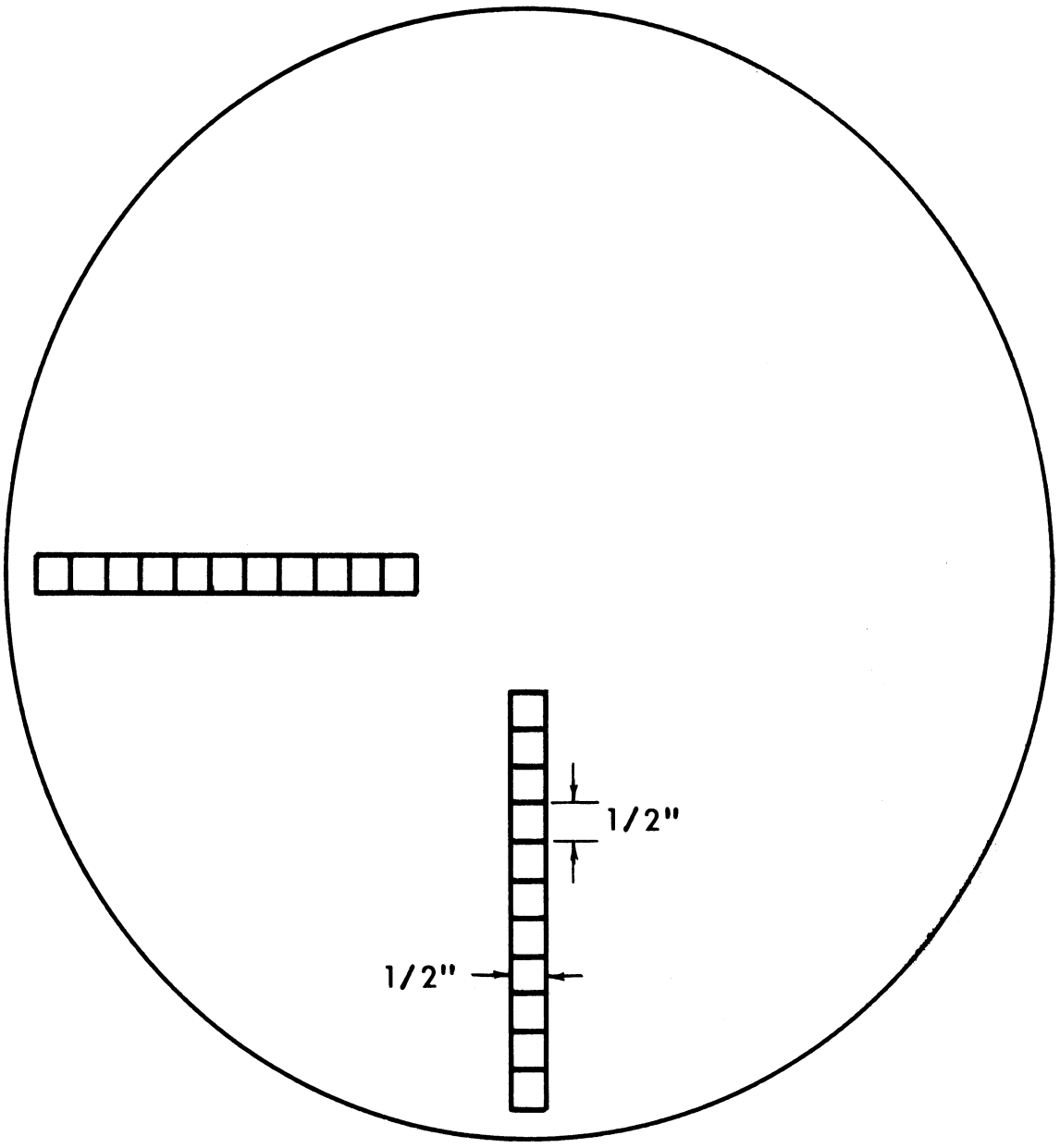

LAYOUT OF GRIDS ON BLANKS BEFORE SPINNING

FIG. 3

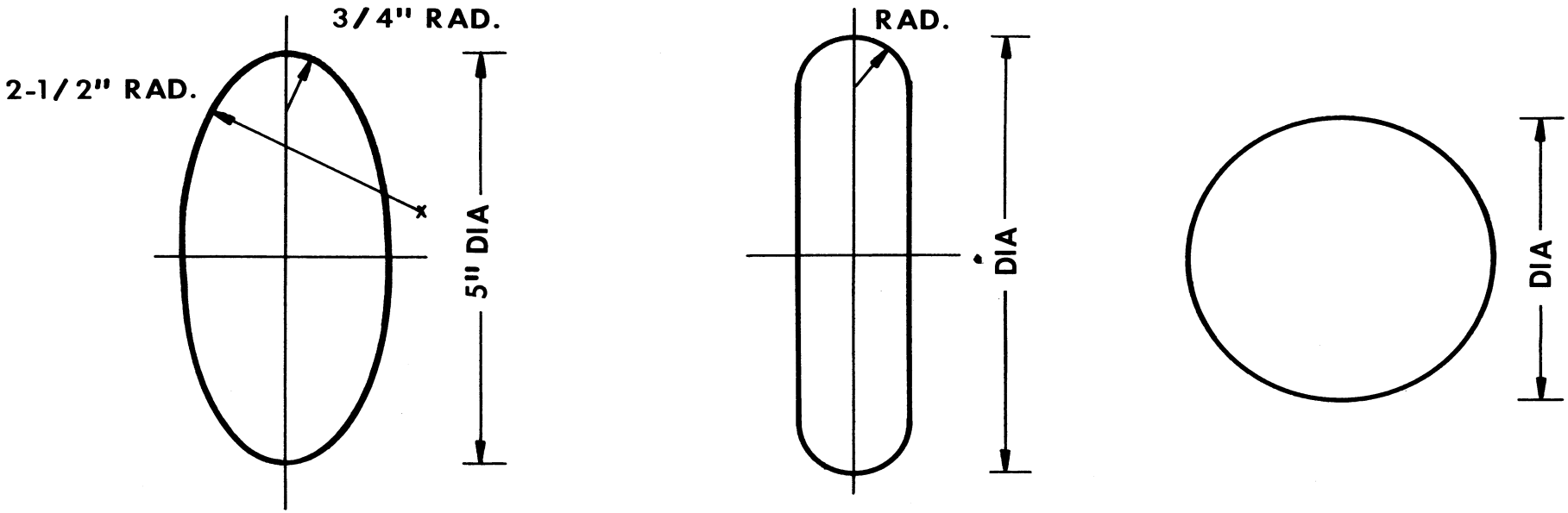

SCHEMATIC VIEW OF VARIOUS SPINNING TOOLS

FIG. 4

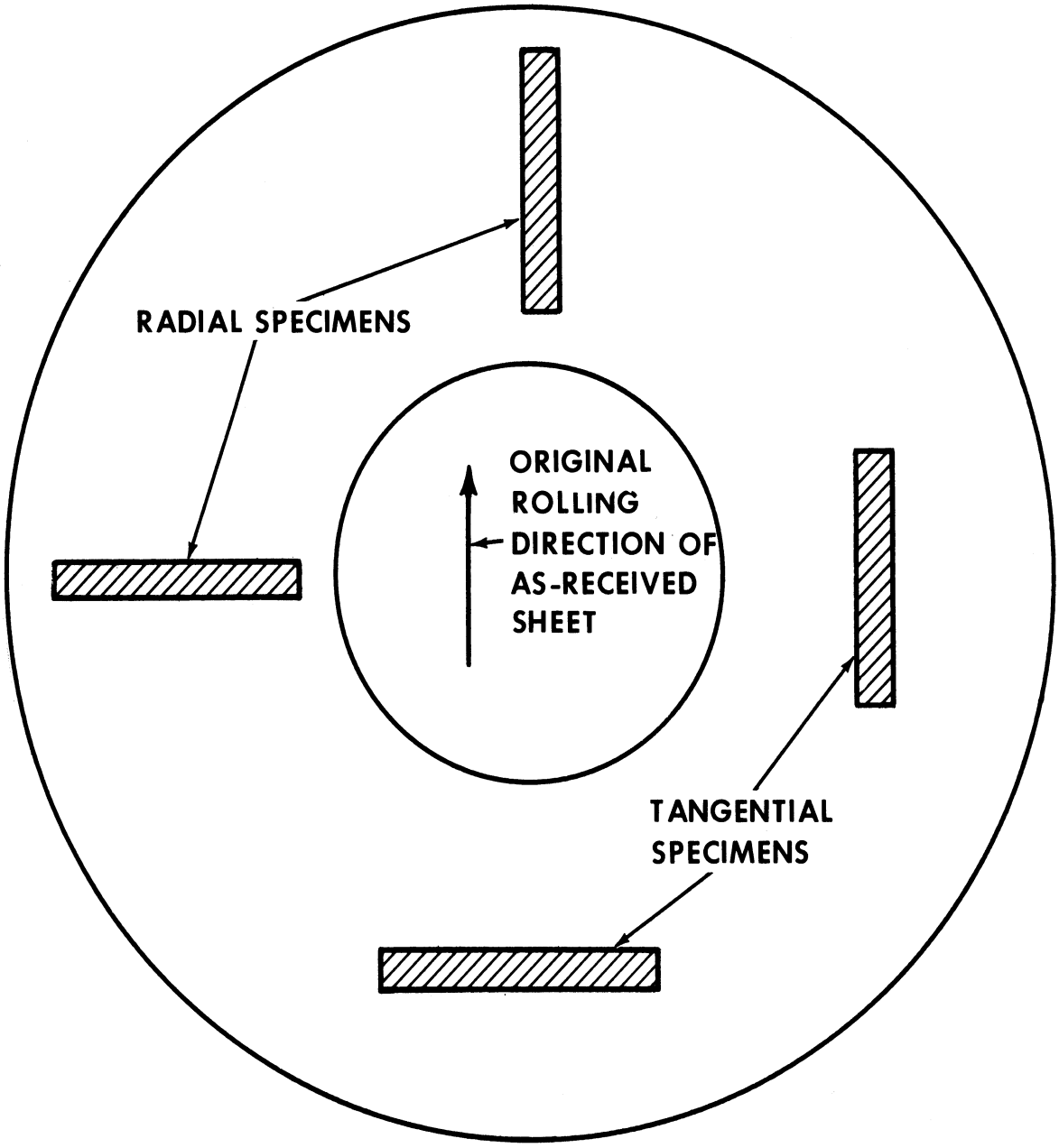

LOCATIONS WHERE TENSILE SPECIMENS WERE CUT FROM CONES

FIG. 5

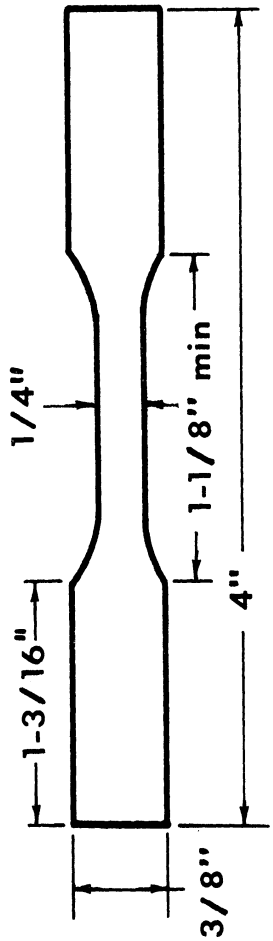

FOUR INCH TENSILE SPECIMEN

FIG. 6

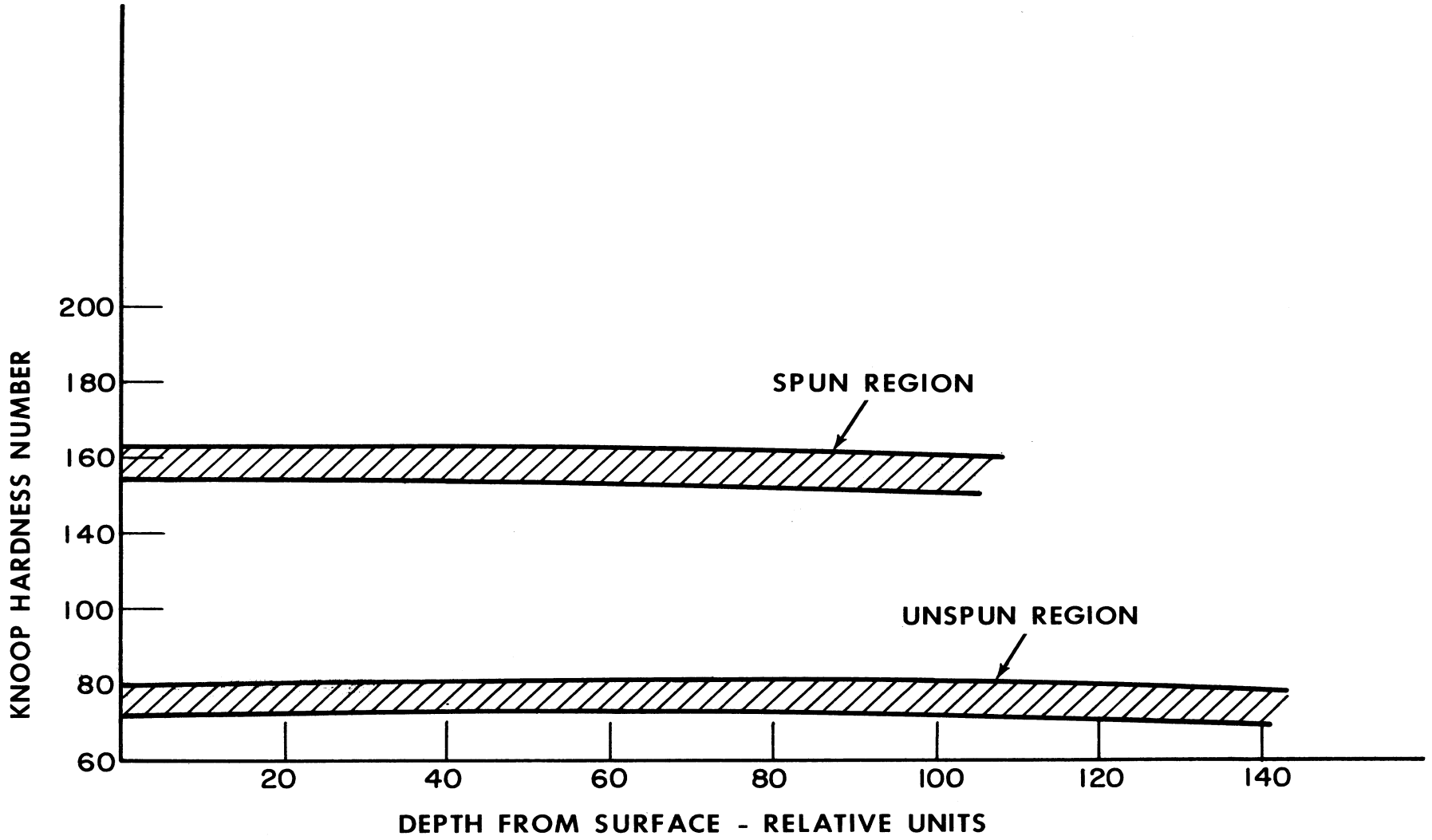

MICROHARDNESS vs DEPTH BELOW SPUN SURFACE – HAND-SPUN BRASS CONES

FIG. 7

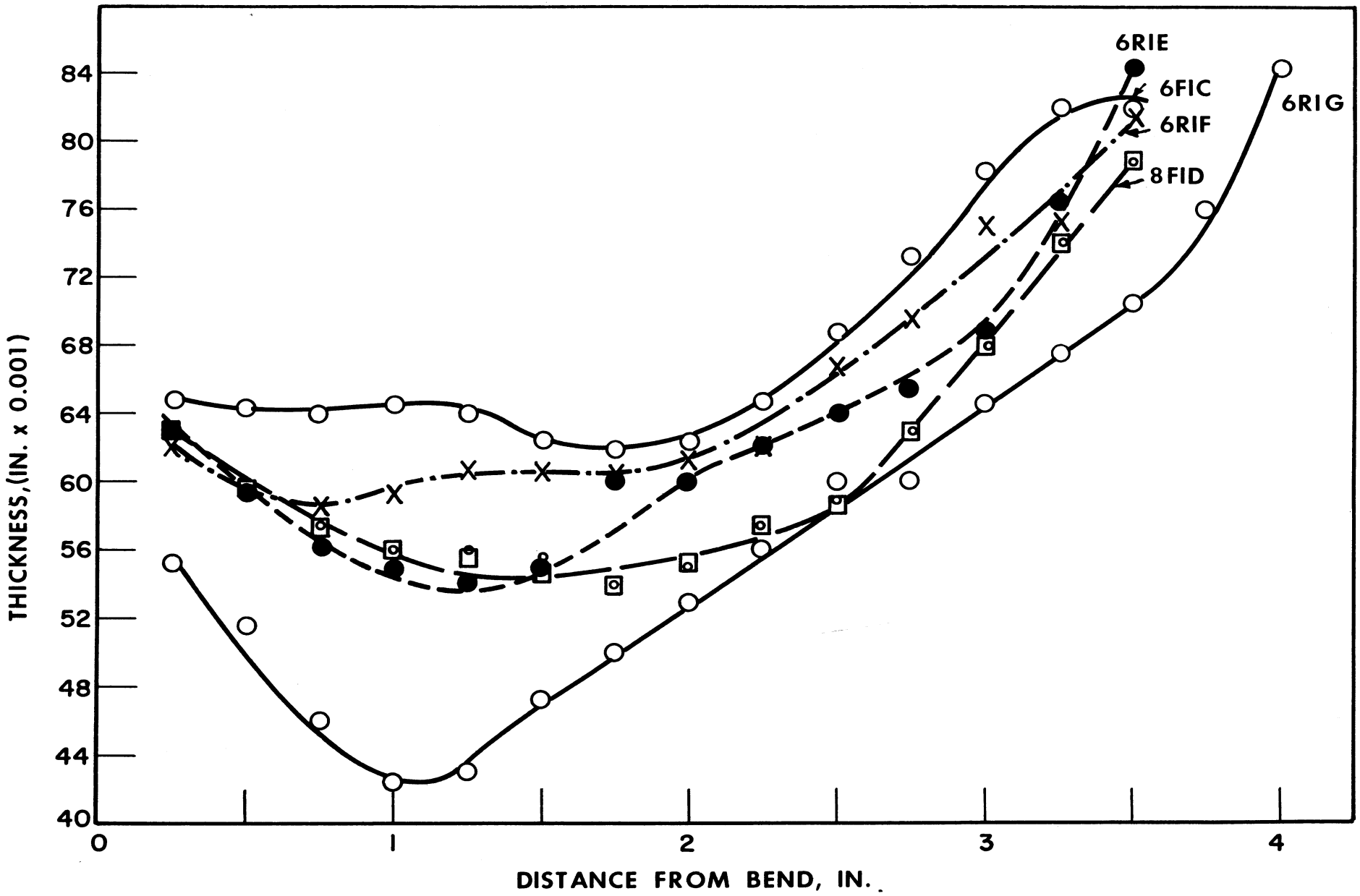

THICKNESS OF HAND-SPUN BRASS CONES - 63°CONE ANGLE

FIG. 8a

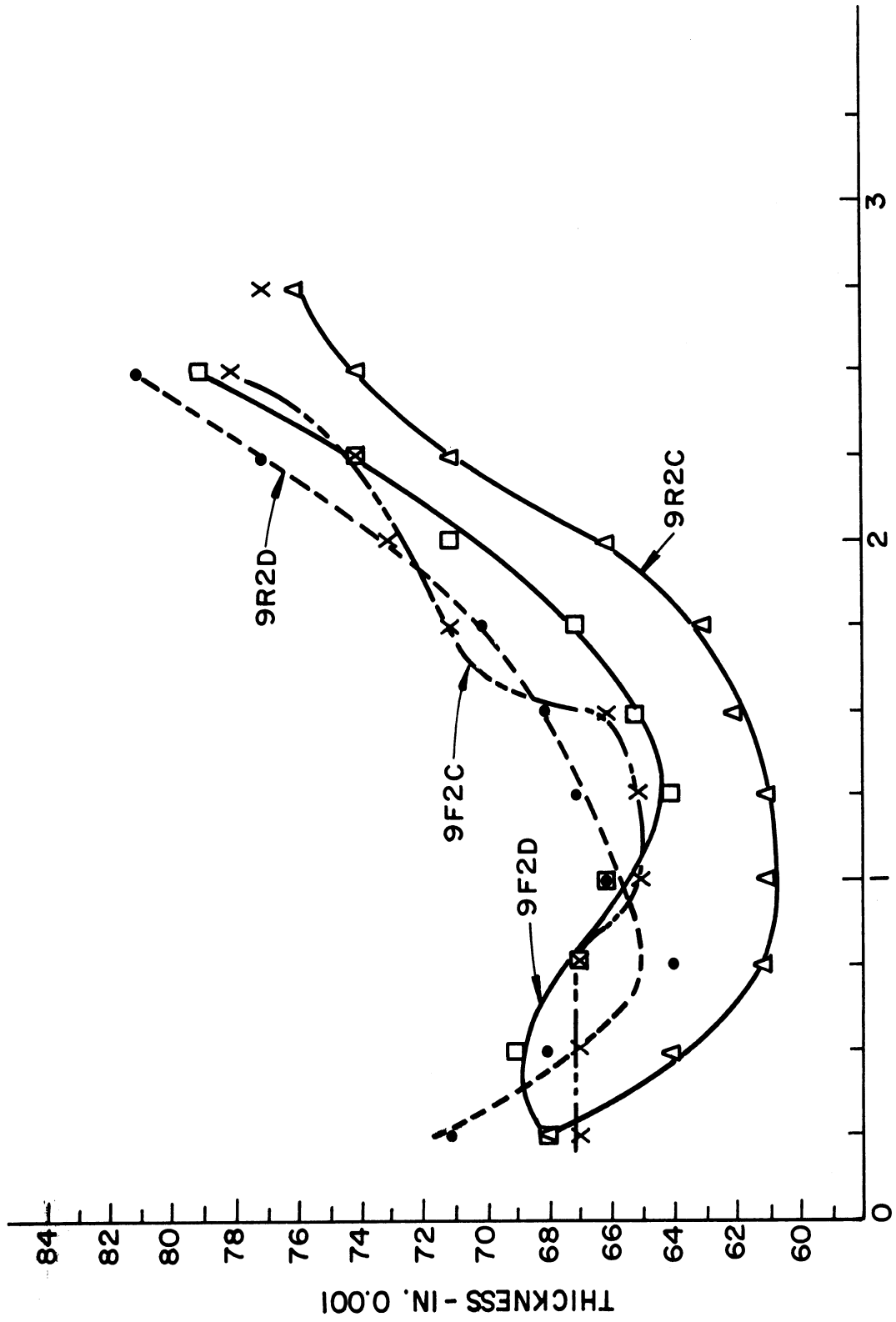

Thickness of Hand Spun Brass Cones 85° Cone Angle

Fig. 8a. (Cont.)

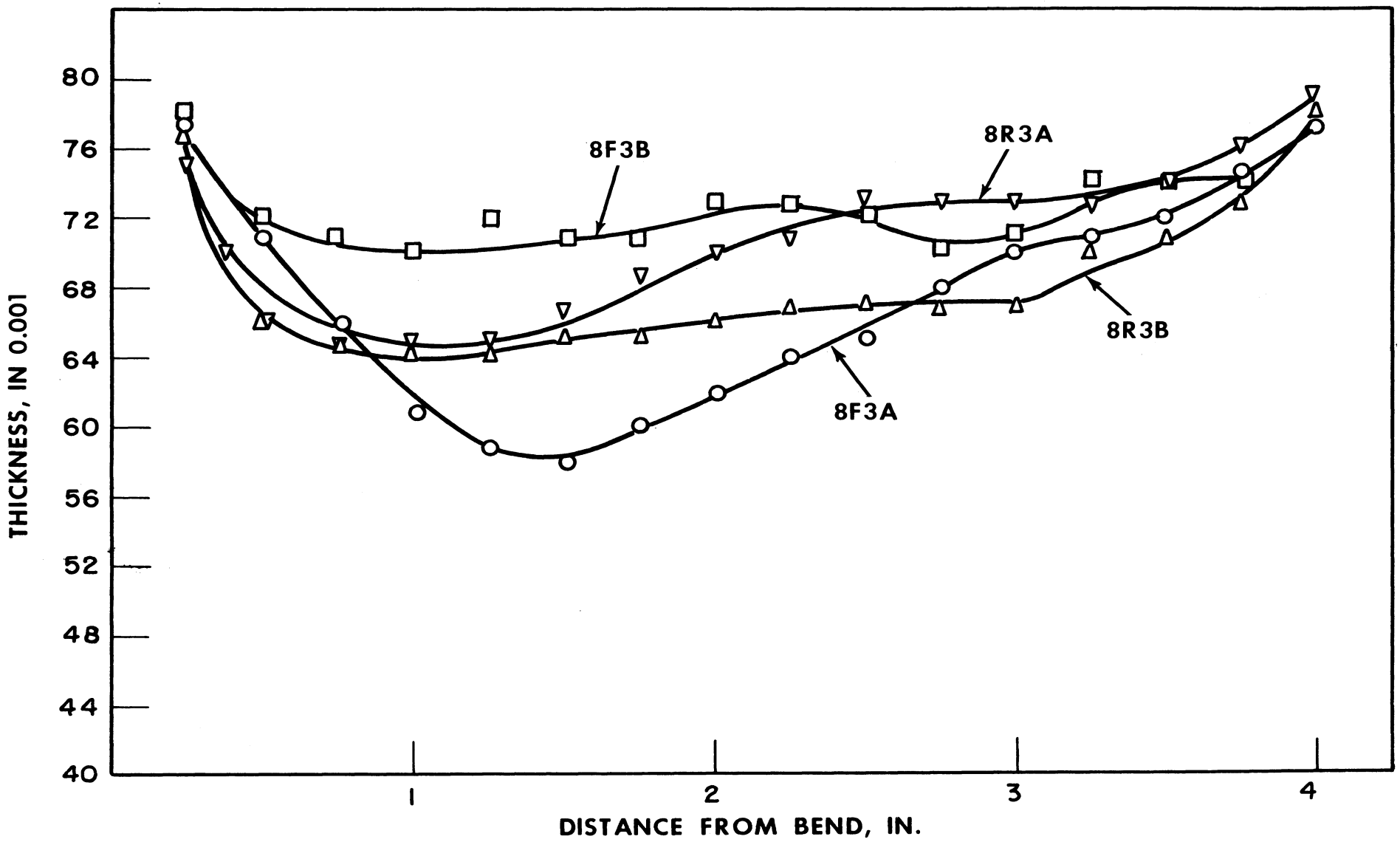

THICKNESS OF HAND-SPUN BRASS CONES - 108° CONE ANGLE

FIG. 8a (CONT.)

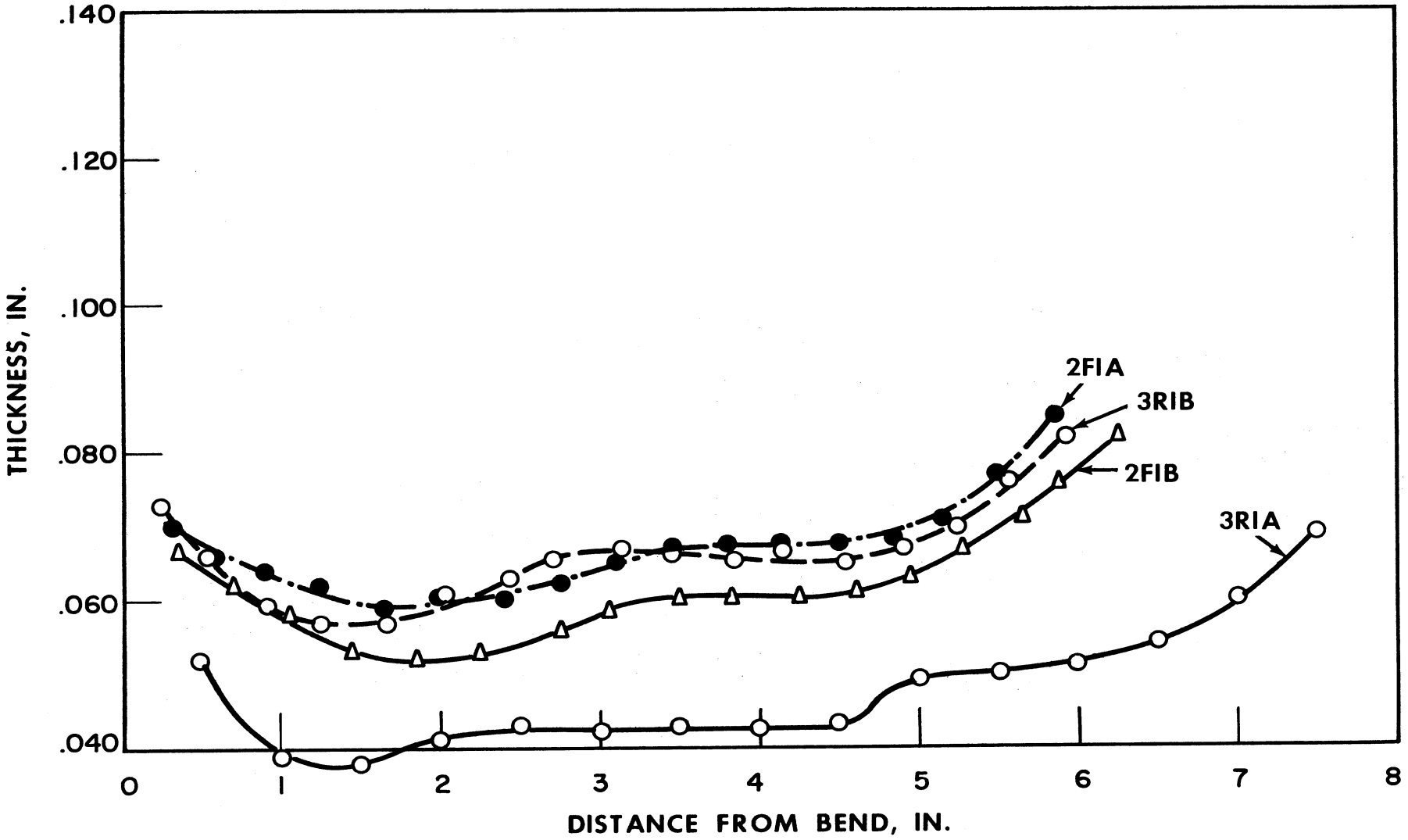

THICKNESS OF HAND-SPUN .081-IN. ALUMINUM CONES - 63° CONE ANGLE

FIG. 8b

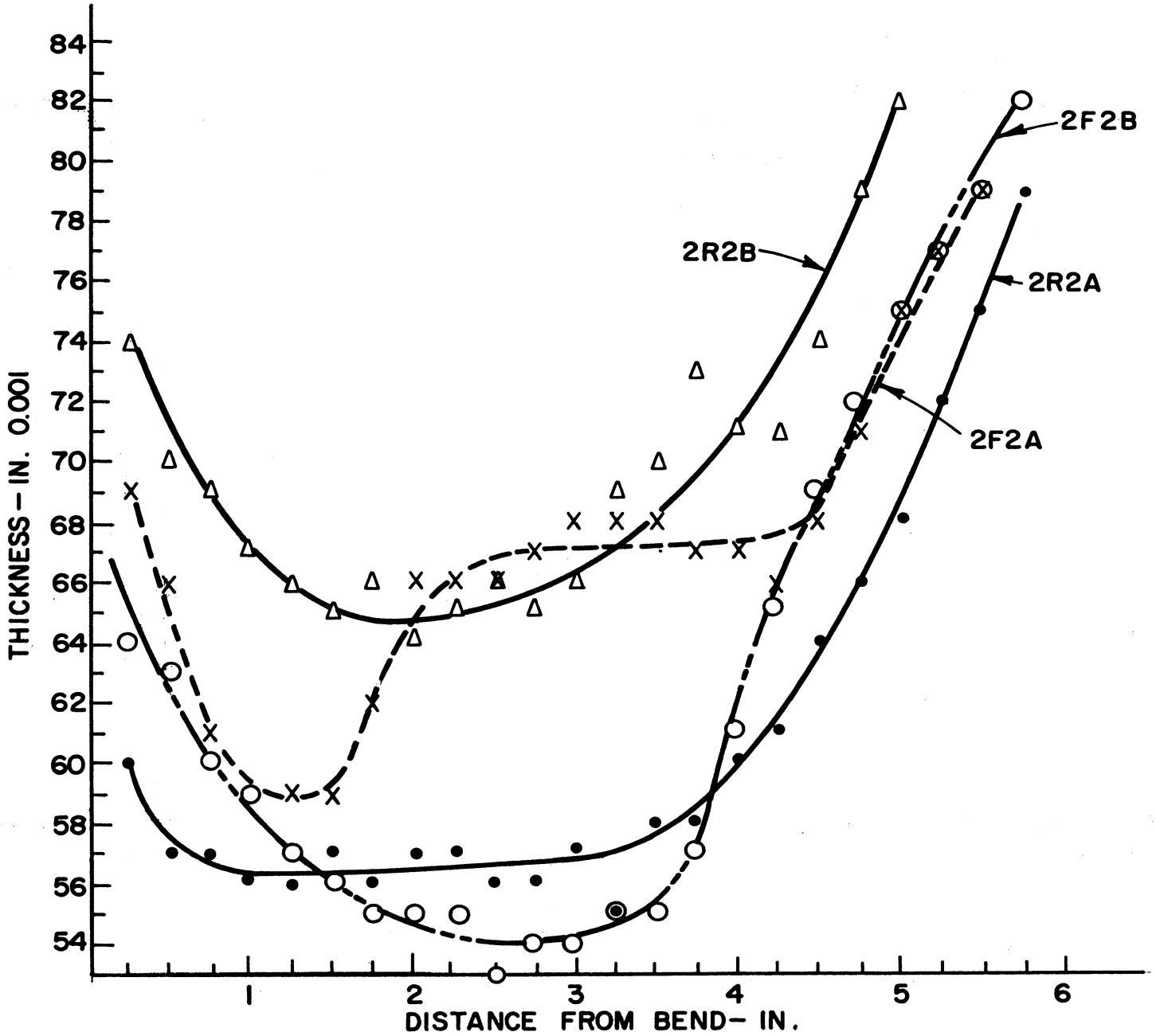

Thickness of Hand Spun Aluminum Cones 85° Cone Angle

Fig. 8b (Cont.)

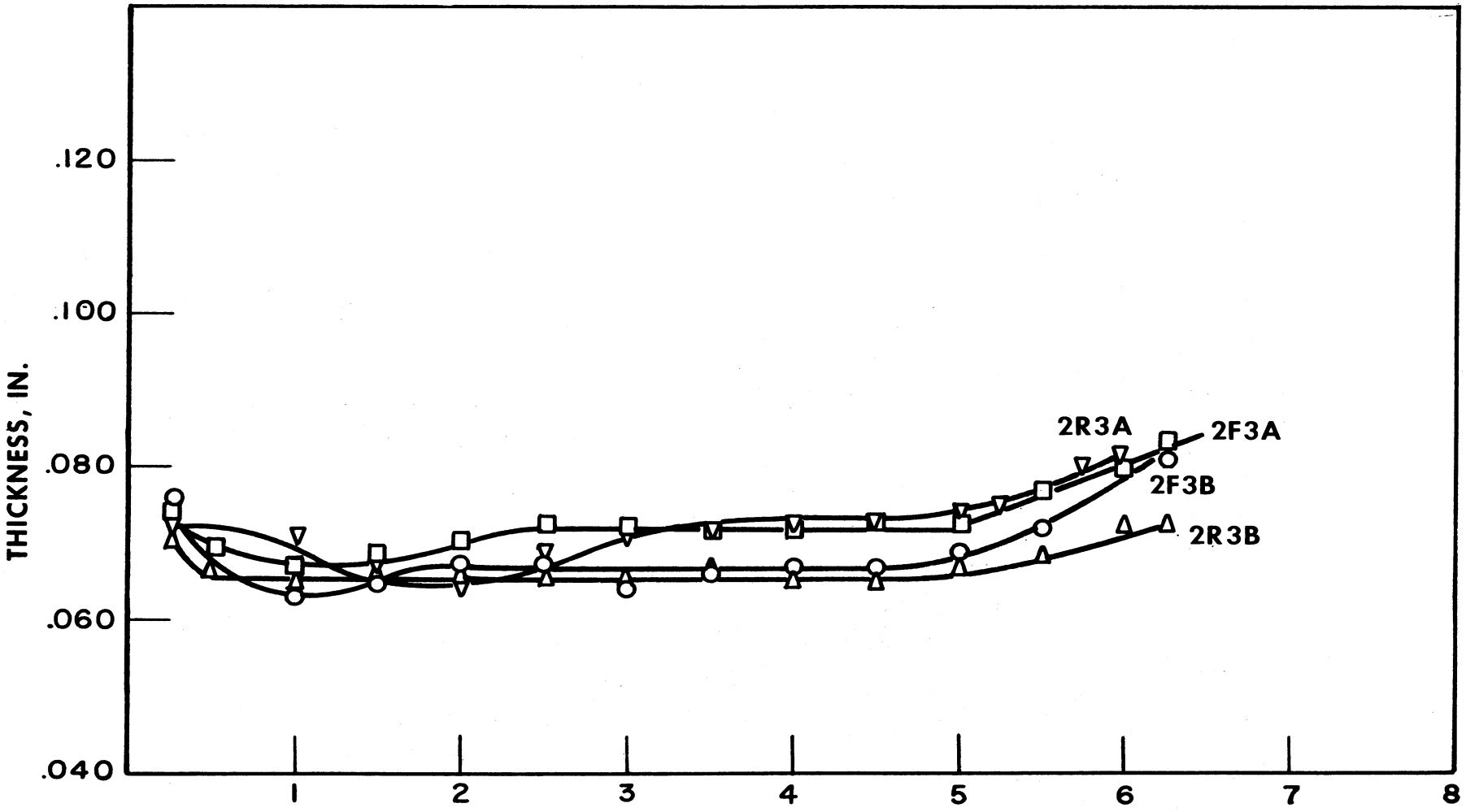

DISTANCE FROM BEND, IN.

THICKNESS OF HAND-SPUN ALUMINUM CONES - 108° CONE ANGLE

FIG. 8b (CONT.)

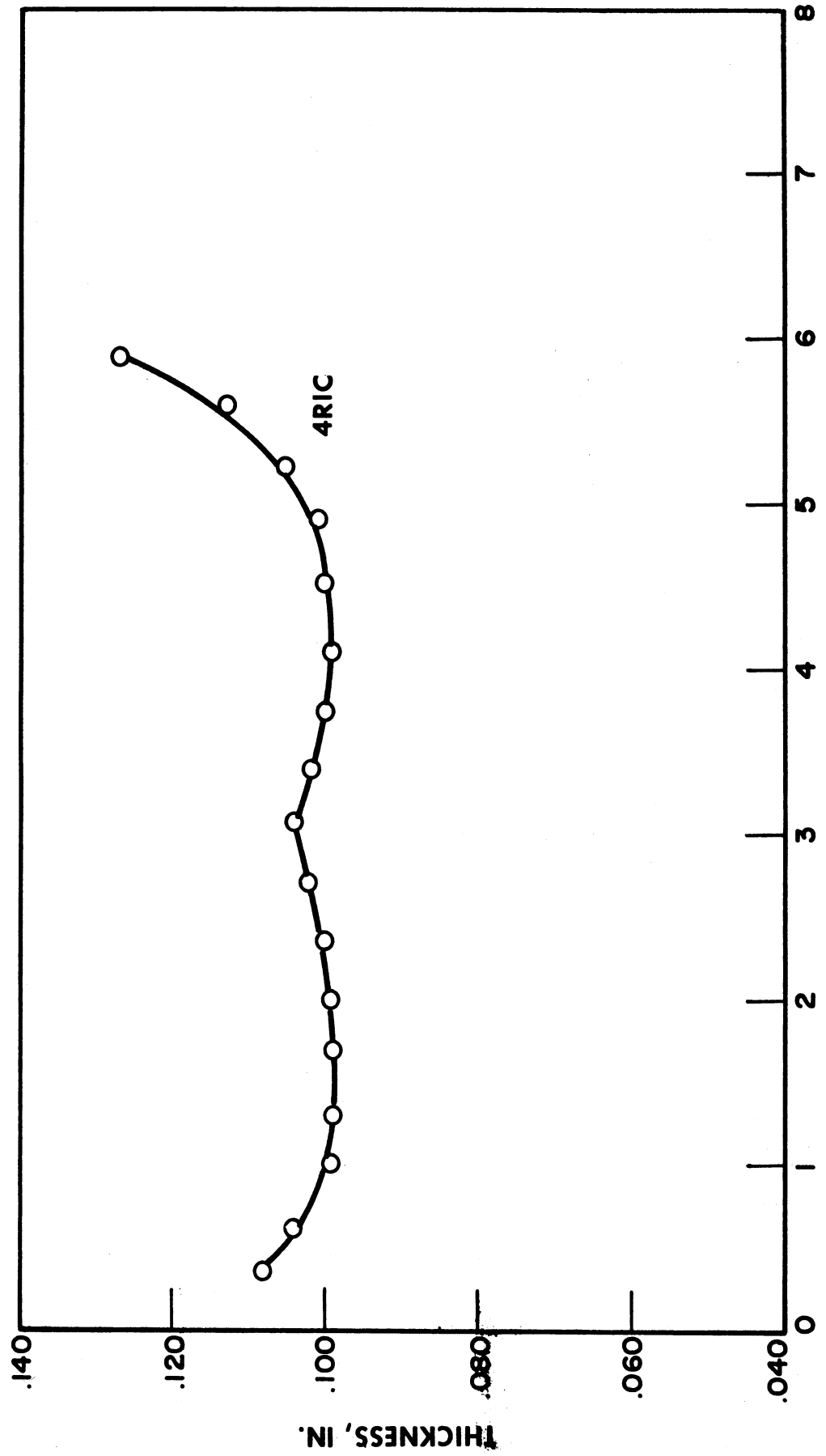

THICKNESS OF HAND-SPUN .125-IN. ALUMINUM CONES

FIG. 8c

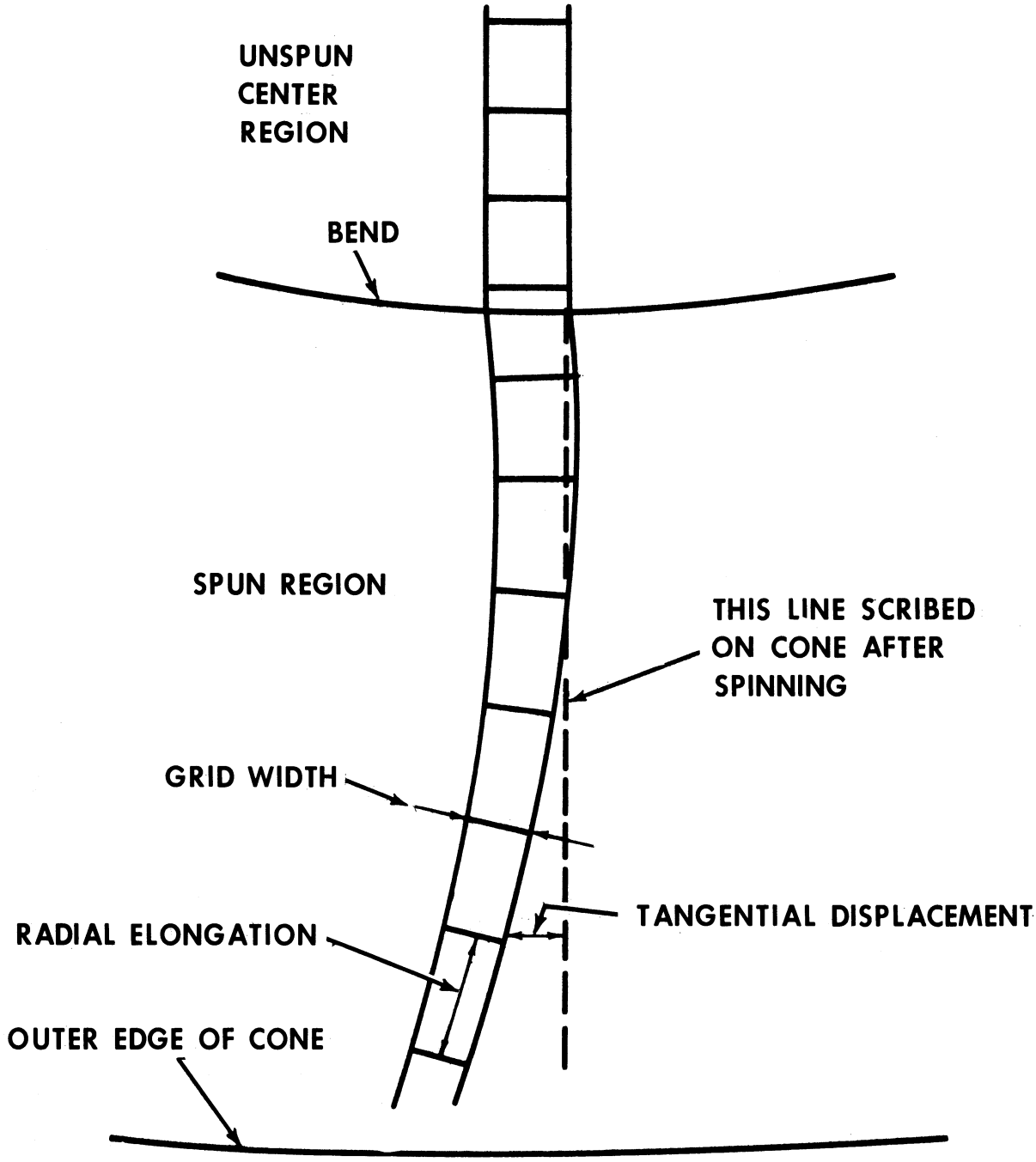

GRID DISTORTIONS IN CONES

FIG. 9

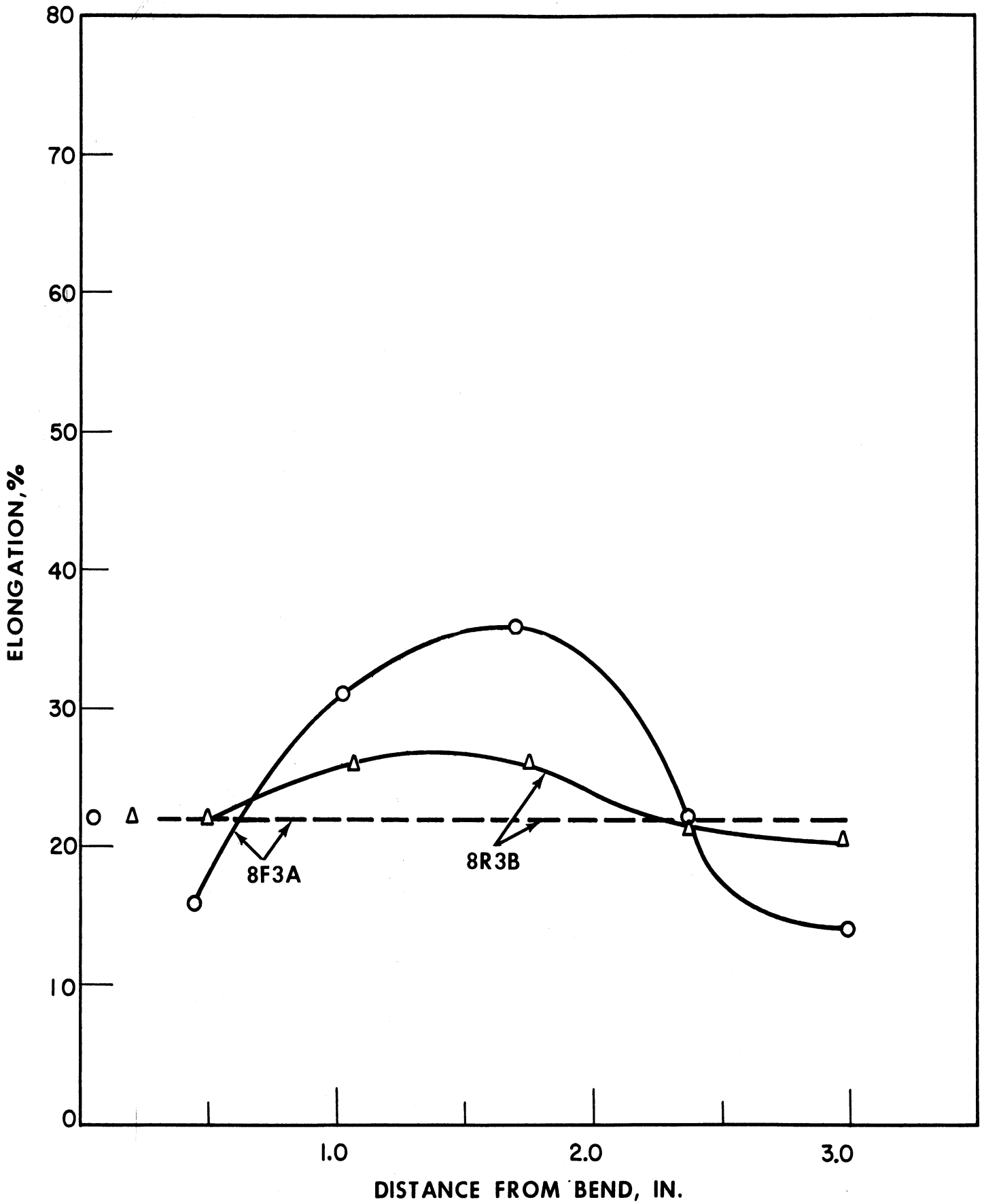

RADIAL GRID ELONGATION - 63° BRASS CONES

FIG. 10a

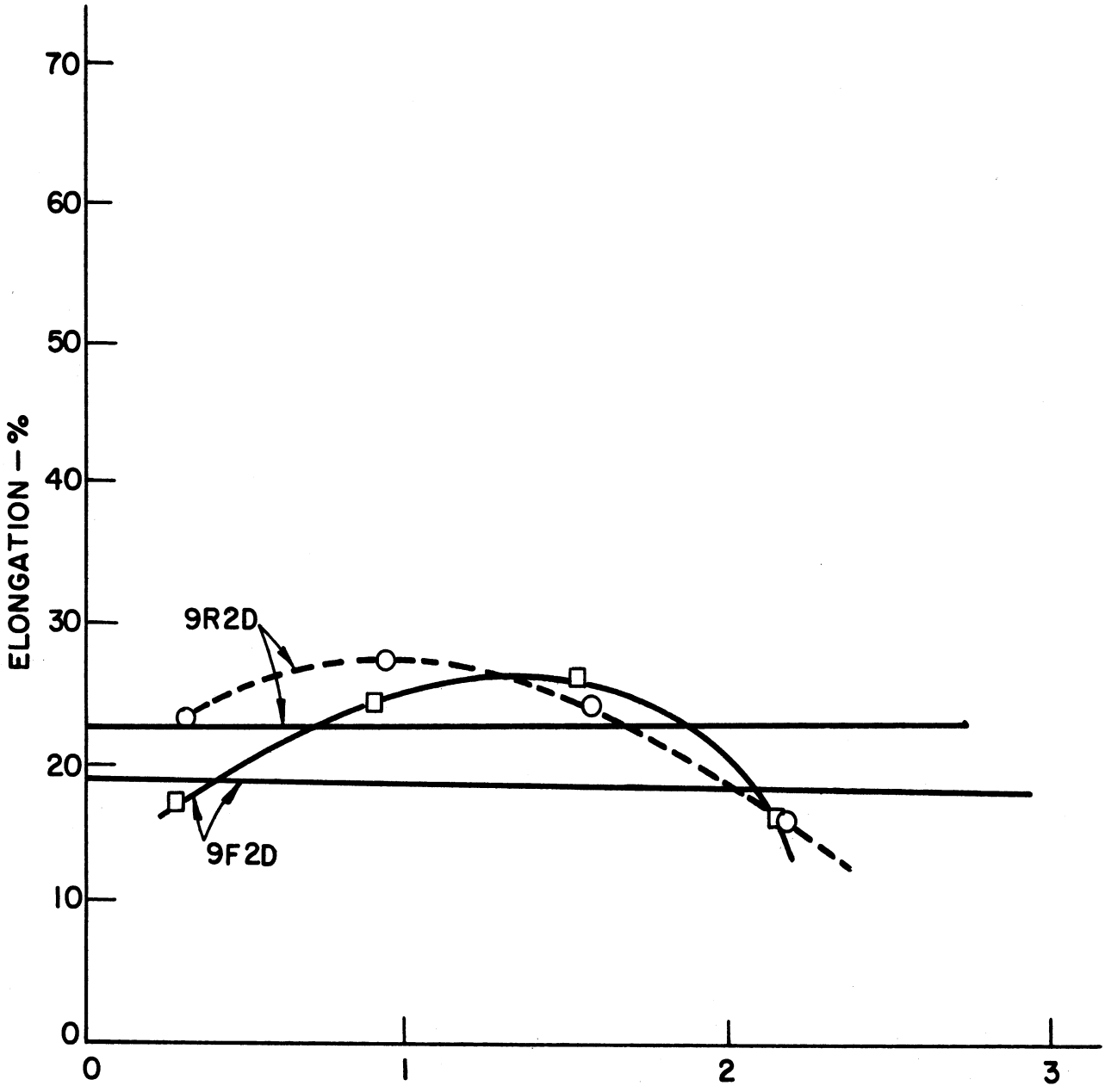

Radial Grid Elongation – 85° Brass Cones

Fig. 10a. (Cont.)

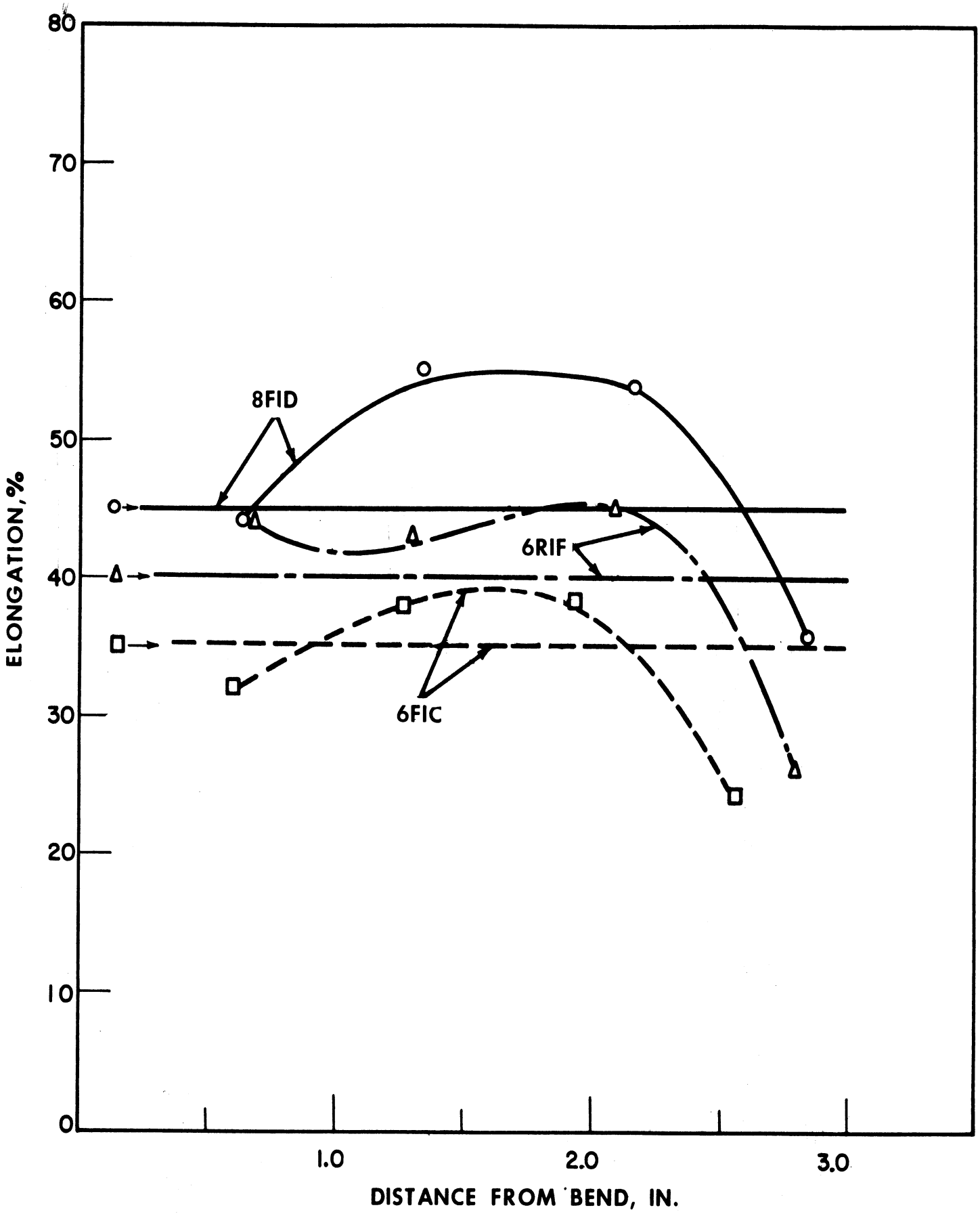

RADIAL GRID ELONGATION - 108° BRASS CONES

FIG. 10a (CONT.)

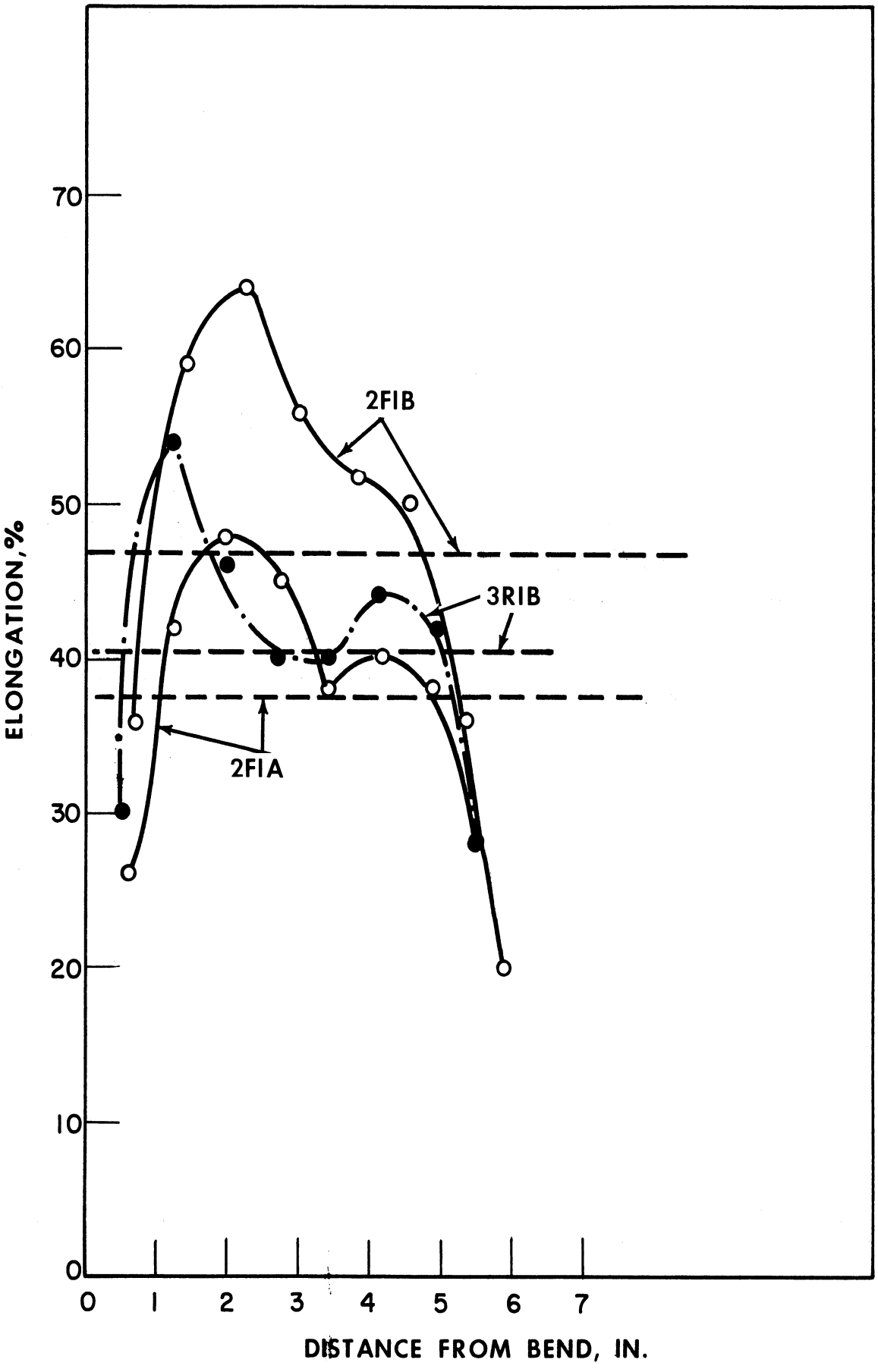

RADIAL GRID ELONGATION 63° ALUMINUM CONES

FIG. 10b

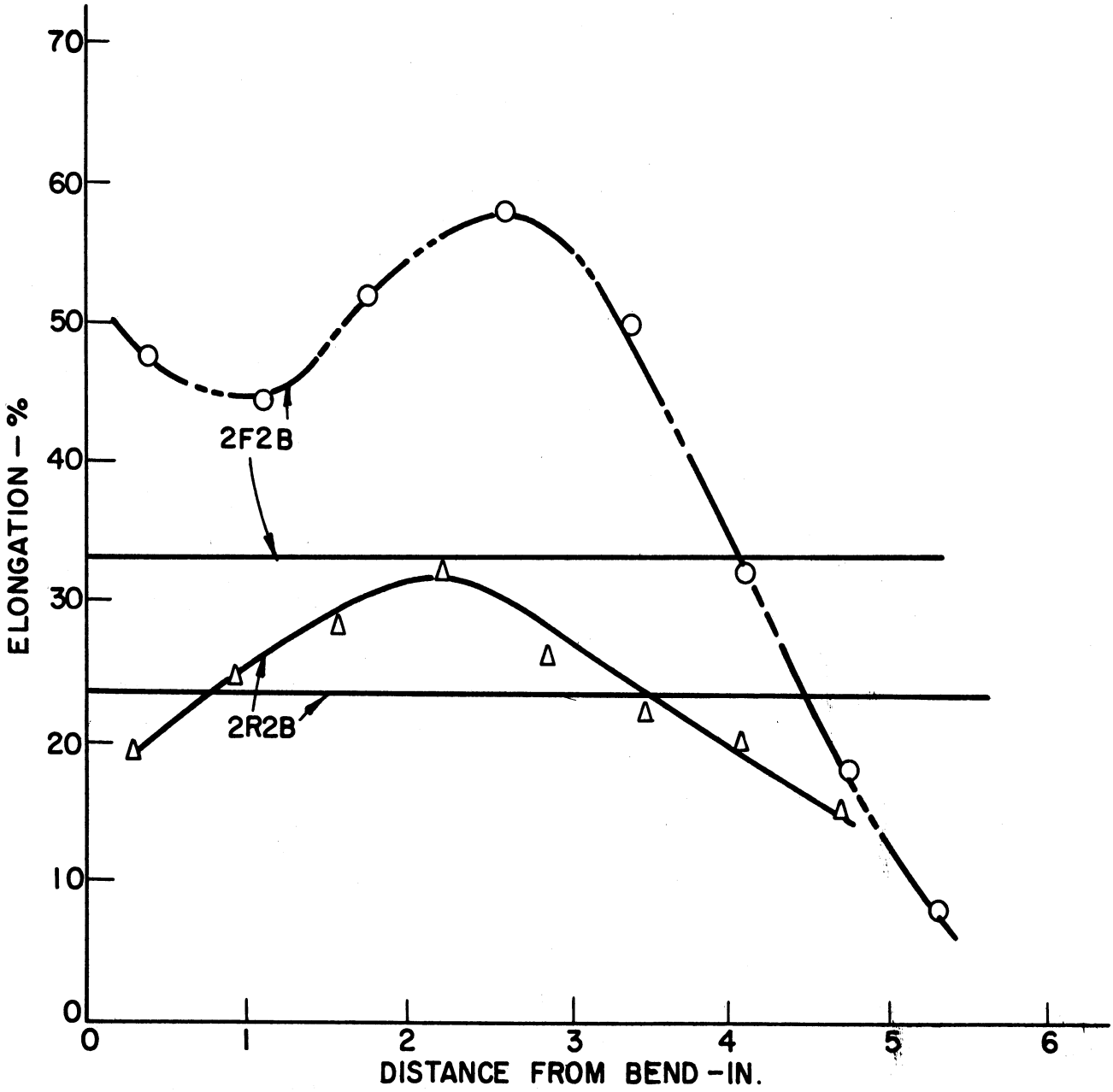

Radial Grid Elongation 85° Aluminum Cones

FIG. 10b (Cont.)

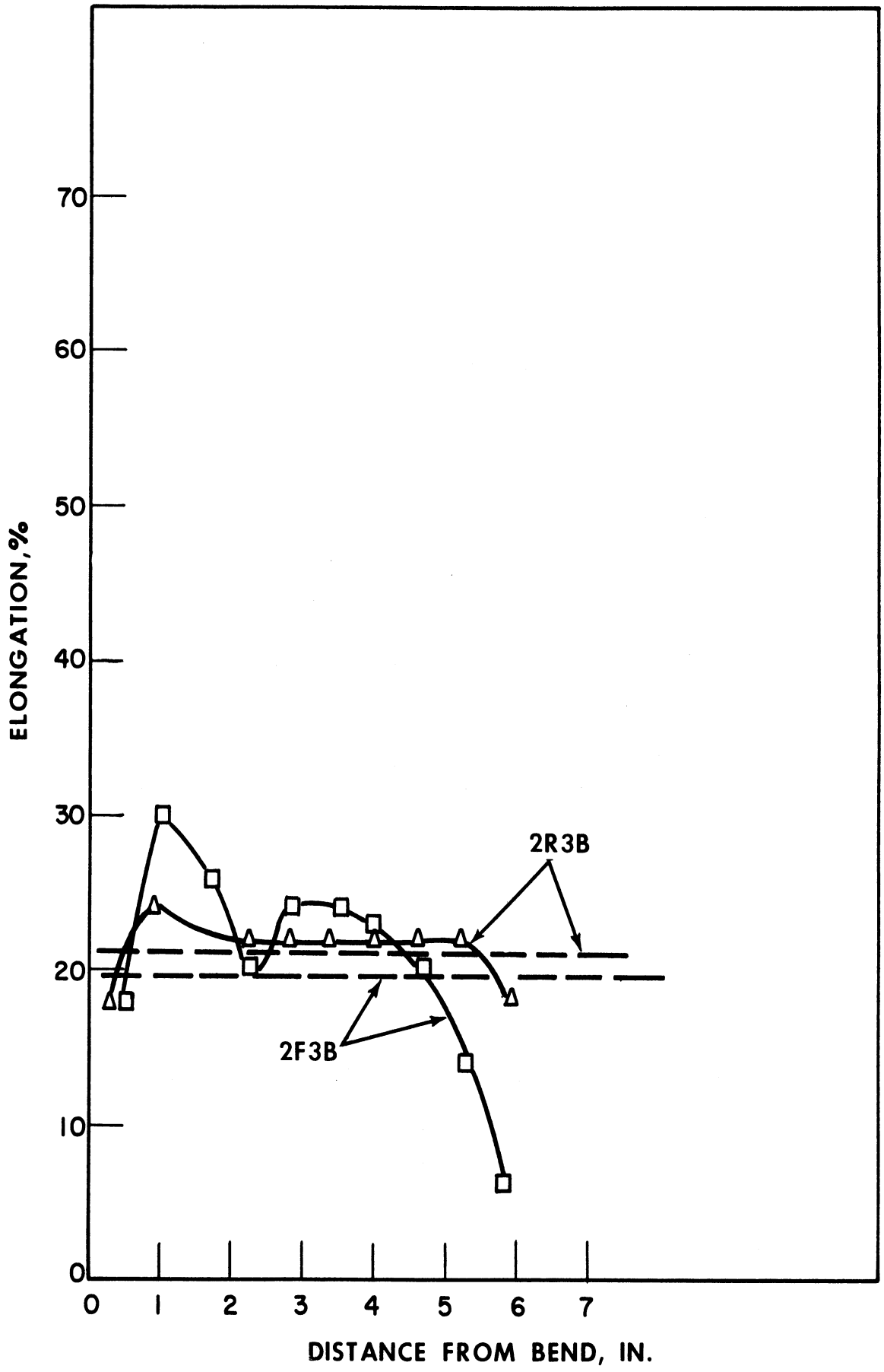

RADIAL GRID ELONGATION 108° ALUMINUM CONES

FIG. 10b (CONT.)

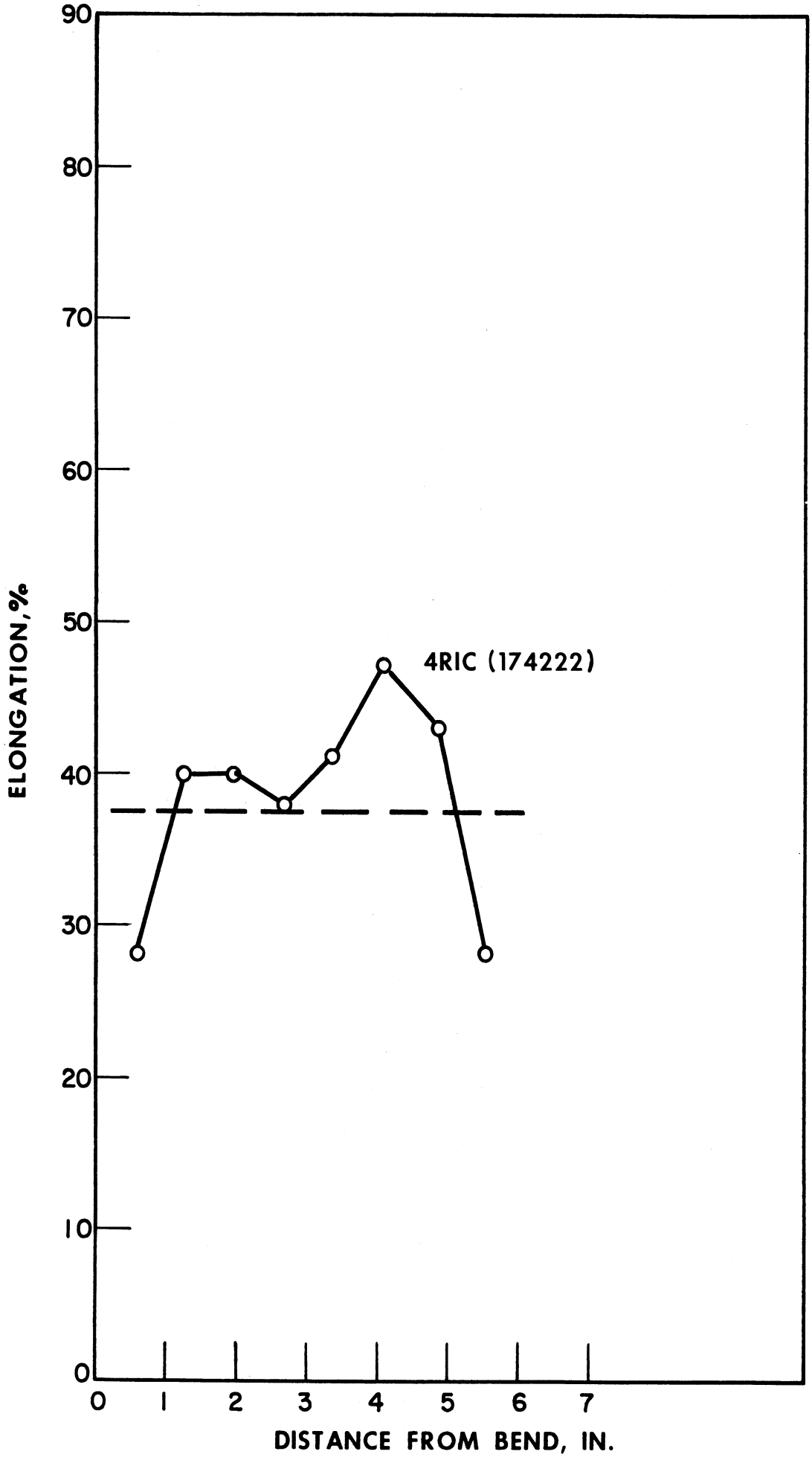

RADIAL GRID ELONGATION– HAND-SPUN .125-IN. ALUMINUM CONES

FIG. 10c

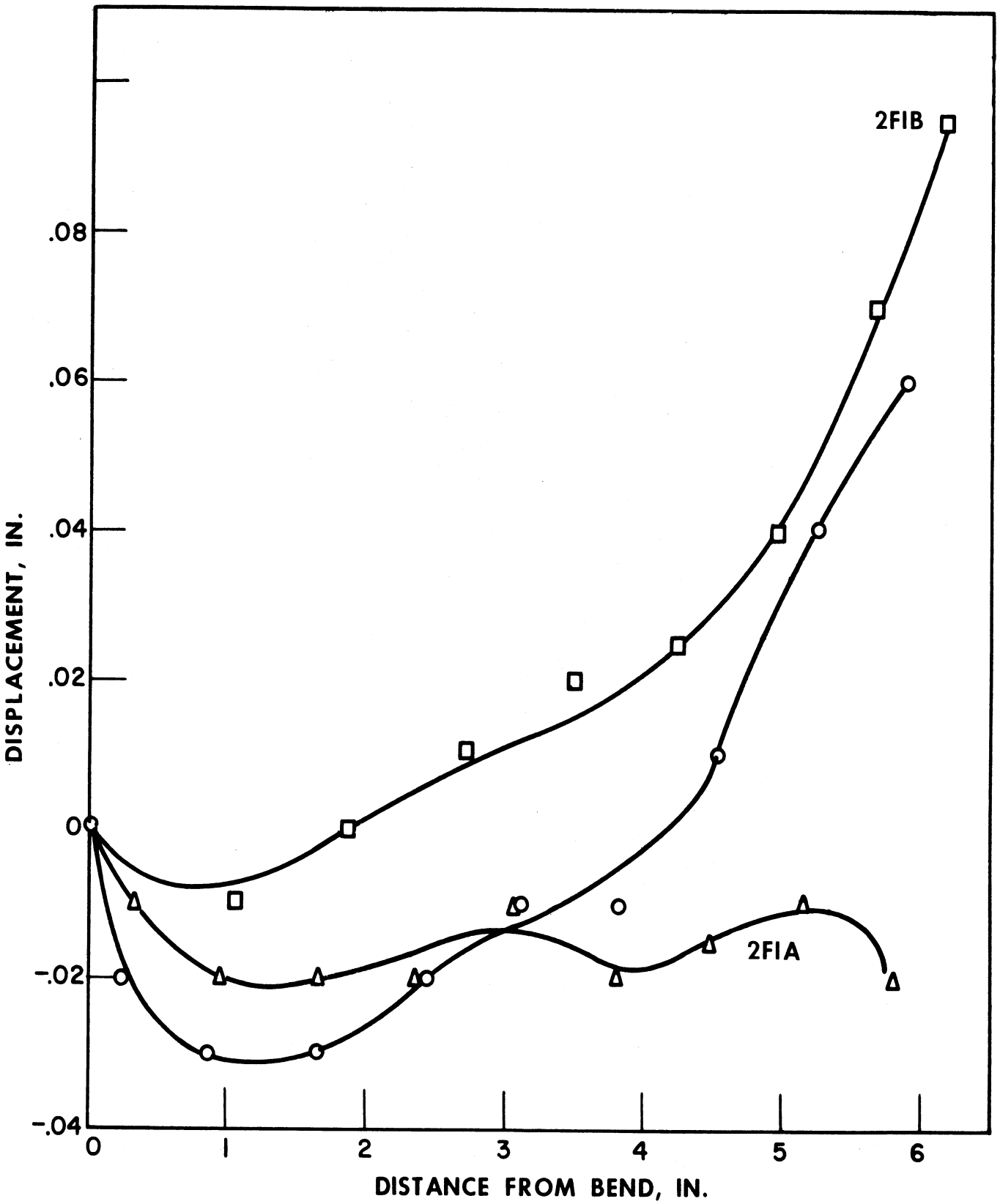

TANGENTIAL GRID MOVEMENT 63° BRASS CONES

FIG. 11a

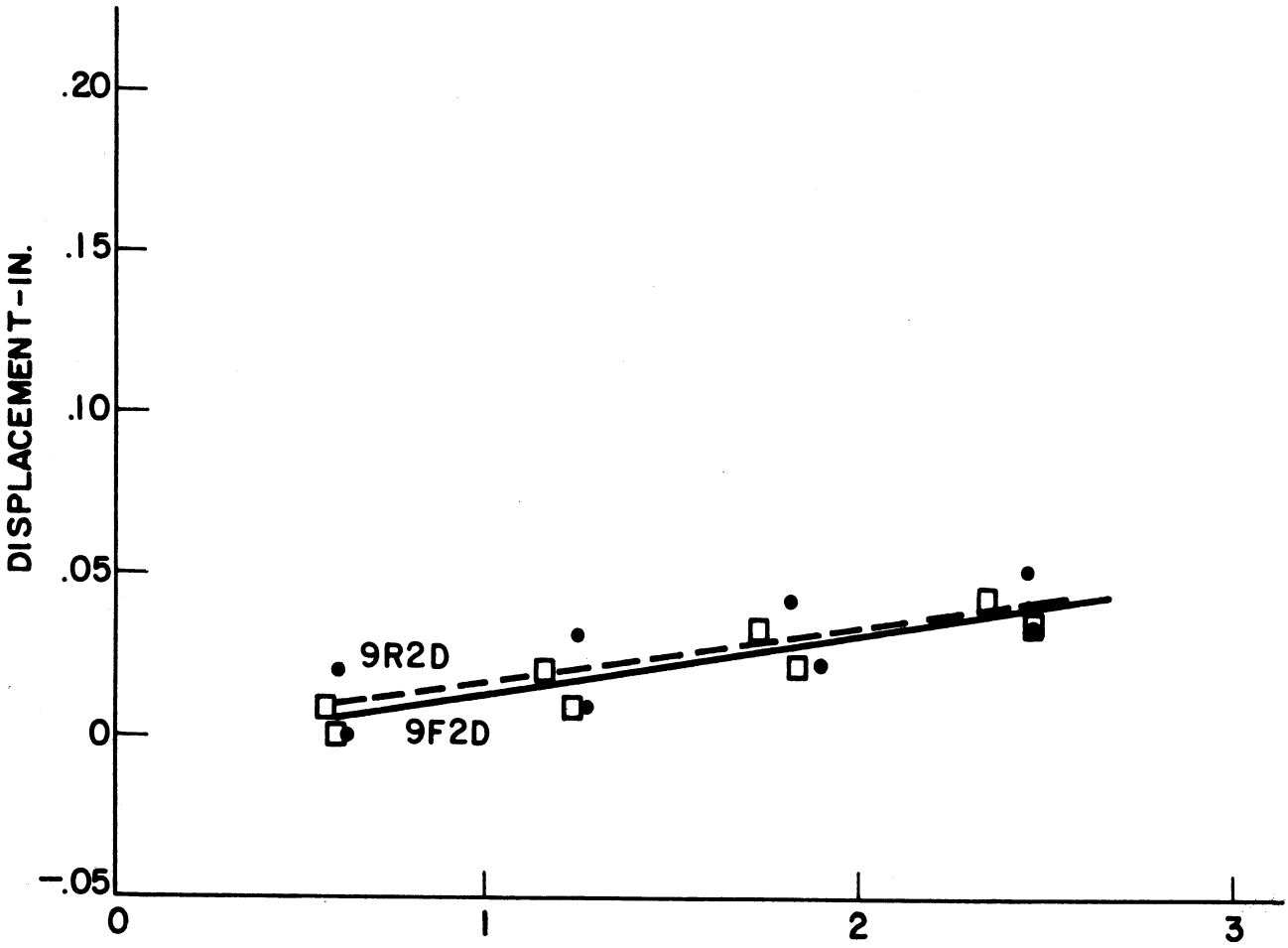

Tangential Grid Movement 85° Brass Cones

FIG. 11a. (Cont.)

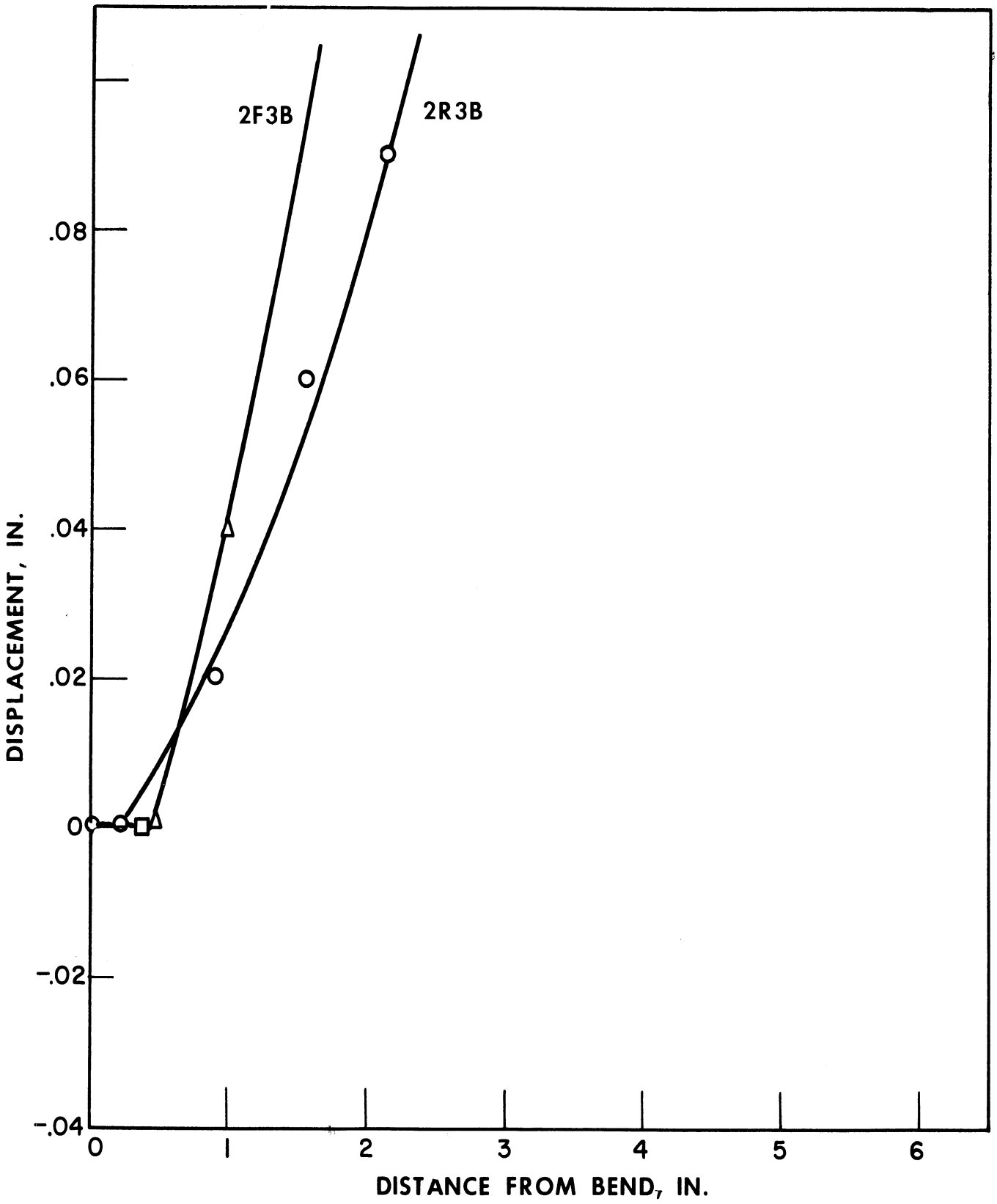

TANGENTIAL GRID MOVEMENT - 108° BRASS CONES

FIG. 11a (CONT.)

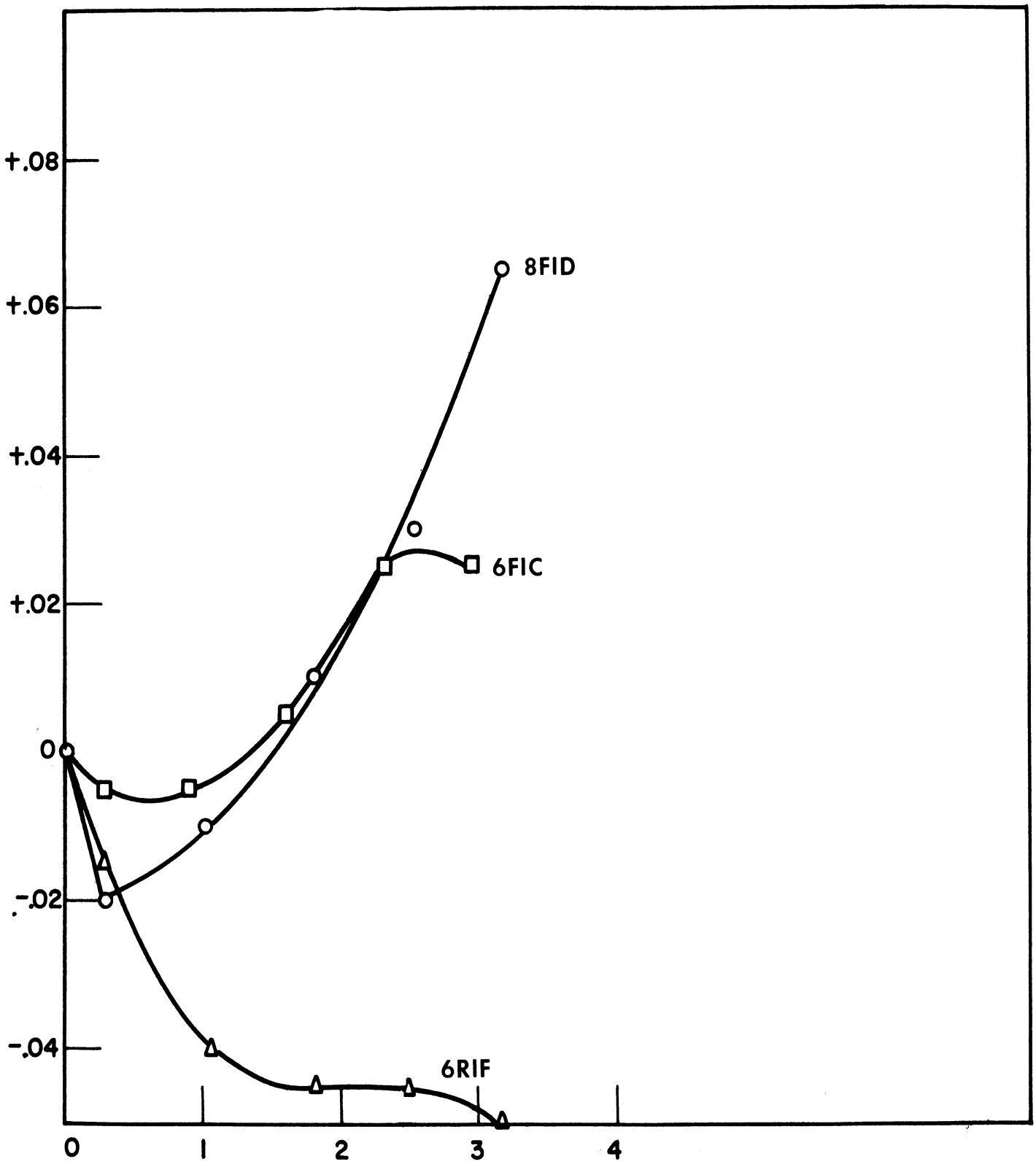

TANGENTIAL GRID MOVEMENT 63° ALUMINUM CONES

FIG. 11b

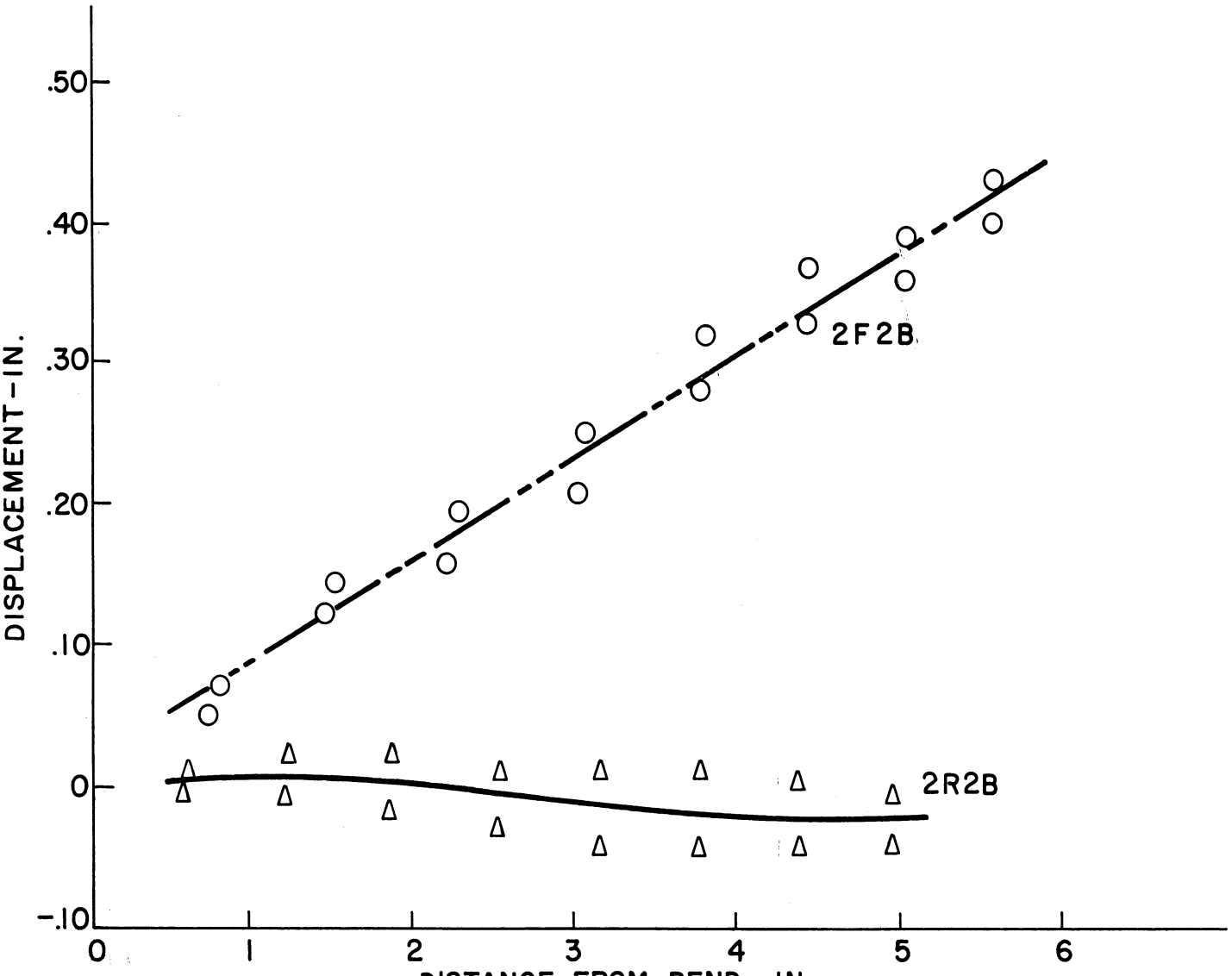

Tangential Grid Movement 85° Aluminum Cones

FIG. 11 b. (Cont.)

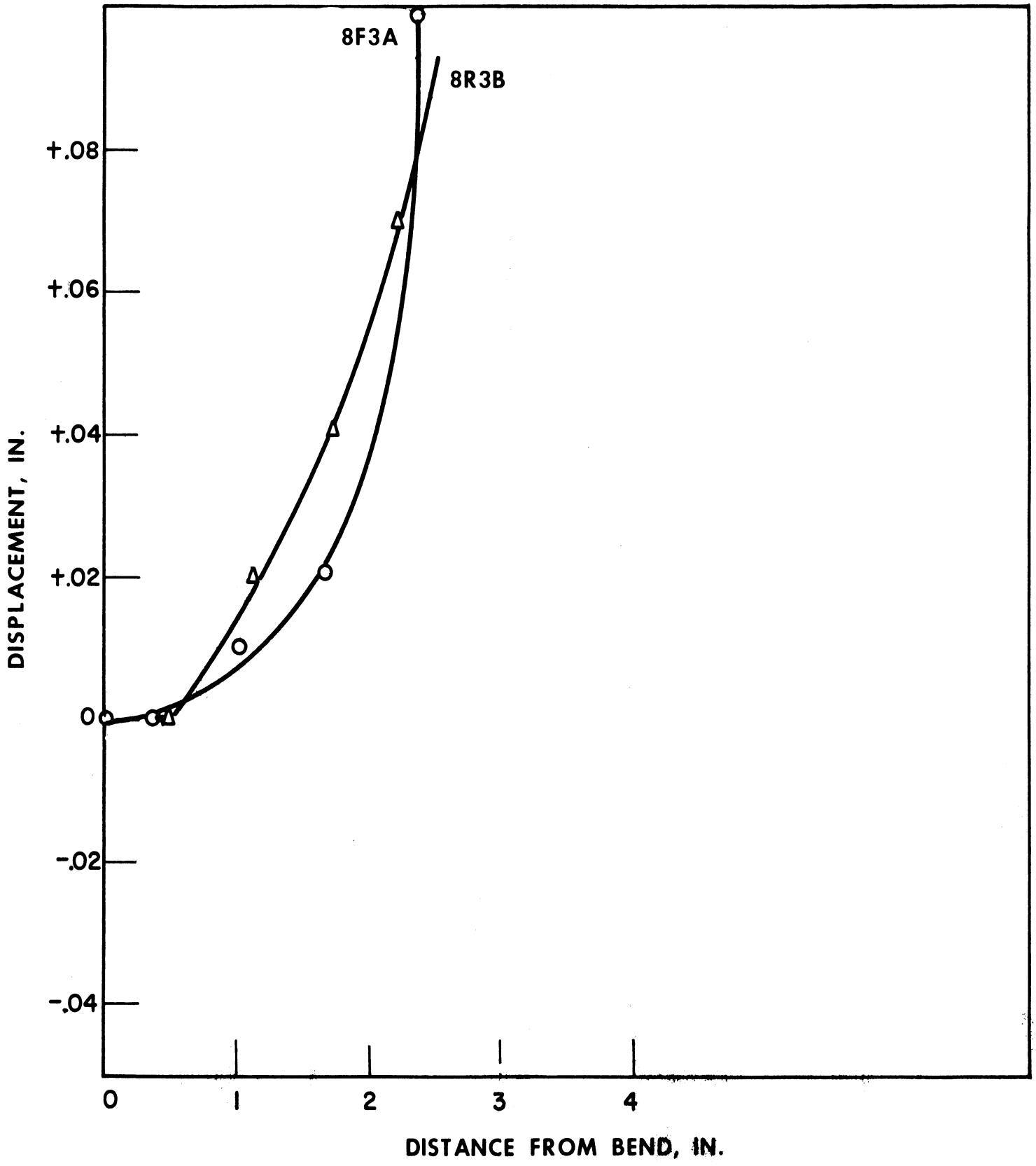

TANGENTIAL GRID MOVEMENT 108° ALUMINUM CONES

FIG. 11b (CONT.)

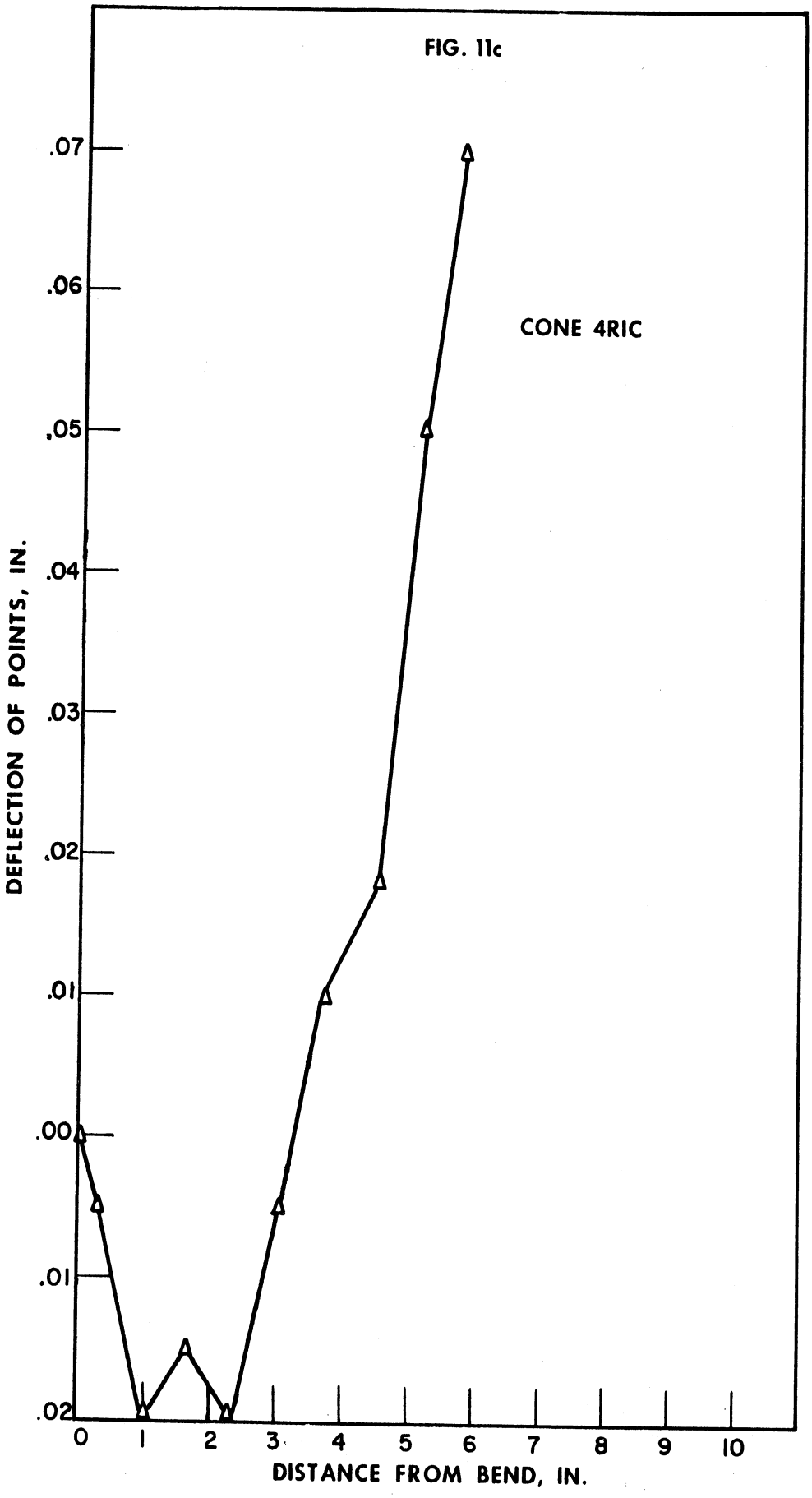

TANGENTIAL GRID MOVEMENT-HAND-SPUN .125-IN. ALUMINUM CONES

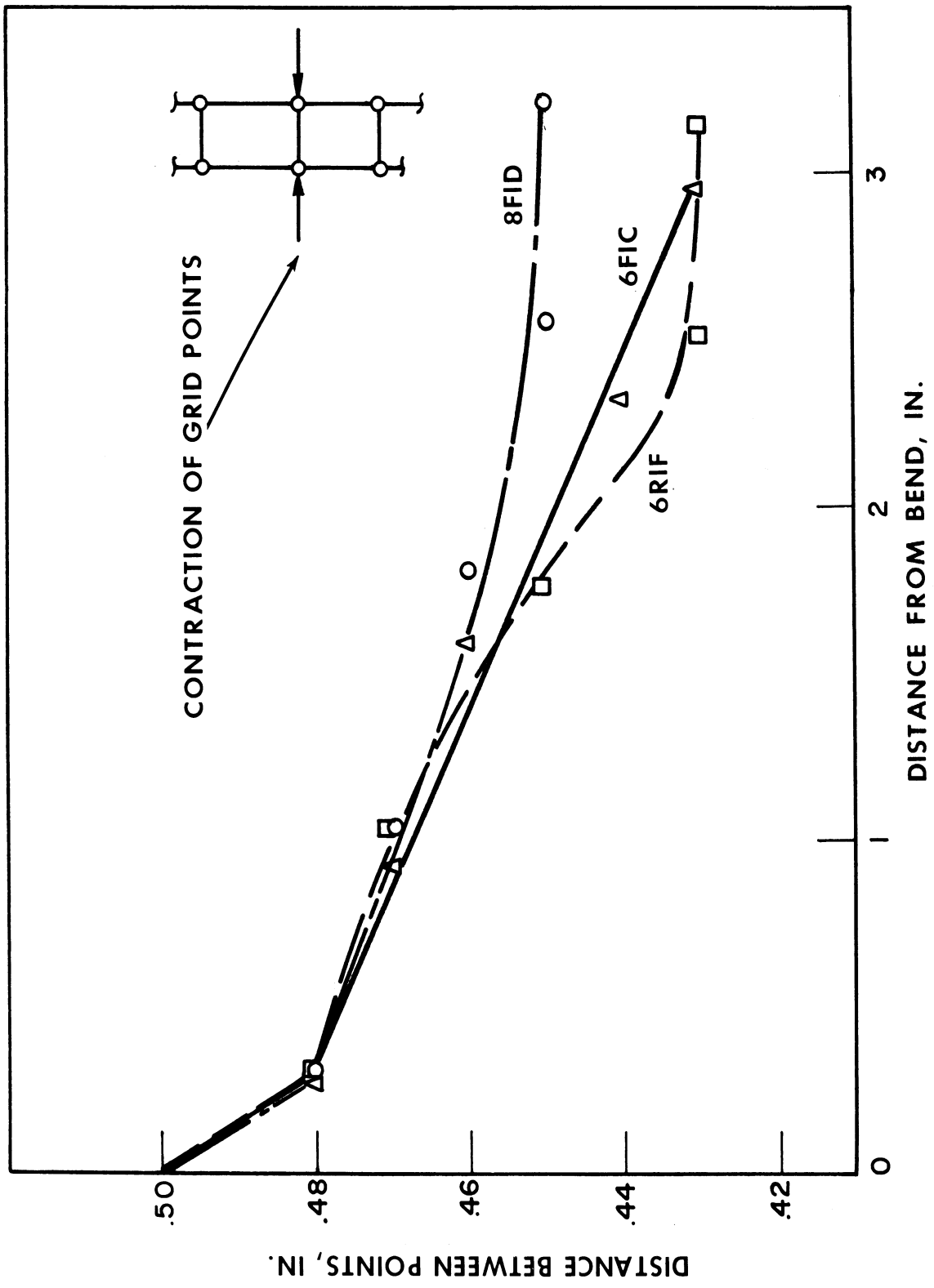

HAND-SPUN BRASS

FIG. 12a

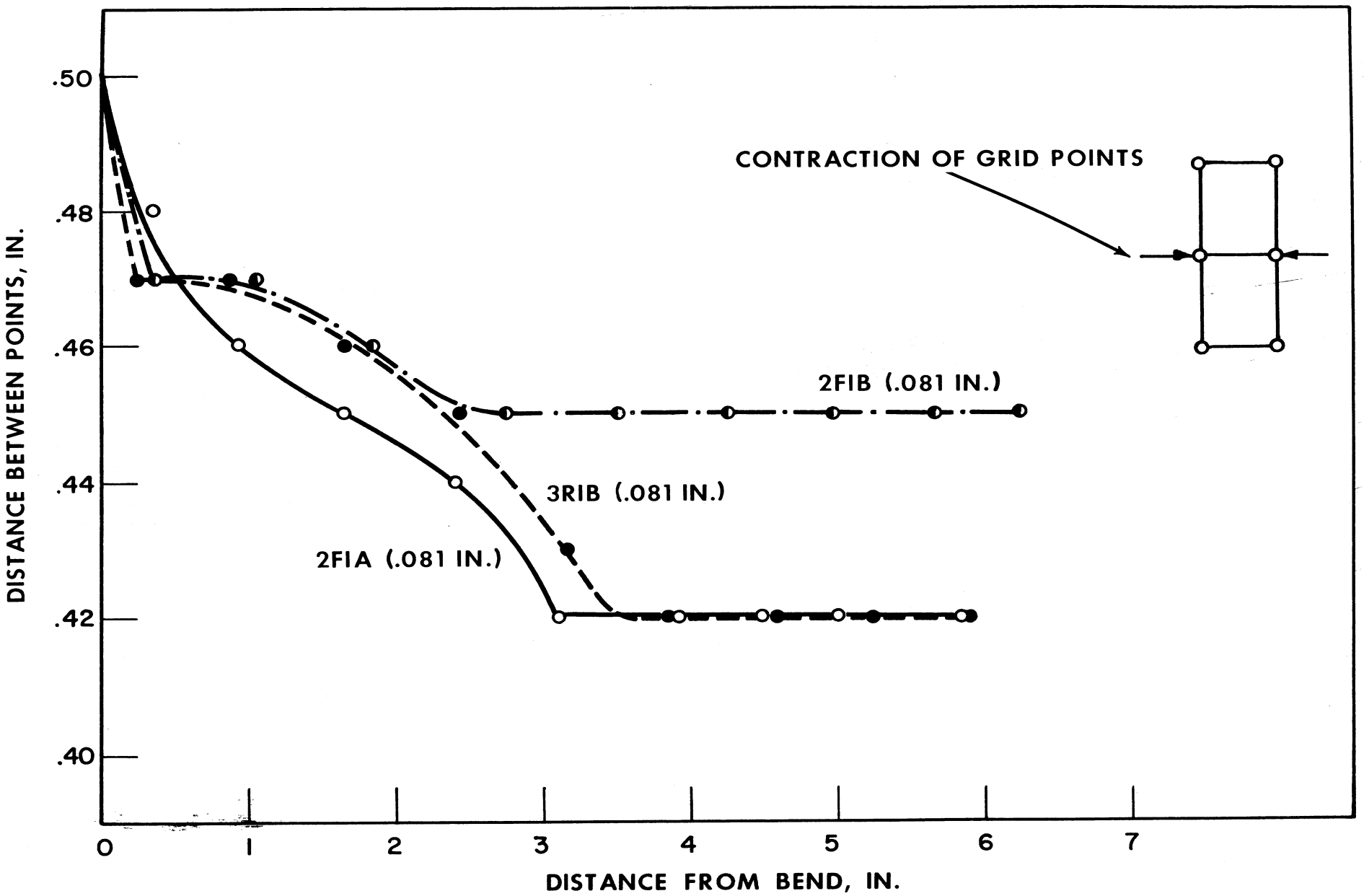

HAND-SPUN .081-IN. ALUMINUM

FIG. 12b

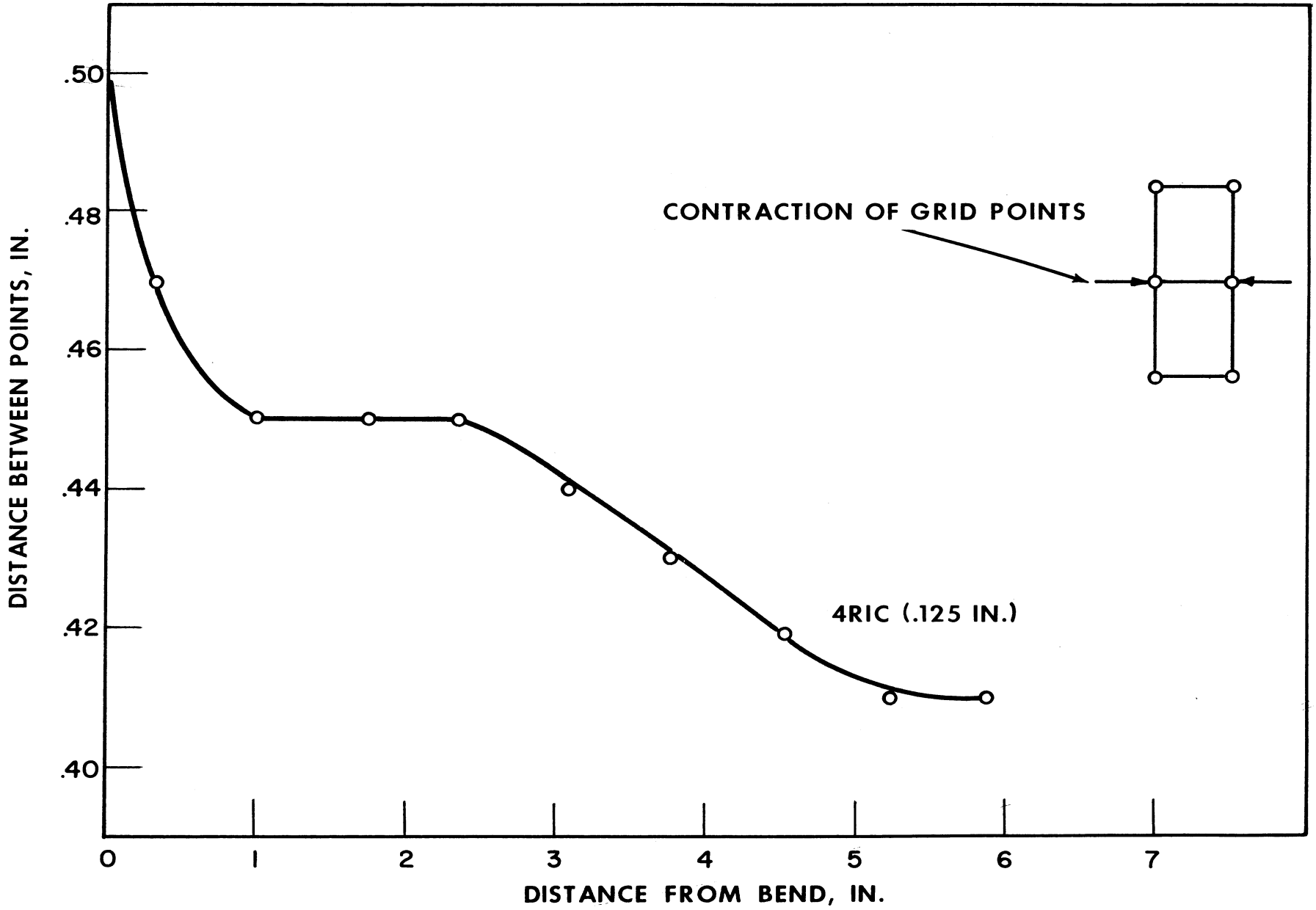

HAND-SPUN .125-IN. ALUMINUM

FIG. 12c

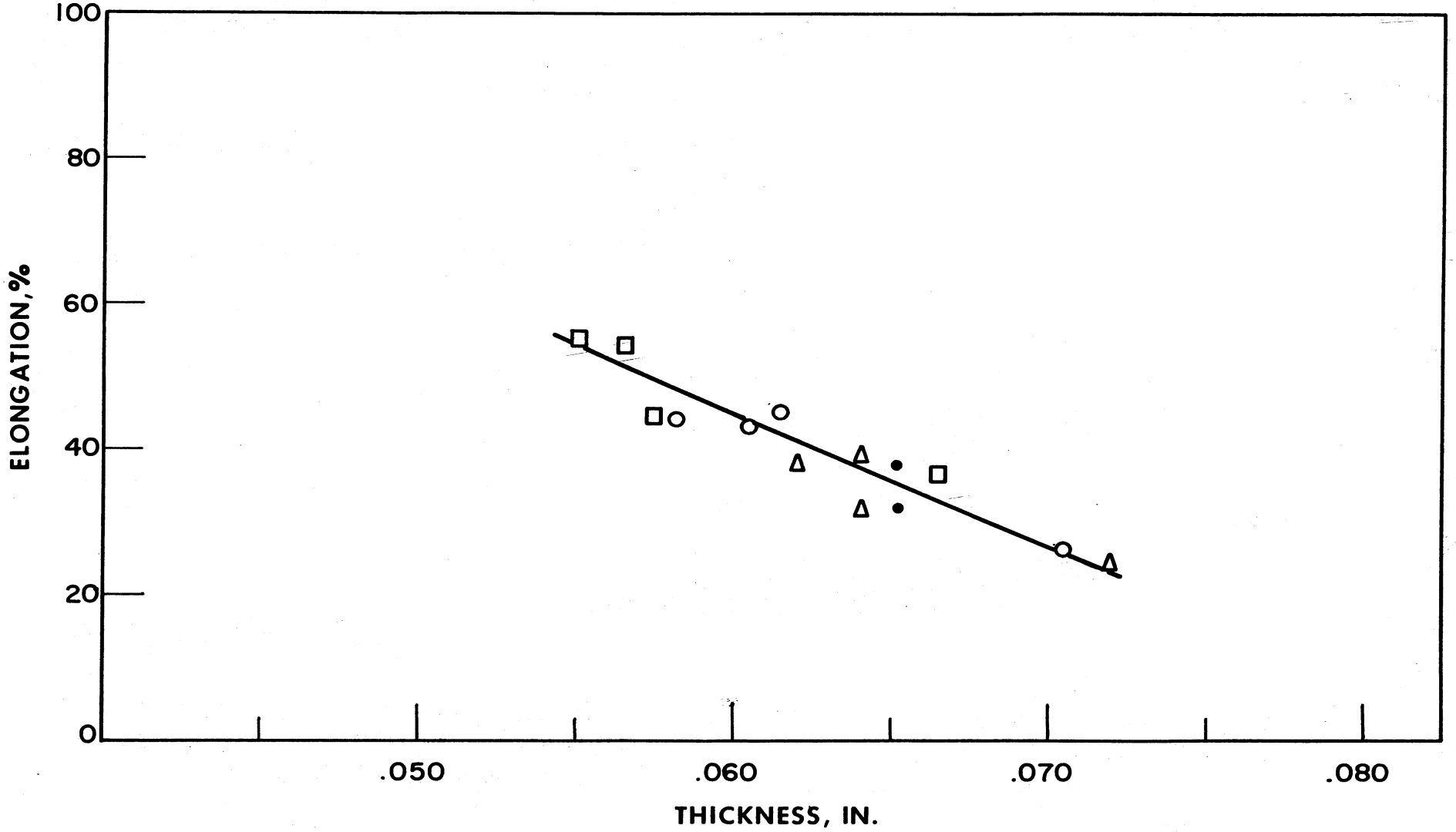

ELONGATION vs. THICKNESS – HAND-SPUN BRASS

FIG. 13a

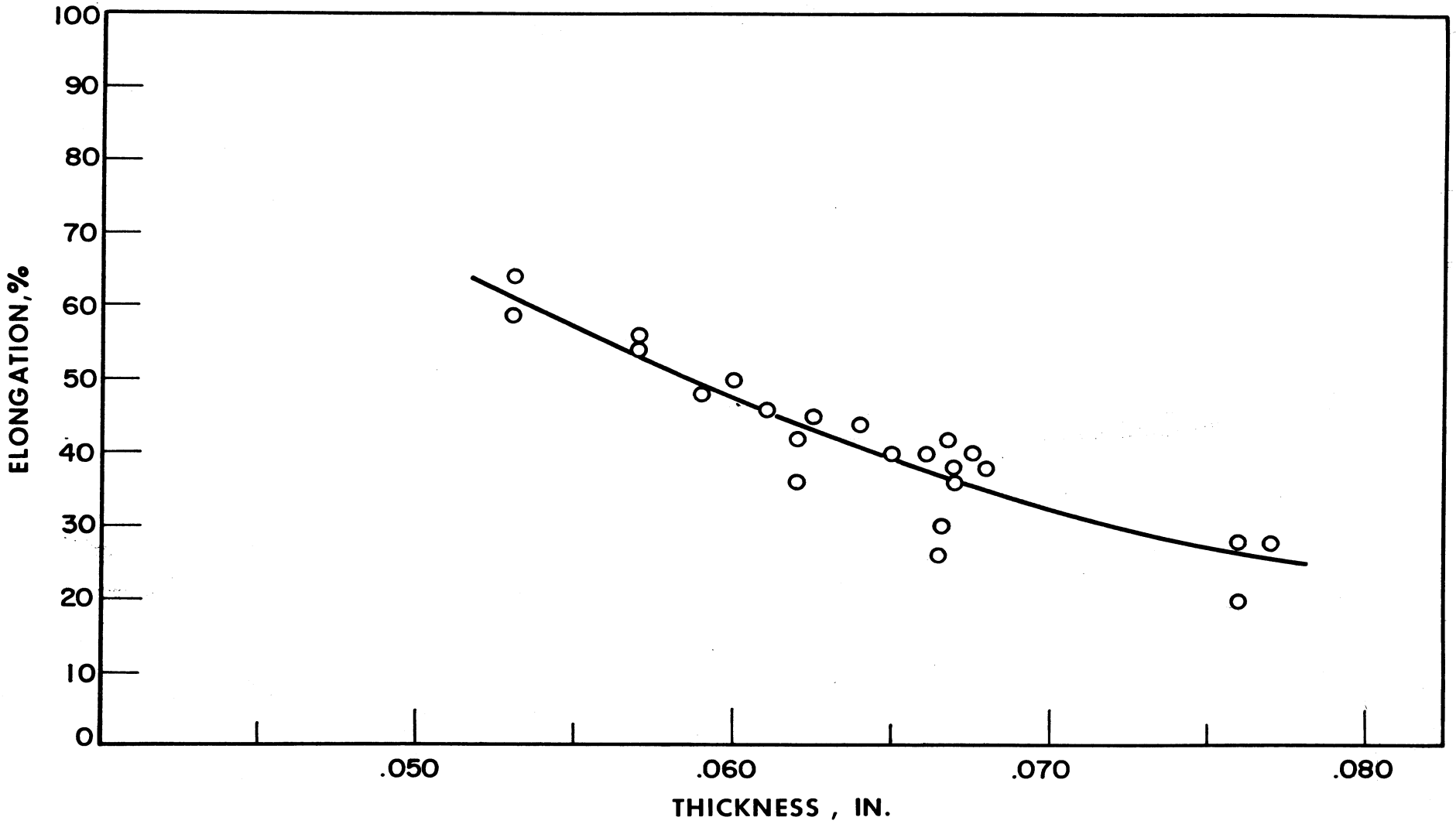

ELONGATION vs. THICKNESS—HAND-SPUN .081-IN. ALUMINUM

FIG. 13b